R-14-25

System design of Dome Plug

Preparatory modelling and tests of the sealing and draining components

Lennart Börgesson, Torbjörn Sandén, Linus Andersson,
Lars-Erik Johannesson, Reza Goudarzi, Mattias Åkesson

Clay Technology AB

Januari 2015

Svensk Kärnbränslehantering AB
Swedish Nuclear Fuel
and Waste Management Co

Box 250, SE-101 24 Stockholm
Phone +46 8 459 84 00

ISSN 1402-3091
SKB R-14-25
ID 1404126

January 2015

System design of Dome Plug

Preparatory modelling and tests of the sealing and draining components

Lennart Börgesson, Torbjörn Sandén, Linus Andersson,
Lars-Erik Johannesson, Reza Goudarzi, Mattias Åkesson

Clay Technology AB

Keywords: Dome plug, Backfill, Delimiter, Bentonite, Drainage, Seal, Swelling pressure, Hydro-mechanical processes, Numerical modelling, KBP1004.

Abstract

The primary requirements of the dome plug are that the water leakage past the plug is small enough to result in a build-up of water pressure inside the pluged volume and to keep water escape from the tunnel at an acceptable level. It is very important that the plug is so tight that the lowest water pressure gradient is moved from the rock/bentonite interface in the tunnel to the plug, since that will give the bentonite time to swell and seal in a non-flow condition. The plug must also be so tight that the water leakage past the plug does not allow for unacceptable erosion of clay from the deposition holes. This is of particular importance during the period before the water pressure in the transport tunnel outside the plug has reached the same level as inside the plug.

In preparation for a plug test in full scale in Äspö HRL a program for investigating critical parts of a plug and design of the plug has been undertaken. The work of designing the seal and draining components of the plug has included the following four subprojects:

- Laboratory testing of the seal materials.
- Laboratory testing of the drainage components.
- Scale tests of the seal and draining function.
- Hydro-mechanical modelling of the tunnel plug.

Laboratory testing of the seal materials

- Compaction tests showed that it was possible to compact blocks of low density and high degree of saturation, although compaction problems occurred if the water content of the powder was higher than 30%. The desired density of the blocks was however increased at a later stage of the project and other tests e.g. the seal tests showed that blocks with lower water content seemed to swell and seal faster.
- The investigation of block strength showed that the strength of the block depends strongly on the water content and on the achieved density of the block. At low water contents (10%) and low density, the block strength was low and the blocks fragile.
- In order to investigate the compression and expansion properties, two oedometer tests were performed. The results from these tests agreed well with what was expected for MX-80 bentonite. The results from these tests were further used in the hydro-mechanical modelling of the plug.
- Measurements of swelling pressure and hydraulic conductivity were completed to check if there were any differences in these parameters as the result of the initial degree of saturation. The investigation showed, as expected, that there was no evident difference although the hydraulic conductivity was somewhat lower than the reference tests. This is probably due to the fact that the blocks, compacted to high degree of saturation were more homogeneous.
- Three tests were performed in order to study if any self-healing effects of an artificial fracture in the rock below the clay blocks could be expected from the bentonite. Two of the tests were performed with bentonite blocks with densities of 1,400 and 1,500 kg/m^3 and with water contents of 35% and 30% respectively i.e. the degree of saturation was very high. The bentonite in these two tests did not manage to seal the artificial fracture (0.01 mm aperture between two steel lids) at the base of the test assembly during the test time. The third test was performed with bentonite blocks with a dry density of 1,500 kg/m^3 and with a water content of 13.9%. In this test the behaviour was quite different. The bentonite sealed the fracture quickly and a water pressure associated with the percolation could be built up without compromising the seal produced (maximum 2 MPa was applied in this test). It is however not clear if the sealing took place in the cylindrical tube containing the blocks or in the artificial slot at the end of the assembly.
- Tests were performed in order to study the effect of initial gap size on sealing ability. In these tests, bentonite blocks with different initial density and different initial water content were allowed to swell and seal a slot with a gap of either 2 or 4 mm. The results from the tests showed, as expected that the slot width is of great importance, with faster swelling pressure increase with a small gap.

It was also observed that the initial water content of the bentonite block also influenced the results. The time for swelling and filling up the slot and start to building up of hydraulic pressure at the upstream end of the bentonite seal was longer for the samples with high initial water contents (and high degree of saturation).

Laboratory testing of the drainage material

This work was done in order to evaluate several different types of draining components that may be used in connection with a concrete tunnel-plug. These draining components will prevent water pressure buildup on the plug prior to completion of initial concrete curing. The candidates tested were three types of geological draining material, two qualities of geotextile and two types of stiff draining materials. An important factor in their evaluation is their durability under the expected swelling pressure of about 2 MPa. Compressibility and hydraulic conductivity were tested for all candidates. Also modified Proctor compaction tests were performed on the draining geological materials so as to ensure that testing is done under realistic field conditions. Finally a clogging test was performed on all candidates to investigate if they would maintain their draining ability when exposed to a water flow with high entrained bentonite content.

The results from the tests led to a recommendation to use the macadam 2–4 mm granulate as a geological draining material. This candidate was the superior option in terms of hydraulic conductivity (very high) and also seemed to maintain its draining ability when exposed to a water flow with high bentonite content. In contrast, the geotextile seem to clog when exposed to a water flow with a content of eroded bentonite and should therefore not be used to drain the system. However it could function as a distributer of water if manual wetting of the system is required. Blocks manufactured of Light Expanded Clay Aggregate, Leca, is the superior stiff draining material in terms of maintaining a high hydraulic conductivity and seems to maintain this ability when exposed to a water flow with high bentonite content.

Scale tests of the seal and draining function

Several tests of a plug scaled about 1:20 with all components included were performed in the laboratory in order to study the drainage and sealing functionality of the plug. The test components interacted as desired and the different materials were successfully separated from each other. The draining function of the filter worked satisfactorily at the inflow rates 0.001 l/min and 0.005 l/min and the measured amount of eroded material was small, about 1 g/l or less, which is in the lower region of the erosion prediction model by Sandén and Börgesson (2010).

The bentonite seal, length of 50 mm, could successfully withstand 5 MPa of water pressure if the available time for swelling was long enough and if the pressure increase rate not was higher than 50 kPa/h.

Based on the test results the following suggestions were made for the full scale field test of the tunnel plug:

- The filter draining function should be tested with a water flow rate that represents the expected total flow of a deposition tunnel.
- The erosion during the drainage period should be measured and evaluated to confirm that it is within an acceptable range.
- The size of the void spaces between concrete beams and between concrete beams and tunnel wall should be minimized to maximize seal functionality. The space between the concrete beams and the tunnel wall should be filled, so far as possible with cement in order to limit the size of the potential water movement pathway.
- The filter should be filled with water early in order to give the bentonite seal access to water as soon as possible.
- The pressurization of the test should be done carefully. If the water pressure needs to be reduced for some reason, the re-pressurization needs to be carefully performed as well.

- This study also provided some data on the radial total pressures and dry densities associated with the seal. It is hard to give a direct recommendation regarding pressurization rate for the full scale field test due to scaling factors, but a radial total pressure of 750 kPa (including a water pressure of 500 kPa) appears to be the lowest radial swelling pressure that could withstand a hydraulic head increase of 50 kPa/h that ultimately reached 5 MPa hydraulic head.

Hydro-mechanical modeling of the tunnel plug

There were two goals to the modeling work: 1) *dimensioning calculations* of the general plug design, and 2) *prediction* of the hydro-mechanical processes in the planned field experiment.

The methods used in these modelling activities also contained two-parts: i) the dimensioning calculations were primarily performed with *analytical methods*, developed for these tasks, and consisted of calculations of dimensions for different plug components in different configurations; and ii) the predictions were primarily performed with *numerical methods*, i.e. the Code_Bright FEM code, and were performed stepwise, becoming increasingly specific during the course of the project.

The analytical models and the general design FEM models were developed with the aim of limiting the final swelling pressure on the concrete plug to 2 MPa. This is considered to be one of the main design criterions for the plug construction. Since the swelling pressure in the backfill can under many conditions, be considerably higher than this limit, this has called for the development of a transition zone. This transition zone allows for swelling pressures generated some distance from the plug to be dissipated by the frictional forces of the fill material against the rock wall. This aim of limiting the pressure to 2 MPa has been given less priority during the planning of the field test. One reason for this has been that the time-scale to reach full saturation in a full-scale test is too long to be studied in a field test. Another reason is that it wasn't possible to manufacture mechanically stable bentonite blocks with a sufficiently low dry density to limit pressure to < 2 MPa.

The mechanical processes simulated in the plug models were generally governed by the main mechanical properties previously established for bentonite: i.e. swelling pressure relation and friction angle of bentonite for which established data was used. More specific data on the mechanical behaviour, i.e. elastic properties of the filter materials, as well as consolidation/swelling data for MX-80 at relevant density levels, were evaluated from results from laboratory tests devoted for this project. Apart from the mechanical aspect of the processes, there was also the issue of bentonite hydration and the time-scale needed for this to be accomplished (largely governed by the hydraulic conductivity), for which established data was used.

The main results from the different numerical models have been:

i. the stress on plug and the stress distribution along the tunnel axis,

ii. the displacements of the different components,

iii. the extent of bentonite homogenization, and

iv. the time-scales associated with bentonite hydration.

Some results have been compared with experimental data. One such data set was the different stress paths in the void ratio vs. net stress plane obtained from oedometer tests. The model results showed quite good agreement with the experimental data set, which strengthens confidence in the validity of the mechanical model used. A similar comparison could be made with water saturation profiles from water uptake tests, by choosing model results for relevant time scales. This comparison indicated that the modelled hydration process was slightly faster than the measured hydration.

Sammanfattning

Kraven på pluggen måste vara sådana att vattenläckaget förbi pluggen ska vara tillräckligt litet för att det ska kunna byggas upp ett vattentryck innanför pluggen och att den samtidigt kan hålla nere eroderande vattenflöden från tunneln på en acceptabel nivå. Det är mycket viktigt att pluggen är så tät att vattentrycksgradienten flyttas från berg/bentonit gränssnittet i tunneln till pluggen, eftersom det kommer att ge bentoniten tid och möjlighet att svälla och täta i stillastående vatten. Pluggen måste också vara så tät att vattenläckage inte orsakar oacceptabel erosion från deponeringshålen fram tills det att vattentrycket i transporttunneln utanför pluggen har nått samma nivå som innanför pluggen.

Som en förberedelse för ett pluggförsök i full skala på Äspölaboratoriet har det utretts vilka de kritiska delarna är när det gäller byggandet och designen av en plugg. Arbetet med att designa och utforma tätningen och de dränerande komponenterna av pluggen har inkluderat följande fyra delprojekt:

- Laboratorietester av bentonittätning.
- Laboratorietester av dräneringskomponenter.
- Skalförsök av funktionen hos tätning och dränering.
- Hydromekanisk modellering av pluggen.

Laboratorietester av bentonittätning

- Kompakteringstester visade att det var möjligt att kompaktera block med låg densitet och hög vattenmättnadsgrad även om det fanns problem när vatteninnehållet i pulvret var högre än 30%. Den valda blockdensiteten ökades emellertid i ett senare skede av projektet eftersom andra tester, till exempel tätningstesterna visade att block med lägre vattenhalt tycktes svälla och täta snabbare.
- Undersökningen visade också att blockens hållfasthet är starkt beroende av vatteninnehållet och av den uppnådda densiteten. Vid låga vatteninnehåll (10%) och låg densitet, var blockhållfastheten ganska låg och blocken spröda.
- Två ödometerförsök har genomförts för att undersöka kompressions och expansionsegenskaper. Resultaten från dessa tester stämmer väl med vad som förväntas av MX-80 bentonit. Resultaten från dessa tester har också använts i den hydromekaniska modelleringen av pluggen.
- Det har gjorts bestämningar av svälltryck och hydraulisk konduktivitet för att undersöka om det finns några skillnader beroende på den initiala mättnadsgraden. Undersökningen visade, som väntat, att det inte fanns någon tydlig skillnad även om den hydrauliska konduktiviteten var något lägre än för referenstesterna. Detta berodde förmodligen på att blocken som komprimerats till hög vatten mättnadsgrad var mer homogeniserade.
- Tre tester utfördes för att studera om man kan förvänta sig någon tätningseffekt från bentonittätningen när det gäller sprickor i berget. Två av testerna utfördes med bentonitblock med densiteterna 1,400 och 1,500 kg/m^3 och med vatteninnehåll på 35% respektive 30%, det vill säga mättnadsgraden var mycket hög. Bentoniten lyckades i dessa två tester inte täta en artificiel spricka (0,01 mm öppning) under testtiden. Det tredje testet utfördes med bentonitblock med en torr densitet av 1,500 kg/m^3 och med ett vatteninnehåll av 13,9%. Resultatet från detta test var helt annorlunda. Bentoniten tätade ganska snabbt och ett vattentryck kunde byggas upp (max 2 MPa). Det är dock inte helt klargjort om tätningen ägde rum i det cylindriska röret där blocken fanns eller i den konstgjorda sprickan.
- Tester har också gjorts för att studera tätningseffekten av befintliga spalter. Här testades om bentonitblock med olika densitet och olika startvatteninnehåll kunde svälla och täta en spalt på antingen 2 eller 4 mm. Resultaten från testerna visade som väntat att spaltvidden är av stor betydelse för om tätningen ska lyckas. Ett annat resultat var att start vatteninnehållet i bentonitblocket också påverkade resultatet. Tiden för att svälla och börja täta var längre för proven med höga startvatteninnehåll (och hög grad av mättnad).

Laboratorietester av dräneringsmaterial

Detta arbete gjordes för att utvärdera olika typer av dränerande material som var möjliga att använda innanför en tunnelplugg av betong. De dränerande komponenterna förhindrar att ett vattentryck byggs upp mot pluggen innan denna har härdat. Materialen som testades var tre typer av geologiska dränerande material, två olika kvaliteter av geotextil och två typer av styva dräneringsmaterial. En viktig faktor vid bedömningen var att de testade materialen skulle utsättas för ett svälltryck på ca 2 MPa. Alla material testades också när det gäller kompressibilitet och hydraulisk konduktivitet. Det gjordes också s.k. modifierad Proctor tester på de dränerande geologiska materialen och även tester för att studera om det fanns tendenser på att något av materialen skulle sätta igen när de utsattes för ett vattenflöde med hög bentonithalt.

Resultaten från testerna ledde till en rekommendation att man ska använda makadam 2–4 mm som ett geologiskt dränerande material. Detta material var överlägset när det gällde hydraulisk konduktivitet och verkade också behålla sin dränerande förmåga även när det utsattes för ett vattenflöde med hög bentonithalt. Geotextilerna verkade täta när de utsattes för ett vattenflöde med ett innehåll av eroderande bentonit och dessa bör därför inte användas för dränering, dock skulle de kunna användas för att fördela vatten om man skulle vilja göra en artificiell bevätning av bentoniten i tätningen. Av de styva materialen är Leca det överlägset mest dränerande material och den verkar dessutom att behålla sin dränerande förmåga även när den utsatts för ett vattenflöde med hög bentonithalt.

Skaltester av tätningen och dränering

För att studera dränering och tätningsfunktionerna i en tunnelplugg har det genomförts ett antal tester i skala 1:20. De ingående komponenterna fungerade enligt önskemålen och lyckades även hålla sig separerade från varandra. Den dränerande funktionen hos filtret var tillfredsställande vid inflöden på 0,001 l/min och 0,005 l/min och den uppmätta mängden av eroderat material var liten, cirka 1 g/l eller mindre, vilket är i den nedre regionen av den erosionsmodell som föreslagits av Sandén och Börgesson (2010).

Bentonittätningen lyckades klara 5 MPa vattentryck om den gavs tillräckligt med tid för att svälla och täta. Tryckhöjningstakten fick dock inte vara högre än 50 kPa/h.

Baserat på testresultaten gjordes följande förslag inför fältförsöket med en tunnelplugg i full skala:

- Dräneringsfunktionen hos filtret bör testas med ett flöde som är i samma storleksordning som det förväntade flödet i en deponeringstunnel.
- Erosionen bör mätas under dräneringsperioden för att säkerställa att den är på en godtagbar nivå.
- Spalterna mellan betongbalkar och mellan betongbalkar och tunnelvägg bör minimeras för maximal tätning funktion. Dessa spalter bör efter inplaceringen av betongbalkar gjutas igen med cement.
- Dräneringsfiltret bör fyllas upp med vatten tidigt för att ge bentonittätningen tillgång till vatten så fort som möjligt.
- Tryckökningen bör göras med försiktighet. Om vattentrycket av någon anledning behöver minskas måste tryckökningen återigen göras med försiktighet.
- Det finns också data när det gäller det radiella totaltrycket från bentonittätningen. Det är svårt att ge rekommendationer beroende på skaleffekter men ett radiellt tryck på 750 kPa (inklusive 500 kPa vattentryck) visade sig vara det lägsta tryck där tätningen kunde motstå en tryckökningshastighet på 50 kPa/h upp till maximalt 5 MPa.

Hydromekanisk modellering av tunnelpluggen

Målsättningen för modelleringsarbetet var väsentligen tvådelat: i) *dimensioneringsberäkningar* för den allmänna plugg-designen, och ii) *prediktioner* av de hydromekansika processerna i det planerade fältförsöket. Metoderna som användes för arbetet var också tvådelade: i) dimensioneringsberäkningarna utfördes i första hand med *analytiska metoder* vilka utvecklades för dessa uppgifter, och utgjordes av beräkningar av dimensioner för olika plugg-komponenter i olika konfigurationer; och ii) prediktionerna utfördes framförallt med *numeriska metoder* (FEM-koden Code_Bright), och utfödes stegvis och blev alltmer specifika under projektets gång.

De analytiska modellerna, samt FEM-modellerna för den allmänna designen, utvecklades med målet att begränsa det slutliga svälltrycket mot betongpluggen till 2 MPa, vilket betraktades som en av de viktigaste designkriterierna för pluggkonstruktionen. Eftersom svälltrycket i återfyllningen kan bli väsentligt högre, så har detta lett fram till en utveckling av en övergångszon, i vilken tryckskillnaderna mellan olika sektioner av pluggen kan motverkas av friktionskrafterna mot bergväggen. Målet på 2 MPa gavs lägre prioritet under planeringen av fältförsöket. En orsak till detta var att tidsskalan för att nå full vattenmättnad var för lång för att studeras i ett fältförsök. En annan orsak var att det inte var möjligt att tillverka lämpliga bentonitblock med tillräckligt låg torrdensitet.

De mekaniska processerna i pluggmodellerna styrdes generellt av de viktigaste mekaniska egenskaperna: det vill säga svälltrycket och friktionsvinkeln för bentoniten för vilka etablerad data användes. Mer specifik data för det mekaniska beteendet, det vill säga elastiska egenskaper för filtermaterialen samt konsolidering/svällnings-data för MX-80 vid en relevant densitetsnivå utvärderades från resultat från laboratorieundersökningar speciellt utförda för detta projektet. Förutom de mekansika aspekterna för processerna så beaktades även bevätningen av bentoniten och tidsskalan för detta, och dessa processer styrdes till stor del av de hydrauliska konduktiviterna för vilka etablerad etablerad data användes.

Huvudresultatet från de olika numeriska modellerna har varit:

i. spänningar mot pluggen och spänningsfördelningen längs tunnelaxeln,

ii. förskjutningar för olika komponenter,

iii. homogeniseringens omfattning, samt

iv. tidsskalan för bevätningen.

Vissa resultat har jämförts med experimentell data. En sådan datamängd var olika spänningsvägar i portal-nettospänningsplanet som var erhållna från ödometerförsök. Modelresultaten visade god överenstämmelse med den experimentella datamängden, vilket därmed skulle styrka giltigheten för den använda mekaniska modellen. En liknande jämförelse kunde göras med vattenmättnadsprofiler från vattenupptagsförsök, genom att välja modellresultat för relevanta tidsskalor. Denna jämförelse indikerade att den modellerade bevätningsprocessen var något snabbare än den uppmätta bevätningen.

Contents

1 Introduction

The deposition tunnels in a planned repository for spent nuclear fuel will be sealed with a plug at the end of each of the tunnels. They are needed to withstand the swelling of the backfill and prevent outflow of groundwater from these tunnels.

The demands on the plug require that the water leakage past the plug is small enough to allow for build-up of water pressure inside the plug until the water pressure in the closed and backfilled transport tunnel outside the plug has reached the same level as inside the plug. This will keep movement of any eroding water flows within the tunnel at an acceptable level, preventing substantial redistribution of buffer or backfill during the pre-closure period. It is very important that the plug is so tight that the lowest water pressure gradient is moved from the rock/bentonite interface in the tunnel to the plug itself, since that will give the bentonite time and ability to swell and seal without needing to resist flow of water.

The concrete part of the plug needs time for hardening and contact grouting and during that time (about 3 months) the concrete dome must be kept free from flowing water, which for wet tunnels (tunnels with water inflow rates too high to be stored in the pellet filling and where there is a risk for water reaching the backfill front during the construction of a plug) requires installation of a drainage system that takes care of the water coming from the inner parts of the tunnel.

The work to design a plug has proceeded over a period of a couple of years and has resulted in a decision to make such a field test. The present report describes the work associated with the design and testing of the sealing and drainage components of that plug.

The two main components of the plug system, apart from the concrete dome, are i) the bentonite seal, which will severely limit water flow through the concrete dome and, especially, between the dome and the rock wall; and ii) the permeable filter, which will enable drainage from the tunnel and/or water injection during the hydration of the bentonite seal.

The dimensioning of the bentonite seal has aimed at limiting the swelling pressure on the concrete dome to a maximum of 2 MPa. The swelling pressure within the backfill may however reach significantly higher levels (~ 6 MPa). This has initiated the development of a transition zone, which provides a component in which the stresses along the tunnel axis can be dissipated due to friction along the rock wall.

The basic layout of the plug was settled in the backfill and plug production report (SKB 2010). The detailed components were settled partly in the beginning of the study and partly during the progress of the study as results of the increased knowledge. The design used for the full scale test is shown in Figure 1-1. The minor details of the layout were changed as the study progressed, mainly regarding the delimiters, separating the different materials (see Figure 3-1). The plug consists of (from left to right):

- A concrete dome that shall resist the swelling pressure from the bentonite and the hydrostatic water pressure in the rock.
- A delimeter that separates the concrete from the sealing zone.
- A sealing zone made of bentonite blocks and bentonite pellets with the purpose of hindering water flow from the filter zone through possible fractures in the concrete or along the concrete-rock interface. It may also be used to cut off a possible excavation disturbed zone in the rock.
- Another delimeter that separates the sealing zone from the drainage filter (this was later removed).
- A drainage filter that has three purposes:
  - To drain water during the installation and hardening phase of the concrete dome.
  - To wet the bentonite seal and assure a fast and even water saturation.
  - To hinder water from leaking out past the plug by applying a water pressure higher than the hydrostatic in the case that the plug is not tight enough.
- A third delimeter separating the filter from the backfill (later changed to draining Leca beams).
- A transition zone made of bentonite blocks with low density and bentonite pellets that together will provide a component in which the stresses along the tunnel axis can be dissipated due to friction along the rock wall.

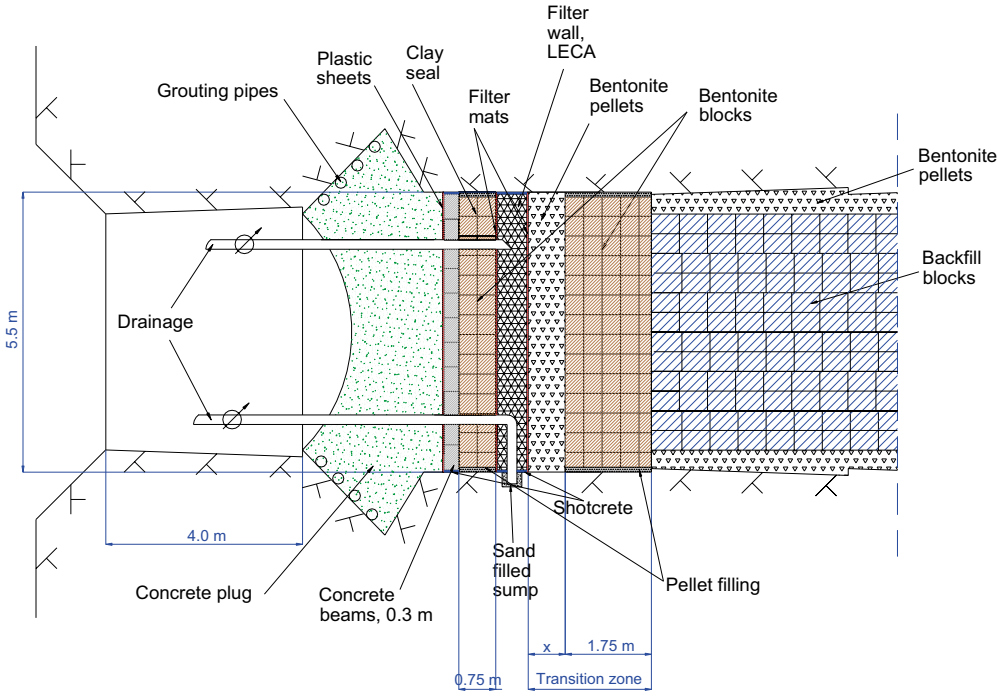

Figure 1-1. *Illustration of main components of plug design.*

The preparatory work done for the design of the sealing and draining sections of the plug have included of the following four main subprojects:

- Laboratory testing of the sealing materials, see Chapter 2.
- Laboratory testing of the drainage components, see Chapter 3.
- Scale tests of the sealing and draining function, see Chapter 4.
- Hydro-mechanical modelling of the tunnel plug, see Chapter 5.

2 Laboratory testing of the sealing materials

2.1 Introduction

The present design of a KBS-3 deposition tunnel end plug includes a bentonite seal, positioned behind the cast concrete dome, Figure 1-1. The sealing blocks were originally planned to be placed in a rock section, sawed out by use of wire sawing technique i.e. the surfaces were meant be very smooth with very precise measures. With this design the sealing blocks could be positioned tight against the rock surface, requiring that the block density be kept rather low in order to limit swelling pressure to less than 2 MPa (which is a preset design parameter). The plug design has however changed with time and in the present design (field test at Äspö HRL) the bentonite sealing blocks are to be placed in a section excavated by blasting, which means that the rock surface is very uneven. This also means that the sealing blocks must be piled on a bentonite pellet flooring fill, used in order to even out the rock surface.. This same pellet material will be used along the walls and also against the ceiling. In this design the sealing blocks must therefore have a higher density in order to reach the same average backfill density for the section. The objectives with the laboratory tests have therefore changed with design evolution, resulting in the test parameters varying.

2.2 Compaction properties

2.2.1 General

In the original planning of the plug design, it was intended to use sealing blocks with low density and high initial water content. In order to investigate the compaction properties of such material, block compaction tests were performed in laboratory scale.

2.2.2 Method and test matrix

The as-delivered material had a water content of about 12%. The bentonite powder was mixed in five different batches to different water contents, 15, 20, 25, 30 and 35%. The mixed materials were then used for compaction tests that were performed according to the following:

1. Small specimens were compacted in laboratory scale (Ø 50 mm, h 20 mm) using bentonite with different initial water contents.
2. Two test series were performed, one with a target dry density of 1,400 kg/m^3 and one with a target dry density of 1,500 kg/m^3. The target dry density, the water content and the final volume of the compacted sample were the fixed data and the weight of the powder was adapted thereafter for each test.
3. During compaction the pressure and displacement was registered.
4. After compaction, the water content and density of the compacted samples were determined. This data was then used to calculate the density as function of the compaction displacement during the compaction procedure.

In total eleven test compactions were made.

2.2.3 Results

A compilation of the sample data determined before and after compaction is provided in Table 2-1. The results from the compaction tests are presented in Figure 2-1 and Figure 2-2 where the compaction pressure is plotted versus displacement. The tests showed that it was very difficult to achieve the target density of the samples when low density blocks are the intended product. This difficulty was the result of both the relatively small scale but also the difference in behaviour of bentonites at different water contents. The samples with lowest water content exhibited expansion/rebound after compaction load was released, while the samples with higher water content showed a much smaller rebound. Figure 2-3 shows the compaction pressure plotted versus the dry density. The compaction pressure

needed to achieve dry densities of 1,400 kg/m^3 or 1,500 kg/m^3 is low, between 4 and 12 MPa. Figure 2-3 shows clearly that compaction of samples with a water content of 30 or 35% will be difficult. As saturation is approached during compaction, the load increase needed to accomplish further densification rises rapidly until refusal is achieved at saturation. The vertical lines in Figure 2-1 and 2-2 shows the displacement needed to reach full saturation and the vertical lines in Figure 2-3 shows the dry density at saturation.

Table 2-1. Compilation of data determined for the different samples before and after compaction.

	Before compaction		After compaction			
Sample ID	**Dry density kg/m³**	**Water content %**	**Bulk density kg/m³**	**Degree of saturation %**	**Void ratio**	**Dry density kg/m³**
1400-12 A	979	12.3	1,672	39.3	0.867	1,489
1400-12B	981	12.4	1,652	38.8	0.892	1,469
1400-15	962	15.0	1,672	45.7	0.912	1,454
1400-20	884	19.8	1,743	60.4	0.910	1,456
1400-25	822	24.8	1,840	77.7	0.886	1,474
1400-30	746	30.2	1,907	93.4	0.897	1,465
1400-35	641	34.2	1,902	98.9	0.961	1,417
1500-12	949	12.4	1,679	40.1	0.861	1,494
1500-15	917	15.0	1,769	51.6	0.806	1,539
1500-20	870	19.8	1,840	67.9	0.810	1,536
1500-25	825	24.7	1,959	89.2	0.769	1,572
1500-30	717	30.4	1,957	99.2	0.853	1,501

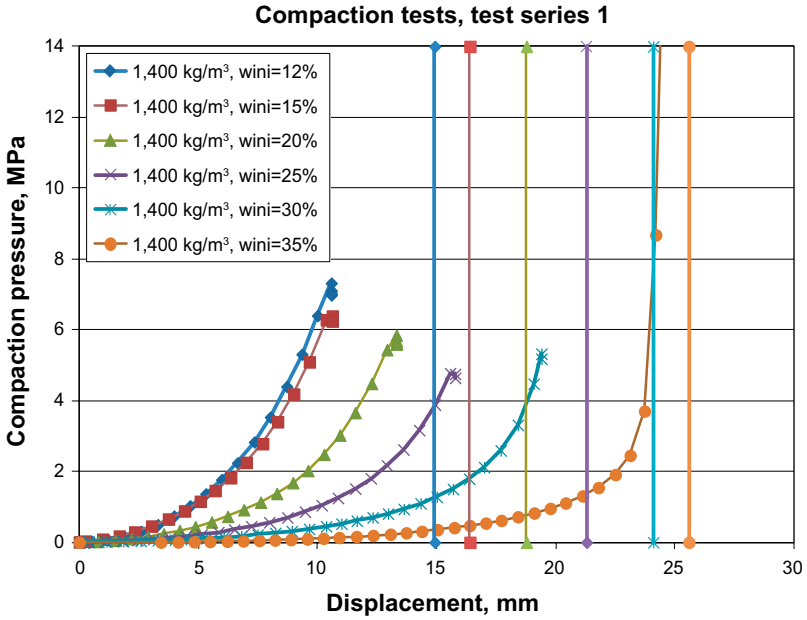

Figure 2-1. *Compaction pressure plotted versus displacement for samples with a target final dry density of 1,400 kg/m^3. The vertical lines shows the displacement needed to reach full saturation for a certain initial water content.*

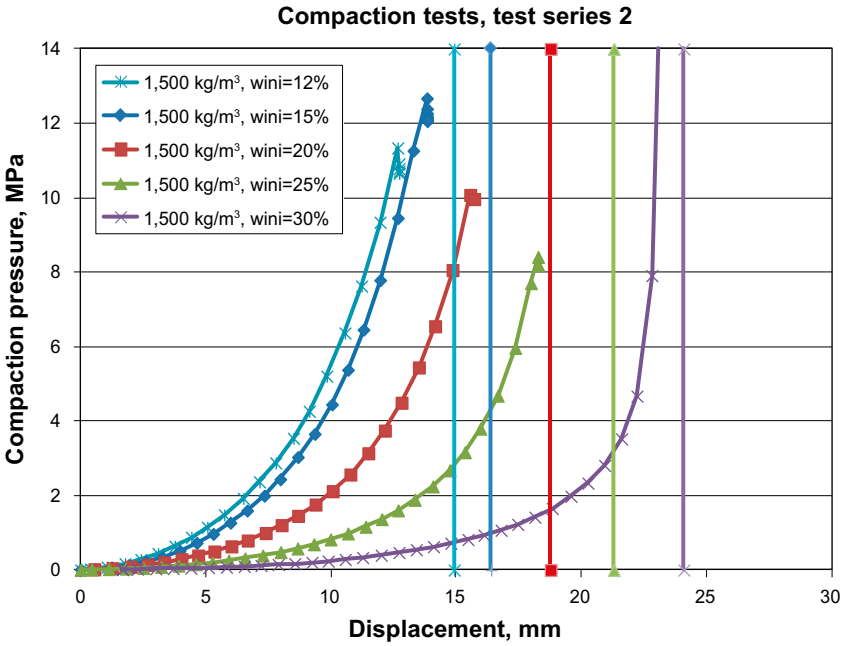

Figure 2-2. *Compaction pressure plotted versus displacement for samples with a target final dry density of 1,500 kg/m³. The vertical lines shows the displacement needed to reach full saturation for a certain initial water content.*

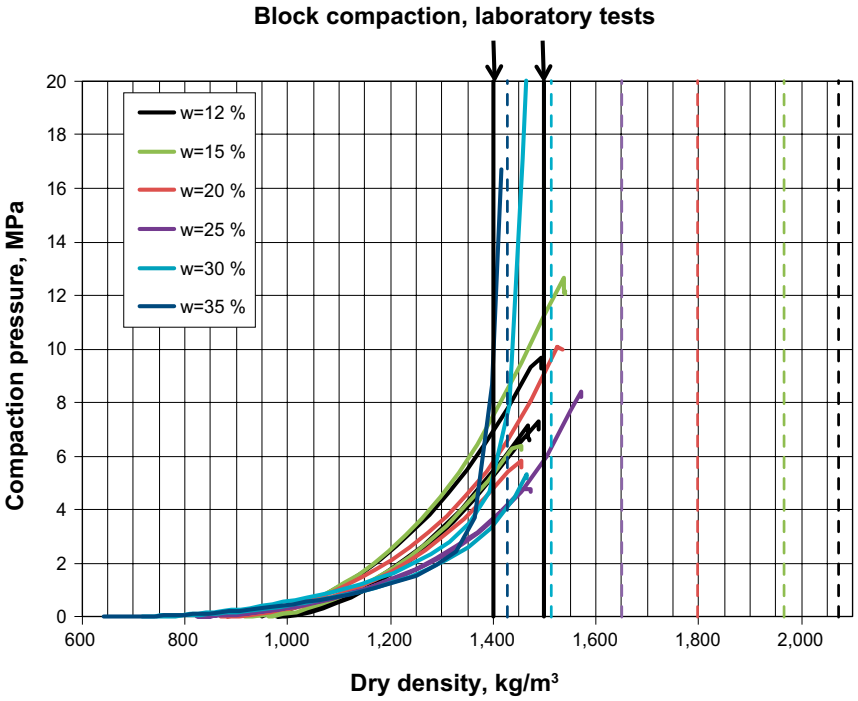

Figure 2-3. *Compaction pressure plotted versus dry density for samples with different initial water content. The vertical lines shows the dry density where the sample reaches full saturation.*

2.2.4 Comments and conclusions

At the time of performing the compaction tests it was of interest to produce blocks with low density, 1,400–1,500 kg/m^3, and with high degree of water saturation. In the course of the study, for a number of reasons, see Section 2.1, this density and saturation design component was changed.

From the performed tests the following conclusions and comments can be made:

1. It is possible to produce blocks of low density and high water content. However, the strength of these kinds of blocks has not been tested since the subsequent design activities focused on blocks with higher density.
2. The compaction pressures needed to reach a density of 1,400 to 1,500 kg/m^3, are low, between 4 and 12 MPa, depending on the water content.
3. At water contents of 30 to 35%, the compaction pressure increases very fast as the bentonite gets close to saturation. This could be an issue if large block compaction is desired. Another issue that can be expected is the handling of material with high water content, since it will not flow readily from mixers or storage locations e.g. silos.
4. The higher water content of the bentonite powder is, the lower the attained dry density of the bulk material will be before compaction. This means that in order to produce blocks with high water content to a certain height, the form has to be filled with powder to a larger volume in order to reach the same density as if the compaction is made with drier material.
5. Larger blocks of low density also have the potential to be problematic in terms of uniformity of density since compactive loads, particularly at lower water contents are very low resulting in uneven densification.

2.3 Strength of blocks

2.3.1 General

The sealing blocks are planned to be installed by use of a vacuum lifting tool, placing the blocks one by one, into position. An important parameter for this block handling is that the strength of the compacted blocks has to be high enough to avoid damage or pieces falling off. The tensile strength of these materials has been investigated by performing beam tests on compacted specimens of differing densities and water contents.

2.3.2 Method

The tensile test procedure was as following:

- Small specimens were compacted in laboratory (Ø 50 mm, h 20 mm) with different compaction pressures and with different initial water contents. From these samples beams were sawn out (a·b·c ~10·20·35 mm^3).
- The beams were forced to tensile failure by applying a constant deformation rate of 0.10 mm/min at the middle of the beam (Figure 2-4). The load and the displacement were measured continuously.
- The tensile stress (σ_t) and the strain (ε_t) were evaluated with the following equations (see Figure 2-3).

$$\sigma_t = \frac{6Qc}{4ba^2} \tag{2-1}$$

$$\varepsilon_t = \frac{a\omega 6}{c^2} \tag{2-2}$$

where

Q = vertical force

a = sample height

b = sample width

c = the length between the support points

ω = the vertical displacement at the middle of the beam

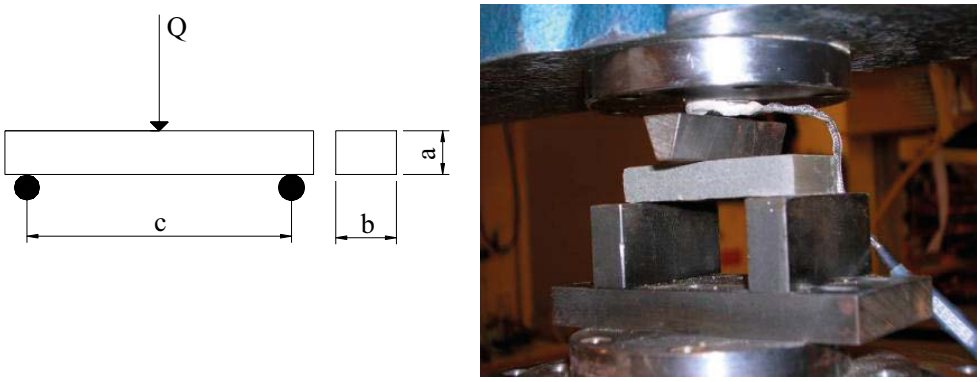

Figure 2-4. *Test arrangement for determination of the tensile strength.*

2.3.3 Test matrix

MX-80 material was mixed with tap water in order to achieve material with five different initial water contents. Four replicate specimens were then compacted for each of the water contents.

2.3.4 Results

The results from the tensile strength measurements are shown in Figure 2-5 and a compilation of data from the measurements is provided in Table 2-2. The influence of the initial water content is obvious when comparing the driest samples, 10% water content, and the wettest, 28% water content. In Figure 2-6, the maximum tensile strength evaluated from the different tests is plotted as a function of the dry density. Even though there is scatter in the results, it is clearly shown in the figure that the strength increases with increasing density but also with increasing water content of the samples.

Blocks with highest dry density for a compaction pressure of 25 MPa were achieved when powder with a water content of 17% was compacted. These blocks also have the highest strength. The strength of blocks compacted with a water content of around 14, 22 or 24%, were high while the samples compacted with 10% water content were very fragile with low strength, mainly due to the low density. The specimen with a water content of 28% had a very low dry density, 1,525 to 1,550 kg/m^3, but the high water content resulted in beams with good strength.

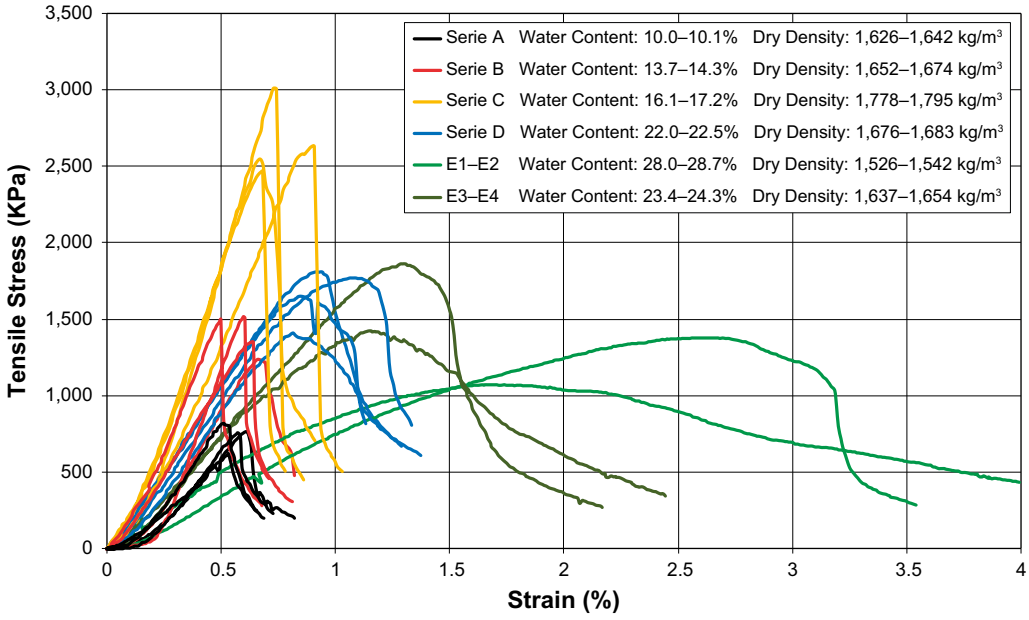

Figure 2-5. *Results from the beam tests performed with MX-80 bentonite. The samples shown in the figure were compacted in laboratory with a pressure of 25 MPa and with different water contents.*

Table 2-2. Compilation of the tensile strength results from the beam tests.

Sample	Water content %	Dry density kg/m ^{3}	Max. tensile strength kPa	Strain at failure %
A1	10.0	1,630	770	0.61
A2	10.1	1,631	758	0.57
A3	10.1	1,642	621	0.53
A4	10.0	1,626	820	0.51
B1	14.3	1,652	1,240	0.67
B2	13.8	1,674	1,519	0.60
B3	13.7	1,674	1,500	0.50
B4	14.2	1,669	1,351	0.64
C1	16.1	1,795	3,008	0.73
C2	16.2	1,795	2,632	0.90
C3	17.2	1,782	2,468	0.68
C4	17.2	1,778	2,544	0.67
D1	22.0	1,683	1,810	0.94
D2	22.5	1,676	1,606	0.92
D3	22.4	1,679	1,771	1.09
D4	22.1	1,680	1,407	0.82
E1	28.7	1,526	1,376	2.69
E2	28.0	1,542	1,070	1.74
E3	23.4	1,654	1,424	1.16
E4	24.3	1,637	1,859	1.31

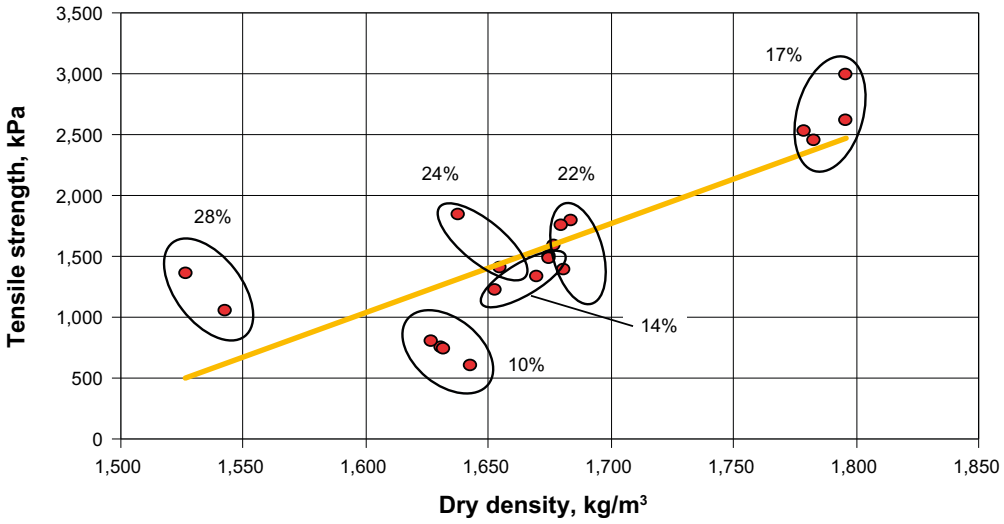

Figure 2-6. *The maximum tensile strength at failure for the beam tests plotted as function of the dry density of the specimens prepared using 25 MPa load.*

2.3.5 Conclusions and comments

The performed beam tests show that in order to produce blocks with the intended density, 1,400–1,500 kg/m^3 and with high strength, too low water content (10%) should be avoided. The highest strength was achieved for the specimens having a water content of 17% and high dry density. With an adjustment of the compaction pressure this water content may be the optimal from a block strength point of view but an alternative is to manufacture the blocks with water content of 28%.

2.4 Oedometer tests (compressibility)

2.4.1 General

Knowing the compressibility properties of the sealing blocks is of considerable importance if modeling of the movements of the backfill behind the deposition tunnel end plug is to be accurate.

2.4.2 Test procedure

The compressibility of the low density blocks that may be used both for sealing just inside the drift end plug as well as in the transition zone needs to be known in order to control the swelling pressure that will be applied to the plug. This information was determined via oedometer tests.

The consolidation equipment used is shown in Figure 2-7. The specimens, pre-compacted as blocks in the laboratory, were placed in the specially constructed test cell, where they were saturated through the two end filters. The water used in the tests had a salinity of 1% by weight (NaCl/$CaCl_2$, 50/50) as this composition simulates the conditions that might be expected in a repository. The specimens were saturated while under a constant vertical stress (2,000 kPa for Test 1 and 3 and 4,000 kPa for Test 2 and 4). After saturation, the vertical load was decreased and/or increased in steps while continuously monitored for displacement and radial pressure. After finishing the test, each specimen was taken out and the water content and density determined. From these data the void ratio, degree of saturation, dry density and saturated density could be calculated.

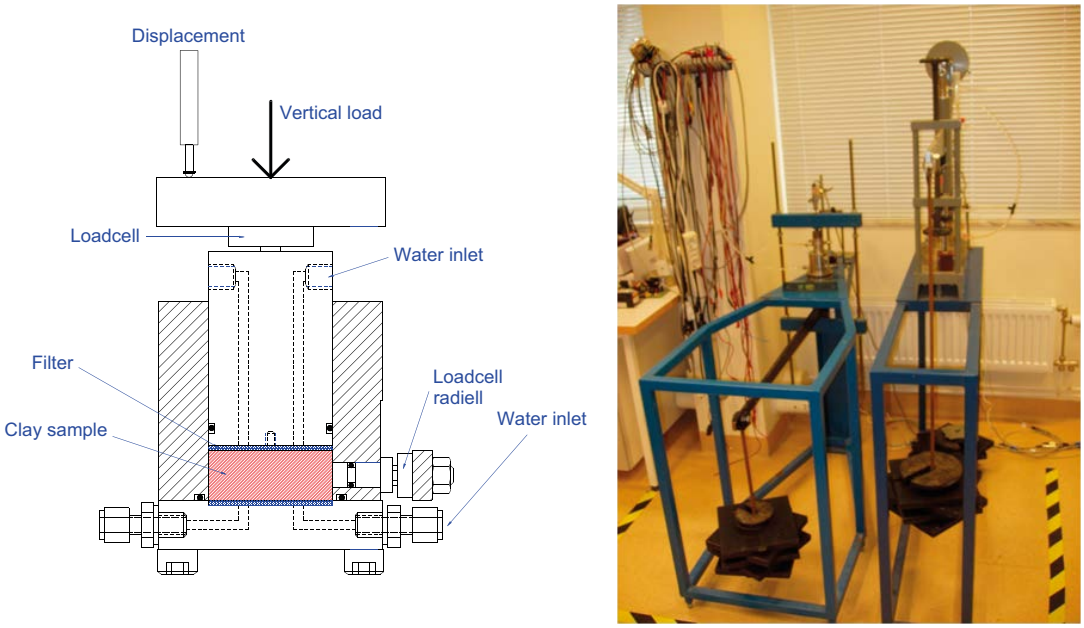

Figure 2-7. *Left: Schematic drawing of the test cell. Right: Photo of the test equipment used for the oedometer tests.*

2.4.3 Test matrix

In total four consolidation tests were performed. The different load steps for each test are described in detail in Table 2-3. The sealing blocks are intended to have a maximum swelling pressure of 2 MPa when fully saturated but will subsequently be affected by conditions around them (e.g. small voids or adjacent, higher density backfill). Therefore from this initial this swelling pressure condition, the blocks can either swell or be compressed depending on the situation. As a result, the chosen load-steps in the oedometer tests began with pressures starting at 2 MPa rather than allowing for excessive swelling that would have occurred if lower initial loads were applied.

2.4.4 Results

Table 2-3 shows a compilation of data from the four tests performed. The table shows the applied axial stress, the measured radial stress and the determined density and void ratio after the last load step which then has been used to calculate the density and void ratio at the previous load steps. Figure 2-8 to Figure 2-11 shows the void ratio as function of time for the four tests and also the void ratio as function of pressure.

The use of the achieved data is further described in the hydro mechanical modelling of the plug components.

Table 2-3 Compilation of test results for the oedometer tests.

Test no.	Axial stress kPa	Radial stress kPa	Saturated density kg/m^3	Dry density kg/m^3	Void ratio	Water content %	Degree of saturation %
Oedometer test 1							
Saturation	2,022	1,781	1,881	1,376	1.021		
Load step 1	1,003	1,283	1,848	1,324	1.099		
Load step 2	497	793	1,810	1,265	1.198		
Load step 3	2,013	1,445	1,855	1,335	1.083		
Load step 4	4,059	2,681	1,900	1,405	0.979	35.4	100.5
Oedometer test 2							
Saturation	4,072	3,651	1,934	1,459	0.906		
Load step 1	2,096	2,508	1,894	1,397	0.990		
Load step 2	1,083	1,611	1,851	1,329	1.091		
Load step 3	3,948	2,849	1,902	1,409	0.973		
Load step 4	8,054	5,552	1,967	1,511	0.840	30.2	100.1
Oedometer test 3							
Saturation	1,988	1,768	1,878	1,371	1.028		
Load step 1	973	1,149	1,844	1,318	1.109		
Load step 2	1,941	1,386	1,866	1,352	1.056	38.1	100.4
Oedometer test 4							
Saturation	4,127	2,444	1,936	1,462	0.902		
Load step 1	2,125	1,846	1,896	1,399	0.987		
Load step 2	4,031	2,217	1,916	1,431	0.943	34.05	100.4

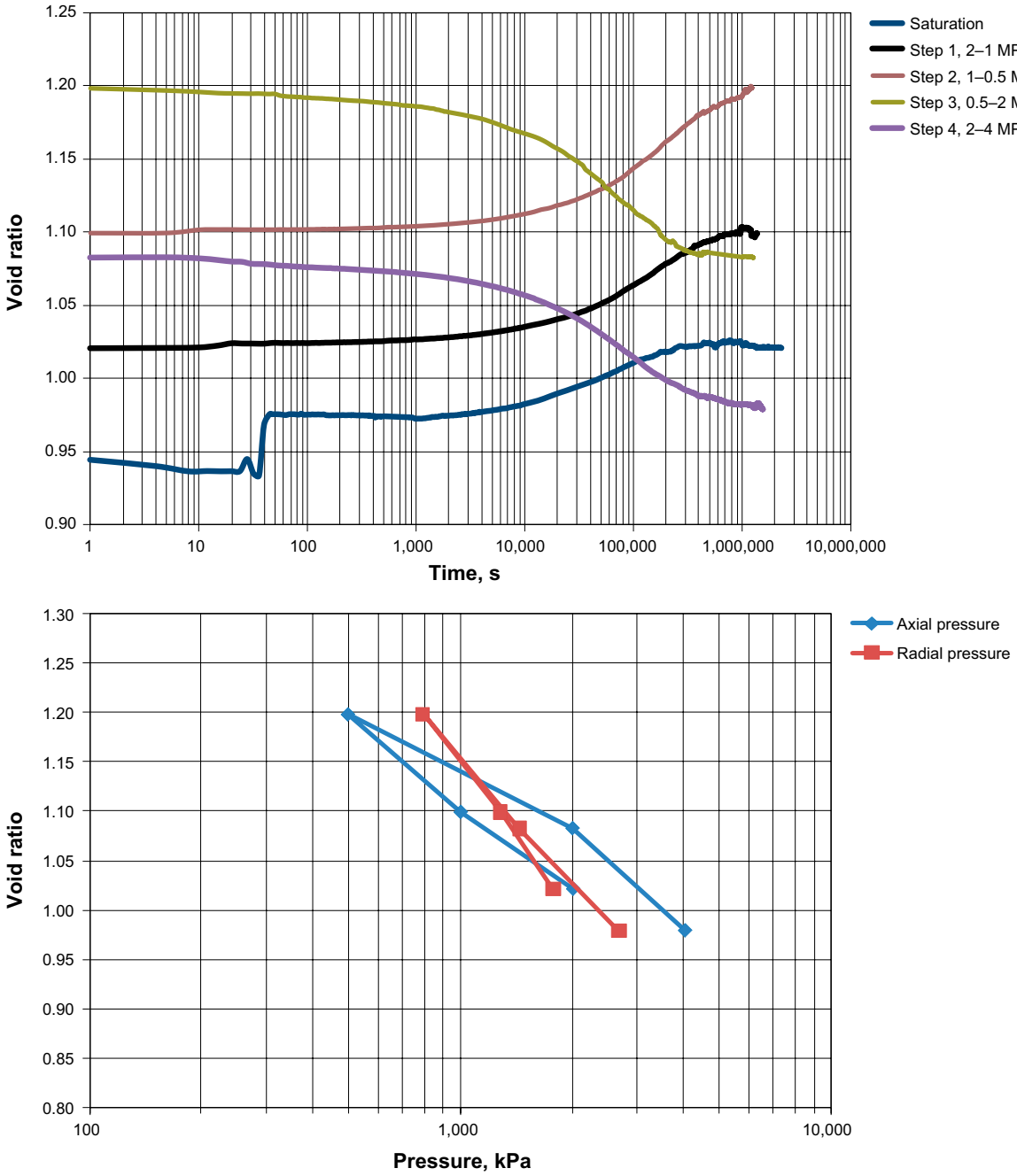

Figure 2-8. *Figure showing the test results from oedometer Test 1. Upper: Void ratio as function of time for the four load steps. Lower: Void ratio as function of the vertical stress.*

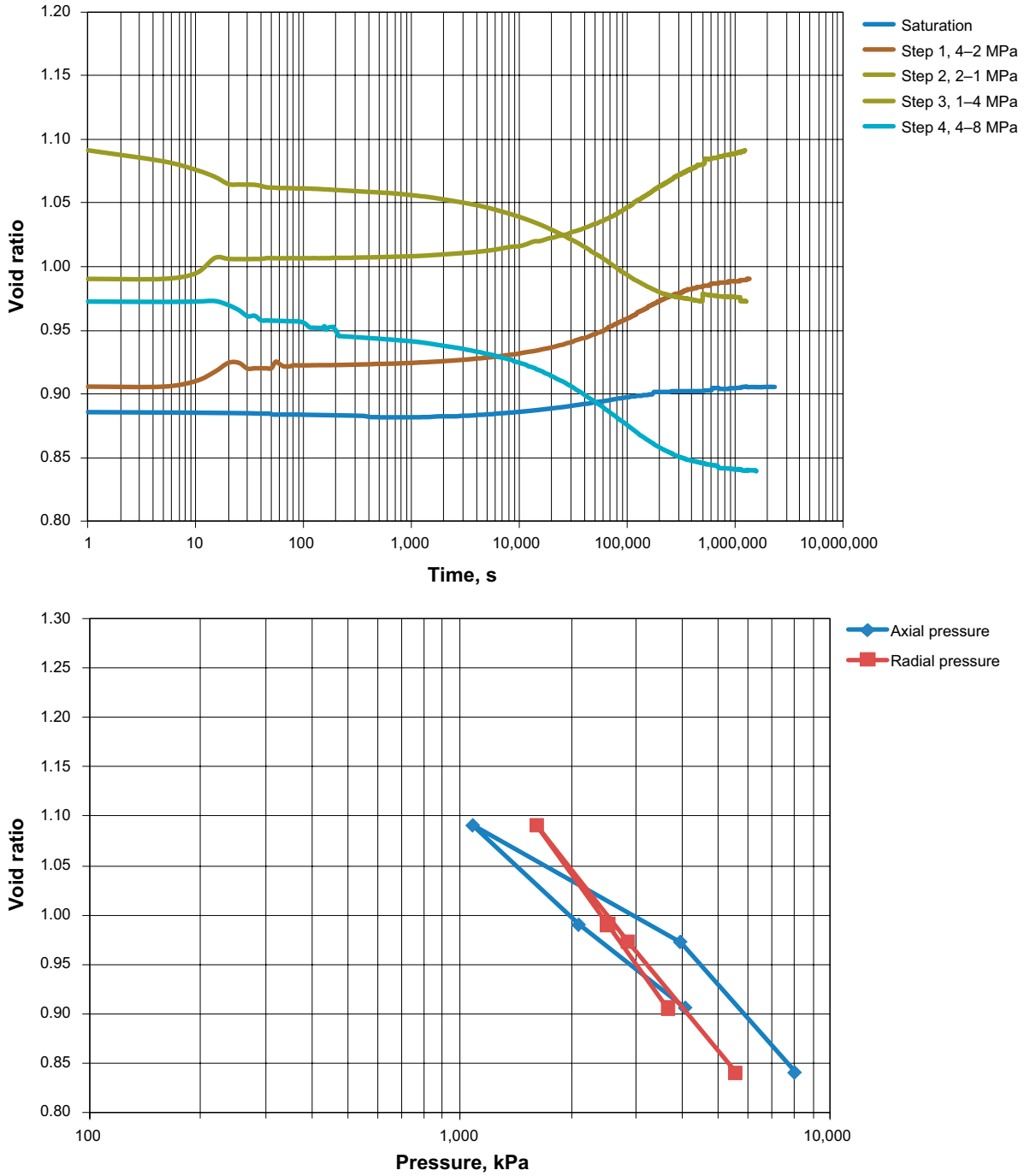

Figure 2-9. *Figure showing the test results from oedometer Test 2. Upper: Void ratio as function of time for the four load steps. Lower: Void ratio as function of the vertical stress.*

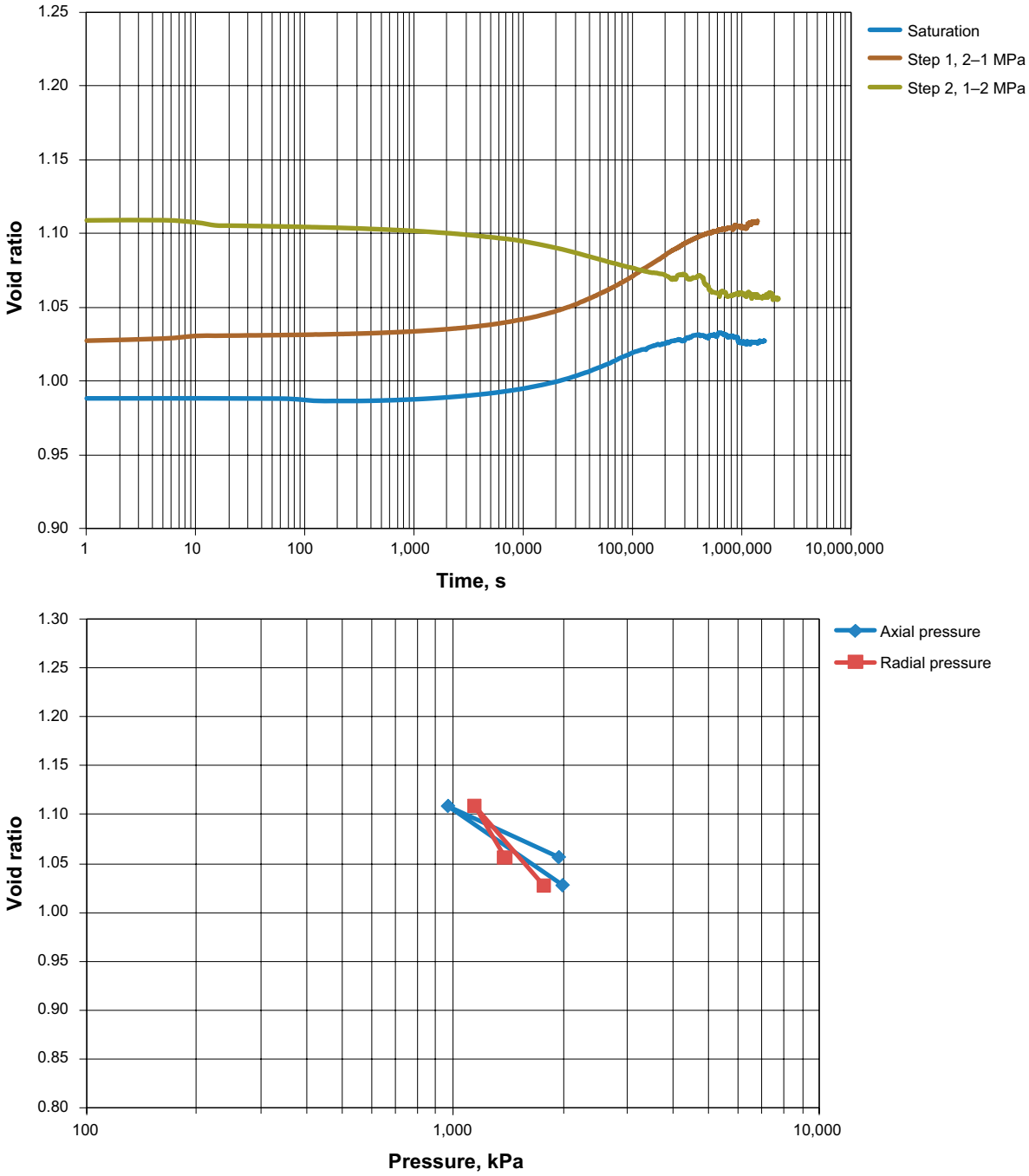

Figure 2-10. *Figure showing the test results from oedometer Test 3. Upper: Void ratio as function of time for the two load steps. Lower: Void ratio as function of the vertical stress.*

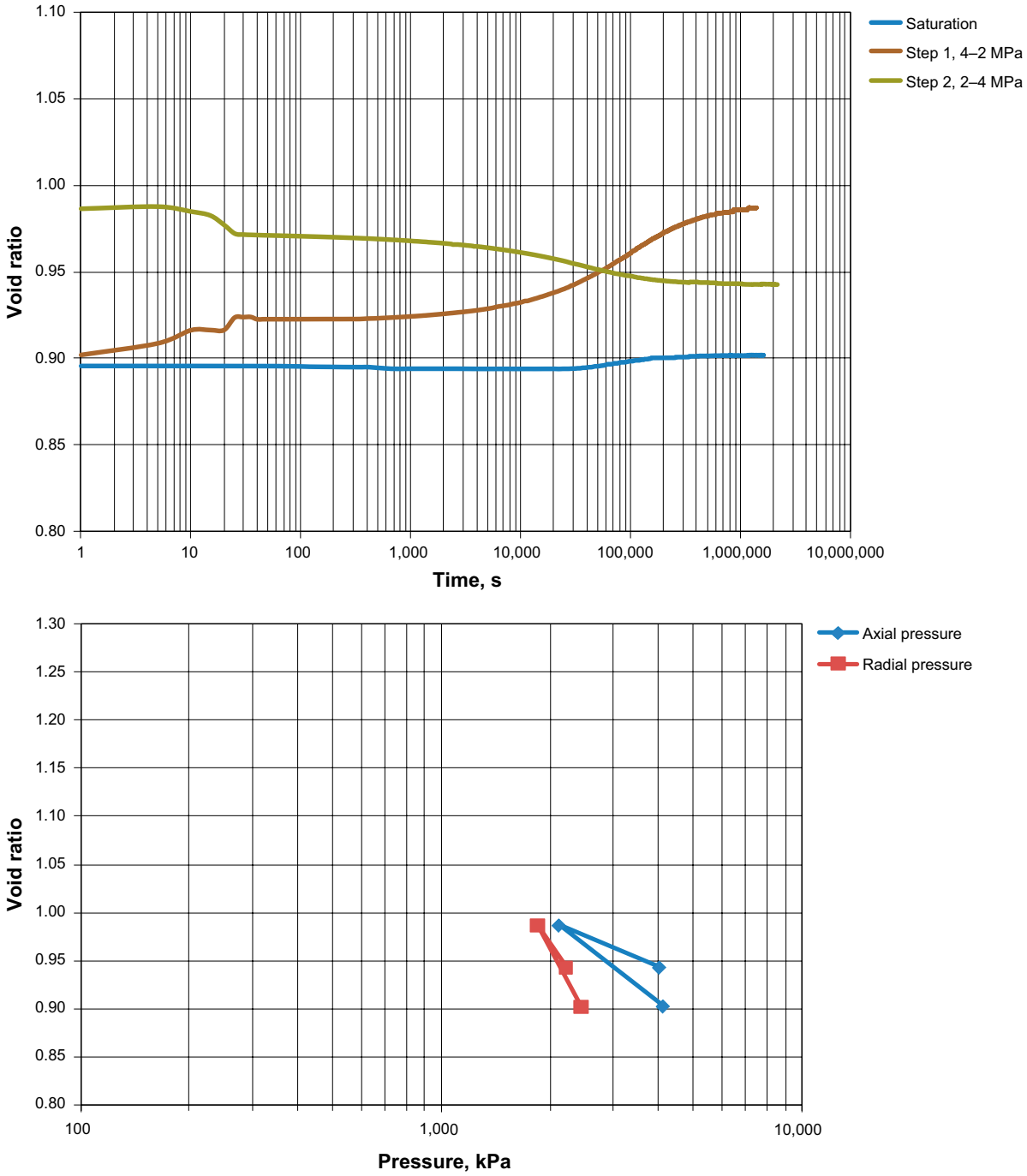

Figure 2-11. *Figure showing the test results from oedometer Test 4. Upper: Void ratio as function of time for the two load steps. Lower: Void ratio as function of the vertical stress.*

2.5 Swelling pressure and hydraulic conductivity

2.5.1 Test procedure

Swelling pressure oedometers made of acid resistant steel were used in the tests, see Figure 2-12. In this test the specimen is surrounded by a rigid steel cylinder with an inner diameter of 50 mm and filters of acid resistant steel are placed at the top and bottom. The height of the specimen is 20 mm. The axial load was measured continuously by the load cell placed between the locked-in-place piston and the upper lid.

The tests were made according to the following procedure:

- The specimen was compacted in compaction device to a specified dry density at a decided initial water content of the material (20–35%), see Table 2-4. The final dry densities of the specimens varied between 1,330 and 1,447 kg/m^3, representing an estimated average dry density of a homogenized bentonite in the sealing zone inside the plug.
- The specimen was placed in the oedometer and a piston was placed on top of it. After evacuating air in filters and tubes by use of a vacuum pump, the specimen was allowed access to water from both the top and bottom filters. Two water types were used in the course of these tests, tap water and water with 1% salinity.
- After saturation, a pore pressure gradient was applied over the specimens and the volume of outflowing water measured. This volume was used for calculating the hydraulic conductivity of the specimens. The hydraulic gradient used for all tests was 2,500 (corresponding to a pore pressure difference over the specimen of Δu = 500 kPa). No backpressure was used. The tests were performed using either tap water or water with a salinity of 1% by weight ($NaCl/CaCl_2$, 50/50).
- After finishing the test, the specimen was pushed out of the oedometer and the water content and density determined. The water content was determined by drying the sample for 24 h at 105°C and the density was determined by weighing the sample, first in air and then submerged into paraffin oil.

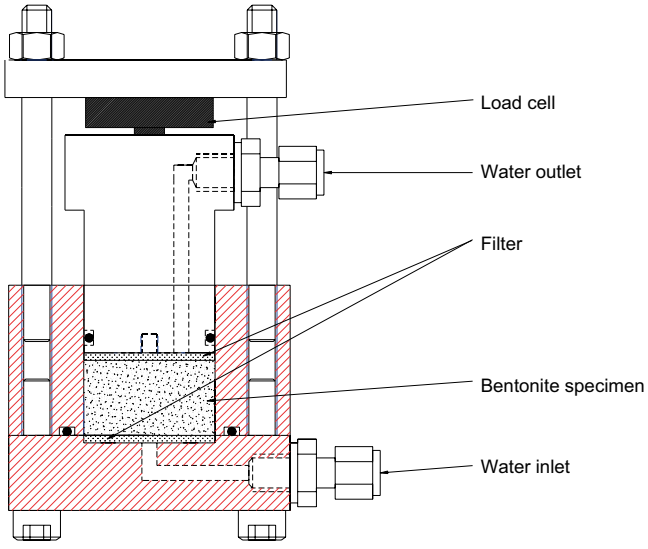

Figure 2-12. *Schematic showing the test equipment used for determining swelling pressure and hydraulic conductivity.*

2.5.2 Results

A compilation of the performed tests is provided in Table 2-4. In Figure 2-13 the results from the measurements of swelling pressure and hydraulic conductivity are presented as function of the dry density. In this figure the results from measurements made on the same material as part of the ABM project (see Svensson et al. 2011) are also provided (this additional data is also used as a reference for the design of field tests). Figure 2-13 shows that there is no significant influence of the initial water content of the bentonite specimen on its swelling pressure and hydraulic conductivity (k). The swelling pressures obtained by the current study is essentially identical to the reference values and the hydraulic conductivities measured are just slightly lower, which is interpreted as being due to the fact that the higher initial water content gives somewhat more homogenized specimens and hence a slightly lower k-value. Based on previous studies and a substantial database, the influence of a 1% salt concentration in the pore-water is as expected to be very small at these densities (Karnland et al. 2006).

Table 2-4. Compilation of the performed tests and the results of the measurements.

Test no.	Water content initial %	Water type	Dry density kg/m^3	Void ratio	Swelling pressure kPa	Hydraulic conductivity m/s
1	20	Tapwater	1,347	1.063	1,572	2.67E-13
2	20	Tapwater	1,349	1.060	1,518	2.45E-13
3	30	Tapwater	1,430	0.945	2,700	1.44E-13
4	35	Tapwater	1,441	0.929	2,900	1.52E-13
5	20	1%	1,404	0.981	3,010	1.60E-13
6	20	1%	1,337	1.080	1,515	2.20E-13
7	20	1%	1,330	1.090	1,466	2.37E-13
8	20	1%	1,447	0.922	3,405	1.20E-13
9	30	1%	1,412	0.969	2,408	1.45E-13
10	35	1%	1,328	1.093	1,410	1.80E-13

2.6 Self sealing of fractures

2.6.1 General

Previously completed tests have shown that eroding bentonite from a pellet filling can seal fractures in the rock up to apertures of 0.15 mm (Sandén et al. 2008). If the materials used in the sealing blocks have the same potential to supply material to clog adjacent fractures or gaps, it would be of great significance regarding the demands on the initial tightness of the plug.

2.6.2 Method

The test equipment used was the same as was used in other projects for sealing tests involving bentonite pellets, see Figure 2-14. In these new tests the pellet filling was replaced with compacted bentonite blocks with a diameter of 96 mm and height of 50 mm. The blocks were piled on each other in the cylindrical volume with a diameter of 100 mm leaving a 2 mm wide slot between the bentonite and the surrounding steel wall. The aperture of the artificial slot can be adjusted at the top by use of shims of various thicknesses. By monitoring the hydraulic pressure increases required to inject water at a constant rate of 0.01 l/min a measure of the degree of gap closure could be determined.

After emplacement of the bentonite blocks and setting of the artificial slot aperture at the top, a constant water flow was applied from the bottom. Inside the water inflow point at the bottom of the test equipment, see Figure 2-14, a thin PVC washer with tracks leading out the inflowing water to the outer slot is positioned. The blocks are standing on the PVC washer. During test time the water pressure build up was registered.

At the end of testing and specimen extrusion, the sample was cut horizontally and the radial water content distribution was determined in order to assess the uniformity of water uptake and density.

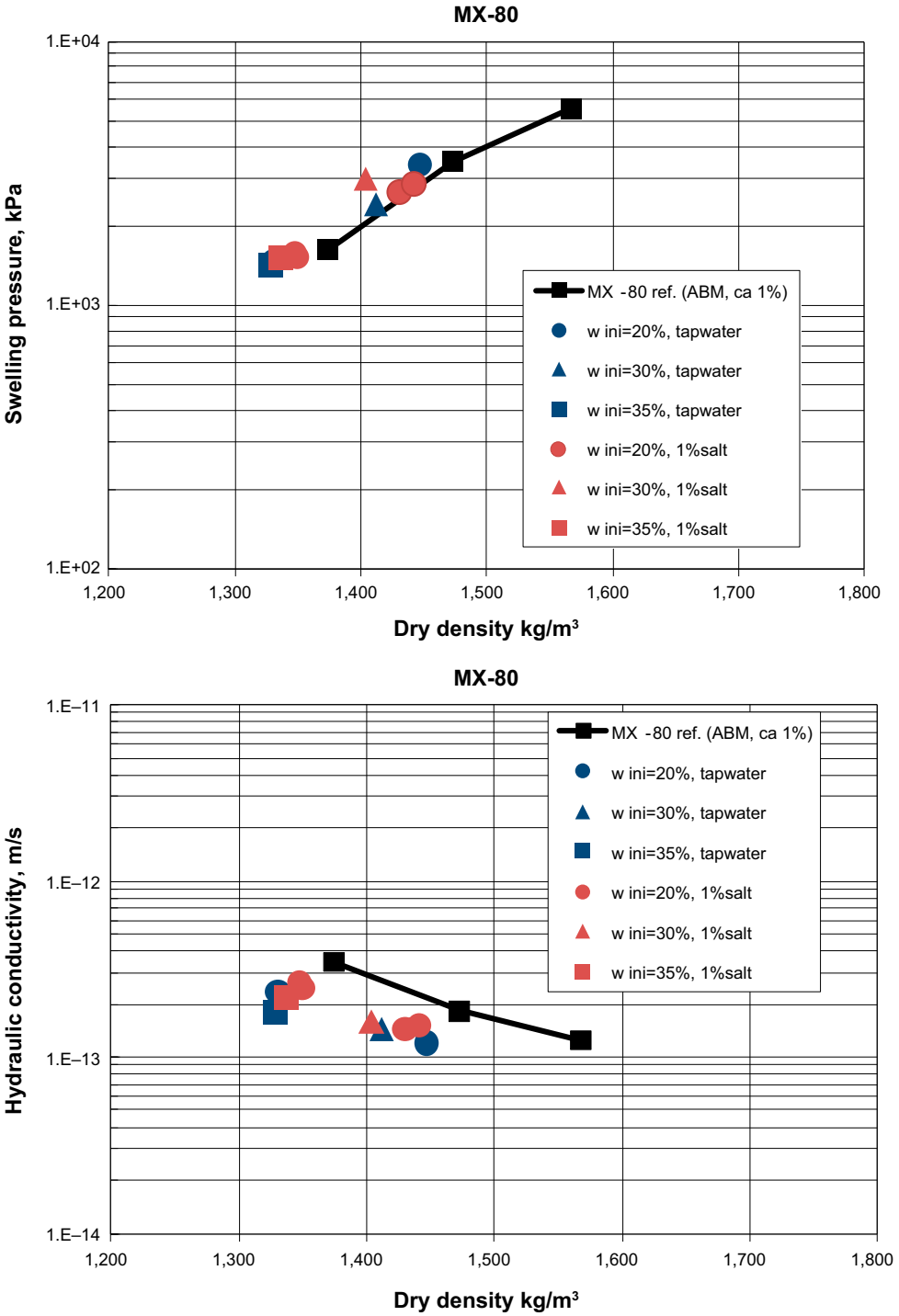

Figure 2-13. *Figures showing the test results. For comparison some results from measurements within the ABM test are also shown in the figures. Upper: Swelling pressure as function of dry density. Lower: Hydraulic conductivity as function of the dry density.*

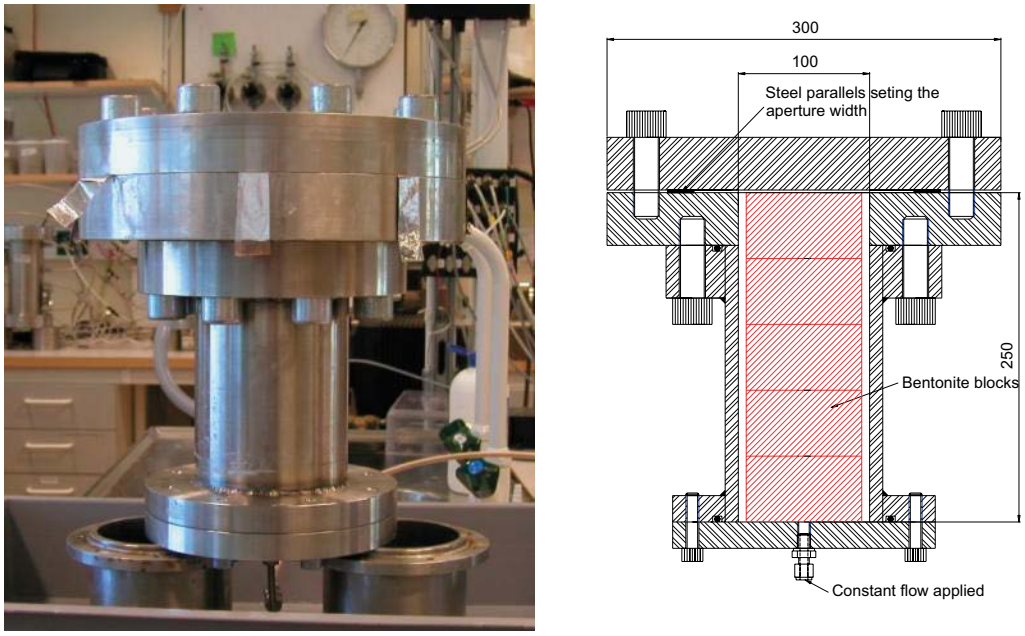

Figure 2-14. *Left: Photo of the test equipment. Right: Schematic showing the test equipment.*

2.6.3 Test matrix

In total three tests have been performed:

1. Target dry density of the blocks = 1,400 kg/m^3 (determined to between 1,378 to 1,404 kg/m^3), initial water content = 35%
2. Target dry density of the blocks = 1,500 kg/m^3 (determined to between 1,450 to 1,471 kg/m^3), initial water content = 30%
3. Target dry density of the blocks = 1,500 kg/m^3, initial water content = 13.9%

All three tests were performed with a water inflow rate of 0.01 l/min and a simulated fracture width of 0.01 mm. The water used in the tests had a salinity of 1% by weight (NaCl/$CaCl_2$, 50/50).

2.6.4 Results

A compilation of the registered water pressure build up during test time is provided in Figure 2-15.

Tests 1 and 2

The two first tests were performed with blocks with high as-built water contents, 35 and 30% respectively but with different target dry densities, 1,400 and 1,500 kg/m^3 respectively. These specimens did not seal during the testing time allowed. After 40 to 45 hours of testing, some pressure peaks could be seen but no permanent sealing occurred. After dismantling, it was observed that a very evident flow channel had been formed on the outer surface of the specimen in Test 1 (Figure 2-17). The radial water content and dry density distribution of the specimens was also determined in one cross-section at specimen mid-height for the two tests (Figure 2-16). The behaviour observed clearly showed that the bentonite swelled in radial direction and filled up the former slot. During dismantling of these two tests, it was observed that no bentonite seemed to have eroded into the artificial fracture. The registered pressure peaks are probably the result of the bentonite sealing locally in the slot and not on eroding bentonite sealing the fracture.

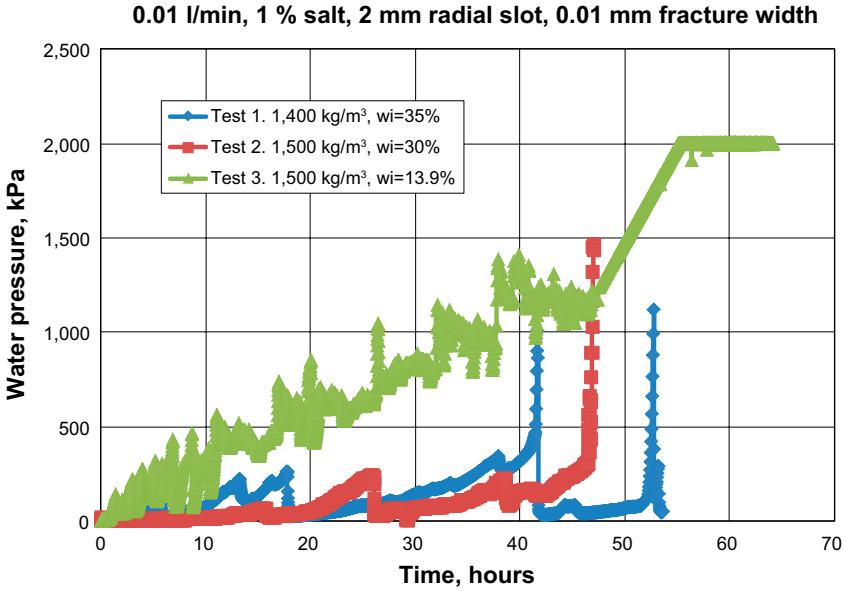

Figure 2-15. Figure showing the water pressure build up plotted versus time for the three tests performed.

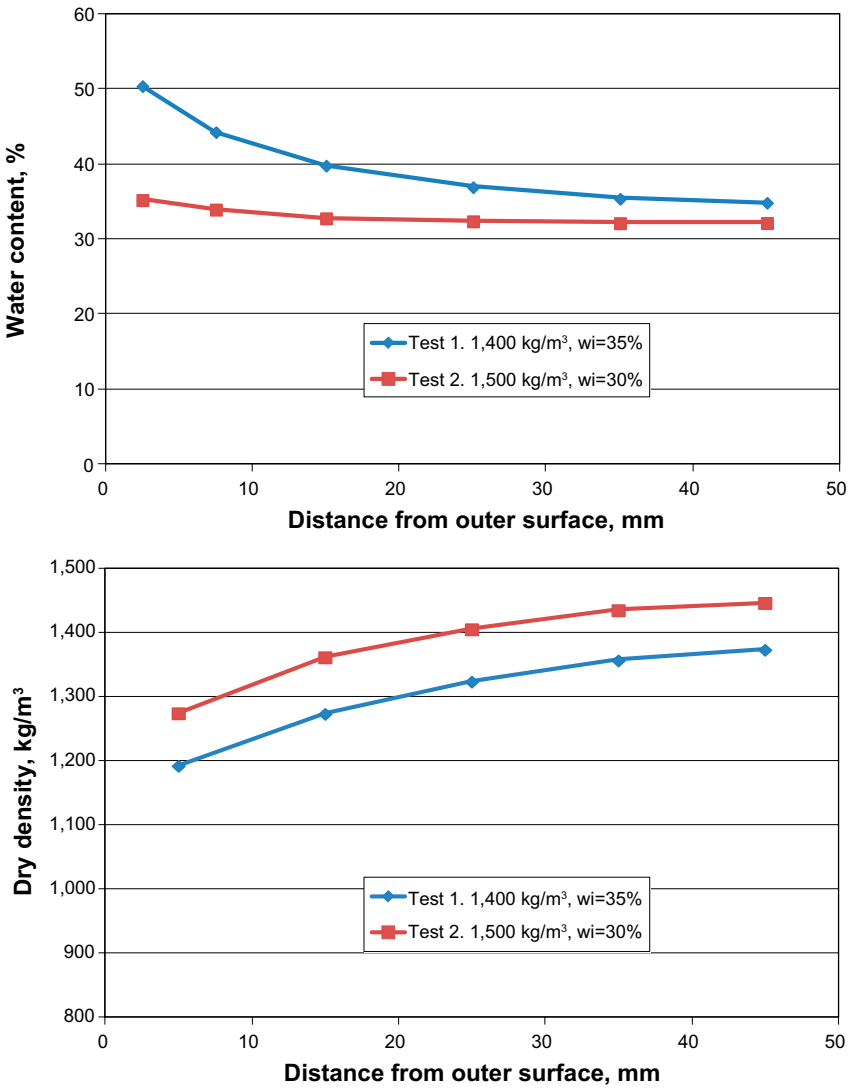

Figure 2-16. Upper: Radial water content distribution determined in a cross-section mid-height of the specimens from Test 1 and 2. Lower: Radial dry density distribution determined in a cross-section mid-height of the specimens from Test 1 and 2.

Figure 2-17. *Photo of the bentonite specimen from Test 1. A very evident flow channel can be seen on the surface.*

Test 3

Test 3 was performed with bentonite blocks having a target dry density of 1,500 kg/m^3 and with a water content of 13.9%. Very soon after test start, there was a water pressure build up registered (Figure 2-15). After about 45 hours test duration, the pump providing the constant inflow rate of 0.01 l/min was changed to a GDS (microprocessor controlled pump). This pump was set to give a water pressure increase rate of 100 kPa/h, up to a maximum of 2 MPa, instead of a constant flow. This change of pumps was made since it was assessed that the constant inflow rate of 0.1 l/min would give very high water pressure increase rates in case of that sealing should occur. After ten hours additional test time with the new pump, the maximum water pressure of 2 MPa was reached.

The examination of the specimen at test termination showed that there were small amounts of bentonite gel in the artificial fracture (Figure 2-18). It is, however, uncertain if the sealing observed took place in the plane of the fracture or represents clogging within the cylindrical container where the blocks are placed. The bentonite blocks exhibited very unsymmetrical water distribution (Figure 2-19). Figure 2-19 also shows the location of the samples taken at the mid-height of the specimen and tested for water content and density (shown in Figure 2-20 and Figure 2-21). The asymmetry is probably caused by lateral displacement of the specimen during testing as the result of the water pressure acting along the location of the channel.

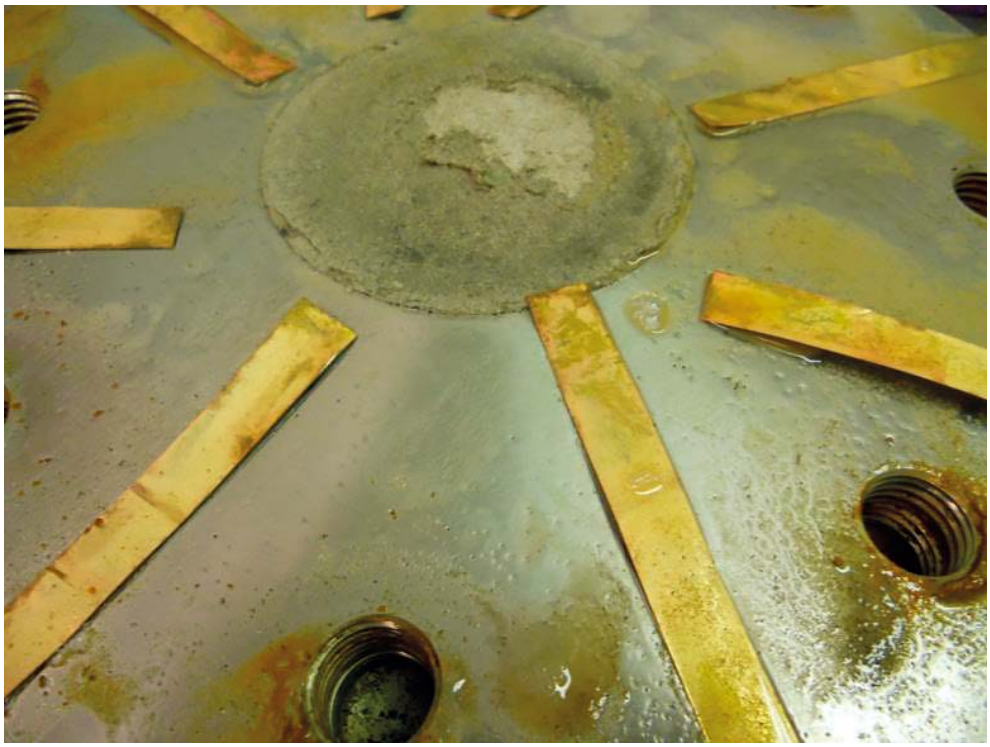

Figure 2-18. *Photo taken during dismantling of Test 3, showing the artificial fracture after removal of the upper lid. The bentonite has swelled and filled the radial slot and some bentonite can also be seen in the "fracture".*

Figure 2-19. *Photo showing a cross-section of the bentonite specimen in Test 3. The bentonite has swelled unsymmetrical, only taking up water at one side.*

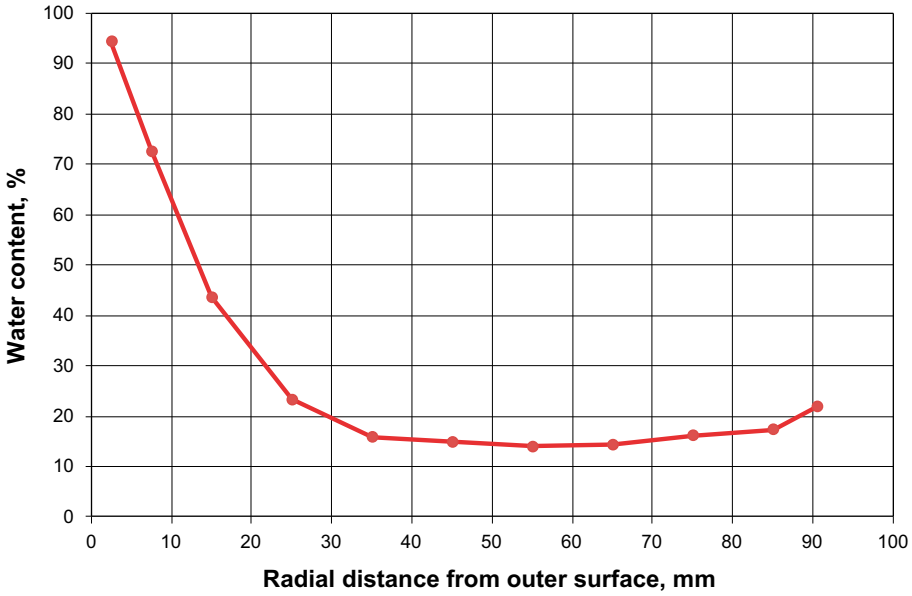

Figure 2-20. *Figure showing the water content distribution across the mid-height of Test 3.*

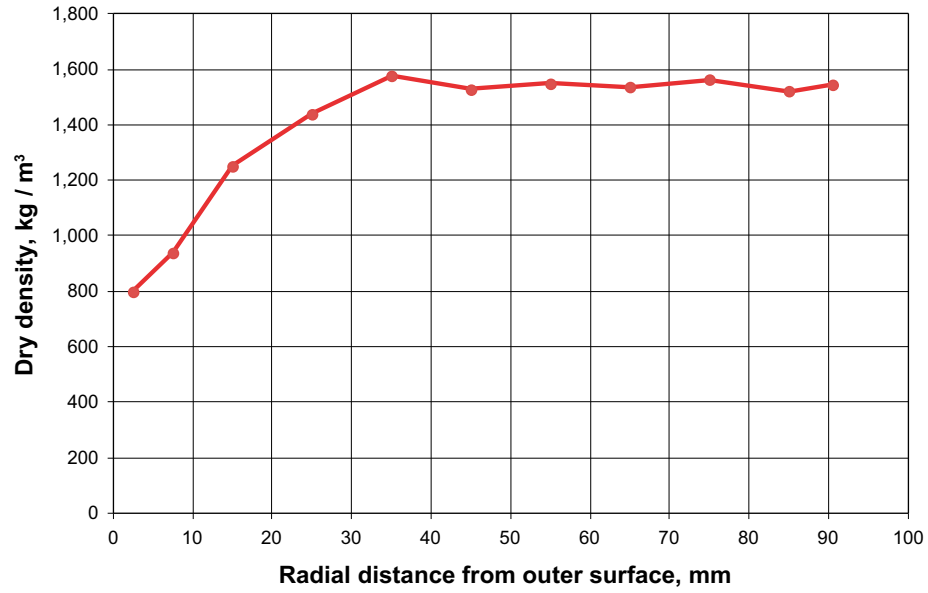

Figure 2-21. *Figure showing the radial density distribution across the mid-height of Test 3.*

2.7 Sealing of initial slots

2.7.1 General

In order to increase the understanding regarding the time for a bentonite seal to swell and seal slots, a number of specially designed tests have been performed.

2.7.2 Test description

Two different types of test equipment were used in this test series:

The first test equipment was the same testing cell as used for the measurement of swelling pressure and hydraulic conductivity but included an additional sensor for measurement of the radial pressure near the mid-height of the specimen (Figure 2-22). The sample holder is manufactured of stainless steel.

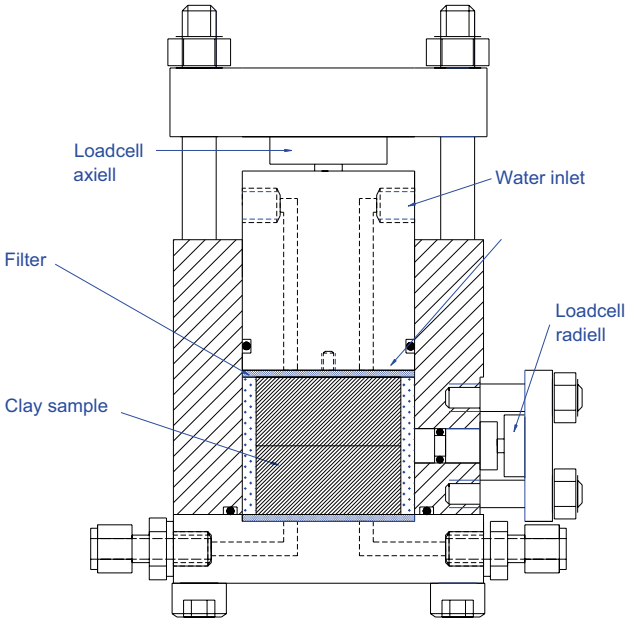

Figure 2-22. *Schematic drawing of the test equipment.*

The inner diameter is 50 mm and the sample height was set to 40 mm. Filters of stainless steel were placed on the top and bottom of the bentonite specimen to allow water access without loss of bentonite. The bentonite specimens were manufactured to different diameters in order to vary the slot width between bentonite and steel. The axial and radial pressure present in the cell is transferred by the load-transferring pistons to load-cells which were continuously monitoring the load applied at that interface.

The second test apparatus was of similar design to the first but the inner diameter was substantially larger (101 mm) and the sample height in the tests was set to 50 mm.

The tests have been performed in two ways:

1. After assembling of a test, a low water inflow rate was applied from the bottom. The water filled up the slot, the upper steel filter and entered the top of the piston. The bentonite sample had access to additional water, from a burette for a period of one week and then the test was terminated. This burette represented a very low head seepage condition allowing water uptake without any substantial gradient being applied. During the test, the swelling pressure development, axial and radial, was recorded registered. After termination the bentonite was divided and the radial water content and density distribution determined.
2. In two of the tests (Test 11 and Test 12), the effectiveness of the bentonite sealing of the former slot location was tested. A stepwise water pressure increase was applied at the bottom filter, after one week of homogenisation time had been completed. As this occurred the radial and axial total pressures were monitored, as was the applied hydraulic pressure.

2.7.3 Results

A compilation of test data and results from the pressure measurements is provided in Table 2-5 and shown in Figure 2-23 to Figure 2-25.

Test 1 and 2 were pilot tests and the radial load cells were incorrectly installed with a 250 kPa pre-stress applied at their contact with the specimen, hence the results from these tests are not included in the Figures. The same type of sensor mounting problem also occurred with the radial pressure measurements in Test 9. The result of this was that it was not possible to measure the radial swelling pressure build up.

Table 2-5. Compilation of data for the sealing tests.

Test parameters					After 7 days test		Test duration	Remark
Test no.	Dry density kg/m^3	Water content %	Radial slot mm	Equipment	Radial pressure kPa	Axial pressure kPa	h	
1	1,500	20	4	50 mm oedometer	–	522	168	Radial sensor was incorrectly installed
2	1,500	30	4	50 mm oedometer	–	975	168	Radial sensor was incorrectly installed
3	1,500	20	4	50 mm oedometer	80	152	168	
4	1,500	30	4	50 mm oedometer	43	158	168	
5	1,400	20	4	50 mm oedometer	36	92	168	
6	1,600	20	4	50 mm oedometer	120	311	168	
7	1,500	20	2	50 mm oedometer	767	1,208	168	
8	1,500	13	4	50 mm oedometer	111	188	168	
9	1,500	20	4	101 mm oedometer	–	480	168	Radial sensor was incorrectly installed
10	1,500	30	2	101 mm oedometer	521	834	168	
11	1,500	20	4	101 mm oedometer	13	475	2,232	Water pressure test of sealing
12	1,500	30	4	101 mm oedometer	0	470	1,275	Water pressure test of sealing
13	1,500	20	4	101 mm oedometer	71	473	455	Long term test

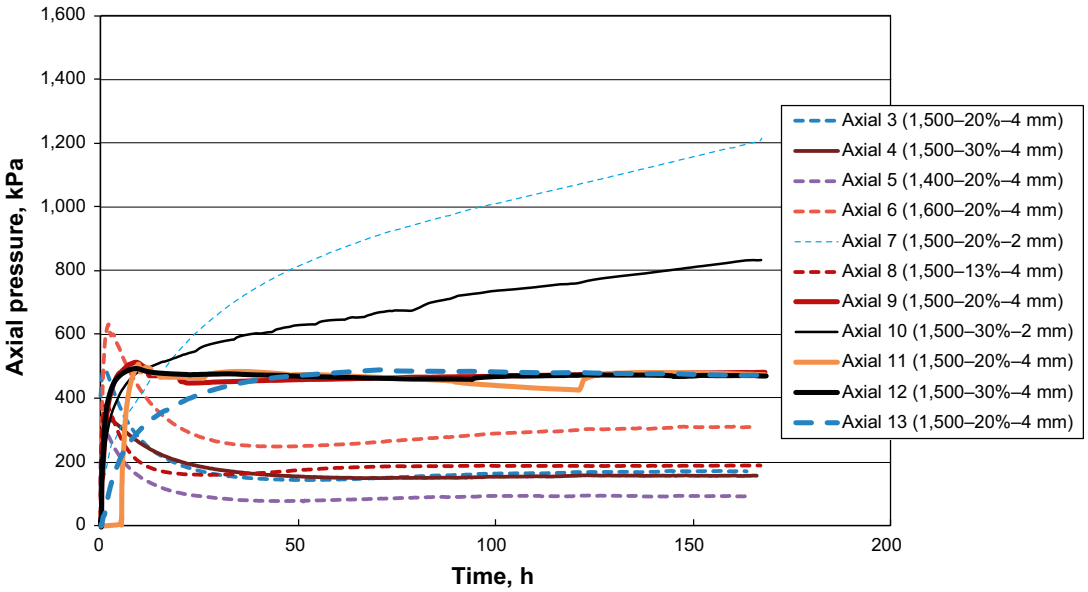

Figure 2-23. *Axial pressure plotted versus time for test 3 to 13.*

The axial pressures registered in all tests are provided in Figure 2-23.

The two tests performed with 2 mm slot width (Tests 7 and 10), have the highest contact pressures. The lowest pressure was registered for Test 5, which was performed with the lowest inital block density. Figure 2-24 shows the radial pressure development for all tests performed with blocks with a starting dry density of 1,500 kg/m^3 but with different initial water content and with different slot widths. The slot width has, as expected, a large influence on the radial pressure development. In Tests 7 and 10 the slot width was only 2 mm and these both tests have the fastest pressure build up.

The initial water content also seems to influence the result, at least in this short term. Comparing the two tests with 2 mm slot (Tests 7 and 10), it can be seen that the sample with the lowest initial water content, 20% (7) compared to 30% for the other test (10), has a higher swelling pressure after one week.

When comparing tests having the same starting density and same slot width, it is obvious that the samples with lowest initial water content swell faster.

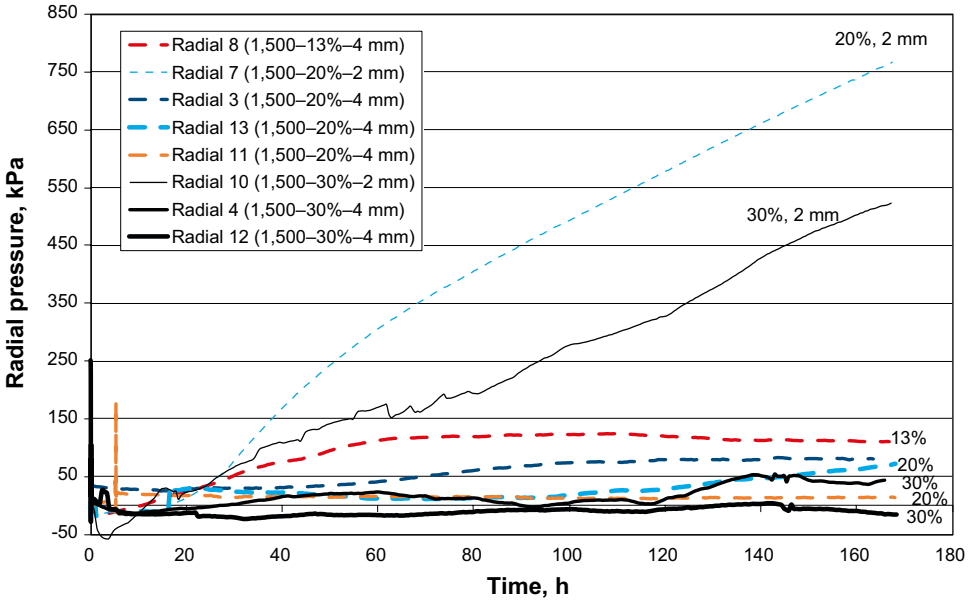

Figure 2-24. *Radial pressure plotted versus time for all tests performed with blocks with a dry density of 1,500 kg/m^3 but with various initial water contents and slot widths.*

The results from the measurements of the radial pressure in Test 11 were, however, not entirely as anticipated or consistent with the other tests results obtained in this study. There was a pressure peak in the beginning of the test and after that the pressure level was almost constant at a very low value. The cause of this is uncertain and could not be identified in the course of dismantling the test. One explanation could be a development of a flow channel at the location of the radial sensor but this is not anything that could be seen during test dismantling.

Figure 2-25 shows samples with the same initial water content but with different initial dry densities and slot widths. This figure also shows that the slot width has strong influence on the pressure development. The as-built dry density of the bentonite block has, as expected, a strong influence on the pressure. The specimen with a dry density of 1,600 kg/m^3 has after one week a pressure of almost 150 kPa while the sample with 1,400 kg/m^3 initial density has less than 50 kPa. As noted previously, the results from Test 11 deviate from the other tests.

Two tests, 11 and 12, had a different test procedure used. In these tests, a constant water pressure was applied at the bottom filter after the first week of low-head water supply to the base.(the results from the first week are provided in Figure 2-23 to Figure 2-25). The evolution of total and water pressure for the entire testing period is shown in Figure 2-26.

The results from Test 11 are rather interesting as only after applying a water pressure of 900 kPa does the radial swelling seemed to start and yield a swelling pressure. The results indicate that the sample likely did not have full access to water in the initial phase, which also could be seen in Figure 2-24 and Figure 2-25. After almost three months of exposure to constant hydraulic conditions, during which specimen homogenization was occurring, the water pressure was again stepwise increased, reaching 3.7 MPa after one week. During this pressurizing period, there was no water leakage observed through the bentonite filled volume.

The behaviour of the bentonite specimen in Test 12 was similar to that observed for Test 11, in that only after having been exposed to a water pressure of 1 MPa did the radial swelling start to register. After about one month of saturation and specimen homogenization, the water pressure was again increased in steps up to 5 MPa. There were also no water leakages through the specimen during the period of increasing hydraulic pressure.

Figure 2-27 shows the results from the pressure measurements performed in Test 13. This test was done by continued at the same initial water uptake conditions after the first week (168 h) as was used for the first week (i.e. water pressure at base was kept constant). The figure shows that the time needed in order to develop a radial pressure of 200 kPa is at least two weeks.

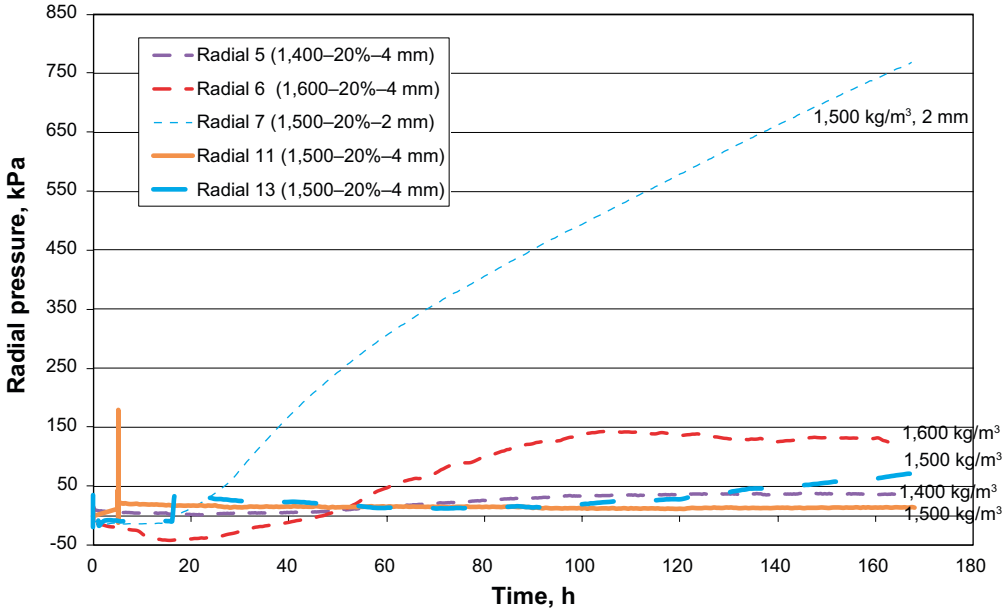

Figure 2-25. *Radial pressure plotted versus time for all tests performed with the same initial water content (20%) but with different start density and slot width.*

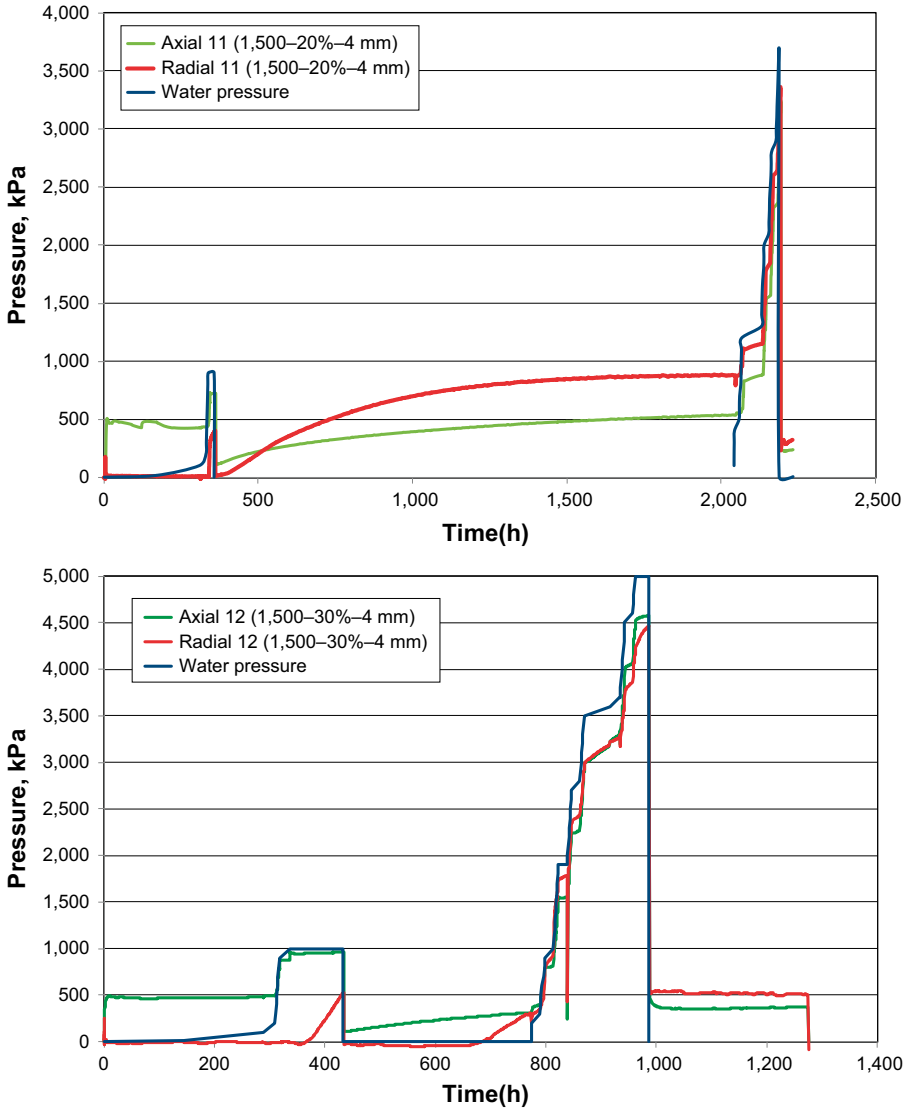

Figure 2-26. *Total pressure and applied water pressure plotted versus time for Test 11 and Test 12.*

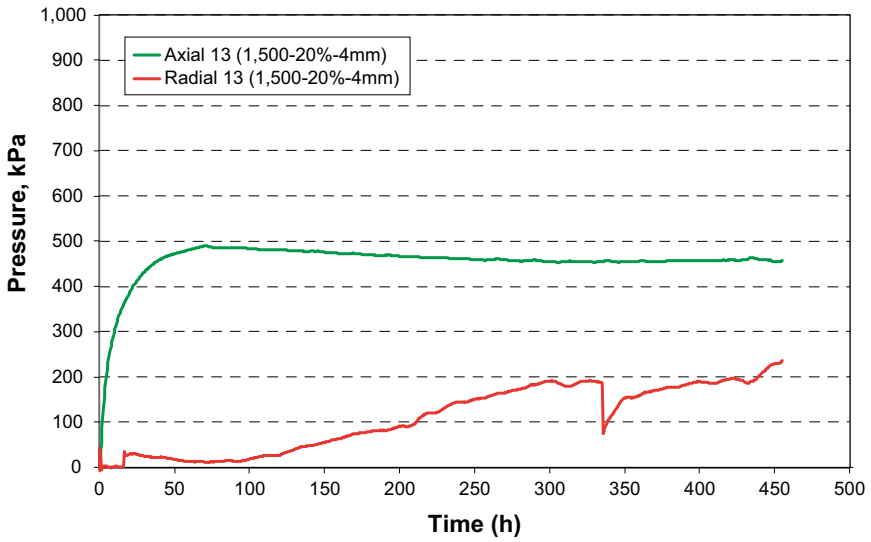

Figure 2-27. *Total pressure development plotted versus time for test 13.*

After termination of the tests, the radial water content and density distribution was determined for all samples and with this data the degree of saturation could be calculated. The results from these determinations for Tests 3 to 8 (performed with a 50 mm diameter oedometer) are provided in Figure 2-28. The density has for Test 7 (2 mm slot width) almost uniform in the radial direction while all the other tests showed a very clear density gradient. The tests only ran for one week which means that the homogenization process was incomplete and radial differences would be expected. The degree of saturation is, however, very high for all specimens in all positions, likely a result of the relatively small size of the specimens.

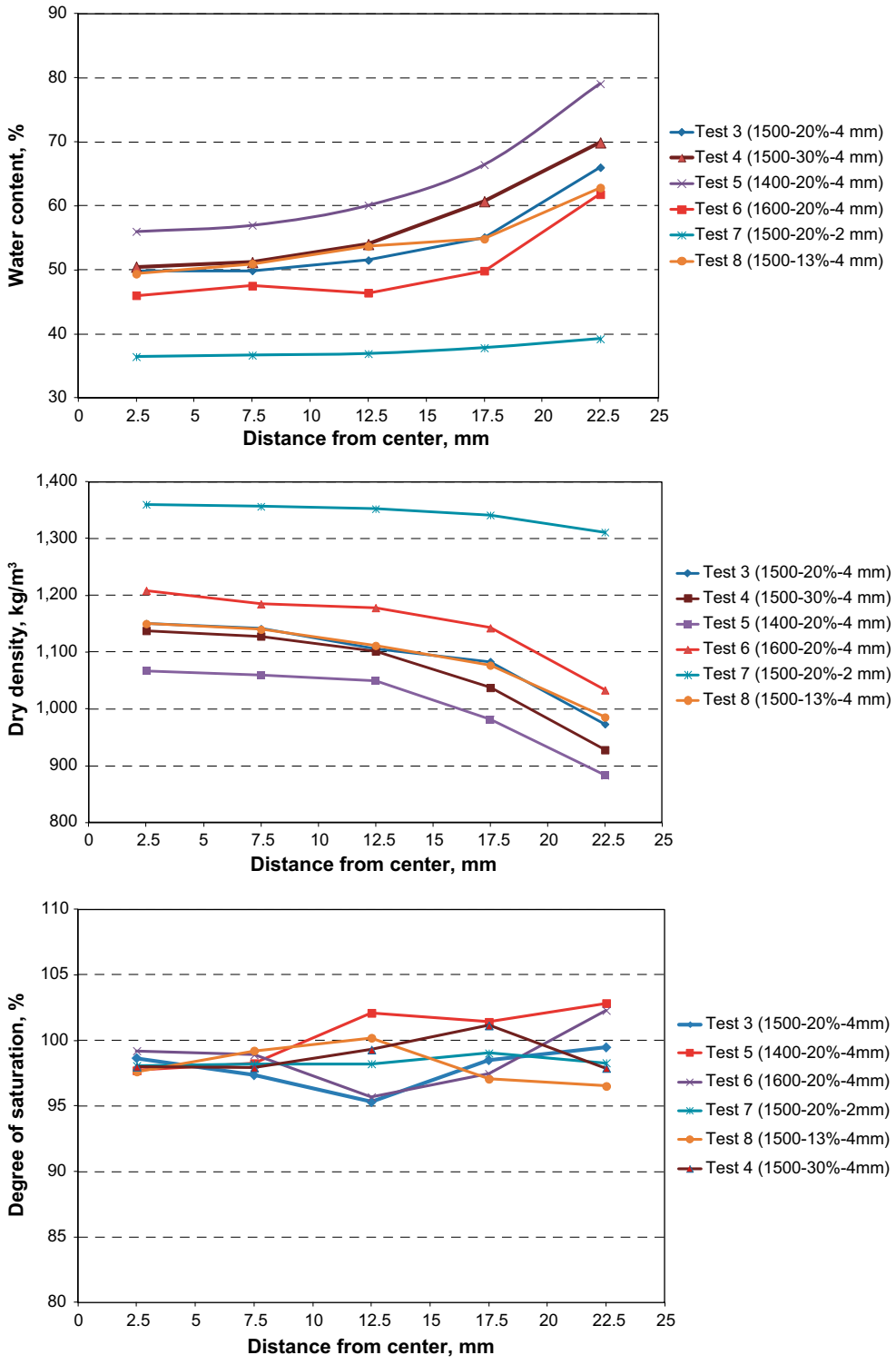

Figure 2-28. *Upper: Radial water content distribution for Tests 3 to 8. Middle: Radial dry density distribution for Tests 3 to 8. Lower: Radial degree of saturation distribution for Tests 3 to 8.*

The results from water content and dry density determinations of Tests 9 to 13 (performed with a 101 mm diameter oedometer) are provided in Figure 2-29. These tests show a density gradient across them and the degree of saturation varies considerably for these tests. There are two main reasons for this:

1. The size of these blocks are larger (d=101 mm compared to d=50 mm for Tests 3 to 8).
2. The test duration for Tests 9 to 13 ranged from 168 h up to 2,230 h.

The lowest degree of saturation was found in Test 9 which only ran for 168 hours and had a low initial water content in the blocks. Test 11 and Test 13 had the same initial density and water content but these tests ran for 2,232 hours and 455 hours respectively, and the degree of saturation is significantly higher for these two specimens.

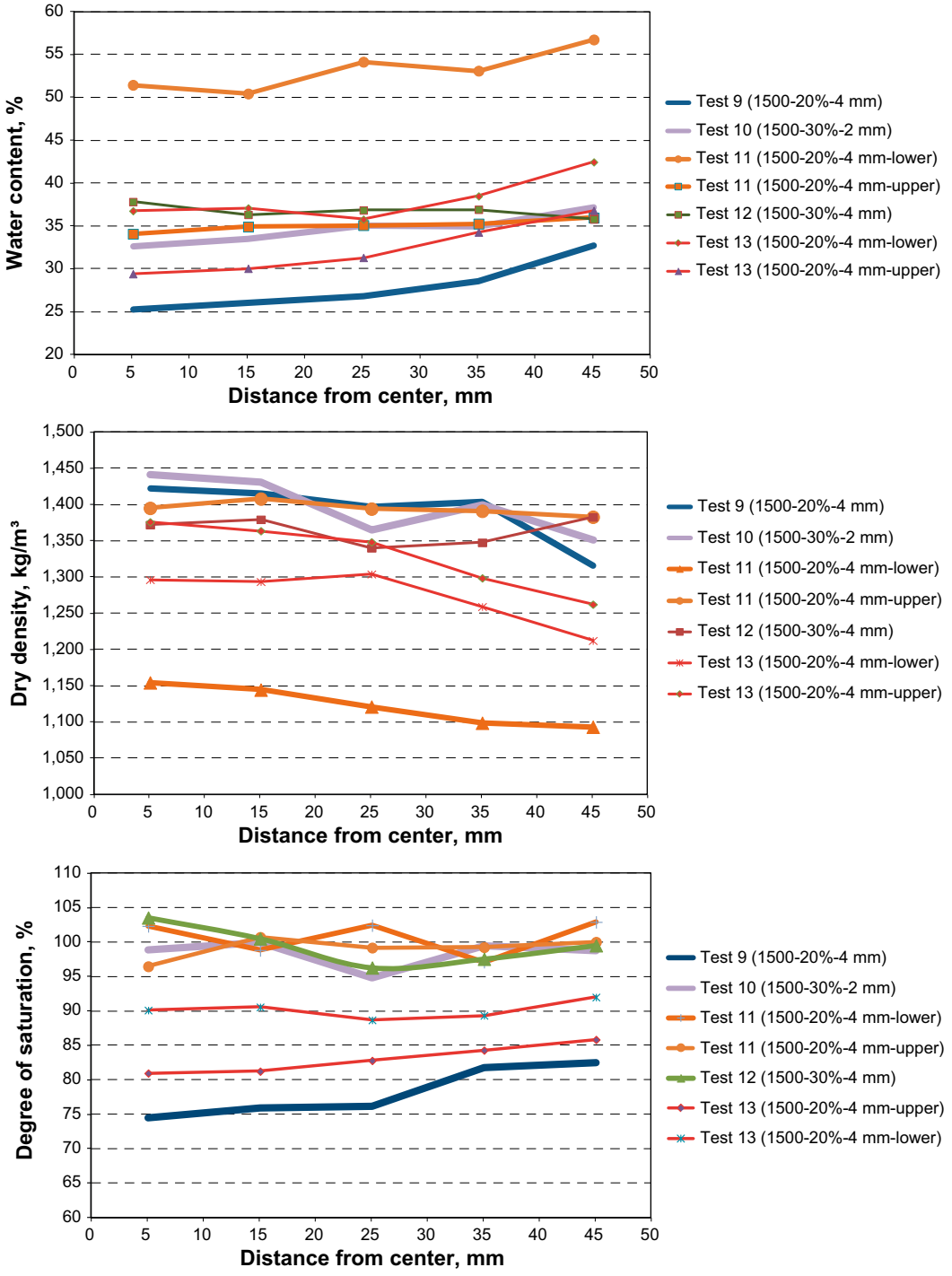

Figure 2-29. *Upper: Radial water content distribution for Tests 9 to 13. Middle: Radial dry density distribution for Tests 9 to 13. Lower: Radial degree of saturation for Tests 9 to 13.*

2.8 Conclusions and comments

The results from the laboratory tests can be summarized as follows:

- **Compaction sealing block**. This test series aimed to investigate the possibility of compacting blocks of low density and high degree of saturation. The tests showed that this was possible although problems could be foreseen if the water content of the powder was higher than 30%. The desired density of the blocks was later increased and other tests e.g. the sealing tests, showed that blocks with lower water content seemed to swell and seal faster.
- **Strength of the sealing blocks**. The results showed that the strength of the block depends strongly on the water content and on the achieved density of the block. The strength seems to increase with increasing dry density and increasing water content (at the same dry density). At low water contents (10%), the strength was rather low and the blocks fragile due to the low density. The tests showed that the highest strength was reached for samples compacted with a water content of 17%. These samples had a dry density higher than that desired, which means that the compaction pressure must be adjusted for the full scale manufacturing.
- **Compression / expansion properties**. The results from these tests agreed well with what was expected for MX-80 bentonite. The use of the results is further described in Chapter 5 describing the hydro-mechanical modeling of the plug.
- **Swelling pressure and hydraulic conductivity**. These tests were done in order to investigate if blocks compacted to high degree of saturation had the same properties as blocks with low degree of saturation. The investigation showed, as expected, that there was no evident difference although the hydraulic conductivity was somewhat lower than the reference tests which probably depends on the fact that the blocks compacted to high degree of saturation were more homogenized.
- **Self sealing of fractures**. Three tests were performed in this test series. Two of the tests were performed with bentonite blocks with densities of 1,400 and 1,500 kg/m^3 and with water contents of 35% and 30% respectively i.e. the degree of saturation was very high. The bentonite in these two tests did not manage to seal the artificial fracture (0.01 mm aperture) during the test time. The third test was performed with bentonite blocks having a dry density of 1,500 kg/m^3 and with a water content of 13.9%. In this test the behavior was quite different. The bentonite sealed quickly and a water pressure could be built up at the inflow end without inducing piping (maximum 2 MPa was applied in this test). One explanation for the observed behavior might be that the erosion rate is higher for bentonite blocks with low initial water content, which means that the eroding bentonite can be more quickly moved into and seal the artificial slot. However, there is some doubt if the sealing took place in the cylindrical tube containing the blocks or in the artificial slot.
- **Sealing of initial slots**. In these tests, bentonite blocks with different initial densities and different initial water contents were allowed to swell and hopefully seal a slot with a width of either 2 or 4 mm. During the tests, one week for most of the tests, the axial and radial pressure build up under low/no applied hydraulic head but access to water at the specimen base was monitored.

The results from the tests showed, as expected that the slot width is of great importance. In the tests performed with 2 mm slot, the radial pressure build up was much faster compared to the tests with 4 mm slot. Another observation was that the initial water content of the bentonite block also influenced the results. The time for swelling and filling up the slot with bentonite and start to build up a pressure at the contact between the bentonite and the cell walls took longer for the samples with high initial water contents (and high degree of saturation).

Two of the samples were, after one week of homogenization exposed to a stepwise increasing water pressure. After 800 and 2,000 hours respectively, both samples could withstand very high water pressures (3.7 and 5 MPa respectively) applied at their base, without exhibiting piping or channeled flow along their length. These hydraulic pressures were much higher than the swelling pressure of these specimens. The explanation for this is probably that the bentonite in the former slot forms an arch within the test cell, which can withstand very high pressures. The same phenomena have been seen in many tests were bentonite pellets have been used (Sandén et al. 2008).

3 Laboratory testing of the drainage components

3.1 General

The concrete plug will consist of a composite structure that uses both geological and stiff draining materials in combination with a bentonite seal, concrete beams and a geotextile as shown in Figure 1-1 and also included in Figure 3-1a. During the course of the project described in this document, different designs were discussed and one proposal was to exclude two of the delimiters (concrete beam walls). The concrete beams between the clay seal and the draining material were judged to be unnecessary since the bentonite blocks are stiff enough to prevent the sand in the draining material from interfering with the clay seal if the system of sand, bentonite blocks and concrete beams are placed successively in parallel. The more massive concrete beams between the sand filter and the backfill was suggested to be replaced by a stiff draining material like Leca or light concrete. Figure 3-1b shows the plug with the proposed new design. The purpose of the geological and the stiff draining material is i.e. to drain the plug to prevent a water pressure build-up prior to the plug is hardened. In order to choose the geotextile, the stiff draining material and the geological draining material a number of tests described in this report were performed.

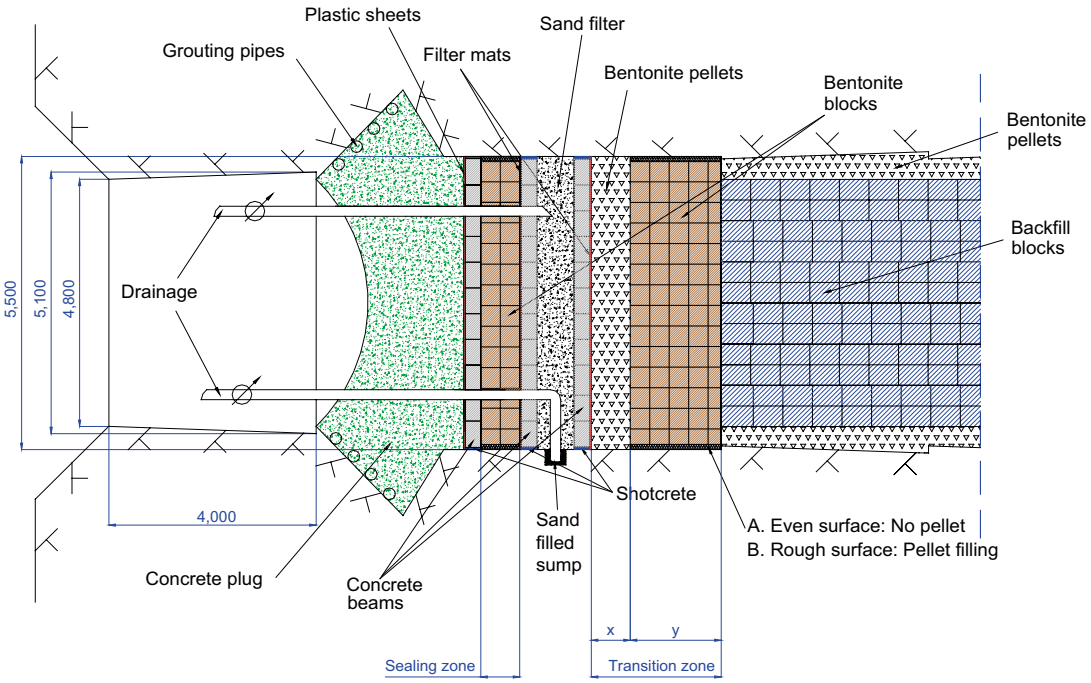

a) Initial Conceptual Design for Deposition Tunnel Plug

Figure 3-1. *The concrete plug outline with the deposition tunnel backfill to the right and the main tunnel to the left. Original conceptual layout is provided as (a) while (b) shows the revised layout with it's stiff draining material and the geological material that will drain the system to prevent a water pressure build-up on the concrete plug before it has hardened. The bentonite blocks to the left in (a) and (b) will eventually swell and seal off water flow past the seal. The concrete beams will act as mechanical support. (Continues on the next page.)*

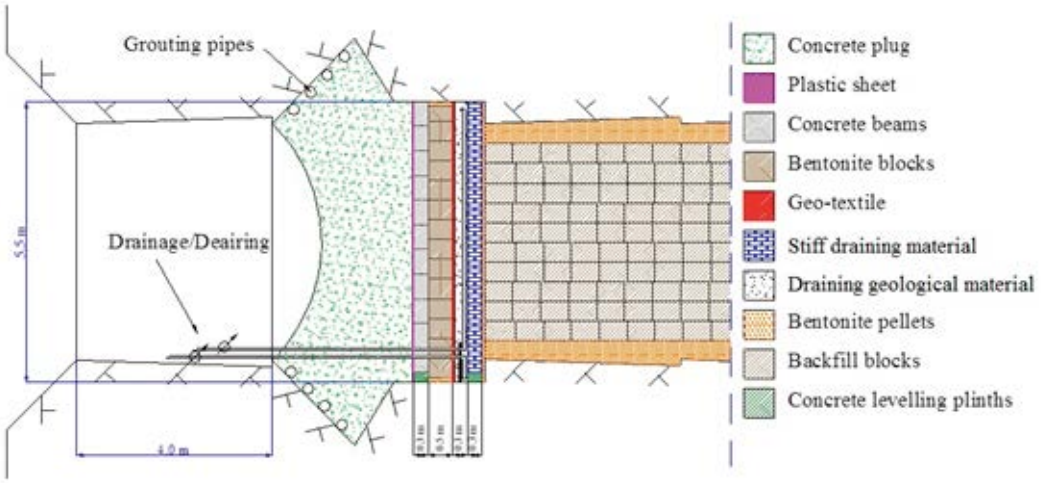

b) Revised Conceptual Design for Deposition Tunnel Plug

Figure 3-1. *Continued.*

3.2 Material and test description

3.2.1 General

Three types of geological draining materials, two types of stiff draining materials and two types of geotextiles were chosen to be tested and evaluated.

3.2.2 Materials

Geological draining material

The aim was to investigate three geological (rock) draining materials with different attributes. For example a poorly graded material with high draining ability and a more packable well graded material were suggested. Samples were taken from both a natural sandpit and a macadam production site. Three candidates were chosen for detailed evaluation;

- **Natural sand/gravel, 0–4 mm.** A natural sand/gravel material with a grain size distribution 0–4 mm was taken at Skånegrus sandpit in Ilstorp/Sjöbo.
- **MakPak® 0–5 mm.** A combination of macadam < 5 mm and stone dust. The product origins from Sydsten AB in Dalby and is described as both packable and draining (Sydsten 2011).
- **Macadam 2–4 mm.** This crushed rock product originates from Sydsten AB, Dalby and was chosen since it was expected to have a very high hydraulic conductivity and also to be self-draining.

Geotextile

Geotextiles were delivered from Svenska Geotech AB in two densities; 1,000 and 1,200 g/m^2 respectively, Appendix 1. The former had a thickness of 7 mm and the latter a thickness of 8 mm. The geotextiles where of needle felted type and made from polypropylene. The product can be used for both material separation and draining purpose and it is also rated as having a high tearing strength.

Stiff draining materials

Two types of stiff draining materials were tested;

- **Leca.** Leca blocks from Beijer Bygg AB in Lund were purchased for testing. Leca-blocks consist of clay aggregate rather than rock aggregate and uses cement as the binding agent. The hydraulic conductivity was expected to be good (high) in this material. During the testing described in this document,,a supplier (Nyströms Cement AB in Norrtälje) of Leca-beams with a length up to 6 meters was found (Nyströms Cement 2011). The supplier provided some test specimens for additional tests to evaluate their specific product in hydraulic conductivity and compressibility.

- **Light concrete.** Light concrete blocks from Beijer Bygg AB in Lund were purchased for testing. Light concrete persist of cement, sand and limestone and was expect to have higher strength but a lower hydraulic conductivity than Leca-blocks.

3.2.3 Test types methods

The test had to be adapted to the tested specimen types. Here follows a brief conceptual description of the tests. Each test is described more in detail in coming text. All tests were performed with tap water.

- **Modified Proctor compaction test**. The Proctor compaction test aims to determine the water content of a geological material where the specimen is most packable for a known compactive effort. It was performed by PEAB AB. This test was only made on the geological draining materials.
- **Compressibility.** The compressibility of the specimen was determined using a CRS-test (constant rate of strain). A constant deformation rate was applied to the specimen and load and deformation was logged. The specimen strain (%) was plotted as a function of the vertical stress (kPa). This test was performed on all components.
- **Hydraulic conductivity**. The hydraulic conductivity was tested by applying a constant water head on one side of the specimen and measuring the flow rate through it. The hydraulic conductivity k (m/s) could then be determined assuming applicability of Darcy's law (see Equation 3-1, Chapter 3.3).
- **Clogging test.** To investigate the clogging risks of the draining components a bentonite-water slurry was percolated through the specimen using a constant flow rate. The test was run for 7 days or until the water pressure exceeded the pump capacity of 1 MPa. The result was displayed by transforming the water pressure into hydraulic conductivity and then plotting it as a function of time.

3.3 Geological draining material

3.3.1 General

The test procedures used on the chosen geological draining material candidates are described below. See Chapter 2.2 for a more detailed description of the tested materials.

3.3.2 Modified Proctor compaction test

General

The modified Proctor compaction tests were performed by PEAB AB. The aim of the test was to see how packable the material is at different water contents. The optimal water content and the maximum Proctor dry density at that specific water content were determined from these results.

Method

Below follows a brief description of the modified Proctor compaction test routine (Fagerström 1973) where;

- A steel cylinder with a volume of 945 cm^3 is used.
- The specimen is packed in five layers. Each layer is impacted 25 times using a 4.5 kg compaction piston dropped from 45 cm height as the cylinder is rotated between impacts to ensure the surface undergoes uniform application of effort.
- When the last layer is completed the dry density of the full specimen is determined by measuring the volume of the compacted specimen and its weight.
- The test is repeated using materials prepared to a number of different water contents (usually at least 3–4 points are required).

Finally by plotting these density and moisture data, the highest Proctor compaction dry density and the optimal packing water content can be determined.

Results

Figure 3-2 displays the results from the modified Proctor compaction tests performed by PEAB AB. The macadam 2–4 mm (see Section 3.3.3) had problems holding water (it drained) and so the test was limited to two water contents. Table 3-1 shows a summary of the maximum dry densities and the optimal water content for each material.

Table 3-1. The maximum dry densities and the optimal water content from the modified Proctor compaction tests performed by PEAB AB.

Material	Optimal water content	Max. dry density
Natural sand/gravel 0–4 mm	14–15%	1,740 kg/m^3
MakPak® 0–5 mm	11–12%	1,960 kg/m^3
Macadam 2–4 mm	1.5%	1,770 kg/m^3

3.3.3 Compressibility

General

A CRS-test (constant rate of strain) was used to investigate the compressibility of the geological drainage materials. The test was planned to be performed with two different initial densities; firstly with lowest possible, loosely-placed density and secondly with 90% of the maximum Proctor dry density. Receipt of the modified Proctor test results was delayed and before the data was available, all tests had already been completed on the geological draining materials. As a result, only the testing of the 90% maximum Proctor dry density macadam 2–4 mm material was done. This reduced scope of compressibility testing was appropriate as the other candidates had already been rejected as being unsuitable due to poor results in the hydraulic conductivity measurements and the clogging tests.

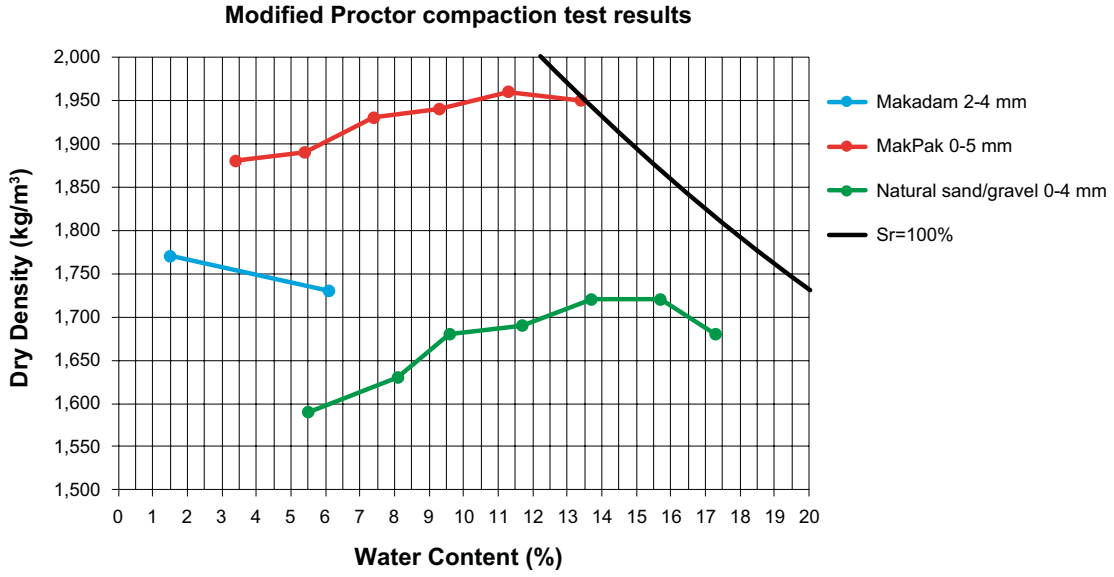

Figure 3-2. *The results of the modified Proctor compaction tests. The black line corresponds to the dry density at full saturation. The test on the macadam 2–4 mm was only performed for two water contents since it had problems holding water.*

Method

The test was arranged as in Figure 3-3 and performed as described below;

- The specimen was placed in an oedometer with the diameter 50 mm. In the tests with low initial density the specimen was carefully placed in the oedometer. In the 90% maximum Proctor dry density test a specific mass of the specimen was compacted in the oedometer until the desired density was achieved. Finally the specimen was confined with a greased piston at the top and fully water saturated.
- A Wykeham Farrance Tritech 50kN press was used for constant deformation at 0.5 mm/min, pushing the piston down to compress the specimen.
- The test was run to a maximum pressure of about 10 MPa.
- Load and deformation were measured with a load cell and a deformation gauge respectively.
- The specimen dry mass was determined by weighing the specimen after drying it for 24 hours at 105°C in a ventilated oven. The specimen height was measured directly after the deformation was stopped when the specimen was in a fixed position. Finally the dry density and the strain were calculated as a function of the stress.

Results

The results from the low initial density tests are shown in Figure 3-4. The modified Proctor compaction test maximum density for each material is added to the figure for comparison. When the samples were water saturated a settling of the fill was observed in MakPak 0–5 mm and Sand/gravel 0–4 mm. The same phenomenon was seen in the hydraulic conductivity tests in described in Section 3.3.4. The initial lowest densities from these tests are also added to Figure 3-4 for comparison.

Figure 3-5 shows the 90% maximum Proctor test result for the macadam 2–4 mm compared to the results from the low initial density and the maximum Proctor dry density.

The compression strain as a function of the vertical stress is compared in Figure 3-6 for all tests.

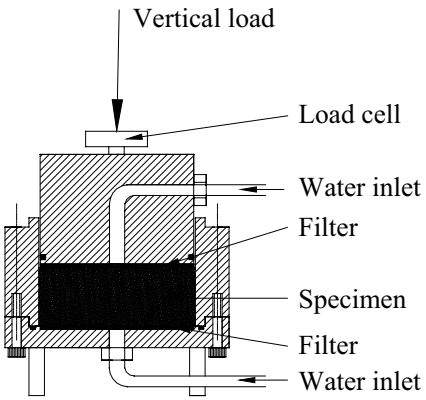

Figure 3-3. *Schematic sketch of the CRS-test.*

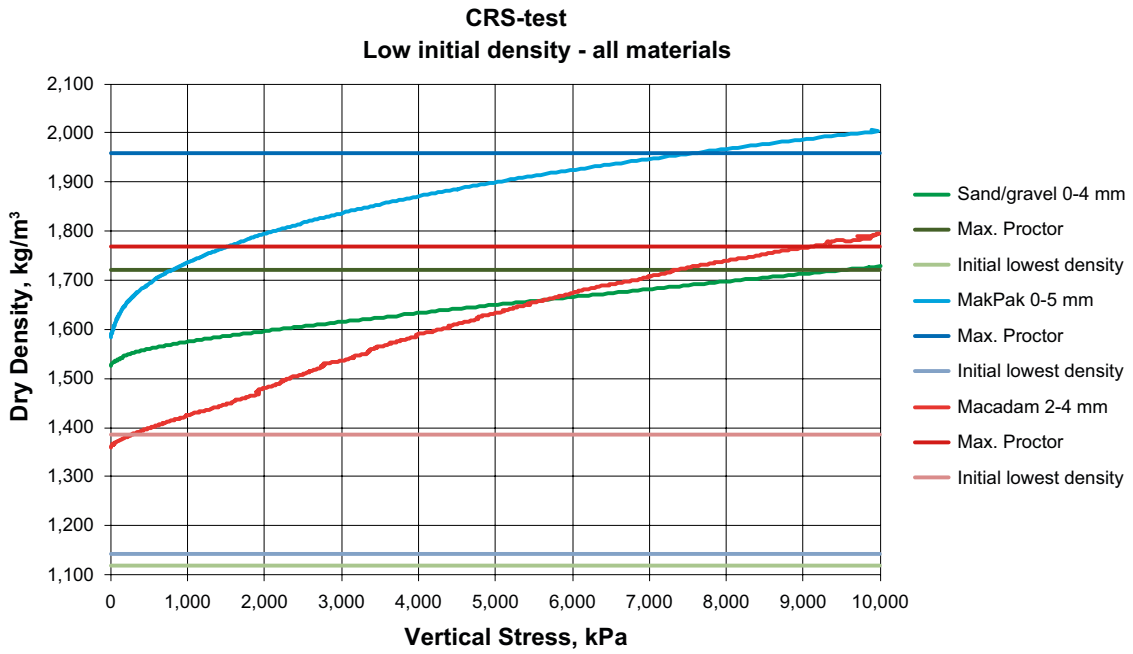

Figure 3-4. *The results from the low initial density CRS-tests for all materials. The maximum Proctor dry density is added for comparison.*

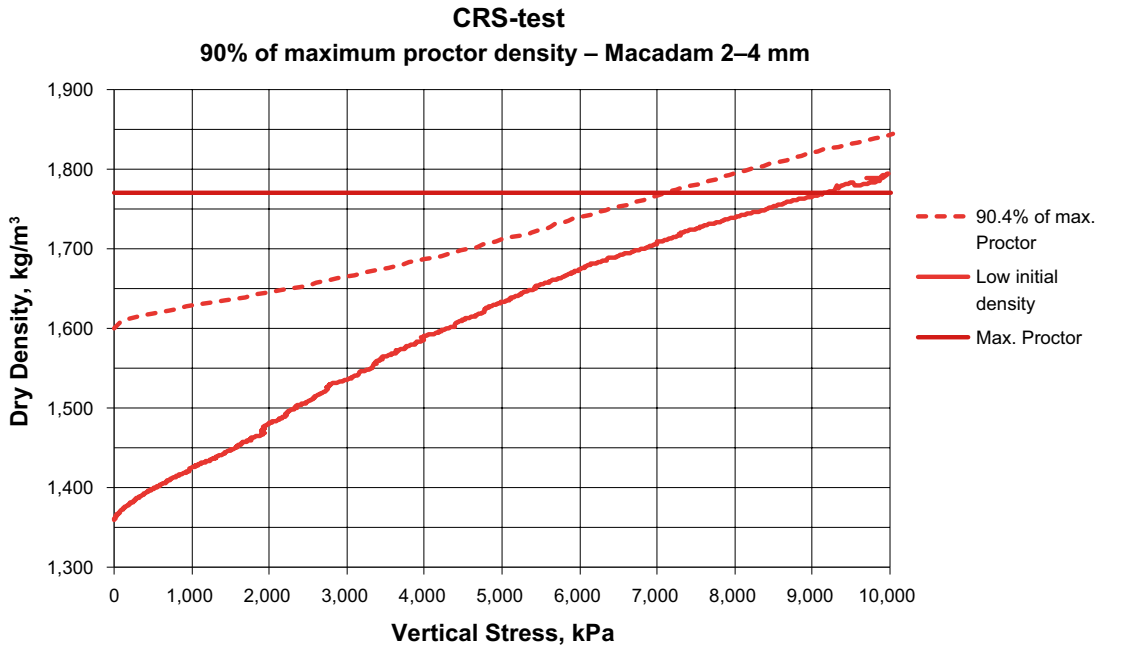

Figure 3-5. *The results of the 90% maximum Proctor dry density test for macadam 2–4 mm. The low initial density results and the maximum Proctor dry density are added for comparison. The dry density of the specimen was determined to be 90.4% of the maximum Proctor dry density.*

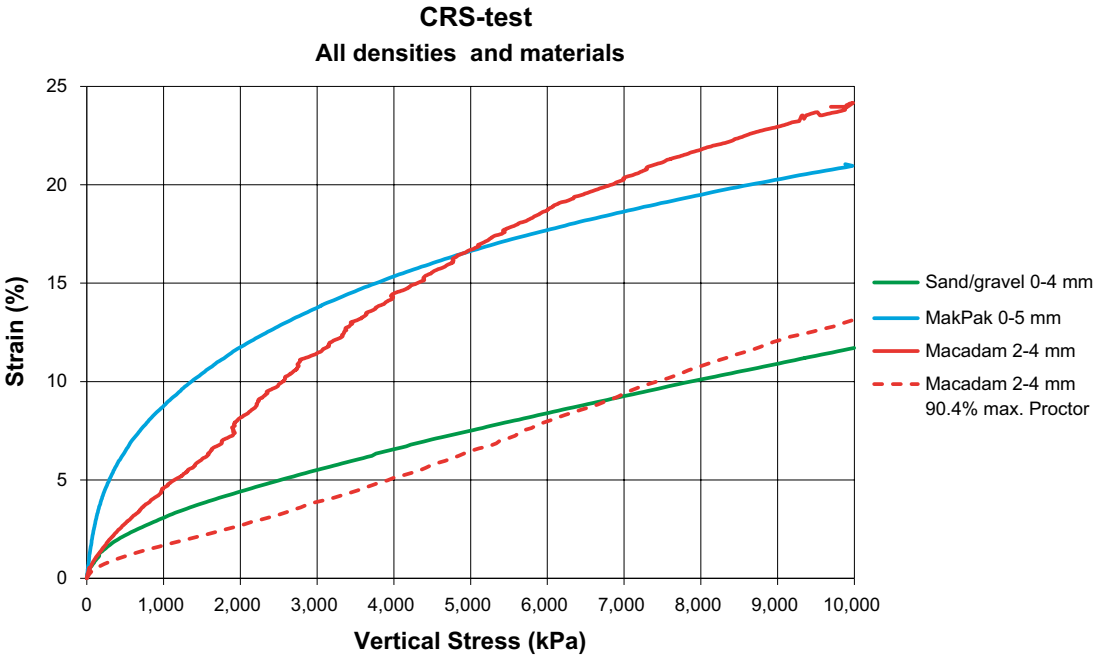

Figure 3-6. *The compression strain plotted as a function of the vertical stress compared for all tests.*

3.3.4 Hydraulic conductivity

General

To confirm the free-draining ability of the geological material the hydraulic conductivity was investigated. The influence of increased dry density on the hydraulic conductivity was also tested since the bentonite swelling pressure is likely to compress the draining geological material and increase its dry density.

Method

The hydraulic conductivity was evaluated using Equation 3-1, Darcy's law.

$$k = \frac{Q}{A \cdot T \cdot i} \qquad 3\text{-}1$$

where

Q = accumulated flow in m^3 during the test runtime,

T = test runtime in seconds,

A = specimen cross section area in m^2,

i = pore pressure gradient dh/dL where dh is the water head and dL is the specimen height.

The test was arranged as in Figure 3-7 and performed according to the following routine;

- The specimen was placed in a steel cylinder with diameter 101 mm and height 116 mm. The specimen was held in place with fixed steel plates at the top and the bottom. A combined fine/coarse-meshed grid was used to distribute the inflow and outflow evenly over the entire specimen area.
- Three different densities were tested for each candidate. The lowest density was prepared by placing the specimen materials carefully into the test cylinder as a loose mass. The medium and the high densities were packed by hand in five layers in the test chamber. The dry density was finally determined after the test by drying the specimen at 105°C for 24 hours before weighing. The specimen volume was calculated from the steel cylinder dimensions, but in the lowest dry densities some settling was observed and the volume was determined from the new specimen height.

- The specimen was fully water saturated and a pore pressure gradient was applied from the bottom to the top. The pore pressure gradient was compensated for the change in specimen height *dL* for the lowest dry densities.
- Flow measurements were taken over 60 second intervals. When the flow was stabilized the hydraulic conductivity was calculated from an average flow rate.

Results

The hydraulic conductivity test results are shown in Figure 3-8. As shown in the method description, a settlement was observed at the lowest densities for MakPak® 0–5 mm and natural sand/gravel 0–4 mm. The initial lowest dry density and also the maximum Proctor dry density are added to the figure as vertical lines. No collapse was observed in the Macadam 2–4 mm tests.

Figure 3-7. *The hydraulic conductivity test arrangement.*

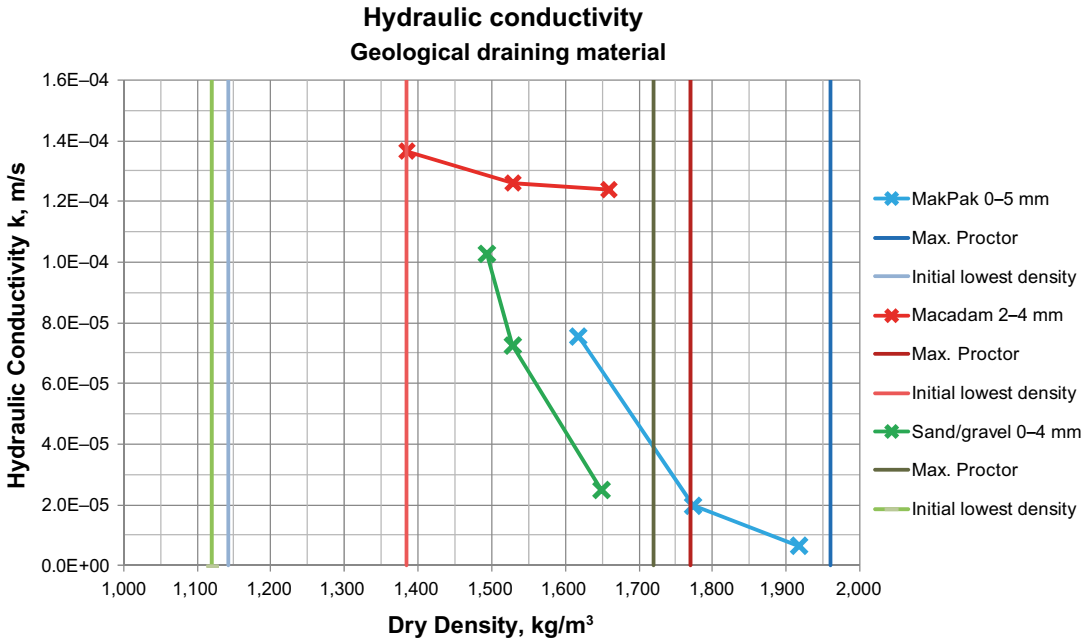

Figure 3-8. *The influence of dry density on hydraulic conductivity. The settling of the low initial density MakPak® 0–5 mm and the natural sand/gravel 0–4 mm specimens caused an increased density for the tests. The initial lowest density is added to the figure as well as the maximum Proctor dry density.*

3.3.5 Macadam 2–4 mm settling test

General

In the MakPak® 0–5 mm and the natural sand/gravel 0–4 mm hydraulic conductivity tests some significant settling of the material was observed in the lowest densities. Figure 3-9 shows the settling of the MakPak® 0–5 mm. Initially the cylinder was entirely filled with material, but after the test it is seen that the specimen height is reduced by about 30%.

The self-settlement phenomenon was not observed in the macadam 2–4 mm. In order to determine whether significant settling at water filling occurs in this material or not a simple test was performed.

Method

A Plexiglas tube of 100 cm length and inner diameter of 10 cm was placed on end and filled with macadam 2–4 mm. The initial specimen height measured 96.0 cm and a point inflow of 1 l/min was applied at the bottom. The arrangement is seen in Figure 3-10.

Figure 3-9. *Significant settling was observed at low initial densities in the hydraulic conductivity tests for MakPak® 0–5 mm (photo) and natural sand/gravel 0–4 mm. Initially the cylinder was entirely filled with material but during the test the specimen settled to about 70% of the initial height.*

Figure 3-10. *The test arrangement for the settling test on macadam 2–4 mm.*

3.3.6 Results

Figure 3-11. shows the results from the settling test on macadam 2–4 mm. The flow rate of 1 l/min was held constant for about 10 minutes. No substantial settling was observed in the specimen over the test period.

Figure 3-11. *The result from the settling test on macadam 2–4mm. No substantial settling is observed in the material.*

3.3.7 Discussion and conclusions

It is important for the draining geological material to maintain its draining ability under the conditions that will occur in the plug. The dry density of all three candidate materials is to some extent affected by a stress exposure. According to the activity plan, a swelling pressure of about 2 MPa is to be expected in the vicinity of the plug. In Figure 3-4 dry density was displayed as a function of stress. Table 3-2 shows the dry densities at no stress and at 2 MPa for all three candidates.

If the hydraulic conductivities provided in Figure 3-8 are compared for the higher and lower dry density conditions provided in Table 3-2, it is clear that macadam 2–4 mm is the only material where the hydraulic conductivity is not significantly affected by an increased dry density. Therefore this candidate is considered the superior option in terms of draining ability and also with respect to its resistance to change under consolidation stress from a swelling pressure. The result from the settling test confirms the observations in the hydraulic conductivity test; no substantial settling can be observed in the macadam 2–4 mm. The clogging test (Section 3.6.2) further evaluates the geological draining material candidates.

Table 3-2. The dry densities of the draining geological materials at 0 and 2 MPa stress.

Pressure (MPa)	MakPak® 0–5 mm (kg/m^3)	Macadam 2–4 mm (kg/m^3)	Natural sand/gravel 0–4 mm (kg/m^3)
0	1,580	1,360	1,520
2	1,790	1,480	1,600

3.4 Geotextile

3.4.1 General

The test procedures for testing the chosen geotextile candidates are described below. See Chapter 3.2.2 for a more detailed description of the tested materials.

3.4.2 Compressibility

General

The compressibility of the geotextiles was evaluated using the same CRS-test as for the geological draining material.

Method

The test was arranged as in Figure 3-3 and performed as described below:

- Specimens were carefully cut out to a circular shape with diameter 50 mm and placed in two layers (yielding a total thickness of 10 and 12 mm respectively) in an oedometer with the same diameter. The specimen was confined with a greased piston at the top and fully water saturated.
- A Wykeham Farrance Tritech 50kN press was used for constant deformation at 0.1 mm/min, pushing the piston down to compress the specimen.
- The test was run to a maximum pressure of about 10 MPa.
- Load and deformation was monitored using a load cell and a deformation gauge.
- The specimen height was measured when the piston was in a fixed position, directly after the deformation was stopped. The strain was calculated as a function of the stress.

Results

The results from the CRS-tests on the geotextile are shown in Figure 3-12. The figure shows that the compressibility is very similar for the two types of geotextile. The results also show that the compressibility is quite high and the thickness will be halved at a pressure of 2 MPa. This is no by itself no problem but may indicate a strong reduction in hydraulic permeability and a vulnerability for clogging after being exposed to high external stresses.

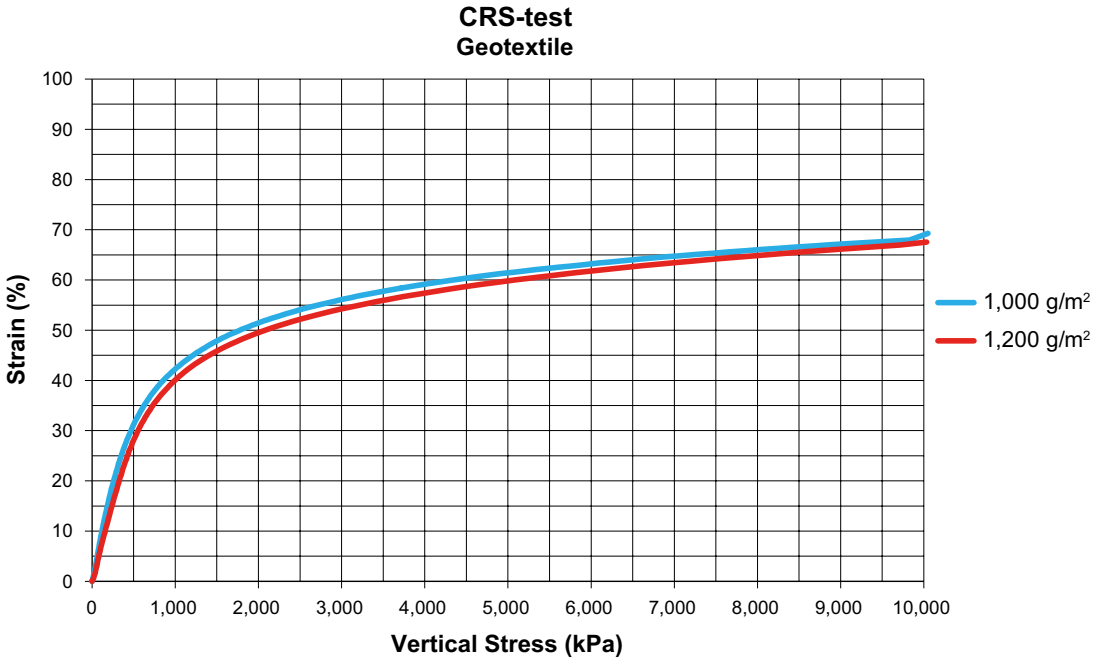

Figure 3-12. *The strain as a function of stress for the geotextiles.*

3.4.3 Hydraulic conductivity

General

The hydraulic conductivity of the geotextile was investigated as a function of the stress. The same equipment was used as in the CRS-test to generate pressure on the specimen and measure the hydraulic conductivity at different rates of compression.

Method

The test was arranged as in Figure 3-13 and performed as described below;

- Specimens were carefully cut out to a circular shape with diameter 50 mm (yielding a total thickness of 10 and 12 mm respectively) and placed in two layers in an oedometer with the same diameter. The specimen was confined with a greased piston at the top and fully water saturated. To minimize flow between the filter and the ring the diameter of the filters were so accurate that the filters had to be pressed into the ring.
- A Wykeham Farrance Tritech 50kN press was used to compress the specimen.
- Seven hydraulic conductivity measurements were done at stresses ranging from 0–10 MPa.
- Load and deformation was monitored using a load cell and a deformation gauge.
- At the inflow and outflow locations a perforated steel filter with rasped recesses was used to distribute the water over the entire specimen.
- A constant drop of water head of 0.6 m was applied between the water inlet and the water outlet.
- The hydraulic conductivity k was evaluated using Darcy's law (Equation 3-1). The actual thickness of the filters was used as the value of dL, which meant that the gradient increased when the filters were compressed since the pressure drop dh was constant. The measured accumulated flow Q during the test time T were then applied in Equation 3-1.

Results

Figure 3-14 shows the hydraulic conductivity in the geotextiles as a function of the stress.

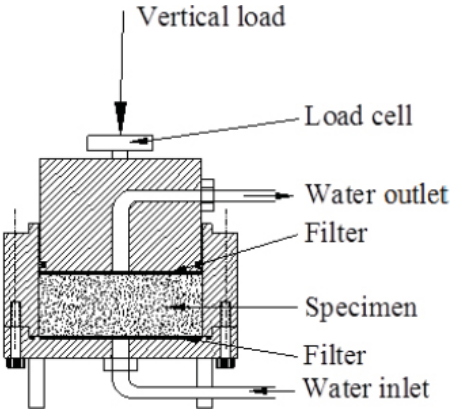

Figure 3-13. *The arrangement of the hydraulic conductivity measurements on the geotextile.*

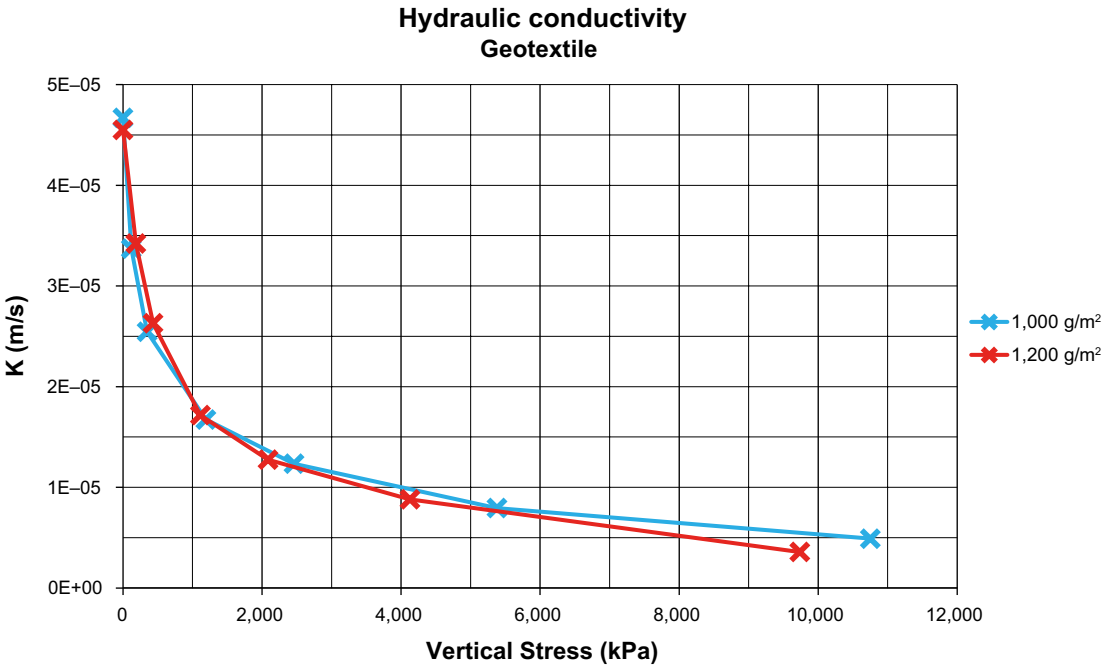

Figure 3-14. *The geotextile's hydraulic conductivity as a function of the stress.*

3.4.4 Discussion and conclusions

No difference can be observed in the hydraulic behaviour of the two tested geotextile densities. Initially the hydraulic conductivity is about $4.5 \cdot 10^{-5}$ m/s. When the stress on the specimen increases the hydraulic conductivity is reduced and at 2 MPa it is less than a third of the initial. The clogging test (Chapter 3.6.3) will further evaluate if the geotextile is suitable for draining the system.

3.5 Stiff draining material

3.5.1 General

Initially all tests were performed on the Leca and light concrete blocks purchased at Beijer Bygg AB in Lund. Later on, specimens from a type of longer Leca-beam were received from Nyströms Cement AB in Norrtälje and some additional tests could be performed on these. The material candidates are described more in detail in Chapter 2.2.

3.5.2 Compressibility

General

The compressibility of the stiff draining material was evaluated using a CRS-test. The first tests were performed using a Wykeham Farrance Tritech 50kN press. Some additional tests were later performed on larger specimens from the Nyströms Cement AB Leca-blocks. The additional tests were performed at the department of Structural Engineering (LTH/Lund University) since the Tritech 50kN was insufficient in capacity. Figure 3-15 shows the press used.

Method

The tests were performed as described below;

- The first tests performed on the blocks from Beijer Bygg AB were done on cylinder shaped specimens with dimensions 35 mm diameter and 70 mm height. The additional tests on the Nyströms Cement AB Leca were performed with cubic specimens with 150 mm sides.
- The smaller specimens were compressed at a constant deformation rate of 0.2 mm/min in a Wykeham Farrance Tritech 50kN press. Since the capacity of the Tritech 50kN was insufficient, the tests on the 150×150×150 mm specimens were performed at the department of Structural Engineering. The latter tests were performed at 1 mm/min deformation rate.
- Deformation and load was measured by a deformation gauge and a load cell for the tests performed in the Tritech50kN. In the tests at the department of Structural Engineering deformation and load was logged by the press.
- The received load and deformation data was transformed into strain as a function of the stress on the specimens.

3.5.3 Results

Figure 3-16 shows the results from the CRS-tests for all candidates. Strain is plotted as a function of the vertical stress. Both materials crack at a high stress in spite of the confinement. The concrete shows brittle behavior with strong reduction in stress with increasing strain at the peak value 5 MPa. The Leca reaches at maximum between 2 and 3 MPa vertical stress.

Figure 3-15. *Compressibility tests performed on the new Leca-block specimens received from Nyströms Cement AB. The tests were performed at the department of Structural Engineering at LTH/Lund University since the available Tritech 50kN press was insufficient in capacity.*

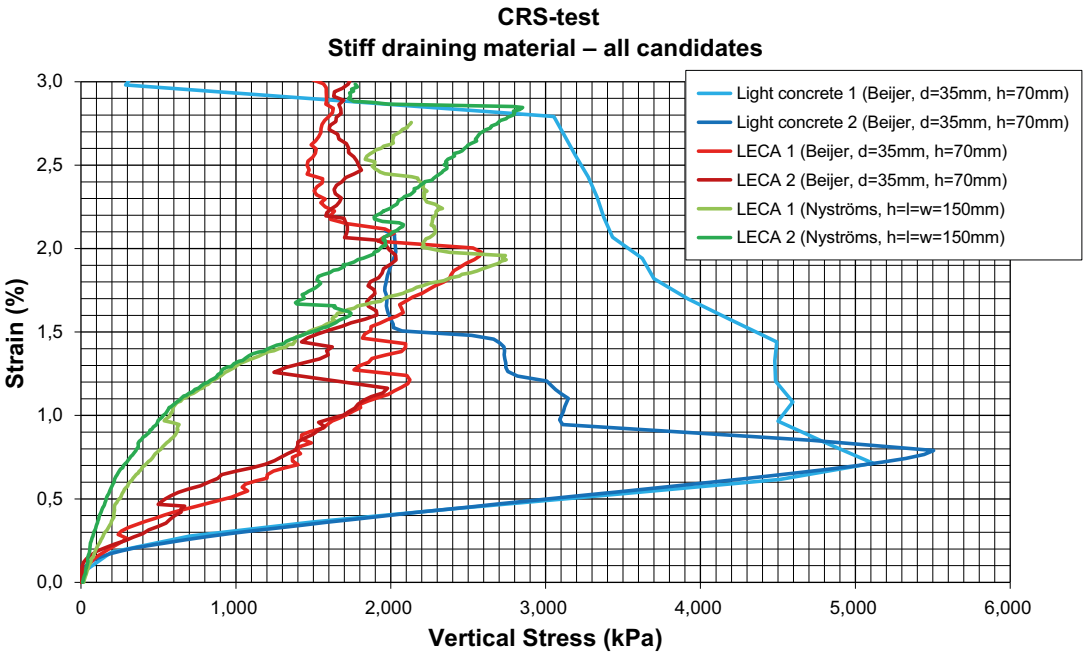

Figure 3-16. *The results from the CRS-tests for all stiff draining material candidates.*

3.5.4 Hydraulic conductivity

General

The hydraulic conductivity was evaluated to investigate the draining ability of the stiff draining materials. Firstly, tests were performed on the light concrete and Leca from Beijer Bygg AB. In addition to this the same test was performed on the Leca specimens from Nyströms Cement AB when they arrived.

Method

The test was done in basically the same way as was used for the geological draining material tests (Figure 3-7). However some changes had to be done when preparing the specimen for testing. The test was performed according to the following routine:

- A cylinder shaped specimen was prepared with dimensions diameter 70 mm and height 100 mm. A rubber membrane was put around the specimen and it was placed in a steel cylinder with diameter 101 mm and height 116 mm (Figure 3-17). A combined fine/coarse-meshed grid was placed at the bottom to distribute the inflow evenly over the entire specimen area.
- To severely limit water from flowing in the slot between the specimen and the cylinder's inner wall, the slot was filled with MX-80 bentonite pellets (Figure 3-18). The slot was then filled with water. A combined fine/coarse-meshed grid was placed on the top of the specimen and it was then vertically confined using a piston.
- The membrane served to prevent flowing water from picking up fines from the confining medium (bentonite) during testing. It also prevented bentonite from swelling into the drainage pores in the Leca. Finally, the bentonite provided some active confinement to the membrane, ensuring that interface flow between the membrane and the LECA did not occur.
- After 24h of swelling, the hydraulic conductivity of the bentonite-sealed slot was considered negligible compared to the hydraulic conductivity of the specimen and the test measurements were started.
- Samples were taken in 60 second intervals for the Leca specimens and one to two hours intervals for the light concrete specimens. When the flow rate stabilized, the hydraulic conductivity was calculated from an average flow rate. The hydraulic conductivity was evaluated using Darcy's law (Equation 3-1).

Results

Table 3-3 shows the results from the hydraulic conductivity tests on the stiff draining materials.

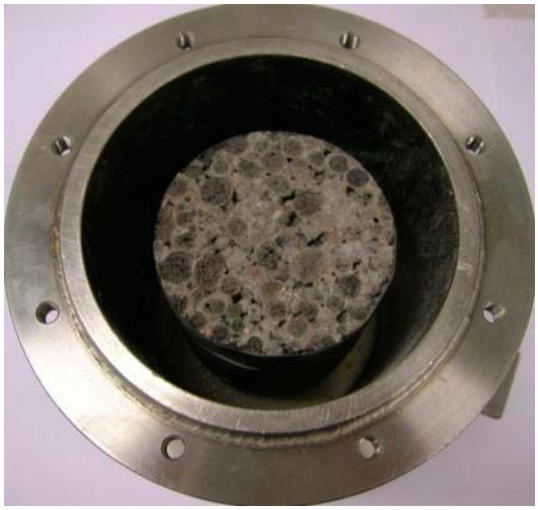

Figure 3-17. *The specimen side is covered with a rubber membrane and placed in the steel cylinder.*

Figure 3-18. *The slot is filled with pellets made from MX80 bentonite to prevent interface flow.*

Table 3-3. The hydraulic conductivity of the stiff draining material candidates.

Material	Light concrete	Leca (Beijer)	Leca (Nyströms)
Hydraulic conductivity, k (m/s)	$1.3 \cdot 10^{-7}$	$1.4 \cdot 10^{-4}$	$1.2 \cdot 10^{-4}$

3.5.5 Discussion and conclusions

The CRS-tests show that the lightweight concrete (LC 1 and LC2 in Figure 3-16), has the highest compression strength, about 5.0–5.5 MPa.

In the CRS-tests performed on the Nyströms Cement AB Leca material, the stress vs. strain graph indicates a more ductile than expected product. In Figure 3-16 this difference in the behaviour of the Leca from Beijer and the Leca from Nyströms is evident. A possible explanation could be strain in the dry cement that was used on the contact sides in the test.

It can also be observed in Figure 3-16 that the compression strength of the Nyströms Leca is about 2.7–2.8 MPa, which is significantly lower than the 4.5 MPa claimed by the supplier. The Beijer Leca also shows a slightly lower peak strength (2–2.6 MPa) than the Nyströms product.

It is uncertain how important the compression strength of the stiff draining material is. Once the component is installed in place a deformation due to stress from swelling pressure is not certain to cause any significant impact on the draining ability. However the reason why the CRS test results differ from the information given by Nyströms Cement AB should be investigated. In general the results indicate that LECA is the superior candidate. The clogging test (Chapter 3.6.4) will further evaluate if LECA is suitable for draining the system.

As seen in Table 3-3 the hydraulic conductivity in the Leca specimens is about a thousand times higher than in the lightweight concrete. There seem to be no major difference of the hydraulic conductivity in the two types of Leca.

3.6 Clogging test

3.6.1 General

The test purpose was to investigate how the hydraulic conductivity of the drainage system components would be affected by high bentonite content in the water moving through it. All drainage system components were tested but due to differences in their characteristics, the methodologies were varied slightly and are therefore described separately.

Common to all tests were the pump- and slurry arrangement. The pump and the slurry it supplies are seen in Figure 3-19. The test was considered conservative as it used a bentonite-water slurry with a concentration of 10 g MX-80 sodium bentonite/liter water, much higher than is anticipated in a repository. A constant flow rate of 0.1 l/min was applied to all the specimens tested and a pressure transducer logged the water pressure in the system. The water pressure data was used to determine the pore pressure gradient i in Darcy's law and then the hydraulic conductivity as a function of time could be plotted. The tests were run for 7 days or until the maximum pump pressure capacity of 1 MPa was reached.

Figure 3-19. *The bentonite-water slurry under constant agitation and the pump.*

The slurry was under constant agitation and samples were taken on a regular basis to survey the concentration. The slurry was diluted when the solids concentration exceeded 10 g/l. Figure 3-20 shows the slurry concentration measurements made in the course of testing.

Tap water was used in these tests. This is a slight drawback since the water in the field test was 1% salt (in situ water). However, viscosity of bentonite slurry decreases when salt is mixed into the slurry so the tests were considered pessimistic.

3.6.2 Geological draining material

Method

The geological draining material was placed in an oedometer with a 50 mm diameter. Figure 3-21 shows the specimen preparation. The inflow point is located in the bottom of the oedometer. A perforated steel filter (1 and 3) with milled grooves was placed at the inflow point to distribute the water flow evenly over the base of the specimen. Then the specimen (2) was placed in the oedometer and a second steel filter (3) was put on top of the specimen. For the materials with finer grains (natural sand/gravel 0–4 mm and MakPak® 0–5 mm) a thin finely meshed filter was also added to prevent erosion of the specimen. Finally the specimen and the filters were confined in the oedometer by a piston through-which the outflow pathway ran. The piston was held rigidly in position by a steel plate fixed with three machine screws (4).

Results

Figure 3-22 shows the hydraulic conductivity in the geological draining materials as a function of time. The macadam 2–4 mm seems to have the lowest reduction in hydraulic conductivity due to clogging by eroded clay. The natural sand/gravel 0–4 mm and the MakPak® 0–5 mm both seem to clog quite quickly and the hydraulic conductivity is reduced significantly.

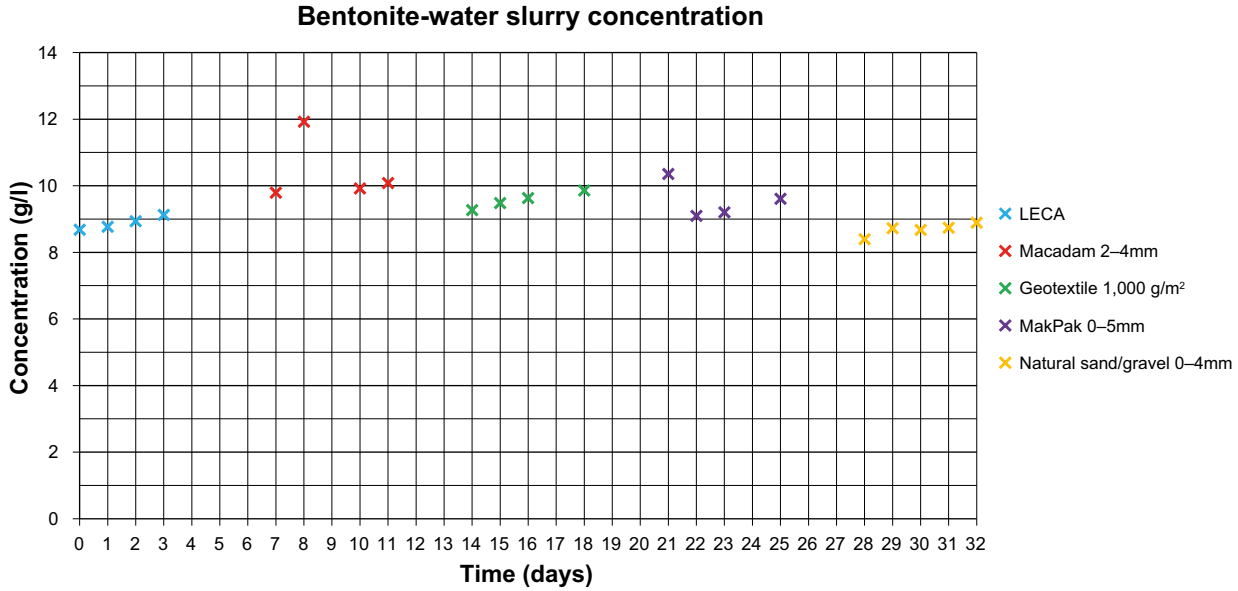

Figure 3-20. *The bentonite slurry concentration for the different clogging tests performed. The slurry was diluted when the bentonite concentration exceeded 10 g/l.*

Figure 3-21. *Geological drainage material specimen preparation for the clogging tests. The specimen is confined between two specially prepared steel filters to keep it in place and distribute the in- and outflow evenly over the specimen area.*

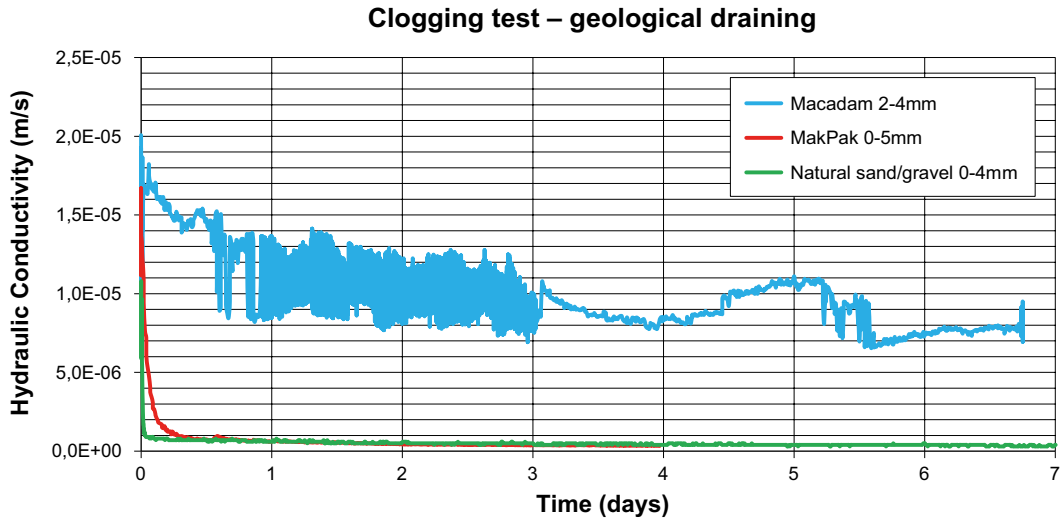

Figure 3-22. *The clogging test results for the geological draining material. Hydraulic conductivity is plotted as a function of time to investigate if the bentonite-slurry clogs the material and reduces its draining ability.*

3.6.3 Geotextile

Method

Since the only difference between the geotextiles examined in this study was their density, only the 1,000 g/m^2 geotextile was tested for its hydraulic properties. The test was performed as for the geological draining material described in Chapter 3.6.2 with exception of the specimen confinement. A double layer of carefully cut out geotextile was used. The diameter of the specimen was the same as the oedometer; 50 mm. To avoid the slurry flow from running along the interface between the specimen and the oedometer inside wall two double O-rings were placed under and over the specimen. These o-rings were located outside of the surface where water supply could reach directly and so there was no means for the slurry to get to the outside edge of the assembly. In this way the flow was forced to run through the middle of the specimen (Figure 3-23).

The final step in test assembly involved mechanically confined the specimen with a piston. The piston was fixed in position by a screwing down a steel plate and the screws were tightened to ensure a tight seal was provided by the o-rings than cut off the flow at the interface between the geotextile and the oedometer's inner side. The reduced specimen surface area was taken in consideration when calculating the hydraulic conductivity with Darcy's law.

Results

Figure 3-24 shows the result from the clogging test on the geotextile having 1,000 g/m^2 density. The hydraulic conductivity shows a pattern of gradual reduction with time for the entire duration of testing. This means that eroded clay particles seems to be stuck in the geotextile structure and with time they will severely limit the water flow through the geotextile.

3.6.4 Stiff draining material

Method

The stiff draining material clogging tests used the cylinder shaped specimens from the hydraulic conductivity tests described in Chapter 3.5.4. The prepared steel cylinder containing the specimen (Figure 3-25) was connected to the clogging test system and water was supplied at a constant rate of 0.1 l/min.

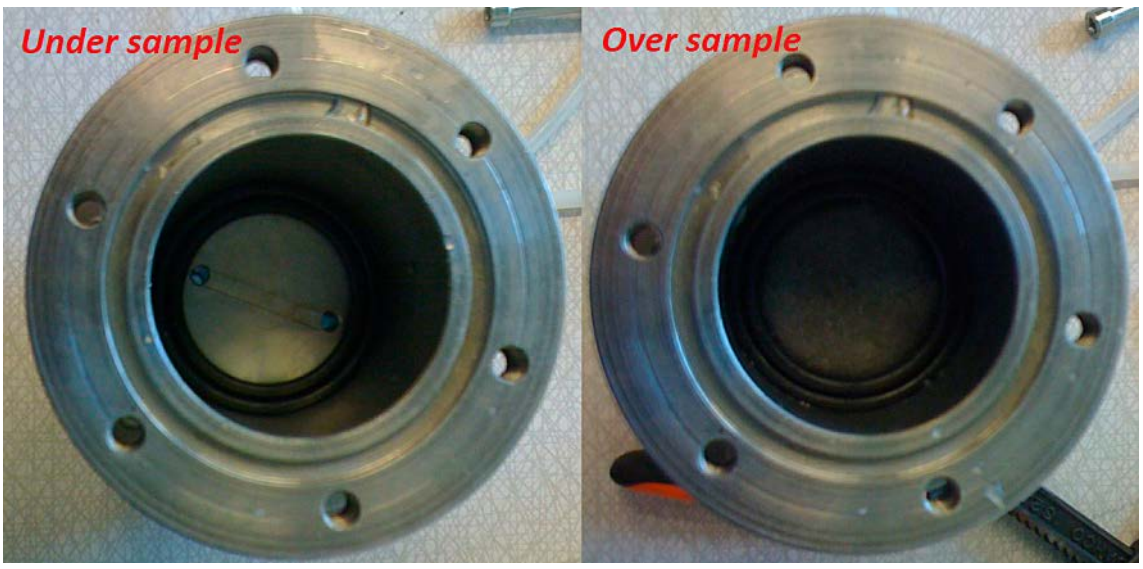

Figure 3-23. *The geotextile specimen was fixed in position between double O-rings to avoid the flow from running in the interspaces between the specimen and the oedometer inner side.*

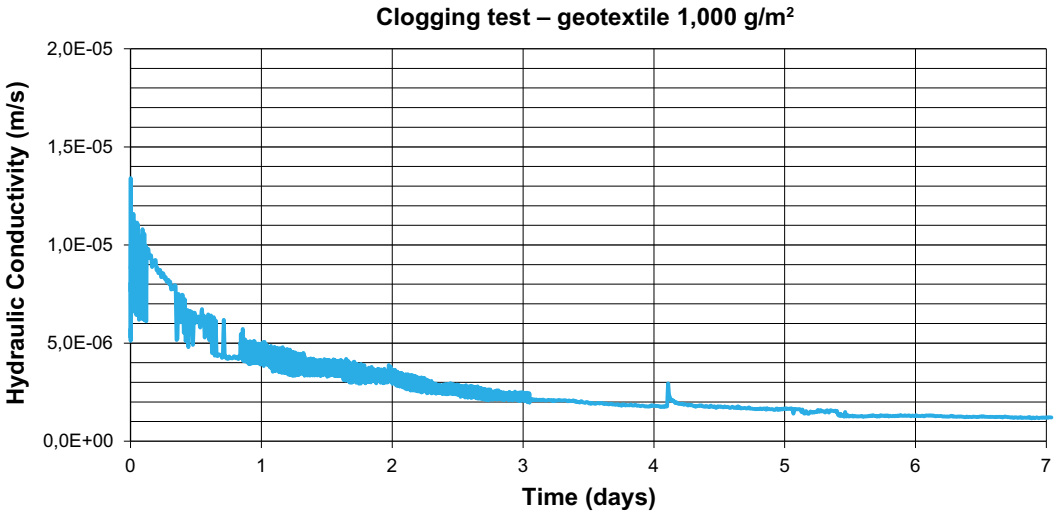

Figure 3-24. *The clogging test results for the geotextile 1,000 g/m². Hydraulic conductivity is plotted as a function of time to investigate if the bentonite-slurry clogs the geotextile and reduces its draining ability.*

Figure 3-25. *The clogging tests on the stiff draining material used the specimens from the hydraulic conductivity tests.*

Results

For the lightweight concrete an instant inflow resistance pressure build-up was observed for the inflow rate of 0.1 L/min and the test was stopped within five minutes due to the pump pressure capacity being exceeded. The registered pressure is displayed in Figure 3-26. This indicates a material that has a very low intrinsic permeability and may have exhibited rapid clogging of what flow paths were available. This is obviously a material that should not be chosen as a drainage material if there is a risk that eroded clay particles will flow through it.

Figure 3-27 shows the result from the clogging test completed on the Leca (Beijer) material. The hydraulic conductivity shows some initial reduction but seems to have stabilized around $1 \cdot 10^{-5}$ m/s after 4 days of percolation. At this level of flow it would not seem that any substantial amount of clogging is occurring as the result of slurry percolation.

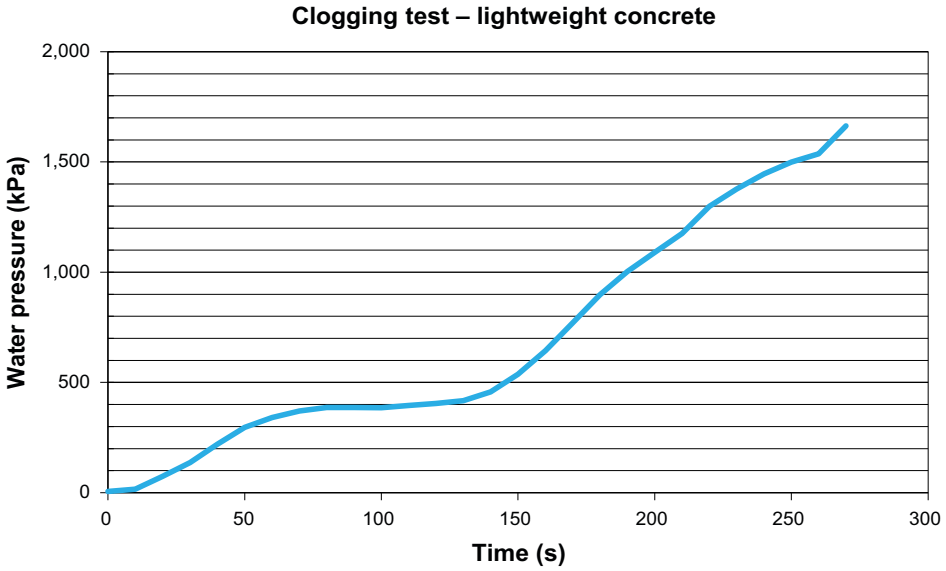

Figure 3-26. *The lightweight concrete clogging test was stopped due to instant pressure build-up.*

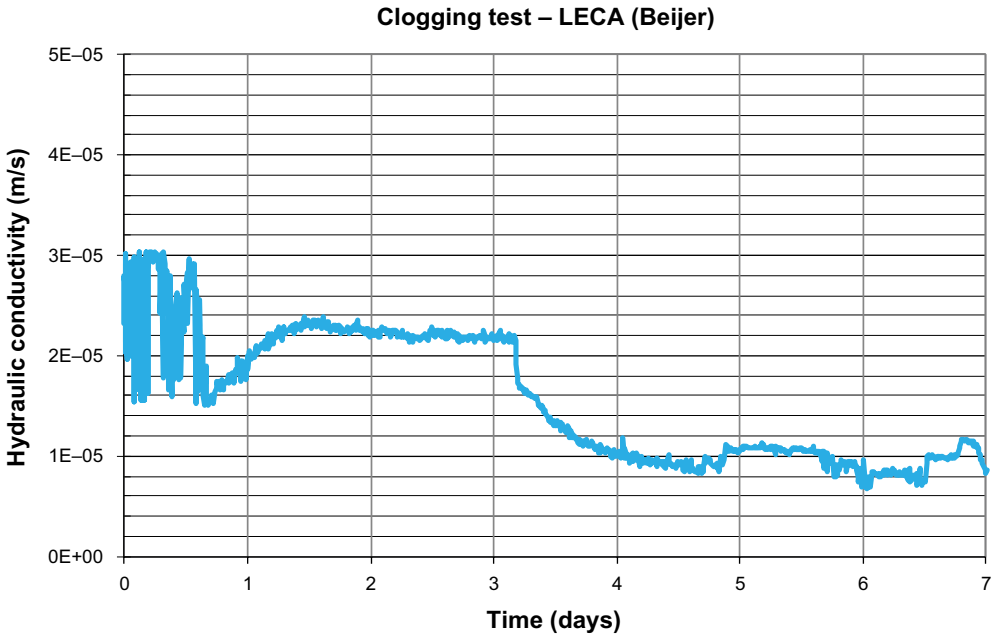

Figure 3-27. *The clogging test results for Leca (Beijer). Hydraulic conductivity is plotted as a function of time to see if the bentonite-slurry clogs the material and reduces its draining ability.*

3.6.5 Discussion and conclusions

The results of the clogging tests can be summarized as follows:

1. The natural sand/gravel 0–4 mm and the MakPak® 0–5 mm specimens had an instant reduction of the hydraulic conductivity. This means that the draining ability in these candidates is likely to be significantly reduced if they are exposed to a water flow containing eroded bentonite. Macadam 2–4 mm was clearly the material least affected by the bentonite slurry percolation. The results indicate that this material can maintain its draining ability despite high bentonite content in the water.
2. The hydraulic conductivity of the geotextile was clearly affected in the test. The geotextile tested exhibited a significant reduction in hydraulic conductivity and is therefore not suitable for draining water with high bentonite content.

3. However, if the system needs to be wetted manually it could still be used to distribute bentonite free water evenly from the draining components.
4. The lightweight concrete was completely clogged by the bentonite slurry and can therefore be excluded as a candidate. The Leca specimen on the other hand seemed to drain the bentonite slurry well and only a slight reduction in the hydraulic conductivity was observed.

Based on these observations, it can be concluded from these clogging tests that macadam 2–4 mm and Leca are potentially the most suitable drainage system components as they could manage to drain water with high bentonite content without clogging. The results of short-term tests indicate that their hydraulic conductivity only seems to be slightly reduced for these candidates when percolated with high suspended solids water.

Worthy of mention is that the viscosity of the bentonite slurry is likely to differ from the viscosity of pure water. The values of hydraulic conductivity determined here can therefore not be directly compared with those values obtained when testing is done using only water.

3.7 Summary and conclusions

3.7.1 General

The work described in this chapter was done in order to evaluate several different types of draining components that could be used in connection with a concrete tunnel-plug. The drainage system components will prevent water pressure buildup on the plug prior to it sufficiently hardening to support the load applied by the materials confined in a closed tunnel. The tested candidates were three types of geological draining material, two qualities of geotextile and two types of stiff draining materials.

An important factor in the evaluation is the expected swelling pressure of about 2 MPa that the components will be exposed to. Compressibility and hydraulic conductivity were tested on all candidates. Also modified Proctor compaction tests were performed on the draining geological materials in order to determine what field densities could realistically be obtained. Finally, a clogging test was performed on all candidates to investigate if they could maintain their draining ability when exposed to a water flow with high bentonite content. The bentonite slurry concentration was about 10 g/liter MX-80 sodium bentonite in fresh water. This section summarizes the main conclusions drawn from the results of the performed tests.

3.7.2 Geological draining material

Three geological draining materials were tested;

- a mix of stone dust and macadam called MakPak® (grain size from 0–5 mm),
- a natural sand/gravel with grain sizes 0–4 mm, and
- pure macadam with grain sizes 2–4 mm.

Initially a modified Proctor compaction test and a CRS-test were performed on the candidates and then the hydraulic conductivity was determined at three different densities.

Macadam 2–4 mm was the candidate with the highest hydraulic conductivity. The hydraulic conductivity of macadam 2–4 mm was also very little affected by an increased dry density.

The results from the CRS-tests showed that the MakPak® and natural sand/gravel candidates experienced a significant reduction in hydraulic conductivity for the densities associated with a 2 MPa external confinement. In the hydraulic conductivity tests some significant autogenous settling was observed in MakPak® 0–5 mm and natural sand/gravel 0–4 mm. A special test was performed on macadam 2–4 mm to determine if self-settlement was also an issue for that material but no discernible settling was observed. Macadam 2–4 mm was also superior in its performance in the clogging test. Initially the Macadam 2–4 mm material's hydraulic conductivity reduced slightly but over time it seemed to maintain its draining ability.

3.7.3 Geotextile

Two qualities of the needle felted geotextile were tested; 1,000 g/m^2 and 1,200 g/m^2. Firstly a CRS-test was performed and then the hydraulic conductivity was investigated as a function of stress on the geotextiles. There was no observed difference in compressibility or hydraulic conductivity. The hydraulic conductivity was clearly reduced when the stress on the specimen increased. The clogging test indicated that the geotextile's draining ability will be reduced with time and that it should not be used for draining water with eroded bentonite present in it. However it could still function to distribute water if artificial wetting of the system is required.

3.7.4 Stiff draining material

The stiff draining material candidates were lightweight concrete and Leca. The first LECA-blocks were bought at Beijer Bygg AB in Lund. Later Nyströms Cement AB in Norrtälje was identified as a supplier of Leca-beams of up to 6 meters in length. Nyströms provided some specimens and the compressibility and hydraulic conductivity tests were performed on these as well. The LECA specimens had hydraulic conductivity from $1.2 \cdot 10^{-4}$ to $1.4 \cdot 10^{-4}$ m/s. The lightweight concrete hydraulic conductivity was determined to $1.3 \cdot 10^{-7}$ m/s. The compression strength was highest in the lightweight concrete, about 5.0–5.5 MPa. The Nyströms LECA had slightly higher compression strength than the Beijer LECA; 2.7–2.8 MPa compared to 2.0–2.5 MPa. However, the results for the Nyströms LECA differ from the received specification, which stated that this product has a compressive strength of about 4.5 MPa. In the clogging test the lightweight concrete had an instantaneous pressure buildup in the water supply system and was considered impermeable to the bentonite slurry. The Leca showed an initial slight reduction in hydraulic conductivity and was considered to likely to be able to maintain its draining ability over an extended time.

3.7.5 Recommendations

It is strongly suggested to use the macadam 2–4 mm as a geological draining material. This candidate is clearly superior in terms of its hydraulic conductivity and also seems to maintain its draining ability when exposed to a water flow with high bentonite content.

The geotextile examined seem to clog when exposed to a water flow with a content of eroded bentonite and should therefore not be used to drain the system. However it could function as a distributer of water if manual wetting of the system is required.

Leca is the superior option for use as a stiff draining material in terms of its hydraulic conductivity and seem to maintain its draining ability when exposed to a water flow with high bentonite content. The main concern is the tested compression strength as the result does not correspond to the product specification. There is however not a current specification regarding this parameter in a tunnel seal. It has been assessed that the strength of the Leca beams should be high enough for the installation process i.e. they should be able to withstand the earth pressure from the pellet filling behind the beams. There is an obvious risk that they will break later due to the swelling pressure from the bentonite, but at this time the consequences will be small if any.

4 Scale tests of the sealing and draining function

4.1 Introduction

The concrete plug is a complex structure using both geological and stiff draining materials in combination with a bentonite sealing, concrete beams and a geotextile. A drawing of the updated conceptual design of the plug was shown in Figure 3-1. The tunnel diameter where this construction is ultimately to function is about 5 meters at full scale.

The function of the filter part of the seal (the macadam and the Leca-beams) is to control the water pressure on the inside of the concrete plug, particularly during the initial period while the concrete is still curing. The function of the bentonite sealing is to prevent leakage past the plug that may occur if the water pressure acts directly on the plug and there is no self-sealing component present. The concrete beams separate the bentonite sealing component from the cast concrete plug and work as a mechanical support during its construction and curing.

A laboratory physical model test at a radial scale of 1:20 has been designed in order to test the functionality of the components and the overall plug. A total of six laboratory model tests have been implemented with the following main purposes;

- Demonstrate the function of the draining components (Leca and macadam filter).
- Demonstrate that the bentonite sealing can withstand a water pressure of 5 MPa without leakage.
- Investigate if a bentonite sealing component is needed when using grouted concrete beams.
- Investigate the bentonite sealing function against grouted and non-grouted concrete beams.
- Investigate how the sealing function is influenced by the void space size between the concrete beams.
- Study how fast and how soon a water pressure can be applied to the sealing after water filling of the filter.

4.2 Test description

4.2.1 Test design

The goal of this study was to design a test at a scale 1:20. A tunnel with the diameter of 5 meters will then correspond to a model tube with a diameter of 25 cm. Geometric constraints made it impractical to scale all the components to 1:20 in axial (length) dimension and therefore the axial scale was set to 1:10 instead. The test equipment used consisted of a steel cylinder with a diameter of 25 cm and the tube inside that is chamfered to simulate the tunnel wall friction. Four windows were installed to allow for visual observation of the test. Load cells were also emplaced in both axial and radial direction to allow for measurement of load and calculation of the total pressure. A total of four 6 mm Swagelok-connections were used for wetting, pressurization and drainage of the system.

The inflow rates used in the test were volumetrically scaled i.e. an inflow rate of 4 l/min in full scale corresponds to 0.001 l/min in the scale test.

The assembled equipment is seen in the upper photograph provided as Figure 4-1. In uppermost photo the observation windows, Swagelok connections and the radial pressure transducers (top photo) are all visible. The steel tube has a chamfered inside surface and simulates the deposition tunnel walls (lower right). The axial load cells can be seen between the restraint cap and the cell body (bottom left photo).

Figure 4-2 shows a cross section sketch of the test. The axial load cells (1) are held in place by a steel plate (2) in each end of the tube. The steel plates are fixed by screws to hold all components positioned in axial direction. Two radial load cells (3) are placed towards the backfill and two are placed towards the bentonite sealing. On both sides inside of the axial load cells there is a PVC plate piston (4). On the backfill side the PVC plate piston is sealed with an O-ring (6) to prevent water leakage in that direction. On the plug side the PVC plate piston has no O-ring. The PVC plate piston

diameter is 249 mm (compared to the tube diameter 250 mm) and the slot that emerges represents a non-hardened concrete dome that allows for leakage or piping if exposed to a water pressure build-up. The windows (5) are placed so that bentonite sealing, geotextile, macadam, Leca and backfill can be observed from the outside. The Swagelok connections are placed in the sections marked "I". Two connections, one at the top and one at the bottom, are placed in contact with the macadam filter for draining and pressurization. The other two are connected at the top and bottom of the backfill to simulate the tunnel flow.

4.2.2 Preparation and installation of components

This chapter describes the preparation and installation of each component. The test equipment was placed standing up with the concrete plug end downwards. Figure 4-3 shows the PVC plate piston that represents the concrete plug. This was the first component to be emplaced in the test equipment.

Concrete beams

Concrete was cast into four beams using a standard cement mortar (Weber cementbruk A). The beams were made approximately 30 mm thick. After hardening the beams were carefully shaped to fit the tube. Figure 4-4 shows the beams emplaced in the test equipment.

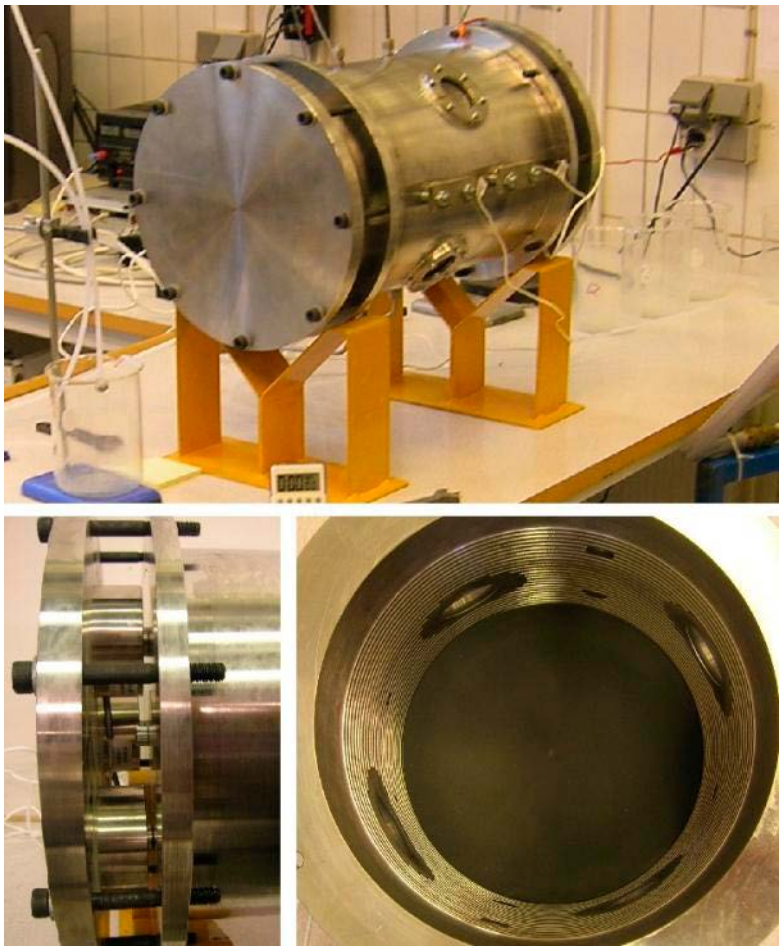

Figure 4-1. *The test equipment.*

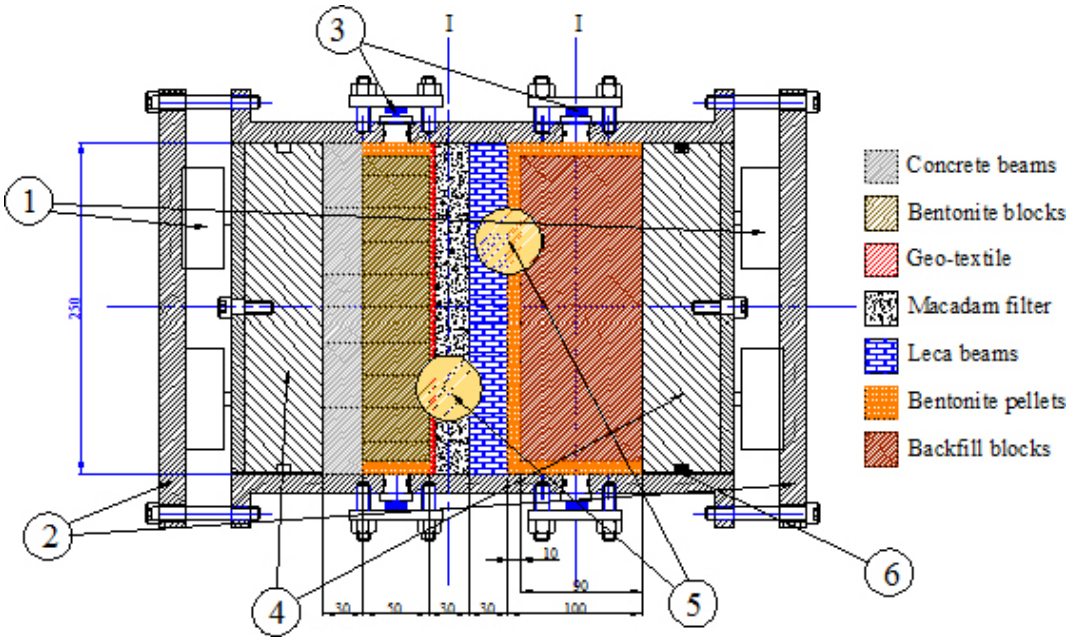

Figure 4-2. *A cross section sketch of the test equipment. The axial load cells (1) are held in place by steel plates (2). Radial load cells (3) are placed on the bentonite sealing and the backfill. There is a PVC plate piston (4) on each side of the components. The PVC plate piston to the left is slightly smaller than the tube and represents a non-hardened concrete dome that allows for leakage. The PVC plate piston to the right is sealed with an O-ring (6) to prevent water from leaking in that direction. On each side of the tube there are two windows (5) showing bentonite sealing, geotextile, macadam, Leca and backfill.*

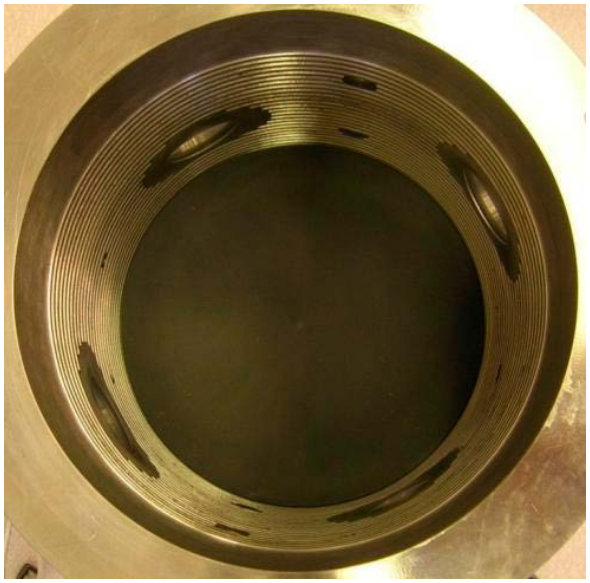

Figure 4-3. *The PVC plate piston that represents the concrete plug was the first component to be emplaced in the test equipment.*

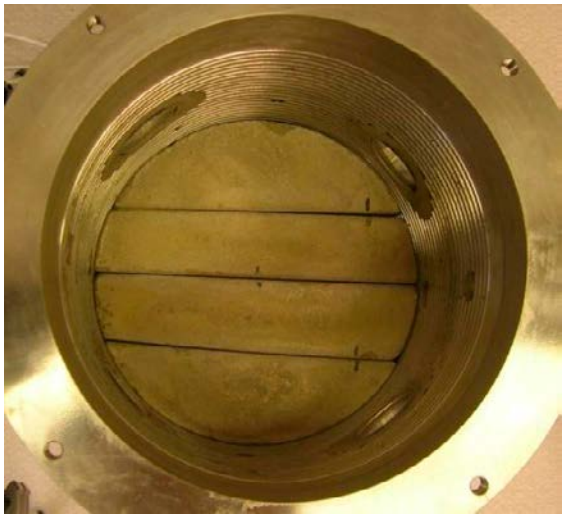

Figure 4-4. *Four concrete beams were cast using a standard cement mortar.*

Bentonite sealing

MX-80 bentonite was used for the manufacturing of sealing blocks. MX-80 is a high grade sodium bentonite from American Colloid Company (Wyoming, USA) with a montmorillonite content of 80% (Karnland et al. 2006). The bentonite sealing blocks were cut out from a larger block. The sealing component was made out of 16 small blocks and had an assembled diameter of 230 mm and a thickness of 50 mm. The blocks were surrounded by a 10 mm slot filled with pellets produced from MX-80 bentonite. Figure 4-5 shows the sealing installed in the test equipment surrounded by pellets. The dry density of the blocks varied slightly (1,790–1,810 kg/m^3), but this will not influence their performance. This block density was used since a number of large blocks were already manufactured and available for use.

Geotextile

A needle felted geotextile from Svenska Geotech AB was used in the test, Appendix 1. The 1,000 g/m^2 quality was selected. It was not possible to scale this component in cell's axial direction. Figure 4-6 shows the geotextile cut to a diameter of 250 mm and placed in the test equipment.

Macadam filter

A 30 mm thick layer of 2–4 mm macadam was placed on top of the geotextile. The macadam was taken from the *AB Sydsten* production site in Dalby. Figure 4-7 shows the macadam emplaced in the test equipment.

Leca beam filter

A standard Leca block was cut to produce four beams, each with a thickness of 30 mm. The beams were then carefully shaped to fit the tube. Figure 4-8 shows the Leca beams emplaced in the test equipment.

Bentonite pellets

The bentonite pellets used in the scale test were manufactured using an extrusion technique where moisture-conditioned MX-80 bentonite was pushed through a matrix. The product is a rod shaped pellet with a diameter of 6 mm and a length of 16–22 mm. The pellets were used both as a cross sectional layer between the backfill blocks and the Leca beams and to fill the outer slot around the backfill and bentonite sealing blocks (as seen in Figures 4-5 and 4-10).

The pellet-filled layer was 10 mm thick (Figure 4-9) and the slots between the bentonite seal (Figure 4-5) and the backfill component (Figure 4-10) were of 10 mm dimension, which was considered the smallest acceptable dimension for this scale of test.

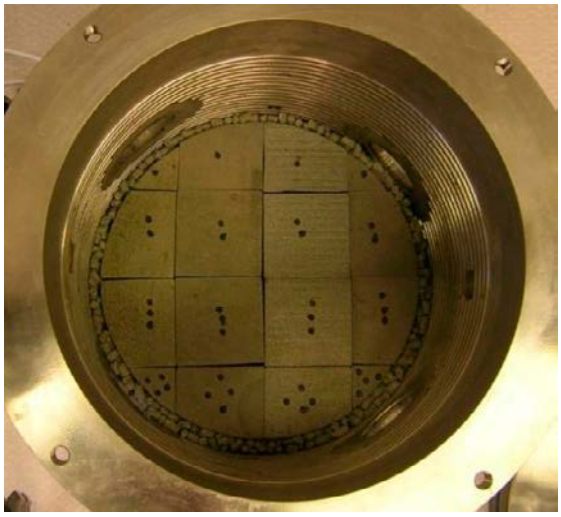

Figure 4-5. *The bentonite sealing was made out of 16 parts and had a diameter of 230 mm and a thickness of 50 mm. The blocks were surrounded by a 10 mm wide, pellet filled slot.*

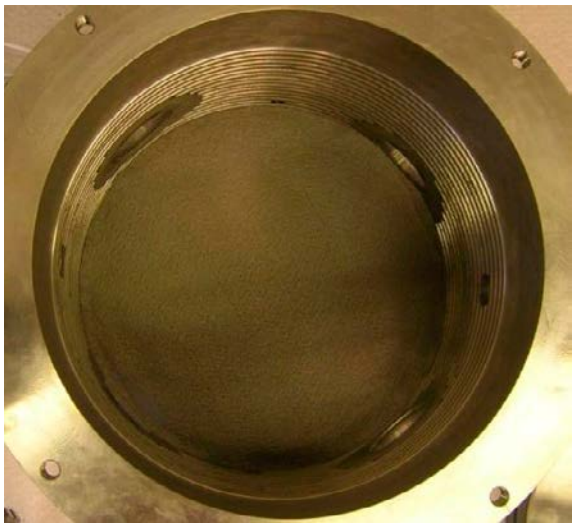

Figure 4-6. *The geotextile cut to a diameter of 250 mm and emplaced in the test equipment.*

Figure 4-7. *The 30 mm layer of 2–4 mm macadam from AB Sydsten emplaced in the test equipment.*

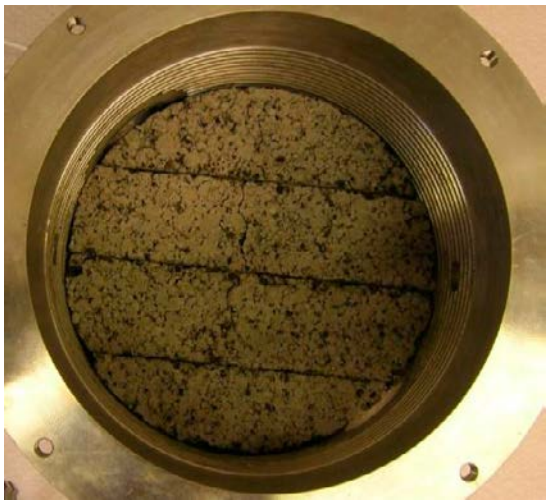

Figure 4-8. *The four 30 mm thick Leca beams emplaced in the test equipment.*

Figure 4-9. *The 10 mm – thick pellet layer between the backfill and the Leca beams. Rod shaped MX-80 bentonite pellets with a diameter of 6 mm were used.*

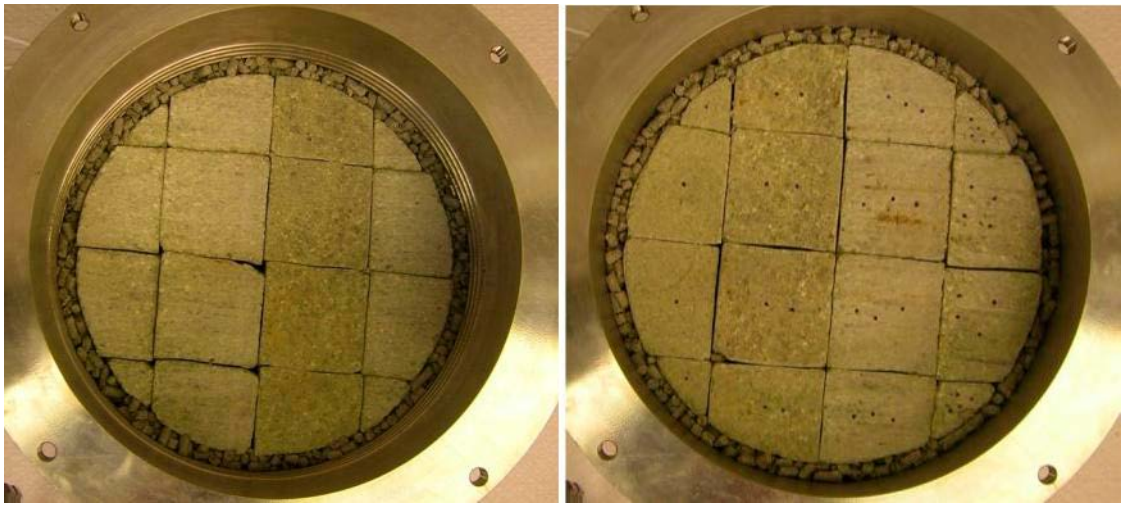

Figure 4-10. *The two 50 mm thick layers of backfill blocks emplaced in the test equipment. The blocks were made of IBECO bentonite from Milos, Greece.*

The small size of the test cell meant that the as-built bentonite pellets were too large for use. Prior to their installation, the pellets were therefore crushed with a rubber hammer and all fines less than 4 mm were separated. This was to reduce the pellet rod length and thereby improve the as-placed pellet density in the relatively thin slots. Figure 4-9 shows the pellet layer between the backfill and the Leca beams. Again, due to the dimensional limitations of the pellet layer and slots in this test setup, the extruded rod pellet material was used instead of the more densely compacted pillow shaped pellet proposed for use in the full-scale construction.

Backfill blocks

IBECO bentonite from the island Milos, Greece, was used for manufacture of the backfill blocks. The material is described by the supplier as a natural calcium bentonite with medium montmorillonite content (Sandén et al. 2014) i.e. it has not been activated or treated in any other way. The blocks were prepared in the same way as the MX80 bentonite blocks. Two 50 mm thick layers consisting of 16 blocks each were made with a diameter of 230 mm. Figure 4-10 shows the emplaced backfill blocks and the surrounding crushed MX-80 extruded pellets.

Water

All tests except Test 1 was performed with tap water mixed to 1% salinity by weight ($NaCl/CaCl_2$, 50/50) i.e. the same type as was used in the laboratory tests described in Chapter 2. Test 1 was performed with tap water.

4.2.3 Additional test equipment

A Grundfos dosing pump (diaphragm type) was used to apply a constant flow of water. The pump flow rate ranges from 0.00125 l/min to 1.0 l/min. The pump manages to provide a constant flow at water pressures up to 1 MPa.

A GDS pressurizing device was used to apply constant pressure and pressure increments. Two different devices were available. The first device had a reservoir volume of about 1.0 liters and a pressure capacity of 2 MPa. The second device had a reservoir volume of 0.25 l and a pressure capacity of 5 MPa. Initially the 2 MPa GDS was used but when 2 MPa of water pressure was achieved the 5 MPa GDS was connected.

4.2.4 Test procedure

The procedure varied slightly from test to test, but in general two phases were performed in every test;

- **Draining/fill-up phase**
  A constant rate of inflow from the dosing pump was applied into the backfill through the bottom Swagelok connection. This flow represented a volumetrically scaled deposition tunnel base flow. The draining function of the filter was tested by allowing the flow to run out through the filter bottom Swagelok connection. Finally the system was filled up by closing the bottom filter Swagelok connection and keeping the top filter Swagelok connection open for air venting. In some of the tests the filter was instantly filled and the draining was done through the top Swagelok connection. The theoretical available volume in macadam filter, Leca filter and macro voids in the pellet fillings is 1.49 liters. For a complete saturation of the system is additional 2.44 liters needed.
- **Pressurizing phase**
  In this phase different strategies were tested to pressurize the filter and test the sealing function of the bentonite sealing. The GDS pressurizing device was used for both constant pressure and pressure elevation steps to test the sealing function of the design.
- **Flow monitoring**
  Water inflow during the drainage period was made with a dosing pump giving a constant flow. The outflows during the drainage period were measured manually by collecting water in a vessel and then weigh it. During the pressurizing period the inflow rate was registered continuously.

4.2.5 Evaluation methodology

Data

During the test total pressure data was obtained using the axial and radial force transducers, photos were taken through the windows and water pressure data was provided by the GDS pressurizing device. In the draining/fill-up phase water pressure was registered by a Druck-transducer connected to the dosing pump. At test dismantling samples were taken primarily in the bentonite sealing regions. Both the test preparation and dismantling were carefully documented with photos.

Component interaction

The photos taken through the windows could tell how the components interacted with each other. Also possible displacement of the components could be observed. In most tests the free drainage from the downstream end of the test assembly was only run for a short time (up to one day) to confirm the function of the components, but in some tests the draining period was longer.

Sealing function

A large part of the evaluation was to determine the properties at which the sealing could hold 5 MPa of water pressure. Dry density profiles were plotted from the samples taken in the sealing. This data was together with measured total pressures/swelling pressures connected to the sealing function. The method of pressurizing was also evaluated in connection to the sealing function.

4.3 Test 1

4.3.1 General

This test was performed as a pilot test to get more acquainted with the equipment. The test was only run to 2 MPa water pressure and the sampling and evaluation of the bentonite was restricted to a dry density profile in the sealing and sampling for water content in both backfill and sealing. A water filling flow rate was selected to represent a full scale tunnel base flow of about 5 l/min. The flow rate was scaled by the filter pore volume relations. The pore volume in the scale test was determined to about 0.02% of the full scale design, which gives a flow rate of 0.001 l/min. This was too low for the Grundfos dosing pump capacity and therefore the GDS was used also for draining and initial filling of the test cell. In this test tap water was used.

The main objectives were as follows:

- Show that all components could be installed properly.
- Show that the equipment was functioning (test container, GDS, connections etc.).
- Confirm that the data assimilation was operating satisfactorily.
- Demonstrate the draining and fill-up function of the macadam-Leca filter.

4.3.2 Results

Timeline summary

The test procedure is described below. Figure 4-11 shows a timeline summary connected to the description below.

- **Day 0–2. Drainage period;** a constant flow rate of 0.001 l/min was applied to the bottom of the backfill. The draining filter is opened in the bottom. The outflow starts after about 12–14 hours and is 90–96% of the inflow (measured to about 0.00090–0.00096 l/min).
- **Day 2–3. Filling up filter;** the bottom connection in the filter is closed and the filter is filled up. The flow rate is temporarily increased to 0.01 l/min but is set back to 0.001 l/min due to observed leakage through the equipment backfill end (It was later discovered that the O-ring had wrong dimensions and it was therefore changed at day 11). The leakage stops as the flow rate is lowered.

- **Day 3–7. Water uptake from burette;** the macadam filter is given access to water from a reservoir connected to the top Swagelok connection, no pressurization.
- **Day 7. Pressure ramp 1 – leakage on backfill side;** a pressure elevation ramp at 100 kPa/hour is applied to the bottom of the macadam filter, all other connections are closed. After about 2 hours leakage is observed through the equipment backfill side.
- **Day 7–14. Water uptake from burette. New O-ring day 11;** the planned ramping of water pressure is cancelled and the burette is reconnected. The sealing O-ring in the equipment backfill end was under dimensioned and is exchanged.
- **Day 14–16. Pressure ramp 2 and 3, leakage through plug;** Pressure ramp 2 is initiated on day 14 at 100 kPa/hour and reaches about 750 kPa before observed leakage through the seal. Pressure ramp 3 is initiated on day 15 at 100 kPa/hour and reaches about 1,100 kPa before observed leakage through the seal**.**
- **Day 16–22. Constant pressure 500 kPa;** a constant water pressure of 500 kPa is applied for about 6 days.
- **Day 22–31. Pressure ramp 4;** the fourth pressure ramp is initiated on day 22 at 100 kPa/hour. The water pressure reaches 2 MPa and the test is terminated.

Data

Figure 4-12 shows the registered axial pressure and the water pressure. An obvious connection between the water pressure and the axial pressure is seen, especially in the pressure elevation ramps. On several occasions the water pressure applied to the macadam-Leca filter exceeded the total axial pressure. This indicates that bentonite sealing and backfill are adhering by friction to the chamfered equipment inside surface. After 11 days the change of the sealing O-ring on the equipment backfill end a drop in total pressure occurred. In the last part of the test, the axial total pressure varies somewhat. It is possible that a volume of air was trapped in the backfill end when the O-ring was changed and this could allow for some creeping displacement of the backfill, which in turn would make the total pressure fluctuate somewhat.

Figure 4-13 shows the radial total pressures and the water pressure. The radial total pressures also seem connected to the water pressure, but not as strongly as the axial total pressure. When the fourth pressure elevation ramp was initiated the total radial pressure in the sealing was 1,000–1,300 kPa including a water pressure of 500 kPa.

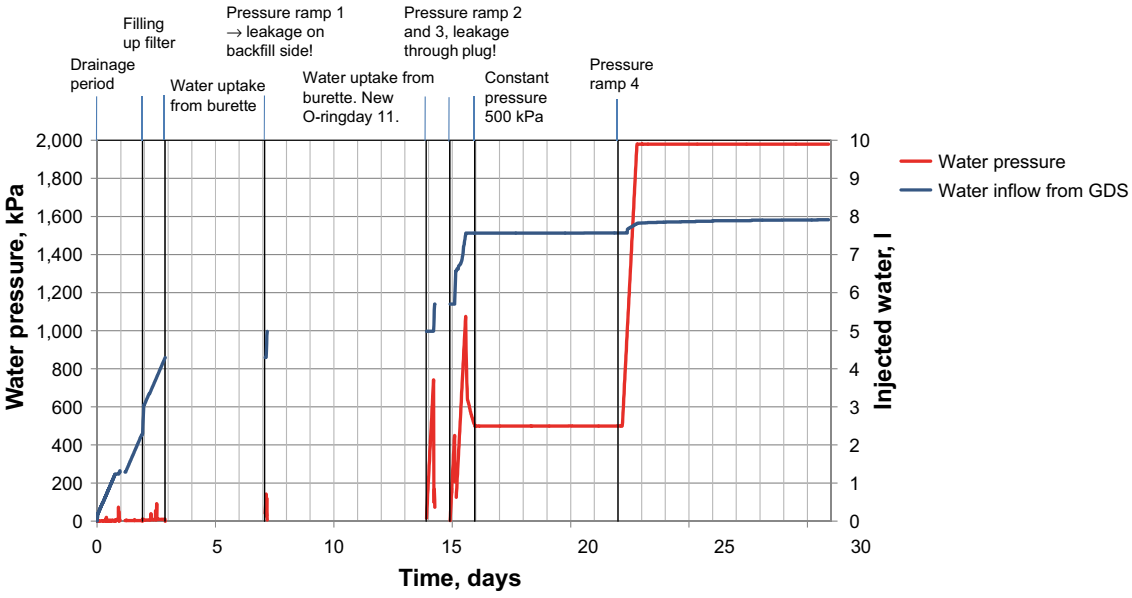

Figure 4-11. *A timeline summary of Test 1. A sealing O-ring on the backfill end of the equipment had to be changed due to leakage. Apart from that the equipment was working satisfactorily. The fourth pressure ramp managed to reach 2 MPa of water pressure and then the test was terminated.*

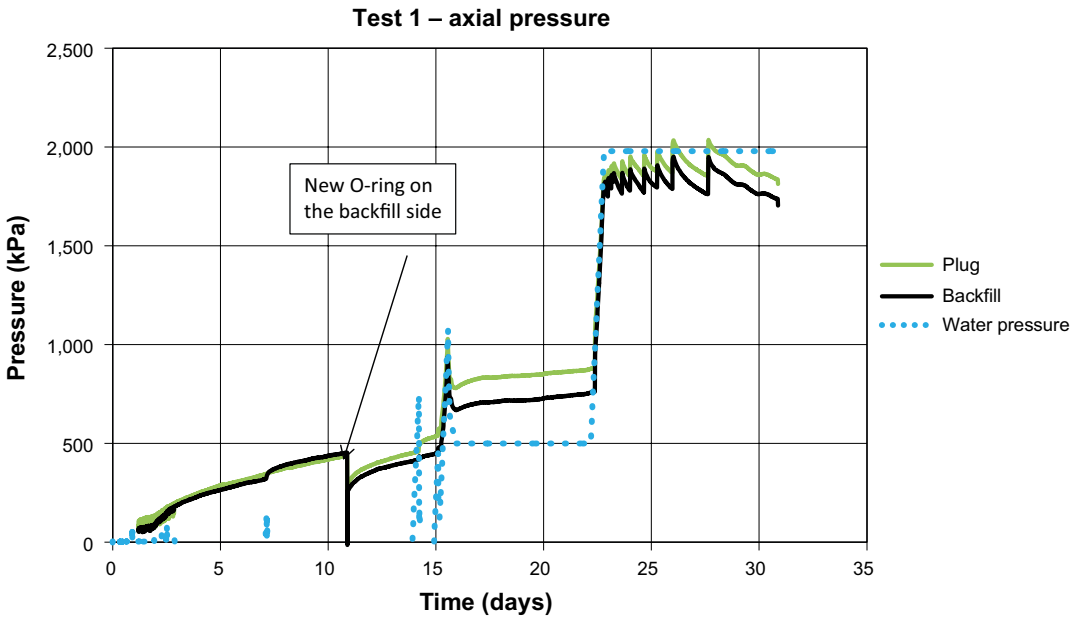

Figure 4-12. *Axial total pressure and water pressure from Test 1. There is an obvious relation between the water pressure and the axial total pressure. Occasionally the water pressure exceeds the total pressure and this indicates that there is significant friction on the chamfered equipment inside. The varying pressure at the end of the test could be explained by creeping motion in the backfill.*

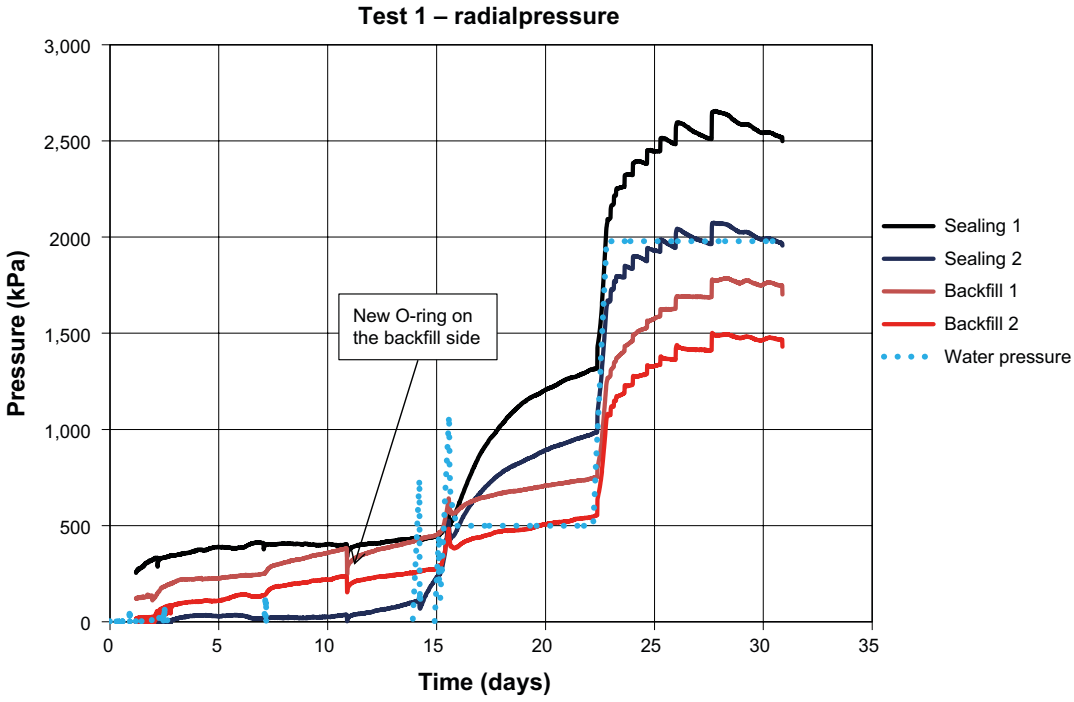

Figure 4-13. *Radial total pressure and water pressure from Test 1. The radial total pressures are not as strongly linked to the water pressures as the axial total pressures. When the final pressure ramp was initiated the total radial pressure in the sealing was between 1,000 to 1,300 kPa, including a water pressure of 500 kPa.*

At test dismantling samples were taken to plot a dry density profile through the bentonite sealing. Figure 4-14 show the dry density and the distance from the concrete beams. The sample is taken in the centre of the sealing. An apparent expansion (in the order of several millimetres), of the originally 50 mm-thick bentonite sealing component has occurred.

Figure 4-15 shows the water content in the pellet-filled section between the filter and the backfill and also the slots surrounding the backfill and sealing blocks. Figure 4-16 shows the water content of the bentonite blocks in the backfill and the sealing. In general the water content is higher in the bottom and lower in the top in both the pellets and the blocks. An exception is the blocks in Section 2 where the bottom sample is the driest.

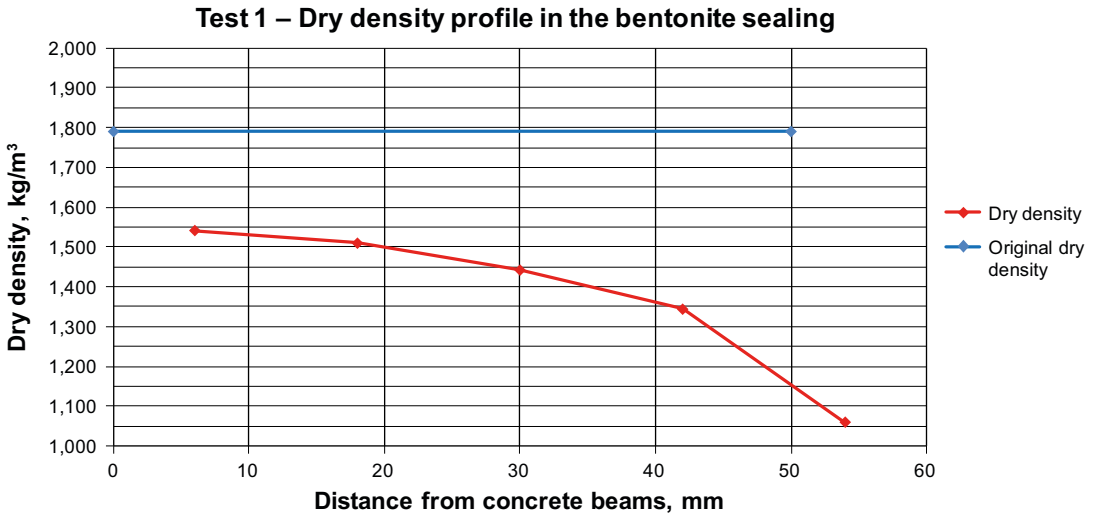

Figure 4-14. *Dry density profile in the bentonite sealing of Test 1 after test completion. The sample is taken in at the centre of the sealing component. An apparent expansion of several millimetres was seen in the bentonite sealing component.*

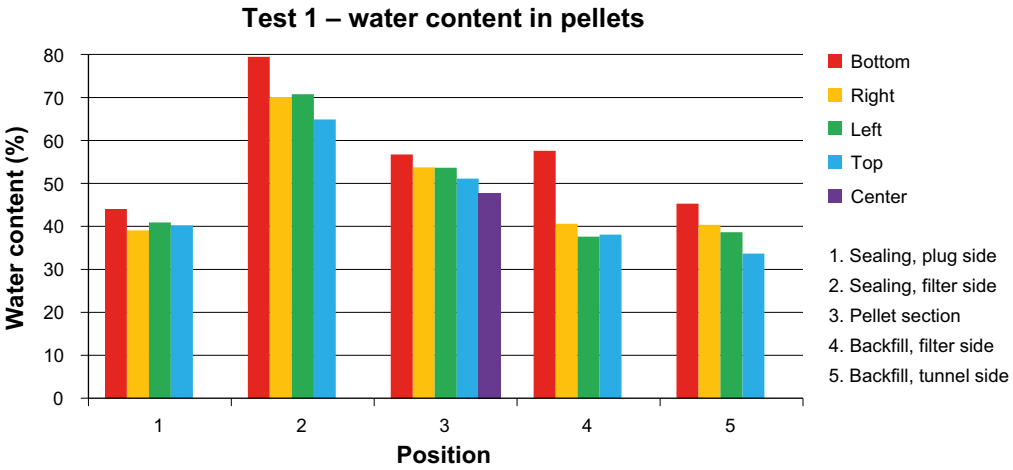

Figure 4-15. *Water content in pellets from Test 1. The water content is higher in the bottom and lower in the top.*

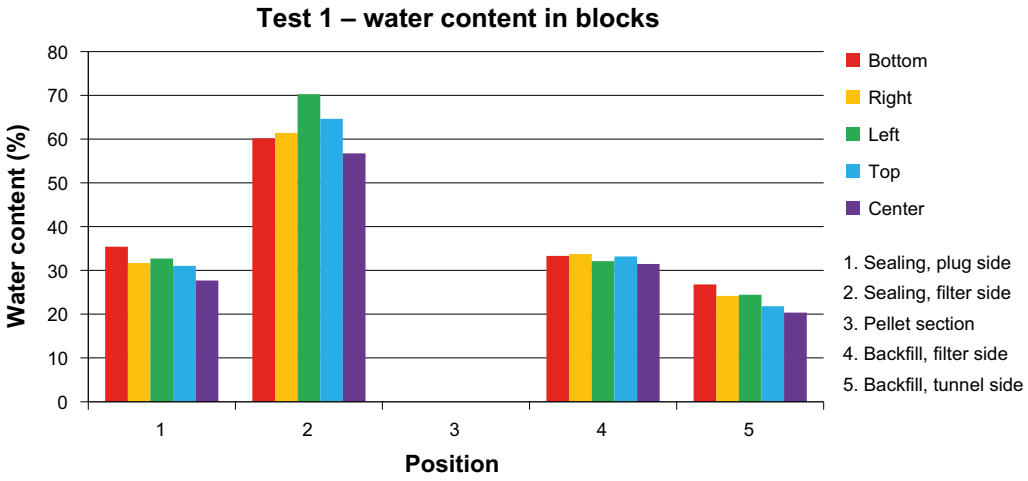

Figure 4-16. *Water content in blocks from Test 1. In general the water content seems somewhat higher in the bottom and lower in the top, with the exception of Section 2 where the bottom is drier.*

Dismantling and visual observations

Figure 4-17 and 4-18 show the view through all the observation windows at test start up and test termination respectively. In windows 1 and 2 the macadam filter, the geotextile and the pellets surrounding the bentonite sealing is visible. When comparing windows 1 and 2 at start up and at termination it is seen that the bentonite sealing segment has swelled and that there has been a displacement of the geotextile and the macadam filter. At test start up in Figure 4-17 the Leca-beams and the pellets surrounding the backfill are seen clearly. In Figure 4-18 at test termination the Leca beams are hardly visible due to backfill bentonite swelling out between the beams and the windows.

The test dismantling started on the backfill side by removing all backfill bentonite until the Leca beams were cleared. Figure 4-19 shows the draining filter seen from the backfill side. One of the Leca beams has been removed and the macadam can be seen. It seems as the Leca beams have separated the backfill bentonite well from the filter, the only observed backfill intrusion into the draining filter occurred between the beams and the windows (windows 3 and 4 in Figure 4-18).

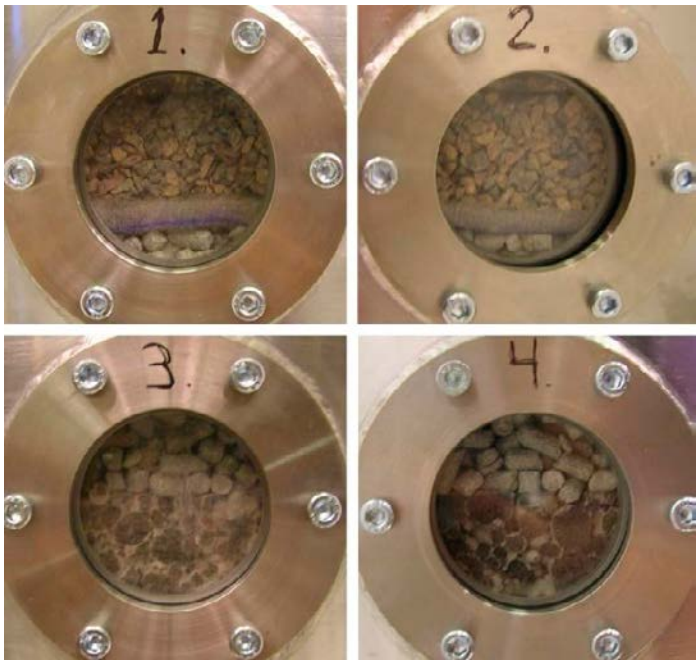

Figure 4-17. *Photos taken at test start up. Windows 1 and 2 shows the bentonite sealing, the geotextile and the macadam filter. Windows 3 and 4 shows the Leca beams and the pellets surrounding the backfill bentonite.*

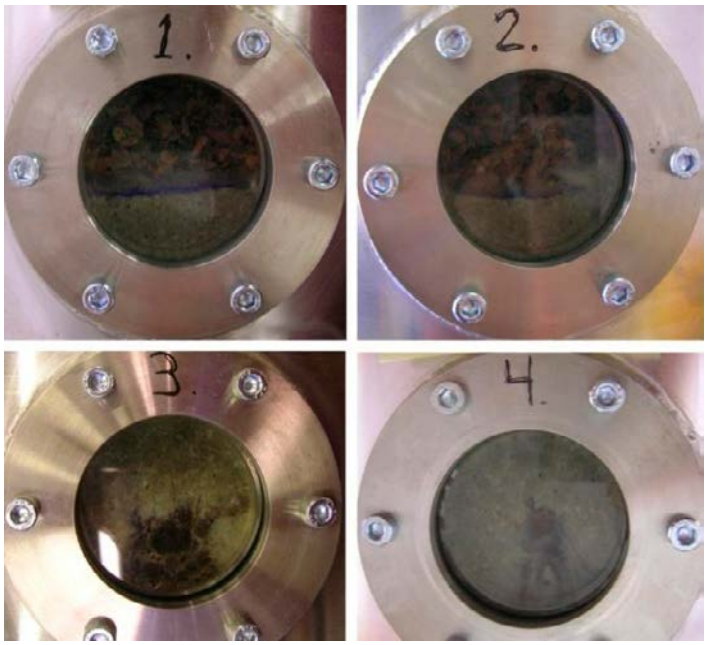

Figure 4-18. *Photos taken at test termination. Windows 1 and 2 shows the bentonite sealing, the geotextile and the macadam filter. Windows 3 and 4 shows the Leca beams and the pellets surrounding the backfill bentonite. The backfill bentonite has swelled out between the Leca beams and the windows.*

Figure 4-19. *The Leca beams and the macadam filter seen from the backfill side. It seems as the backfill bentonite is successfully separated from the draining filter.*

At test dismantling the Leca beams were inspected. Figure 4-20 shows a cross section view of one of the beams split in two. The backfill bentonite was in contact with the upper side of the beam. It looks like bentonite has intruded about half way through the 30 mm thick beam.

Figure 4-21 shows a view of the bentonite sealing from the concrete plug side. In the upper part a concrete beam is removed and the bentonite is visible. In the lower part a concrete beam is still in place. It is clearly seen how the bentonite sealing has swelled into the void space between the beams.

Figure 4-20. *A cross section view of a Leca beam split in two. Backfill bentonite has intruded about half way through the 30 mm thick beam.*

Figure 4-21. *View of the bentonite sealing from the concrete plug side. The bentonite sealing has swelled into the void space between the beams.*

4.3.3 Discussion and conclusions

The main complication of the test was water leaking through the backfill end of the equipment. The O-ring that was supposed to seal the PVC plate piston was under-dimensioned and had to be changed during the test. A part of the test objective was to test the equipment and this malfunction could be successfully corrected.

In the pressure elevation ramping stages, the sealing failed at 750 kPa (ramp 2) on day 14 and at 1,100 kPa (ramp 3) on day 15, so based on the increased pressure required to initiate throughflow, it seems that the sealing ability was improved somewhat despite the piping that occurred. When ramp 2 was initiated the total pressure was about 450 kPa at "sealing 1" and 100 kPa at "sealing 2" and this ramp managed to reach 750 kPa before leakage occurred. When ramp 3 was started the total pressure was still about 450 kPa in "sealing 1" and 200 kPa in "sealing 2". These values are considered to represent the actual swelling pressure since no water pressure is being applied at those times. After failing during the third ramping state, a constant hydraulic pressure of 500 kPa was applied on the sealing component for about six days. During this time the total pressure reached 1,300 kPa at "sealing 1" and 1,000 kPa at "sealing 2". Finally on day 22 a ramp 4 was initiated and successfully reached 2 MPa.

Based on the results and the discussion presented above the following conclusions are made;

- The test components can be installed as designed. The equipment and the data logging system worked satisfactorily, capturing the evolution of the system.
- The draining function of the filter worked as intended. The drainage was measured to about 90–96% of the inflow.

- The backfill bentonite was successfully separated from the macadam filter by the Leca beams. Only some minor intrusion was observed in the space between the beams and the observation windows.
- The bentonite sealing component clearly swelled into the voids between the concrete beams.
- At a radial total pressure of about 1,000–1,300 kPa (including 500 kPa of water pressure) the bentonite sealing section could withstand 2,000 kPa of water pressure without piping occurring.
- Applying a constant water pressure (in this case 500 kPa) on the bentonite sealing seemed to help increase the radial swelling pressure.

4.4 Test 2

4.4.1 General

The material structure of the components used in these scaled tests are unchanged or only little changed (crushing of the pellets) compared to the full scale case. It has been shown in the project "System Design of Backfill" that the water flow rate strongly influences the wetting behavior in pellets, especially at low flow rates (Andersson and Sandén 2012). It was concluded that the flow rate of 0.001 l/min used in Test 1 was too low to provide conservative conditions within the test cell. Therefore it was decided to raise the flow rate somewhat and it was increased to 0.005 l/min for Test 2. At this flow rate the dosing pump could now be used for draining and filling the cell. The water used had 1% salinity (a 50:50 mix of sodium and calcium chloride).

In addition to determining the sealing ability of the test assembly and the effectiveness of the drainage components under the higher inflow conditions, an additional, important part of Test 2 was to investigate if a significant amount of material was lost during the draining period. Therefore monitoring during the draining period was a large part of this test as it allowed determination of erosion. This erosion measurement was accomplished during the draining period by taking, at regular intervals, samples of the outflow water. The amount of dry material in these samples was determined using the same evaporation method as in the System Design of Backfill-project erosion tests (Andersson and Sandén 2012).

In addition to these objectives, it was also planned to make a more extensive analysis of the dry density distribution in the bentonite sealing. Like the previous test, Test 2 was also only run to a maximum of 2 MPa water pressure.

The objectives of Test 2 can be summarized as follows:

- Demonstrate the draining function of the macadam-Leca filter at the higher flow rate (0.005 l/min).
- Investigate if significant amounts of material is lost during draining.
- Undertake extensive end-of-test analysis of the dry density distribution in the bentonite sealing components.
- Complete a test with 1% water salinity that can be compared to previously completed tests using fresh water.

4.4.2 Results

Timeline summary

The test procedure is described below. Figure 4-22 shows a timeline summary for the activity description below.

- **Day 1–10. Drainage period;** a constant flow rate of 0.005 l/min was applied to the bottom of the backfill. The draining filter was open in the bottom and the outflow starts after only 50 minutes. The drainage outflow comes in pulses and this indicates that there is water pressure build up/release. This is confirmed by the registered water pressure which initially varies up to 50–70 kPa but after 5–6 days reaches peaks of more than 500 kPa. A total of 5.75 liters of water was used up during 11 days of drainage and filling testing.

- **Day 10–11. Filling up filter;** the bottom connection in the filter is closed and the filter was filled up and drained from the top Swagelok connection for 24 hours.
- **Day 11. Pressure ramp 1;** day 11 a pressure elevation ramping rate of 100 kPa/h was applied to the bottom of the filter. At about 400 kPa leakage occurred through the seal. The ramping is then ceased and a constant water pressure of 50 kPa is applied.
- **Day 14. Pressure ramp 2;** a second pressure elevation ramping of 100 kPa/h is started on day 14. The pressure reached about 950 kPa before leakage through seal occurred. Ramping is then stopped and a constant water pressure of 100 kPa was applied.
- **Day 21. Pressure ramp 3;** on day 21 pressure elevation ramp 3 of 100 kPa/h was begun. The pressure almost reached 1,050 kPa before leakage occurred through the seal. Ramping was then ceased and an attempt to apply a constant water pressure of 500 kPa is tested but there was still leakage. The pressure was then reduced and is set to 100 kPa with no discernible leakage occurring.
- **Day 31. Constant pressure 500 kPa;** on day 31 the constant hydraulic pressure is increased to 500 kPa.
- **Day 36. Pressure ramp 4;** on day 36, pressure elevation ramp 4 was initiated with 100 kPa/h occurring. The pressure was elevated to 1,000 kPa and then the pressure was held constant.
- **Day 37. Pressure ramp 5;** on day 37 pressure elevation ramp 5 is initiated with 100 kPa/h being applied. The water pressure was raised to 1,500 kPa and then the pressure was held constant.
- **Day 38. Pressure ramp 6;** on day 38 pressure elevation ramp 6 was initiated with 100 kPa/h rate of increase. The pressure was elevated to 2,000 kPa and then the test was terminated.

Data

Figure 4-23 shows the registered axial pressure and the water pressure. Like in Test 1 an obvious connection between the water pressure and the axial pressure is seen, especially in the pressure elevation ramps. It is also seen how the axial pressure on the backfill side responds to the varying water pressure in the drainage period.

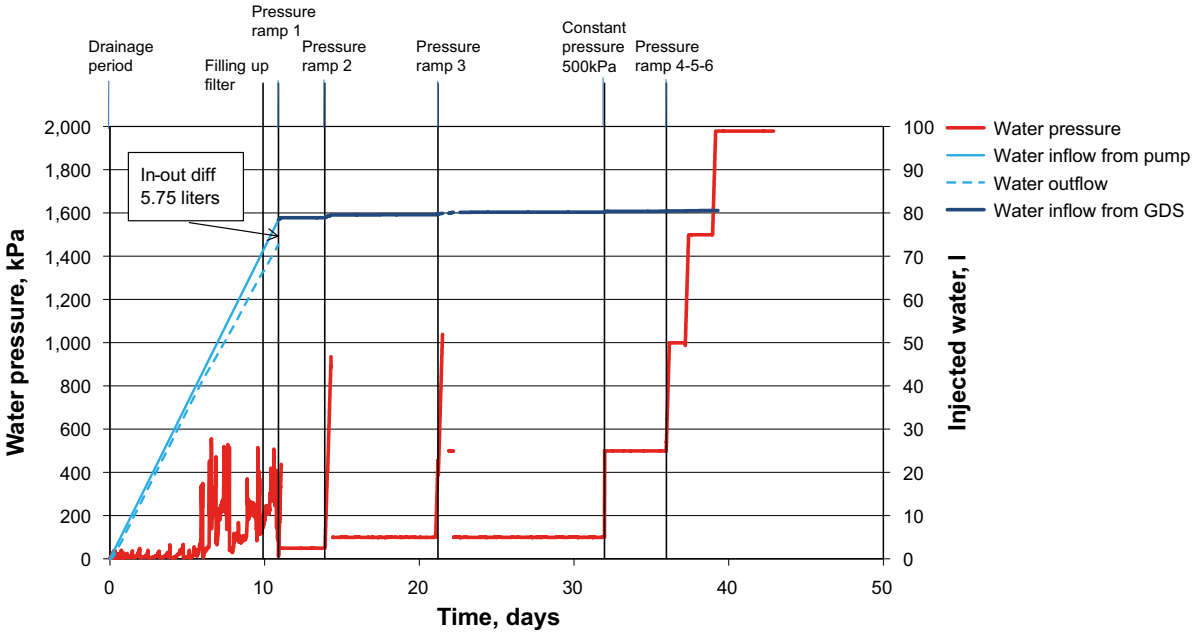

Figure 4-22. A timeline summary of Test 2. The test was started with long draining periods to determine erosion and confirm the filter drainage function at a higher flow rate than Test 1. A number of attempts were performed to elevate the pressure. After about 36 days water pressure ramps 4–5–6 were initiated and eventually 2 MPa water pressure was reached.

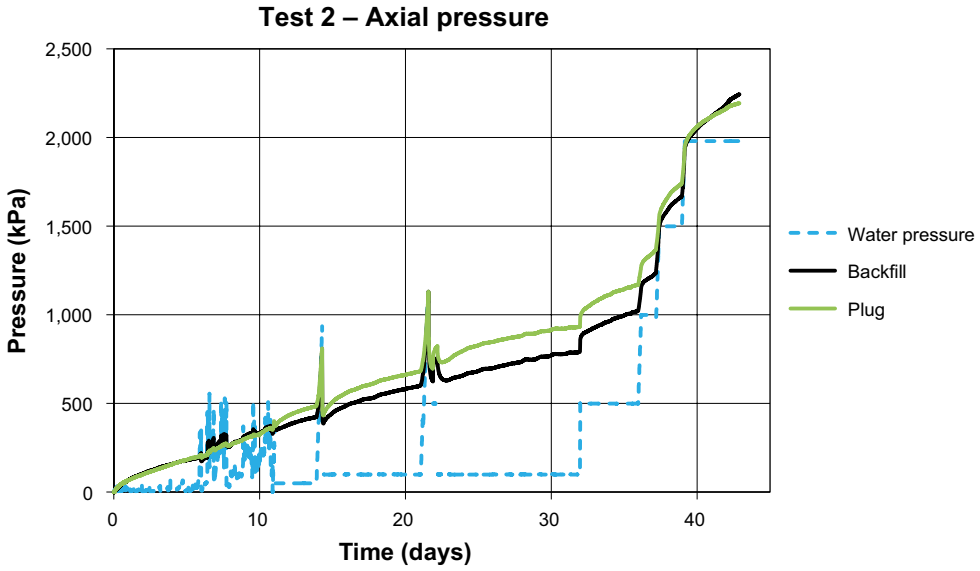

Figure 4-23. *Axial total pressure and water pressure from Test 2. There is an obvious relationship between the water pressure and the axial total pressure. In the drainage period(day 1 to 11) the registered backfill pressure respond rapidly to the water pressure variations.*

Figure 4-24 shows the radial total pressures and the water pressure. The total pressure registered in "Backfill 2" is reacting very closely to the applied water pressure during the first 10 days. The two sensors registering the pressure in the sealing have, however, hardly responded before the first two pressure elevation ramps are initiated. The pellet filling around the sealing blocks seem to have sealed and limited the water inflow to the position of the sensors. On day 21 when ramp 3 is started the total pressure is between 500–700 kPa (100 kPa water pressure included) in the sealing. When ramp 4 is initiated the radial pressure is about 1,000 kPa (100 kPa water pressure included) and the water pressure at the inflow end finally reaches 2 MPa. The radial total pressure in the sealing material was approx. 900 to 1,000 kPa when the pressure elevation that reached 2 MPa was initiated.

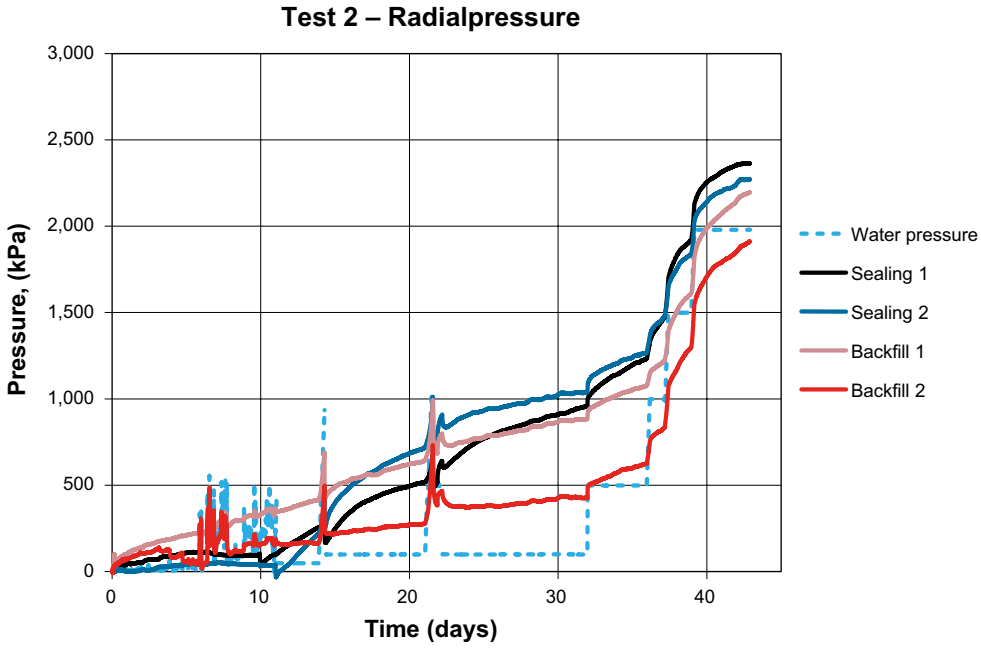

Figure 4-24. *Radial total pressure and water pressure from Test 2.*

At test dismantling, samples were taken to plot a number of dry density profiles through the bentonite sealing section. Figure 4-25 shows the dry density profile in axial directions at five different positions. The bottom, right, left and top samples are taken approximately 6–7 cm from the centre. Figure 4-26 shows the radial dry density profile in four directions. The samples are taken in the cross section 30 mm from the concrete beams. It is seen in Figure 4-26 that the dry density is between 1,250–1,350 kg/m^3 in the outermost parts of the sealing section.

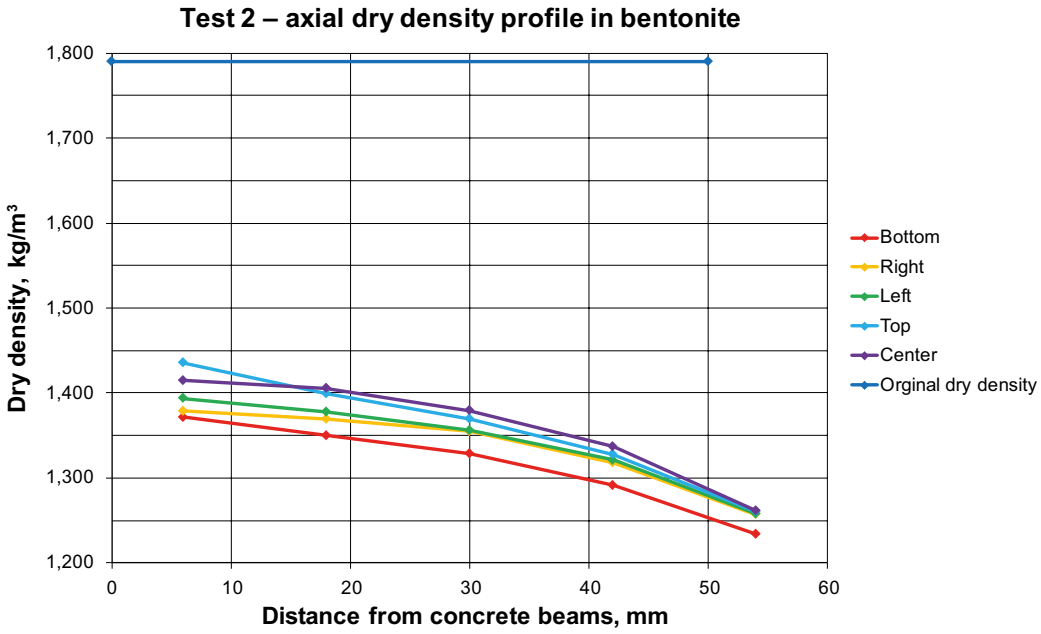

Figure 4-25. *The bentonite sealing dry density profile in axial direction at five different locations. The bottom, left, right and up samples are taken 6–7 cm from the centre.*

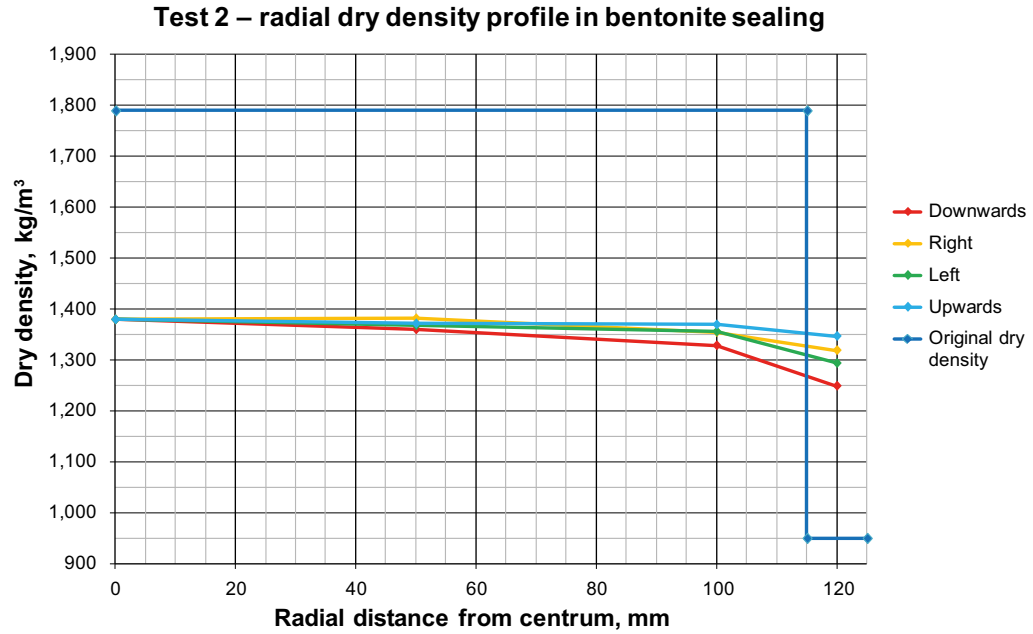

Figure 4-26. *The bentonite sealing radial dry density profile in four different directions. The samples are taken in the cross section 30 mm from the concrete beams.*

The amount of material determined in the outflow during the drainage period is plotted as a function of accumulated flow in Figure 4-27. With exception of the first sample the concentration is less than 1 g/l in all samples. In Figure 4-28 the accumulated eroded material is estimated by extrapolating the bentonite concentrations in the outflow over its corresponding time interval. The straight black lines in the figure show a model that describes the expected maximum and minimum accumulated eroded material (Sandén and Börgesson 2010). The total amount of eroded material is about 30 g by the end of the drainage period (about 70 liters accumulated outflow).

In Figure 4-29 the water contents of the bentonite pellets in the slots are plotted. The water content is somewhat higher closer to the filter section.

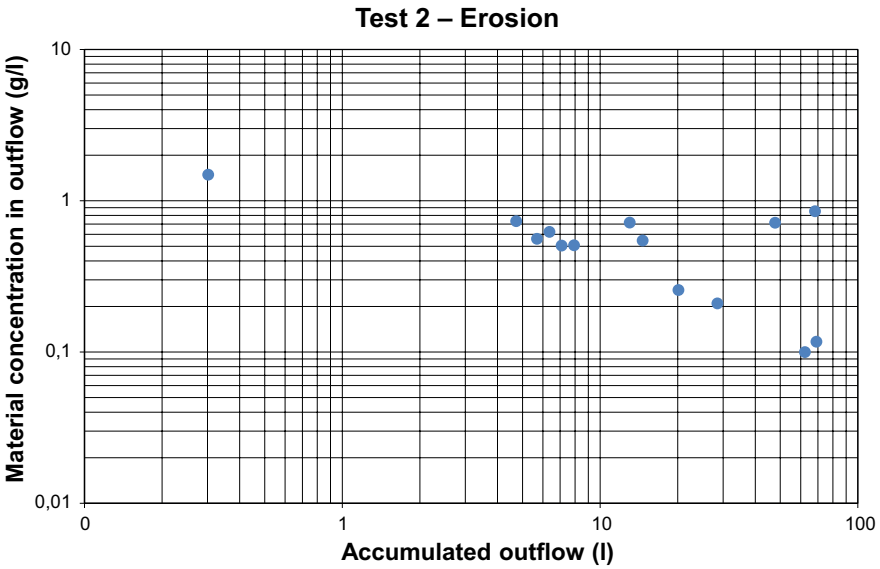

Figure 4-27. *The determined erosion in the outflow of Test 2. With exception of the first sample the material concentration in the outflow is less than 1 g/l.*

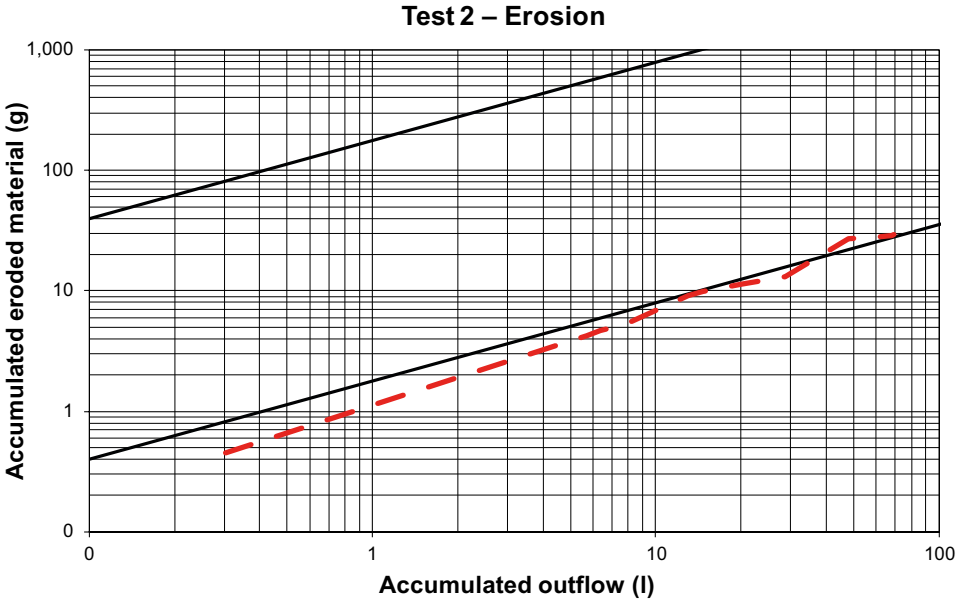

Figure 4-28. *The estimated accumulated eroded material and the accumulated outflow from the drainage period of Test 2. The measured outflow concentrations are extrapolated over their corresponding time interval to estimate the total amount of eroded material. The straight black lines in the figure show a model that describes the expected maximum and minimum accumulated eroded material (Sandén and Börgesson 2010).*

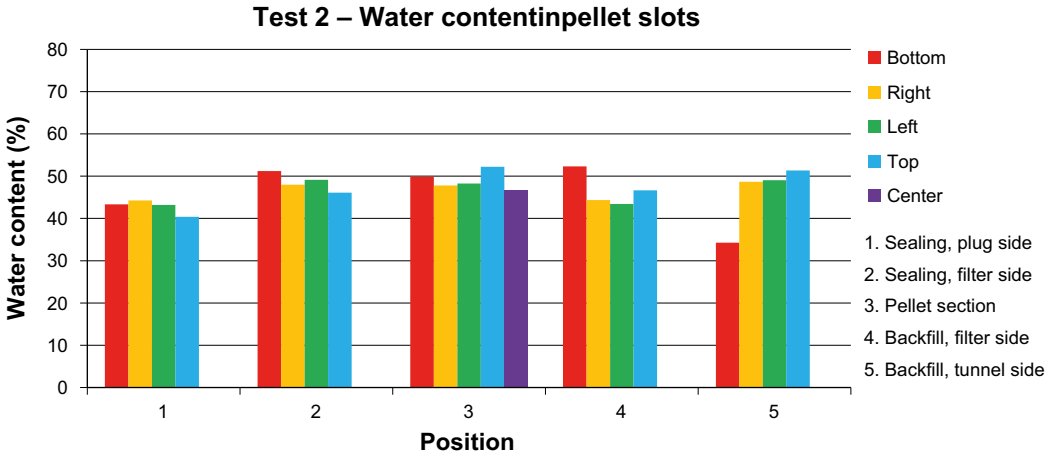

Figure 4-29. *Water content in the pellet slots.*

Dismantling and visual observations

Figure 4-30 and 4-31 shows the view in the windows at test start-up and dismantling respectively. It looks like there has been about the same displacement of the components as in Test 1, several millimeters towards the backfill end. The bentonite intrusion between the Leca-beams and the windows seem somewhat more extensive in this test. In Window 1 it is also seen how bentonite has intruded into the macadam filter. This is confirmed at dismantling. In Figure 4-32 it is clearly seen that there is bentonite present in the macadam filter. This may be a result of the Leca-beam not being so well fitted towards Window 3, which is on the same side as Window 1 were the bentonite intrusion is observed.

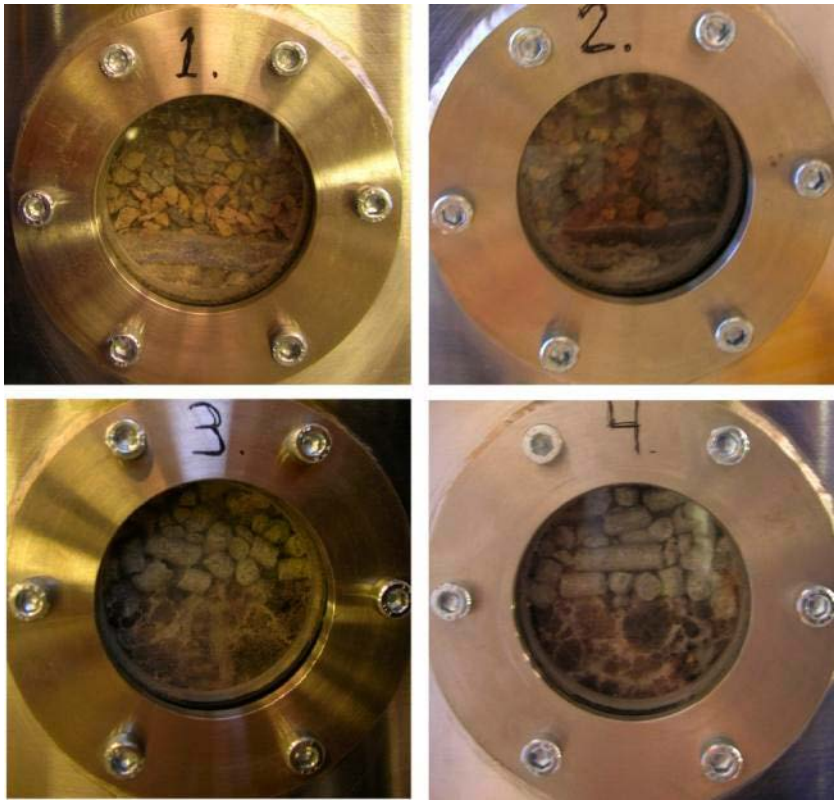

Figure 4-30. *Photos taken at test start up. Windows 1 and 2 shows the bentonite sealing, the geotextile and the macadam filter. Windows 3 and 4 shows the Leca beams and the pellets surrounding the backfill bentonite.*

Figure 4-31. *Photos taken at test termination. Windows 1 and 2 shows the bentonite sealing, the geotextile and the macadam filter. Windows 3 and 4 shows the Leca beams and the pellets surrounding the backfill bentonite. The backfill bentonite has swelled and intruded into the space between the Leca beams and the windows. Window 1 seems to show that the bentonite intruded all the way into the macadam filter.*

Figure 4-32. *The Leca-beam and macadam filter at test dismantling. Bentonite has intruded into the macadam filter to the right (Window 1 side). It is likely that the bentonite intrusion occurred between the Leca-beams and the windows.*

4.4.3 Discussion and conclusions

The draining of the system was tested for a long time period at the new higher flow rate (0.005 l/min) and functioned well. Erosion samples were taken throughout the entire drainage period and the erosion rate was initially about 1 g/l and then decreased. This rate of loss is considered low as the amount of eroded material is in the lower region or below what the model describes.

The radial swelling pressure was responding quite late in the tests. On day 21, when starting the third pressure elevation ramp, the radial total pressures were only 500–700 kPa (100 kPa water pressure included) and the bentonite sealing leaked at about 1,050 kPa. On day 32 the radial total pressure had increased to about 1,000 kPa (100 kPa water pressure included) in the sealing section. The final pressure elevation was initiated and 2 MPa of water pressure was reached.

At the time of dismantling, the bentonite sealing was sampled and dry density profiles were plotted. As expected the dry density was lowest in the outermost parts. The section against the equipment inside (were the pellet slot was initially), had reached a dry density of 1,250–1,350 kg/m^3 and this seems to be sufficient to withstand a water pressure of 2 MPa.

It was also seen through the windows that the backfill bentonite hade intruded past the Leca-beams. Through Window 1 it was possible to see bentonite that had reached into the macadam filter. At dismantling it was seen that bentonite was present in the macadam filter on the Window 1 side. This had probably happened due to the Leca-beam not being well enough fitted to the window.

The Test 2 results can be summarized as follows:

- The draining function of the filter works satisfactorily at 0.005 l/min inflow rate.
- The erosion of material in the draining period is not considered significant. An average erosion rate of less than 1 g/l is observed at 0.005l/min.
- At day 31, a radial total pressure of approx. 1,000 kPa (100 kPa water pressure included) was registered for the bentonite sealing. At this time the water pressure was started to be increased up to 2 MPa. The total pressure after the water pressure increase was determined to approx. 2.2–2.3 MPa.
- Backfill bentonite had intruded all the way into the macadam filter, likely due to bad fitting of the Leca-beams towards the windows.

4.5 Test 3

4.5.1 General

In Test 3 0.005 l/min flow rate and 1% water salinity was used. The test main objective was to reach 5 MPa of water pressure at the inflow end of the chamber without a piping failure occurring. A significant difference in the conduct of the drainage period was that the filter was prefilled and the draining was done through the filter upper Swagelok connection. This way the bentonite sealing was given full access to water from the start of the test. It was also decided to try a pressure elevation ramping rate of 50 kPa/h instead of 100 kPa/h. The exact position of the sealing was also measured in axial direction when the test was prepared. Then the exact expansion of the sealing could be measured at dismantling. The voids between the concrete beams were also inspected in the test preparation. The largest void/slot between the concrete beams was measured to about 0.80 mm. The test three main objectives are listed below:

- Filter fill-up at test start to gave the bentonite sealing access to water directly.
- Reach a water pressure of 5 MPa.
- Test a pressure elevation ramp at 50 kPa/h.
- Measure the axial expansion of the bentonite sealing.

4.5.2 Results

Timeline summary

The test procedure is described below. Figure 4-33 shows a timeline summary connected to the description below.

- **Day 1–4. Fill-up and drainage period;** a constant flow rate of 0.005 l/min was applied to the bottom of the backfill. The draining filter was closed in the bottom and opened at the top. The drainage outflow comes in pulses and this indicates that there is water pressure build up/release. This is confirmed by the registered water pressure which occasionally has peaks close to 500 kPa. About 2.74 liters of water was taken up by the system during the four days of fill-up and drainage.
- **Day 4–5. Pressure ramp 1;** on day 4 a pressure elevation ramp of 50 kPa/h was applied to the bottom of the filter. Right before the water pressure reaches 500 kPa some leakage occurred through the sealing. The ramping was then ceased and a constant water pressure of 50 kPa was applied.
- **Day 5–6. Pressure ramp 2;** on day 5, pressure elevation ramp 2 of 50 kPa/h was initiated. The water pressure reached close to 800 kPa before leakage occurred through the sealing.
- **Day 6–11. 500 kPa constant pressure;** a constant water pressure of 500 kPa was applied to the filter for about 5 days.
- **Day 11–15. Pressure ramp 3;** on day 11 a third pressure elevation ramp of 50 kPa/h was initiated. The water pressure reached 5 MPa by the end of day 14. The test was then terminated.

Data

Figure 4-34 shows the registered axial total pressure and the water pressure. Figure 4-35 shows the radial total pressures and the water pressure. Like in Test 2, the total pressure in "Backfill 2" followed the water pressure very close in the drainage period and it looks like the water pressure is acting directly on the transducer. Around day 4 the radial total pressure was about 450–500 kPa in the sealing (including a water pressure of less than 50 kPa). After the first pressure elevation ramping (which almost reached 500 kPa before leakage) the radial total pressure drops to about 200 kPa in "sealing 2" but slowly increases to about 450 kPa again within one day. On day 5 the second pressure elevation ramp was initiated. Leakage occurred through the bentonite sealing at about 800 kPa inflow water pressure and a reduced constant pressure of 500 kPa was then applied. During these actions it did not seem like the water pressure affected the radial total pressure very much. After 5 days of 500 kPa constant pressure the final ramp that reached 5 MPa was initiated. At this point the radial total pressure was between 750–950 kPa including the 500 kPa water pressure.

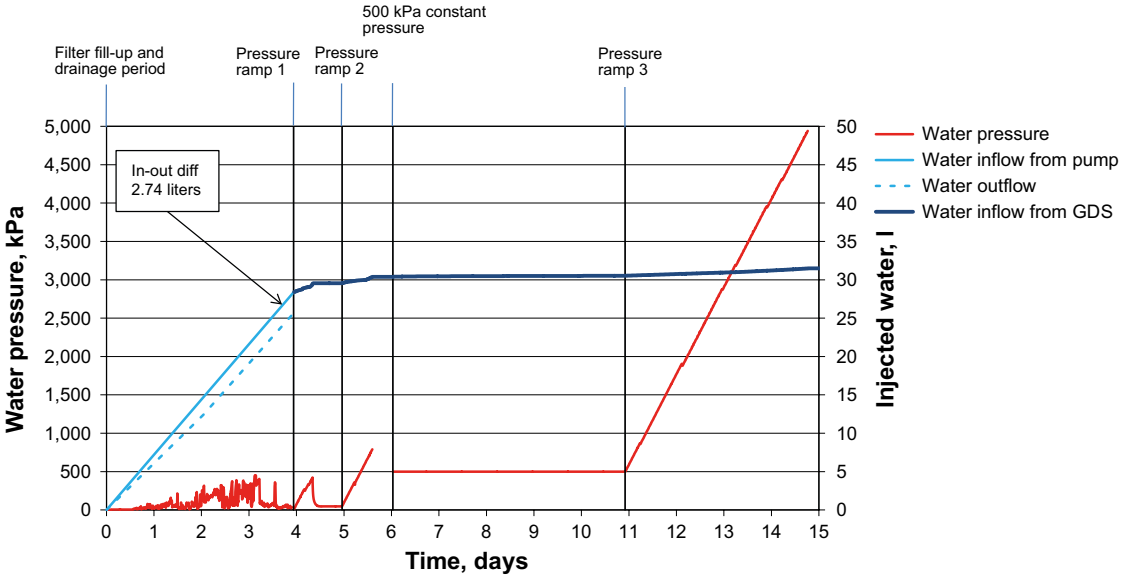

Figure 4-33. *A timeline summary of Test 3. The test was started with shorter drainage period than Test 2. A number of attempts were performed to elevate the pressure and after about 11 days, ramping phase 3 was initiated at 50 kPa/h and eventually 5 MPa water pressure was reached.*

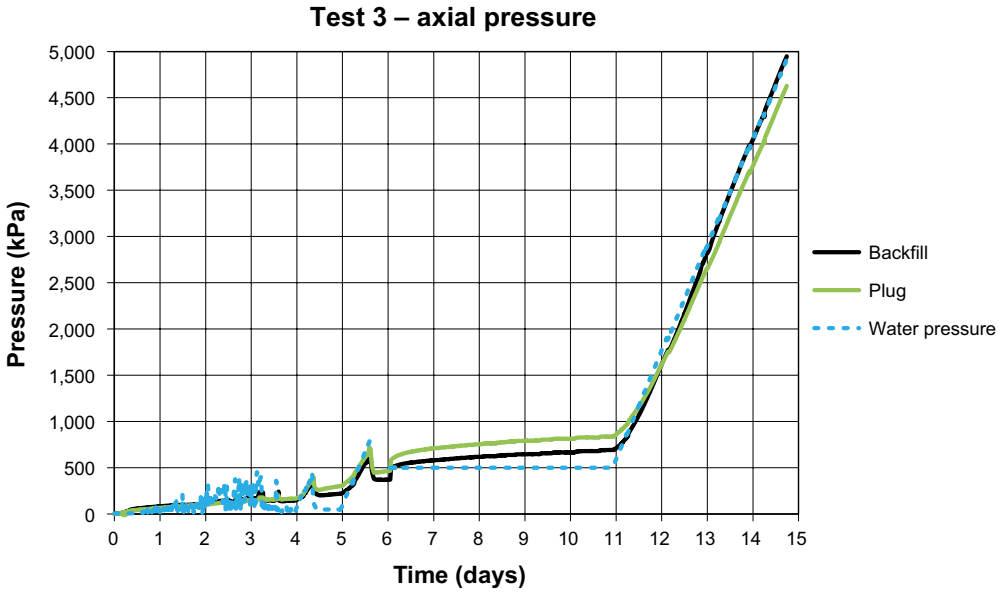

Figure 4-34. Axial total pressure and water pressure from Test 3.

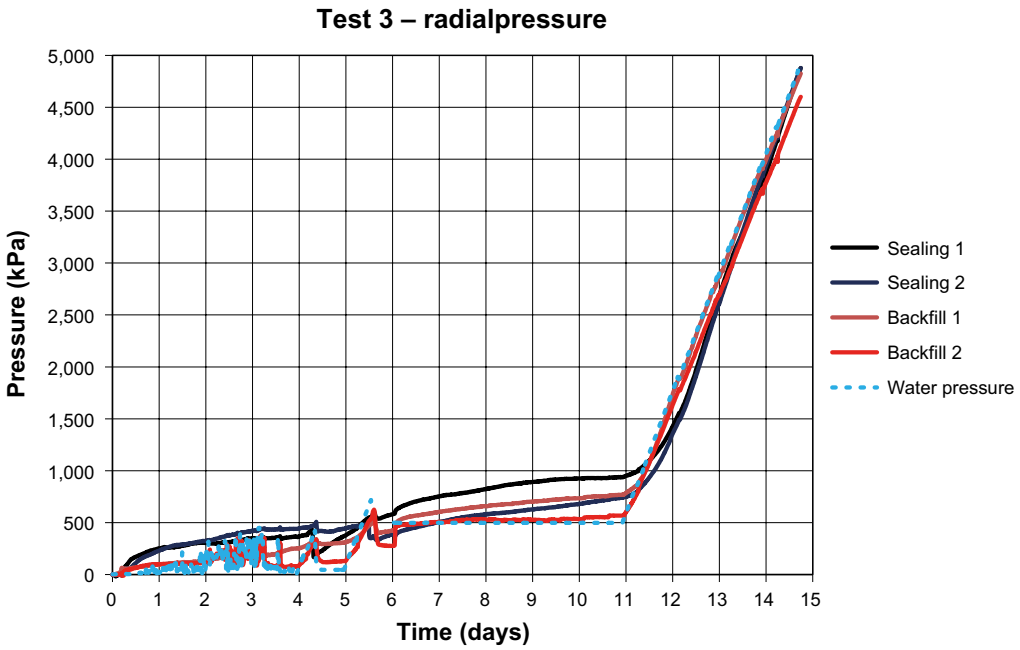

Figure 4-35. Radial total pressure and water pressure from Test 3. The water pressure seems to act directly on the "Backfill 2" sensor. The radial total pressure in the sealing was between 750–950 kPa (including 500 kPa water pressure) when the final pressure ramping to 5 MPa was initiated (day 11).

Figure 4-36 shows the axial dry density profiles taken in five different positions at dismantling. The bottom, right, left and top samples are taken approximately 6–7 cm from the centre. On the concrete beam side the dry density is between 1,440–1,530 kg/m^3. On the filter side the density has decreased to about 1,250 kg/m^3. Figure 4-37 shows the radial dry density profiles. The samples are taken in the cross section 30 mm from the concrete beams. The dry density is lowest in the outermost parts were it is 1,310–1,350 kg/m^3.

For this test the water content was only determined in the backfill pellets. Figure 4-38 shows the backfill pellets water content. As expected the water content is higher in the bottom and closer to the filter.

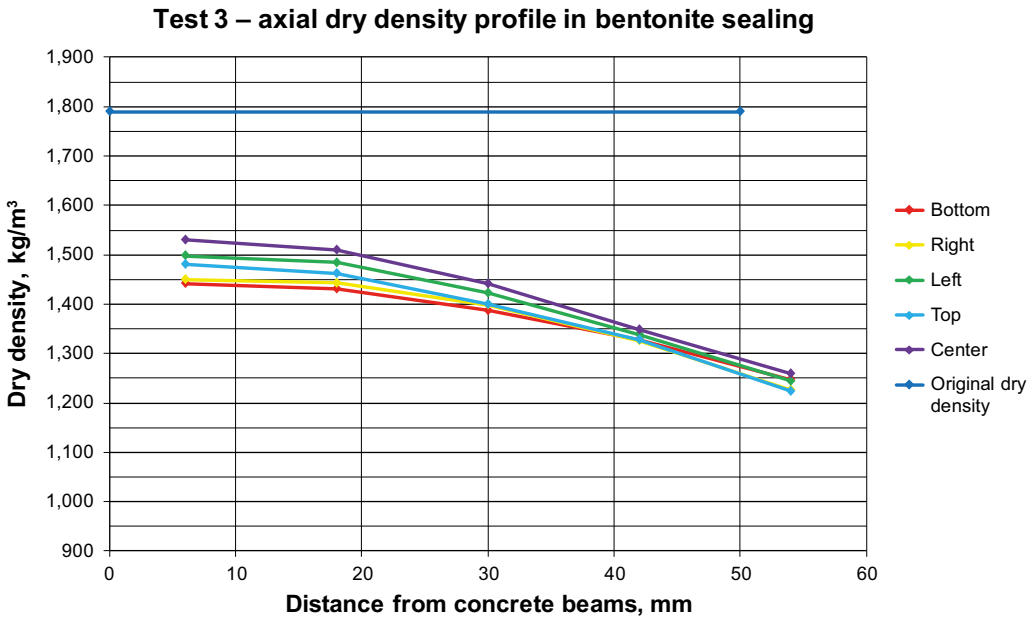

Figure 4-36. *Axial dry density profiles at five different positions in the bentonite sealing. The bottom, left, right and up samples was taken 6–7 cm from the centre.*

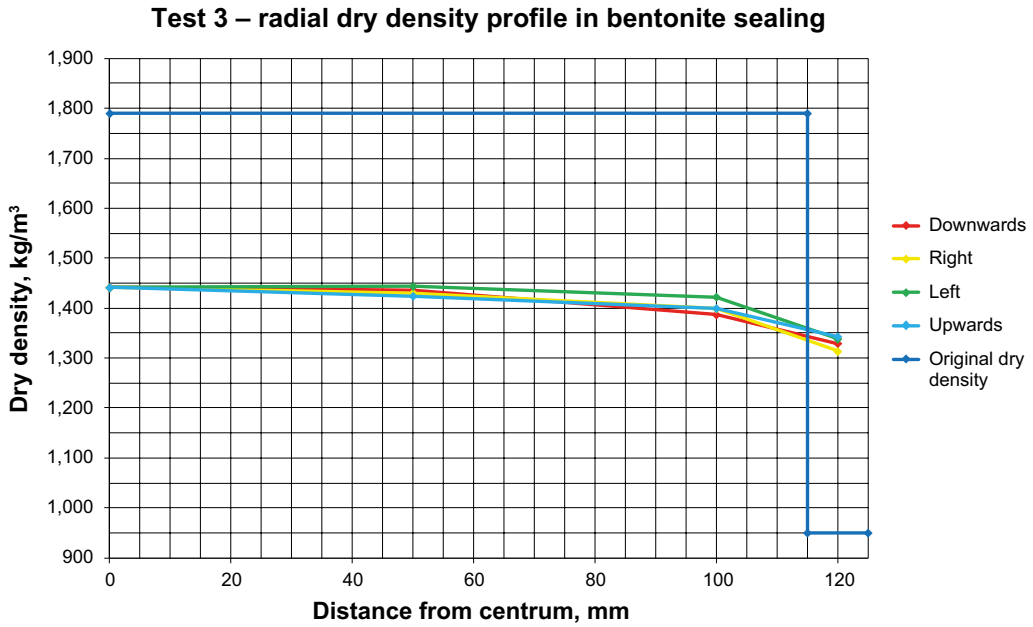

Figure 4-37. *Radial dry density profiles in the bentonite sealing taken in four directions. In the outermost parts the dry density is 1,310–1,350 kg/m^3. The samples are taken in the cross section 30 mm from the concrete beams.*

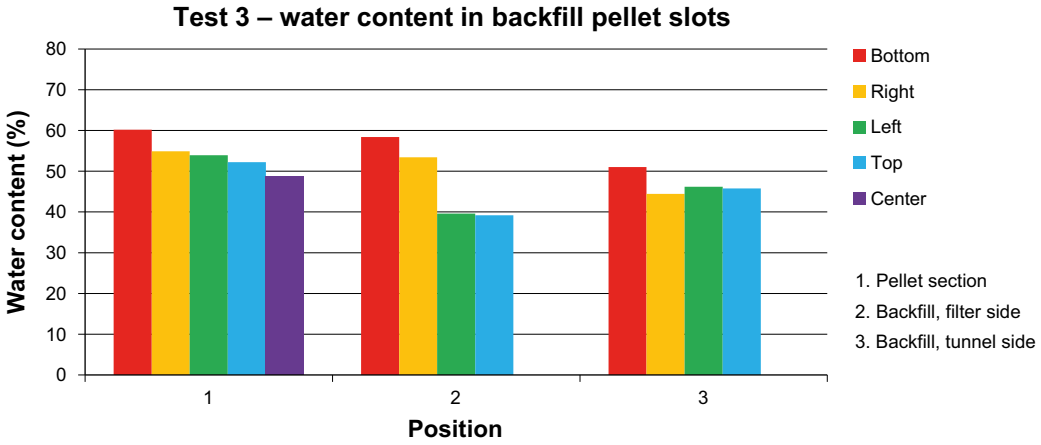

Figure 4-38. *Water content of the backfill pellet slots.*

Dismantling and visual observations

As mentioned above, the sealing axial position was accurately determined at time of test preparation. This was done by placing thumbtacks on two sides and measure the distance from these to the steel tube equipment end. The thumbtacks and the sealing at dismantling are seen in Figure 4-39. The distance was 228/230 mm at test start and 221/224 mm at test dismantling. The axial expansion is thereby determined to 6–7 mm which corresponds to 12–14%.

In Figure 4-40 and 4-41 the view in the windows are seen at test start up and dismantling respectively. The measured displacement of 6–7 mm seems to consist with the visual observations in window 1 and 2. The same backfill bentonite intrusion that was observed in Test 2 has occurred again. In Figure 5-8 it is seen (especially in Window 4) how the backfill has intruded past the Leca-beams. Some bentonite can also be seen in the macadam filter (Window 1 and 3).

4.5.3 Discussion and conclusions

Test 3 was performed with two major differences compared to previous tests; the filter was instantly filled-up at the start of testing and the pressure elevation ramping had a rate of 50 kPa/h instead of 100 kPa/h. This may very well be the explanation why the sealing of the assembly occurred relatively fast in this test. The water pressure was also elevated all the way to 5 MPa. The radial total pressure was however surprisingly low at the initiation of the final pressure elevation ramp. In Test 2 the radial total pressure was about 1,000 kPa, including 100 kPa of water pressure. In this test the radial total pressure was about 750–950 kPa, including water pressure of 500 kPa which means that the swelling pressure is at least between 250 and 450 kPa. The dry density of the outermost parts of the sealing was very similar to Test 2, about 1,310–1,350 kg/m^3. It is thereby shown that the sealing can manage a water pressure of 5 MPa at this dry density.

The largest void spaces between the concrete beams were measured to be about 0.80 mm, or less. In the previous tests the size of the void spaces was not determined but more attention was paid in Test 3 in terms of fitting the concrete beams tightly and so minimizes the voids between them. This has likely contributed to the sealing function in the design.

The axial expansion of the bentonite sealing was determined to 12–14%. This expansion is likely a result of compression primarily in the geotextile and the pellet section next to the backfill. The volume of this expansion would cause the dry density to drop from the original 1,790 kg/m^3 down to 1,539–1,575 kg/m^3, if the bentonite was completely homogenized. If we also consider some additional radial expansion into the pellet slot this is consistent with the determined dry densities in Figure 4-36.

A similar intrusion of backfill bentonite into the filter section as in Test 2 was observed also in this test. However it does not seem to affect the function in the filter and the test outcome in any way.

Figure 4-39. *The bentonite sealing and the thumbtacks used to measure the axial expansion. The sealing expanded about 6–7 mm in axial direction which corresponds to about 12–14%.*

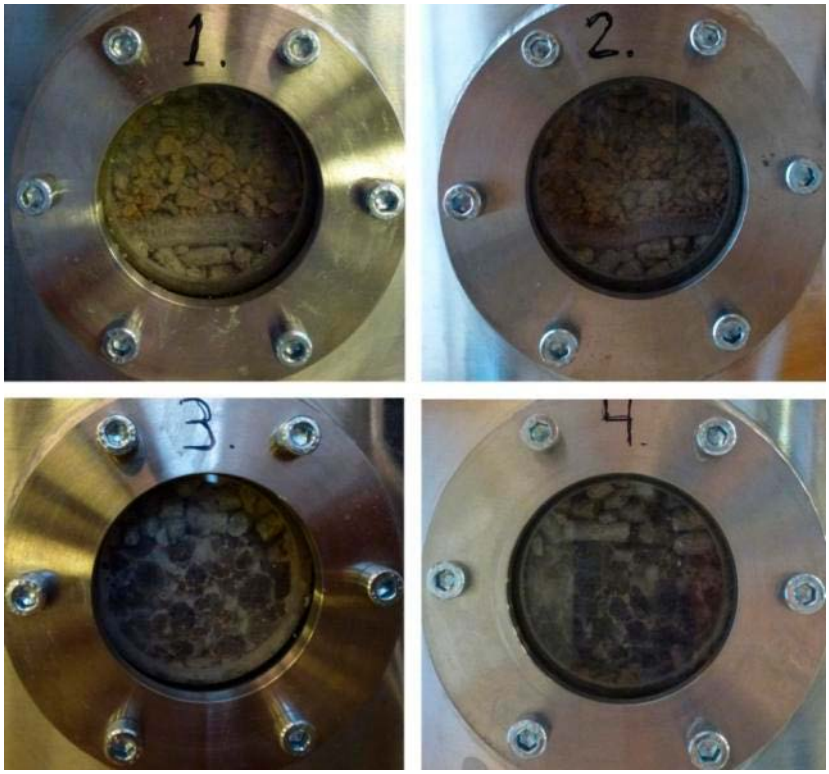

Figure 4-40. *View through the windows at test start up.*

Figure 4-41. *View through the windows at test dismantling. There is bentonite intrusion from the backfill past the Leca-beams into the macadam filter.*

The conclusions of Test 3 are as follows:

- 5 MPa water pressure was reached after 14 days on the third pressure elevation ramp attempt. At this point the outermost part of the sealing had a dry density of 1,310–1,350 kg/m^3. The radial total pressure in the sealing was about 750–950 kPa (500 kPa water pressure included) at the time of the final ramp.
- A 50 kPa/h water pressure elevation ramp seems to work better than a 100 kPa/h ramp.
- It seems important to give the bentonite sealing access to water as early as possible.
- It is suggested that small void spaces between concrete beams improve the sealing function significantly.
- The axial expansion of the bentonite sealing was about 6–7 mm.

4.6 Test 4

4.6.1 General

Test 4 persisted of two parts – Test 4A and Test 4B. In both tests the concrete beams were cast with concrete from the inside to minimize the void spaces between them. In Test 4A a water pressure elevation ramp was applied on the concrete beams without any bentonite sealing present. This was to investigate what water pressure the cast concrete beams would withstand without a bentonite sealing component. Test 4B was fully prepared with all components and performed according to the normal routine but with a slightly more aggressive approach in the pressurization. The filling and drainage period was shortened to about 20 hours and the strategy was to raise the water pressure rapidly with pressure elevation ramps of 100 kPa/h.

The concrete beams before and after molding are seen in Figure 4-42. The molding was performed identically in both Test 4A and 4B using 0.5 liters of wet cement. After hardening the cement thickness was 10 mm.

Figure 4-42. *The concrete beams in Test 4A and 4B were cast with cement to minimize all void spaces between the beams.*

The Test 4 objectives are listed below:

- Comparison of sealing function in cast concrete beams with and without bentonite sealing.
- Investigate if the bentonite sealing ability is improved with reduced void spaces between the concrete beams.
- Try a more aggressive approach in Test 4B with pressure elevation ramping of 100 kPa/h and a short fill-up and drainage period.

4.6.2 Results

Test 4A

In Test 4A all components except the concrete beams and the in-situ casted cement were left out and instead the entire equipment was filled with macadam. The sealing PVC plate piston was placed in the backfill end and a water pressure elevation ramp was applied directly on the cast concrete beams through a Swagelok connection. A 500 kPa/h pressure elevation ramp was used and at 30–35 kPa water pressure leakage was observed. This only took about four minutes.

Test 4B – timeline summary

The test procedure is described below. Figure 4-43 shows a timeline summary connected to the description below.

- **Day 0–1. Filling and drainage period;** a constant flow rate of 0.005 l/min was applied to the bottom of the backfill. The draining filter was closed in the bottom and opened at the top. The fill-up and drainage period only lasted for about 20 hours and the water uptake was determined to 2.29 liters.
- **Day 1–5. Pressure ramp 1–7;** during the following four days a total of seven pressure elevation ramping attempts at 100 kPa/h were made. The highest ramping sequence reached a water pressure close to 2 MPa on day three (ramp 6) before leakage occurred and the water pressure was again decreased. In ramp 7, day five, the pressure is instantly raised to 1,500 kPa but then leakage occurred quite quickly.
- **Day 5–7. Manually stepped pressurization: 200–500–1,000–1,500 kPa;** the pressure was raised in large single increment pressure steps and reached 1,500 kPa before leakage.
- **Day 7. Leakage at 1,500 kPa;** when leakage was observed at 1,500 kPa the pressure was lowered to 1,000 kPa.

- **Day 7–11. Leakage at 1,000 kPa, 500 kPa constant pressure;** leakage was still observed at 1,000 kPa and the water pressure was lowered to 500 kPa. This pressure was kept for about five days without any observed leakage.
- **Day 11–13. Pressure ramp 8;** on day 11 pressure elevation ramp 8 was initiated at 100 kPa/h.
- **Day 13. Window leakage;** during pressure ramp 8 there was some leakage through Window 1. The first time the test was quickly paused and the window was successfully sealed. But at about 4,500 kPa water pressure the windows started leaking again and the test was terminated.

Test 4B – data

Figure 4-44 shows the registered axial total pressure and water pressure. Figure 4-45 shows the radial total pressures and water pressure. The backfill total axial pressure is somewhat higher than in the sealing through the entire test. It is likely that the water pressure is working directly on the backfill end of the test tube.

On day 3 after a number of pressure elevation ramp attempts the radial swelling pressure is about 400 kPa in the sealing. This is right after pressure elevation ramp 6 and no water pressure is working on the sealing. On day 11 when pressure elevation ramp 8 is initiated the radial total pressure is about 1,250–1,400 kPa in the sealing (500 kPa water pressure included).

Figure 4-46 shows the axial dry density profiles taken in five different positions at the time of dismantling. The bottom, right, left and top samples are taken approximately 6–7 cm from the centre. On the concrete beam side, the dry density is between 1,380–1,450 kg/m^3. On the filter side the density has decreased to about 1,180–1,300 kg/m^3. Figure 4-47 shows the radial dry density profiles. The samples are taken in the cross section 30 mm from the concrete beams. The dry density is lowest in the outermost parts where it is 1,250–1,290 kg/m^3.

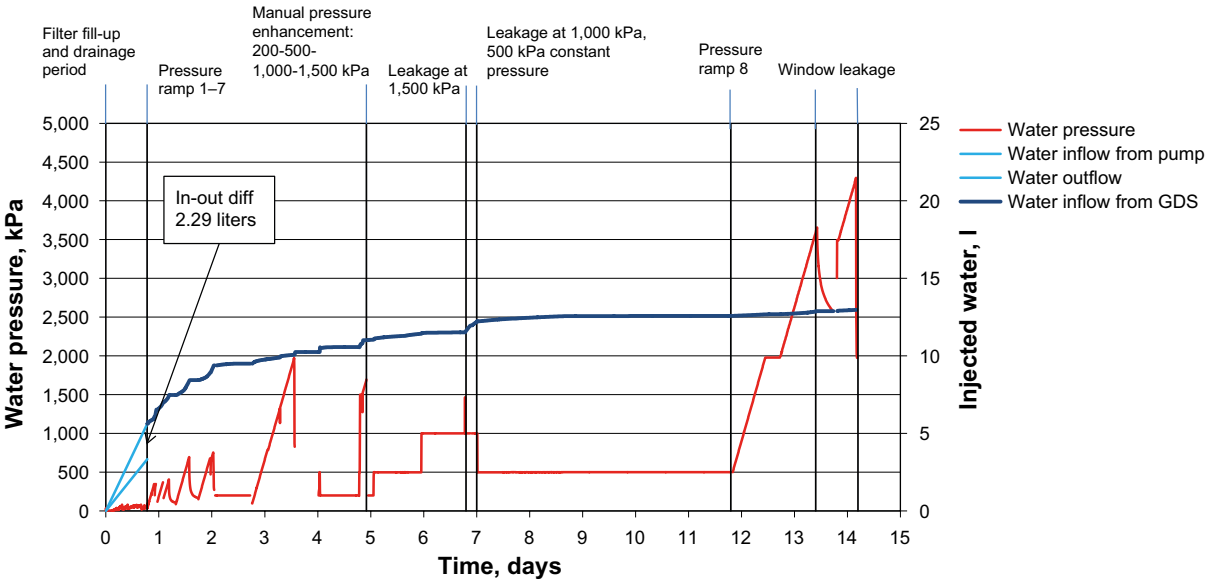

Figure 4-43. *Timeline summary of Test 4B. The initial filling and drainage period was only 20 hours. After about 12 days pressure elevation ramp 8 was initiated and the water pressure was raised to about 4,500 kPa before Window 1 started to leak and the test was terminated.*

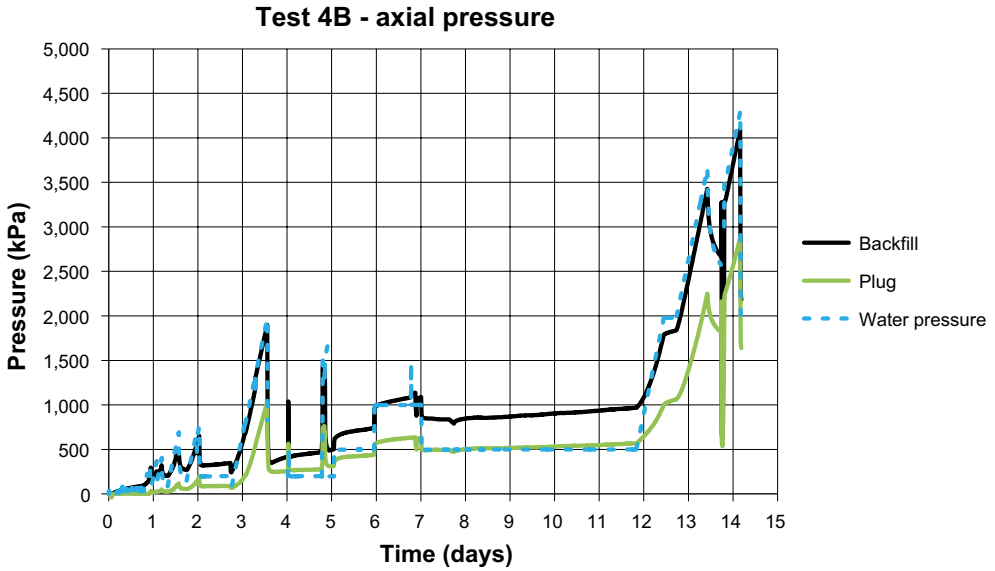

Figure 4-44. *Axial total pressure from Test 4B. The backfill total pressure is higher through the whole test, probably because of the water pressure working directly on the backfill end of the test tube.*

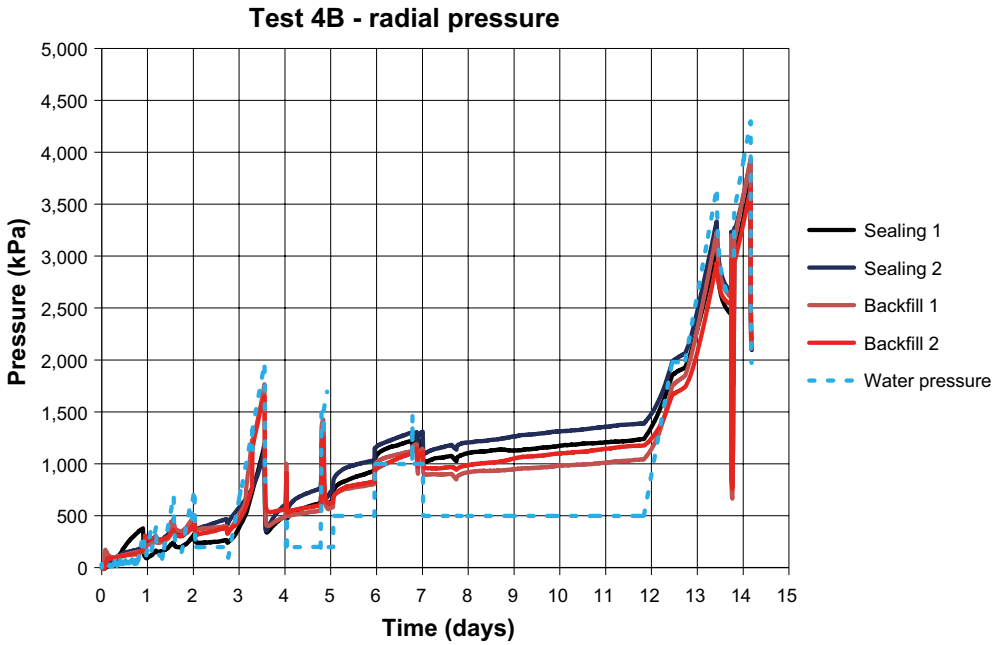

Figure 4-45. *The radial total pressure in Test 4B. After about 3.5 days there is no water pressure present and the radial total pressure is approx. 400 kPa in the sealing material. After 11 days the radial total pressure in the sealing has increased to 1,250–1,400 kPa, including some contribution from the 500 kPa water pressure being supplied at the cell inflow.*

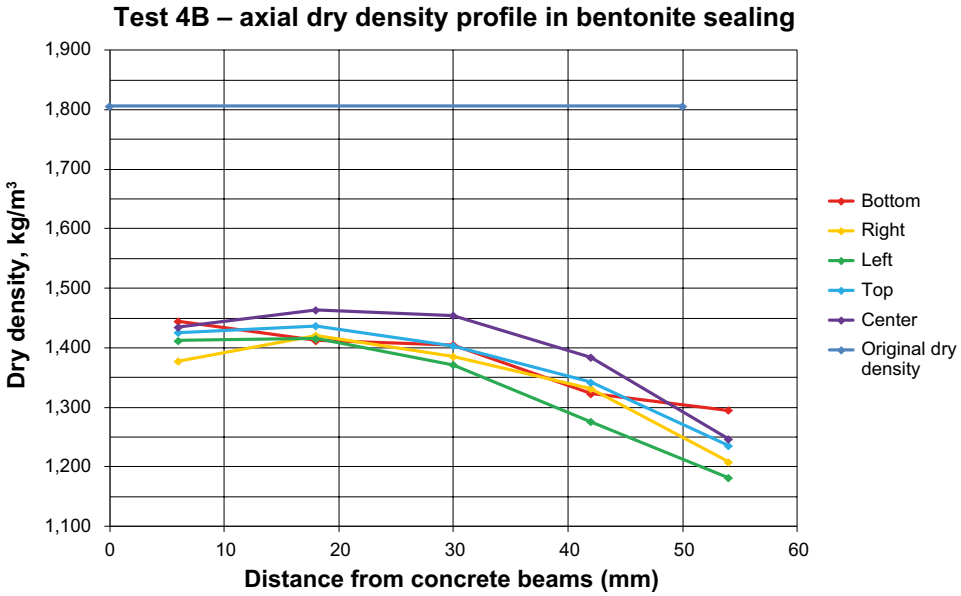

Figure 4-46. *Axial dry density profiles at five different locations in the bentonite sealing. The bottom, left, right and upper samples are taken 6–7 cm from the center.*

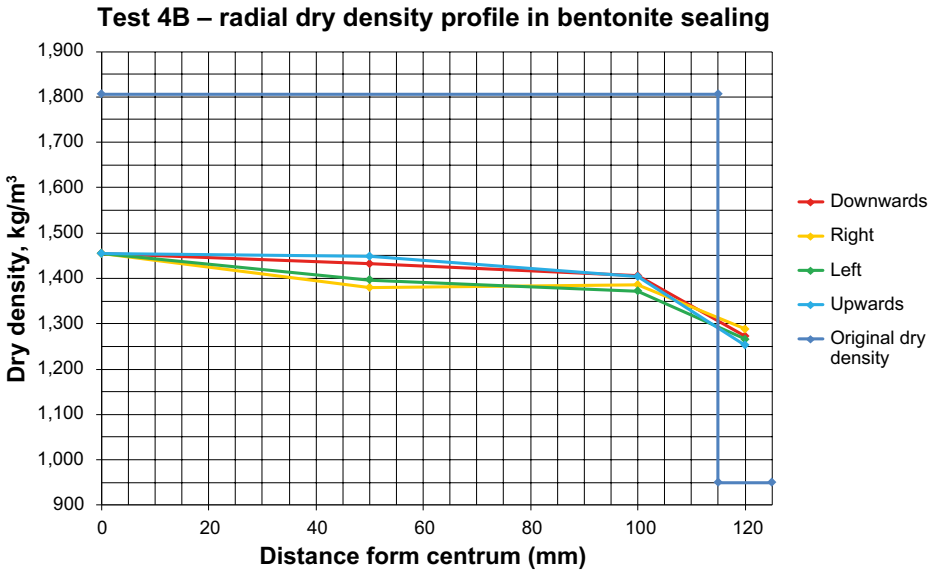

Figure 4-47. *Radial dry density profiles in the bentonite sealing taken in four different directions. The dry density in the outermost parts is 1,250–1,290 kg/m³. The samples are taken in the cross section 30 mm from the concrete beams.*

Test 4B – dismantling and visual observations

Figure 4-48 shows how the bentonite sealing section was excavated. The concrete beams were first taken out from the plug side of the equipment. A ring of the cast cement against the equipment chamfered inside was left in place and finally the bentonite sealing was carefully removed from the filter side. The objective was to leave the cast cement intact towards the chamfered inside surface to allow for a good visual inspection to be made.

Figure 4-49 shows a close-up example of the cast cement outermost part. There were no visible traces of piping or leakage seen at dismantling.

Figure 4-48. *Dismantling of Test 4B. LEFT: First the concrete beams were removed from the outside. MIDDLE: The outermost part of cast cement was left in place to be able to make observations from the inside once the bentonite sealing was removed. The bentonite sealing is seen in the centre. RIGHT: The bentonite sealing was removed carefully from the filter side.*

Figure 4-49. *Example of the cast cement outermost part. The outer edge was visually inspected. No visible traces of piping or leakage were observed.*

4.6.3 Discussion and conclusions

In Test 4A the leakage was almost instant; the cast concrete beams could not withstand any significant water pressure and leakage was observed already at 30–35 kPa. The water leaked out in the interface between the in-situ casted cement/concrete beams and the test cell wall. In Test 4B the same preparation of the concrete beams was performed, but with the bentonite sealing present. This system could withstand at least 4.5 MPa and thereby it is obvious that the bentonite sealing is required.

Test 4B was performed using a more aggressive pressurization approach. The pressure elevation ramps were again set to 100 kPa/h and the filling and drainage period was shortened to 20 hours. Already after 3.5 days a water pressure of 2 MPa was reached in ramp 6, but then leakage occurred through the bentonite sealing and the pressure needed to be reduced. When ramp 7 was started the pressure was re-raised directly to 1,500 kPa and the ramp was started from there. This was too tough on the sealing and leakage occurred almost directly. This was followed by a manually controlled pressure enhancement in four steps over two days until 1,500 kPa was reached. This rate was too aggressive and leakage occurred again at 1,500 kPa. It is suggested that the leakage in ramp 6 at 2 MPa may have caused some piping or similar damage to a section of the sealing. Therefore the sealing was weakened and leakage could easily occur again at lower water pressures, about 1,500 kPa.

Finally on day 11 after about five days of 500 kPa constant pressure, the sealing managed to withstand the water pressure of ramp 8. When the pressure ramp was initiated the radial total pressure was about 1,250–1,400 kPa (including a contribution from 500 kPa of water pressure) which previous tests have shown to be sufficient to withstand piping. The dry density of the outermost parts of the sealing was 1,250–1,290 kg/m^3 which is also in the same order of magnitude as previous tests.

The test objective was to investigate the difference using the cast or the non-cast concrete beams. 2 MPa of water pressure was reached within 3.5 days, which is very fast compared to Test 2 (almost 40 days) and also a lot earlier than Test 3 (about 12 days). As mentioned the approach in Test 4 was more aggressive than in previous tests and it finally took somewhat more time to reach 4.5 MPa than in Test 3. It is suggested that molding of the concrete beams improves the sealing ability, based on the results from the early part of the test. The repeated leakages that occurred from day 3–6 are suspected to have reduced the functionality of the sealing and therefore the final water pressure was reached later than in Test 3. In general the aggressive approach with 100 kPa/h ramps and a short fill-up and drainage period does not seem preferable.

At test dismantling a visual observation was done on the interface between bentonite sealing and cast cement, but no weak spots or traces of piping were observed. It is possible that previously existing damage to the sealing had healed and that the visual tracing of a piping feature was no longer possible.

The conclusions from Test 4 are listed as follows:

- The bentonite sealing is crucial for the sealing function also when the concrete beams are cast in cement.
- Molding of the concrete beams seems to improve the sealing function of the design.
- When the sealing managed to withstand a water pressure of 4.5 MPa the radial total pressure was 1,250–1,400 kPa (including some contribution from the 500 kPa water pressure) and the dry density in the sealing outermost parts was 1,250–1,290 kg/m^3.
- The aggressive approach using the 100 kPa/h pressure elevation ramp and the short fill-up and drainage period does not seem preferable.

4.7 Test 5

4.7.1 General

The strategy of Test 5 was to increase the pressure manually in steps (100–200–500 kPa) and finally initiate a pressure elevation ramp when a constant pressure of 500 kPa had been working for some time. The voids between the concrete beams were about 1–2 mm in the largest gaps, which is considerably larger than in Test 3. The test could thereby provide additional information on how the sealing ability is affected by the void space size between the concrete beams. Also the swelling pressure and dry density of the sealing was evaluated as in previous tests.

Figure 4-50. *The gaps between the concrete beams in Test 5 were considerably larger than in previous tests. The largest voids were about 1–2 mm.*

The objectives of Test 5 were as follows:

- Use manual pressure enhancement in controlled steps to build up the water pressure.
- Further evaluate the influence of the void space size between the concrete beams.
- Provide more information on dry density and swelling pressure in the bentonite sealing.

4.7.2 Results

Timeline summary

The test procedure is described below. Figure 4-51 shows a timeline summary connected to the description below.

- **Day 0–1. Filter fill-up and drainage period;** a constant flow rate of 0.005 l/min was applied to the bottom of the backfill. The draining filter is closed in the bottom and opened at the top. The fill-up and drainage period lasted for about 24 hours and the water uptake of the system was determined to 2.01 liters.
- **Day 1-6. Constant pressure 100 kPa – 200 kPa;** the water pressure was directly set to 100 kPa and after about 3 days it was increased to 200 kPa.
- **Day 6. GDS empty;** the GDS pressurizing device was emptied during the night and was refilled in the morning. The water pressure was reset to 200 kPa.
- **Day 6. Rise to 500 kPa – window and sealing leakage;** on days 6 the pressure was increased to 500 kPa with a 100 kPa/h ramp slope, but leakage occurred directly in both the sealing and through Window 2 and 4.
- **Day 6–10. Constant pressure 200 kPa – 500 kPa;** the windows were sealed and a constant pressure was set at 200 kPa for 24 hours, then the pressure was stepped up to 500 kPa and held constant for four days.
- **Day 11. Pressure ramp 1 – window leakage at 1,500 kPa;** pressure elevation ramp 1 at 100 kPa/h is initiated. At 1,500 kPa there was leakage in Window 2. All windows are replaced by steel plates.
- **Day 11–14. Constant pressure 1,500 kPa – sealing leakage – 500 kPa constant pressure;** after sealing the windows the pressure is returned to 1,500 kPa and leakage occurred in the sealing. The pressure was lowered to 500 kPa and kept constant for three days.
- **Day 14–18. Pressure ramp 2;** the pressure was quickly raised to 1,500 kPa and then pressure elevation ramp 2 was initiated at 50 kPa/h.
- **Day 15. GDS empty;** the GDS was emptied twice during ramp 2 but finally on day 18, 5 MPa water pressure was reached.

Data

Figure 4-52 shows the registered axial pressure and the water pressure. The total pressure on the plug side and the backfill side are identical throughout the test. On day 11 there is no water pressure being supplied to the system and the registered total pressure must thereby be swelling pressure, which is about 600 kPa at this point. Figure 4-53 shows the radial total pressures and the water pressure. At day 11 during a second period of no water pressure existed and the swelling pressure in the sealing is about 800–900 kPa. At this point the water pressure was quickly returned to 1,500 kPa and leakage was observed requiring depressurization to 500 kPa to be done. On day 14, after a few days of 500 kPa constant pressure, the radial total pressure in the sealing is about 1,200–1,300 kPa. The actual swelling pressure is likely somewhat higher than the 800–900 kPa registered on day 11 and at this point the sealing withstands the pressure elevation ramp and 5 MPa is reached on day 18.

Figure 4-54 shows the axial dry density profiles taken in five different positions at time of dismantling. The bottom, right, left and top samples are taken approximately 6–7 cm from the centre. On the concrete beam side the dry density is between 1,520–1,630 kg/m^3. On the filter side the density has lowered to about 1,200–1,220 kg/m^3. Figure 4-55 shows the radial dry density profiles. The samples are taken in the cross section 30 mm from the concrete beams. The dry density is lowest in the outermost parts were it is 1,230–1,330 kg/m^3.

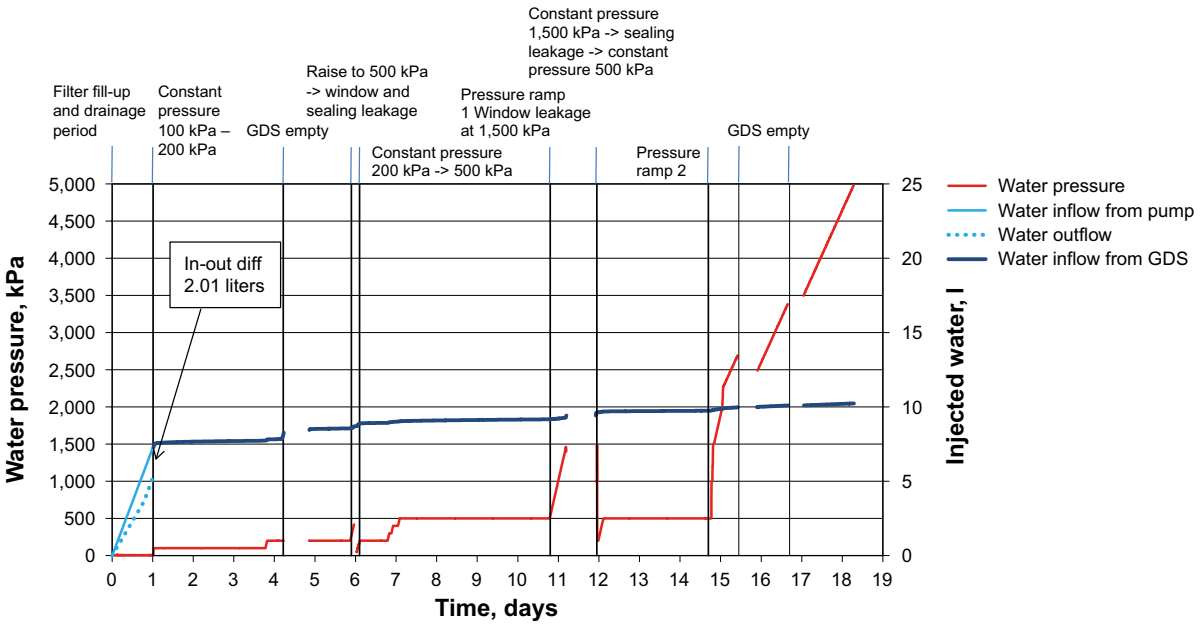

Figure 4-51. *Timeline summary of Test 5. The filling and drainage period was only 24 hours. Leaking windows caused some complications in the test. The water pressure reached 5 MPa after about 18 days.*

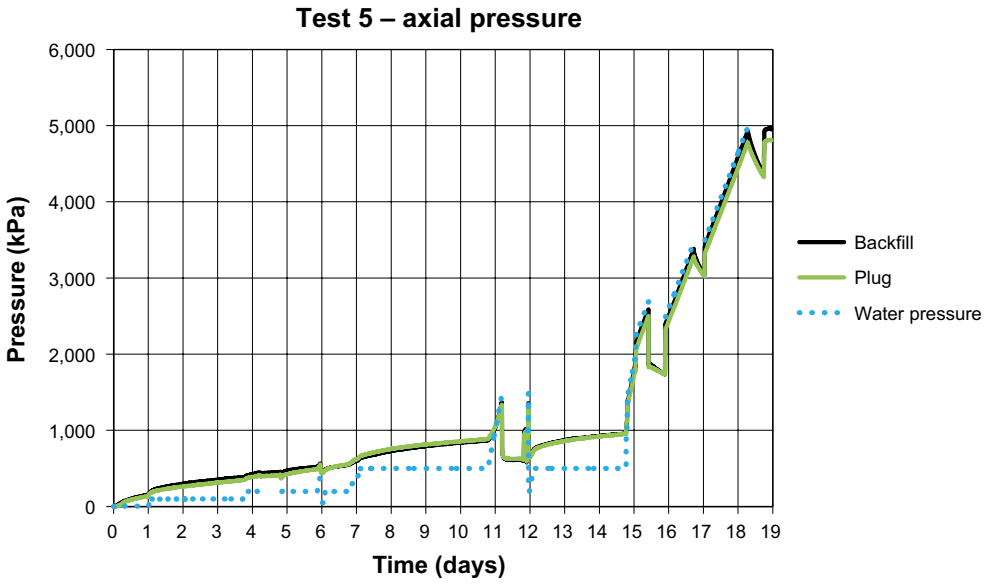

Figure 4-52. *Axial total pressure in Test 5. The pressure is the same on the backfill and on the plug side throughout the entire test.*

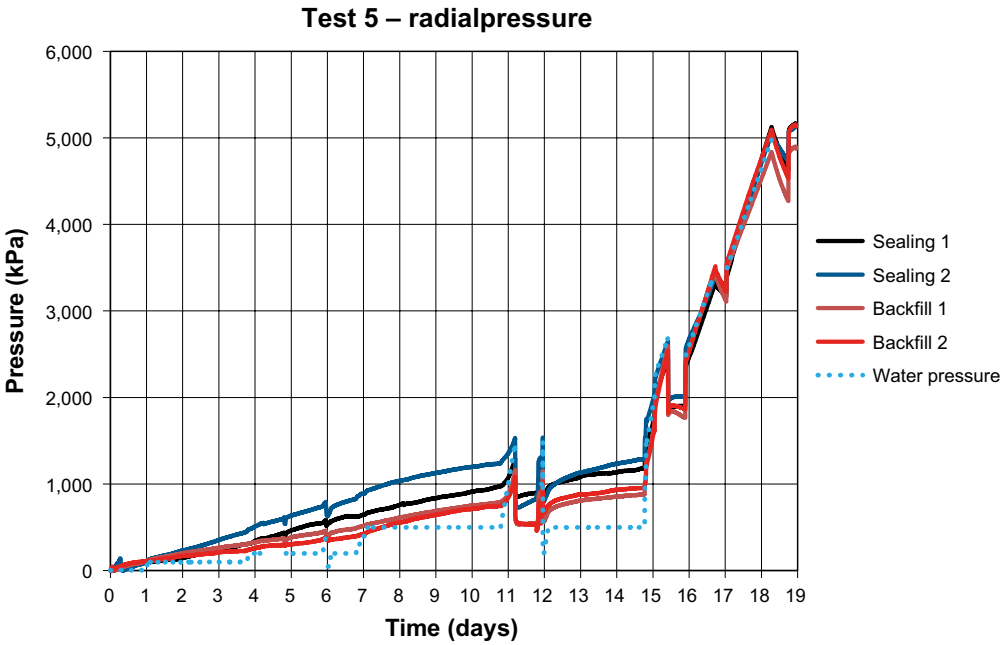

Figure 4-53. *Radial total pressure. The total pressure in the sealing is 1,200–1,300 kPa (including 500 kPa water pressure) on day 14 when the final pressure elevation ramp is initiated.*

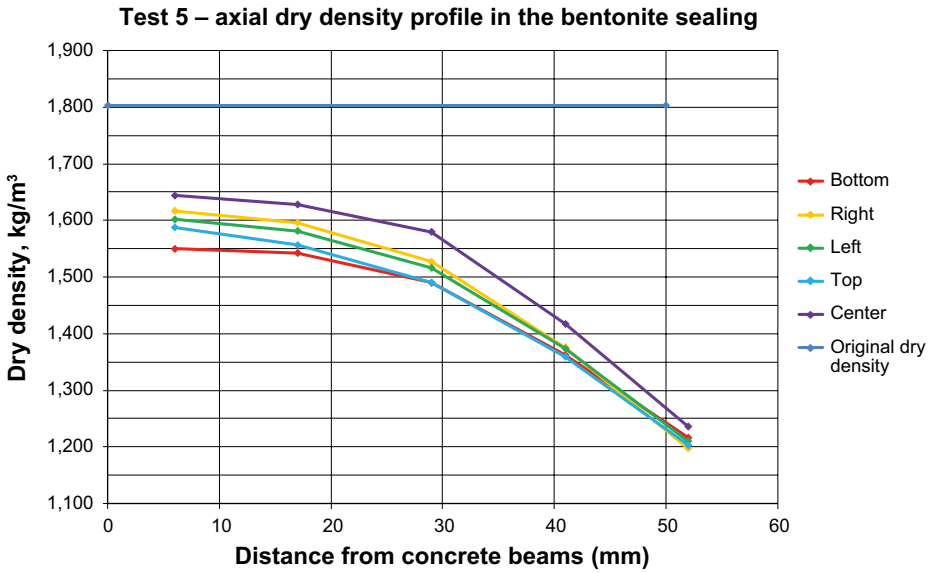

Figure 4-54. *Axial dry density profiles at five different locations in the bentonite sealing. The bottom, left, right and up samples is taken 6–7 cm from the centre.*

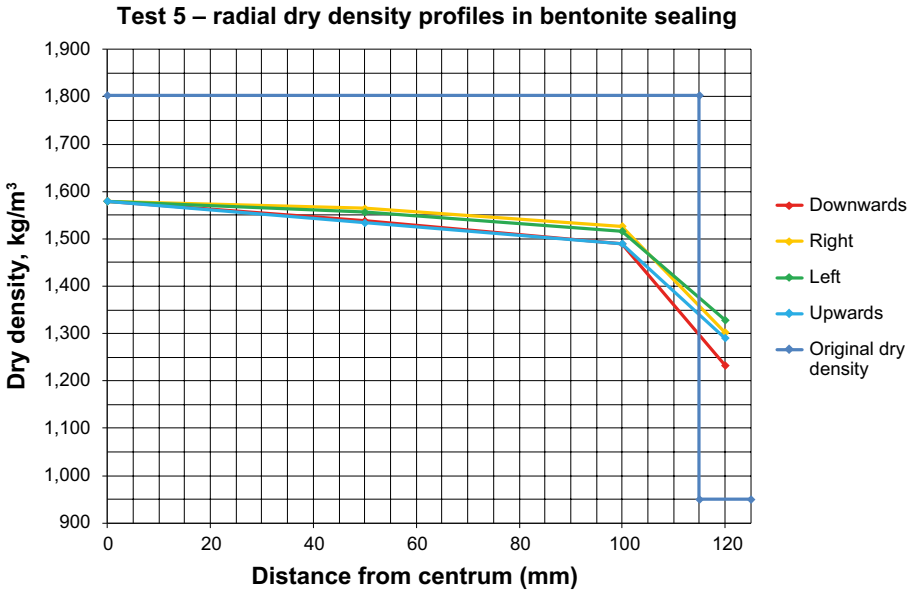

Figure 4-55. *Radial dry density profiles in the bentonite sealing taken in four different directions. The dry density in the outermost parts is 1,250–1,290 kg/m³. The samples are taken in the cross section 30 mm from the concrete beams.*

Dismantling and visual observations

No new observations were made in the dismantling of Test 5 relative to what had been observed in previous tests. When excavating the Leca-macadam filter no backfill bentonite intrusion was found in the filter. A view from the backfill side into the Leca-macadam filter is shown in Figure 4-56. Also, the geotextile is seen behind the macadam.

4.7.3 Discussion and conclusions

A new approach was tested where the water pressure initially was increased in smaller steps. The idea was to build up the water pressure in a more controlled way. However, there was leakage observed early at relatively low water pressures (500 kPa after 6 days). This can be compared to Test 4B where a water pressure of 2 MPa was reached after only half the time (about 3 days). The main difference in the tests is that the concrete beams in Test4B were cast and the concrete beams in Test 5 had voids as large as 1–2 mm between them. It seems as the sealing function is reduced with increased void space size between the concrete beams.

Figure 4-56. *View from the backfill side of the equipment. Behind the Leca-beams both the macadam filter and the geotextile is visible. No backfill bentonite intrusion was observed in the Leca-macadam filter in Test 5.*

Also an interesting observation is made around day 10–12. First a water pressure of 1,500 kPa is reached but then a window starts to leak. However, the sealing managed to withstand the water pressure. Once the window leakage was sealed the pressure was quickly returned to 1,500 kPa and now leakage occurred in the sealing. It seems as the pressure needs to be built up slowly. Even in the case where the sealing already has managed to withstand a certain pressure it seems as the water pressure increase needs to be done with a certain slope to regain the same level.

It took about 18 days to reach 5 MPa. The dismantling and analysis of the bentonite sealing did not provide any new information. The dry density in the outermost parts of the sealing was 1,230–1,330 kg/m^3, which is within the expected order of magnitude. The radial total pressure was 1,200–1,300 kPa (including a contribution from 500 kPa water pressure) at the point where the final pressure elevation ramp was initiated.

The conclusions drawn from Test 5 are as follows:

- The void space sizes between the concrete beams were relatively large and this is suggested to reduce the sealing function.
- Even if a certain water pressure has been held by the sealing, a rapid re-pressurization after a drop in pressure needs to be performed carefully.
- When the final pressure elevation ramp was initiated the dry density in the outermost parts of the bentonite sealing was 1,230–1,330 kg/m^3 and the radial total pressure was 1,200–1,300 kPa (including a contribution from the 500 kPa water pressure).

4.8 Test 6

4.8.1 General

Test 6 was performed with a similar manual pressure enhancement method as in Test 5. The void space sizes were also quite large in Test 6, up to a few millimeters as seen in Figure 4-57.

This test suffered some complications. After about 13 days of testing the GDS pressurizing device started leaking. The pressure elevation ramp had to be cancelled and the GDS replaced. At 21 days the power went down for several hours. This did not affect the test outcome significantly since it happened during a pressure increase ramp, see Figure 4-58, and only resulted in that there was a stop at 3.5 MPa for approx. 6 hours. The main problem was that the axial and radial total pressure data collected prior to this event was lost. Therefore data is only available from day 21 and onwards.

Figure 4-57. *The void spaces between the concrete beams in Test 6. The voids are up to a few millimeters wide.*

When 5 MPa of water pressure was reached, the test was kept running and the pressure held constant at 5 MPa for an additional 54 days before dismantling. This provided information of how the bentonite sealing and the concrete beams would interact over a longer exposure to high water pressure. For example, what bentonite intrusion could occur during extended testing was of interest.

The main objectives of Test 6 can be summarized as follows:

- Further testing of manual pressure enhancement.
- Repetition of test with large void spaces between concrete beams.
- Investigate effects on the bentonite sealing from exposure to high water pressures over longer time periods.

4.8.2 Results

Timeline summary

The test procedure is described below. Figure 4-58 shows a timeline summary connected to the description below.

- **Day 0–1. Filter filling and drainage period;** a constant flow rate of 0.005 l/min was applied to the bottom of the backfill. The draining filter is closed in the bottom and opened at the top. The fill-up and drainage period lasted for about 24 hours and the water uptake into the system was 1.12 liters.
- **Day 1–3. Constant pressure 100 kPa – 200 kPa – 300 kPa;** the water pressure was increased stepwise in intervals of 100 kPa.
- **Day 3–6. Sealing leakage at 300 kPa, pressure enhancement restarted;** Leakage occured through the sealing at 300 kPa. Manual pressure enhancement in 100 kPa steps is restarted.
- **Day 6–9. Constant pressure 500 kPa;** 500 kPa is reached and held constant for three days.
- **Day 9–10. Pressure ramp 1 – leakage at 1,850 kPa;** Pressure elevation ramp 1 is initiated. The pressure ramping rate is 100 kPa/h up to 1,000 kPa, then 50 kPa/h until leakage occurs through the sealing at 1,850 kPa (day 10). At this time pressure is decreased to 500 kPa.
- **Day 10–13. 500 kPa constant pressure;** the water pressure is set to 500 kPa and held constant for about three days
- **Day 13–14. Pressure ramp 2 – GDS leakage;** pressure elevation ramp 2 is started with a rate of 100 kPa/h to 1,000 kPa and then decreased to 50 kPa/h. At about 1,250 kPa the ramp is cancelled due to leakage in the GDS. The GDS is replaced.
- **Day 14–18. Pressure ramp 3 – leakage at 3,600 kPa;** pressure ramp 3 is initiated after one day of 500 kPa constant pressure. The slope is 50 kPa/h and the water pressure reaches about 3,600 kPa before leakage through the sealing occurs. The water pressure is reset to 1,000 kPa and held at that level until the next stage of testing.
- **Day 18–23. Pressure ramp 4;** pressure elevation ramp 4 is initiated on day 19 and successfully reaches 5 MPa with a slope of 50 kPa/h. When the pressure had reached about 3,500 kPa the power went out, but the ramp could be resumed after about six hours.

After the full water pressure of 5 MPa was reached it was held constant for about 54 days before dismantling. During this time a total of 0.918 liters of water was taken up by the system.

Data

Figure 4-59 shows the water pressure and the axial total pressure. Figure 4-60 shows the water pressure and the radial total pressure. On day 21 the power went out and all collected data from the force transducers was lost. Therefore no pressure data is available from when the final pressure elevation ramp was initiated.

During the 54 days of 5 MPa constant pressure, the axial total pressure is significantly higher on the backfill side. By the end of the test, when the water pressure is removed the actual axial swelling pressure is around 850–900 kPa on both sides. At this point the radial swelling pressure is about 1,150–1,300 kPa in the sealing material.

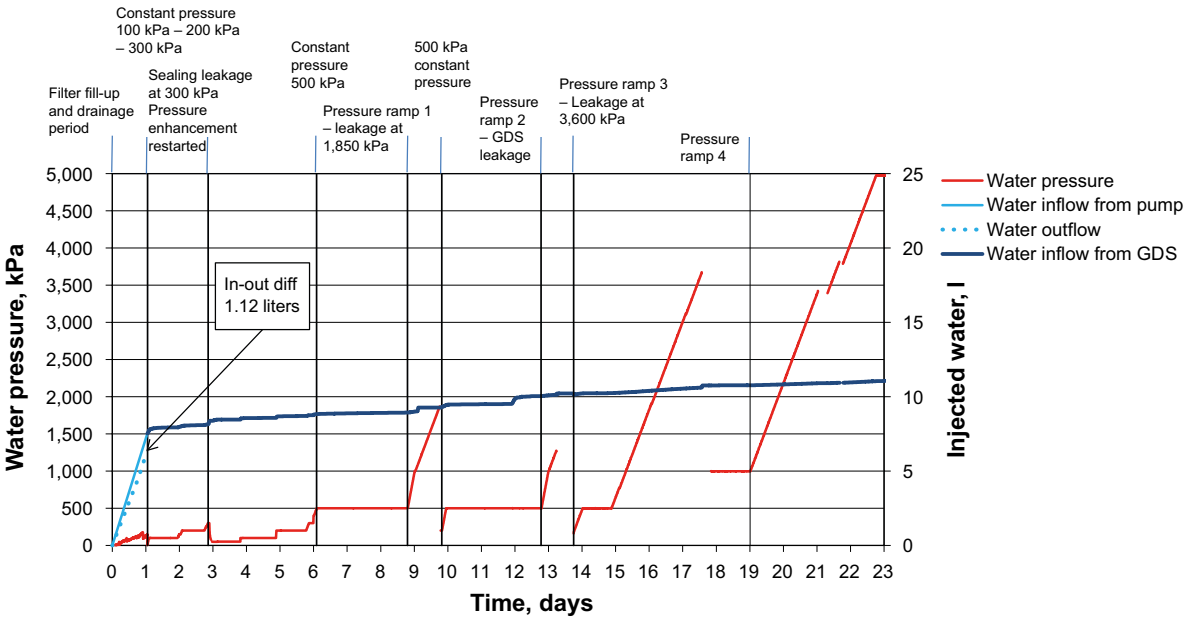

Figure 4-58. *Timeline summary of Test 6. The fill-up and drainage period was about 24 hours. After 13 days the GDS started to leak and was replaced. The pressure elevation ramp that reached 5 MPa was initiated on day 19. After 21 days the power went out for about 6 hours but the test could be resumed without complications.*

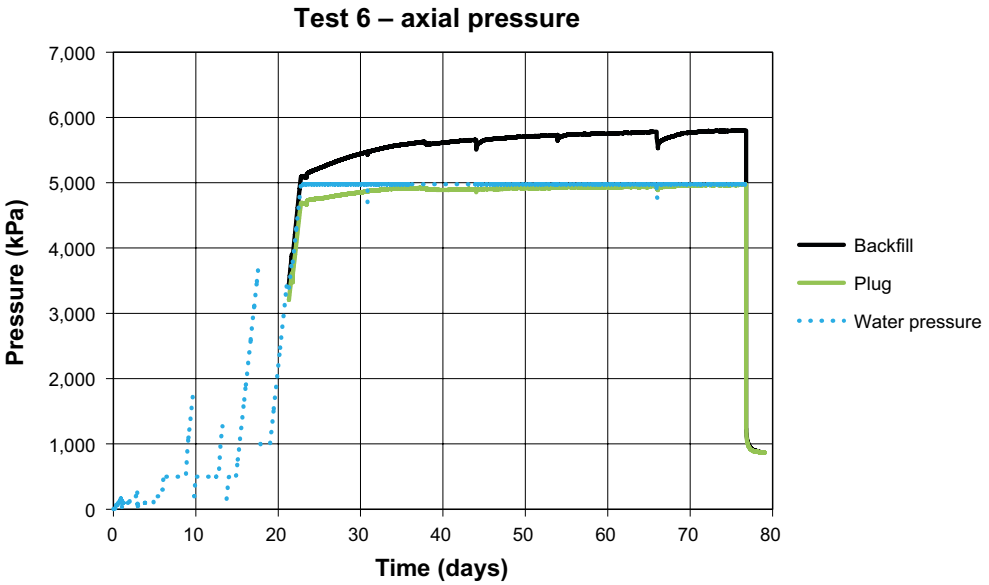

Figure 4-59. *Axial total pressure and water pressure in Test 6. On day 21 the power went out and all registered data was lost.*

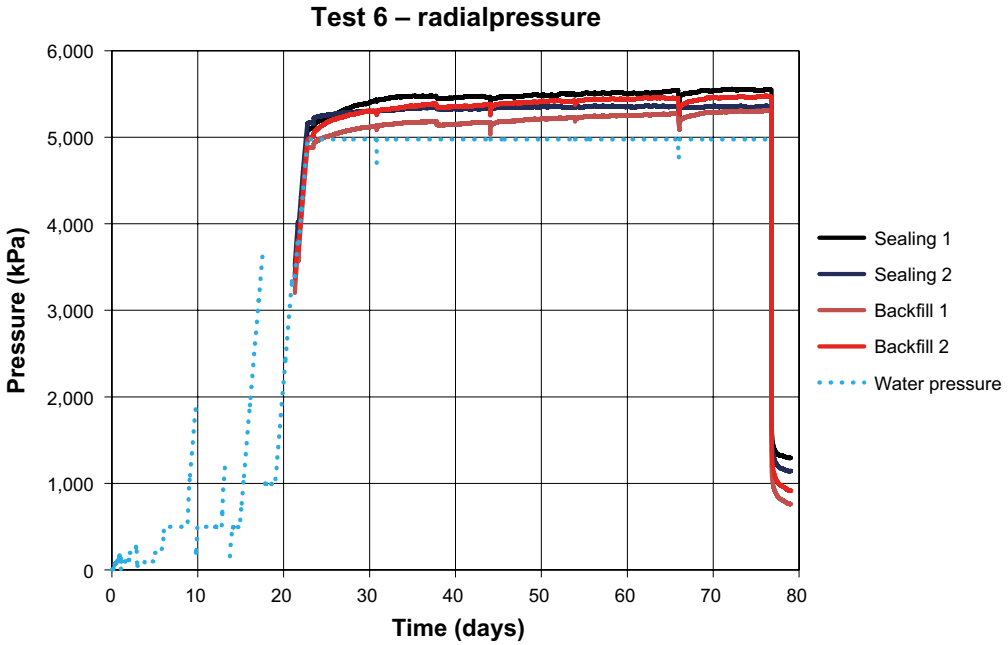

Figure 4-60. *Radial total pressure and water pressure in Test 6. On day 21 the power went out and all registered data was lost.*

Figure 4-61 shows the axial dry density profiles taken in five different positions at the time of test dismantling. The bottom, right, left and top samples are taken approximately 6–7 cm from the center. On the concrete beam side the dry density is between 1,430–1,510 kg/m^3. On the filter side the density has decreased to about 1,170–1,200 kg/m^3. Figure 4-62 shows the radial dry density profiles. The samples are taken in the cross section 30 mm from the concrete beams. The dry density is lowest in the outermost parts were it is 1,250–1,320 kg/m^3. Figure 4-63 and 4-64 shows the saturation rates at the same profiles.

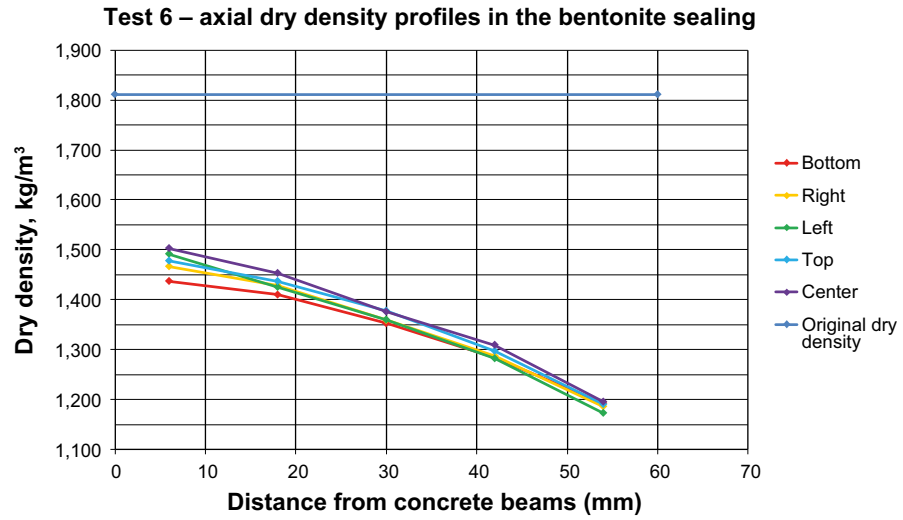

Figure 4-61. *Axial dry density profiles at five different locations in the bentonite sealing. The bottom, left, right and up samples are taken 6–7 cm from the center.*

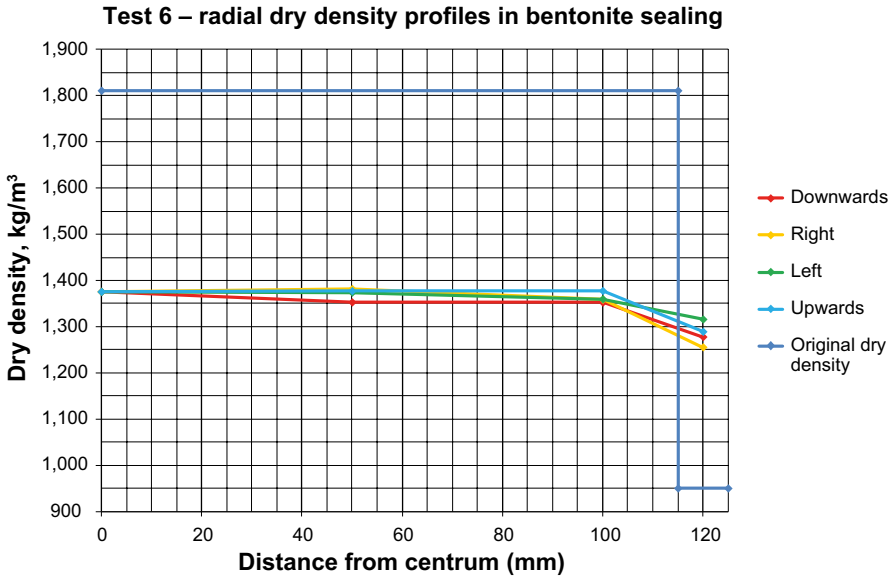

Figure 4-62. *Radial dry density profiles in the bentonite sealing taken in four different directions. The dry density in the outermost parts is 1,250–1,320 kg/m³. The samples are taken in the cross section 30 mm from the concrete beams.*

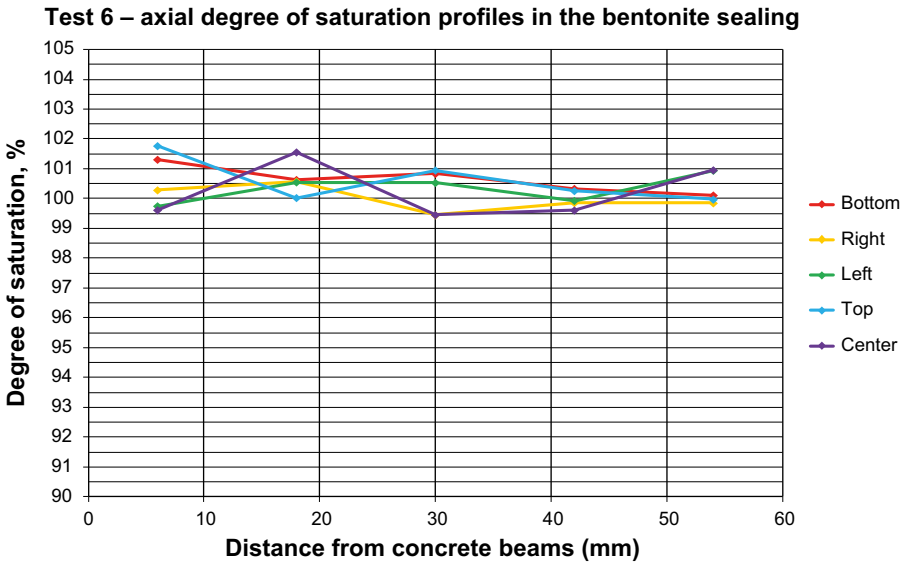

Figure 4-63. *Saturation rate profile in axial direction (same samples as in Figure 8-5).*

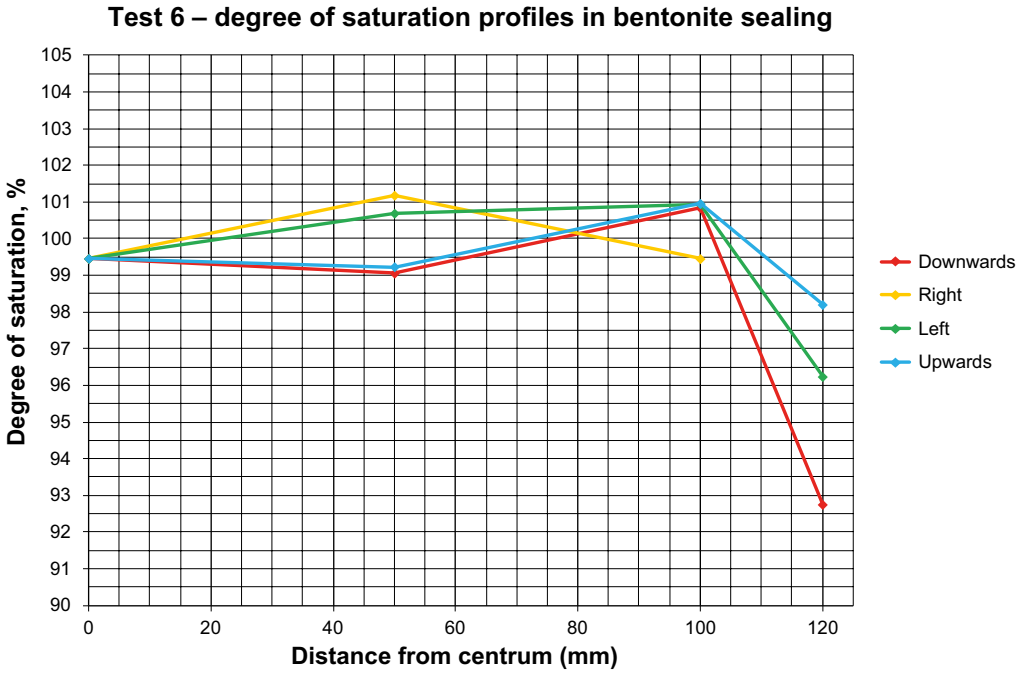

Figure 4-64. *Saturation rate profile in radial direction (same samples as in Figure 8-6).*

Dismantling and visual observations

No new observations were made in the Leca-macadam filter section. Since the windows were replaced with steel plates no observations could be made.

When removing the concrete beams some interesting observations were made on the plug side of the sealing. It was clearly seen how the bentonite sealing had swelled into the voids between the concrete beams. Figure 4-65 shows a view of the sealing from the concrete beam side. It was also seen that the bentonite had swelled along the chamfered inside of the steel tube.

4.8.3 Discussion and conclusions

Test 6 had two complications that occurred during its operation. First, the GDS pressurizing device started leaking on day 13 and had to be replaced. Then on day 21 the power supply went out for about six hours. However, none of these deviations are considered to have affected the test outcome significantly. Unfortunately all collected data from both the axial and radial force transducers were lost during the power loss and therefore the radial swelling pressure in the bentonite sealing could not be estimated at the time of starting the final ramp on day 19.

Figure 4-65. *During the long time of 5 MPa water pressure the bentonite sealing had swelled into the voids between the concrete beams.*

The only new element introduced in Test 6 was to hold the water pressure constant after 5 MPa was reached. After 54 days, the test was finally dismantled and as shown in Figure 8-9 the bentonite had swelled into the voids of the concrete beams to quite a large extent. This is not considered negative for the sealing function since the open void spaces are actually filled with bentonite and thereby potential for leakage is reduced.

The void spaces between the concrete beams were large and this is suspected to be the reason why the sealing ability in Test 6 was relatively poor. Despite a careful, small increment, manually set pressurization process there was leakage at 300 kPa (at less than 3 days). In the first major pressurization ramping there was leakage at 1,850 kPa on day nine. This can be compared to Test 4B with grouted concrete beams that managed to resist almost 2 MPa by day four.

A clear difference in Test 6 is that only 1.12 liters of water was taken up by the system during the drainage and filling period. The time spent on the drainage and filling period was in the same order of magnitude (20–24 hours) as Test 4B and 5 but in these tests the water uptake was 2.29 and 2.01 liters respectively. A lower water uptake could contribute to the observed behaviour by reducing the initial sealing ability. The reason for the low water uptake is not known.

The analysis of the bentonite sealing shows that the dry density in the outermost parts of the sealing is about 1,250–1,320 kg/m^3. These values can be compared to Test 4B and 5 with 1,250–1,290 kg/m^3 and 1,230–1,330 kg/m^3 respectively. Both these are in the same order of magnitude as Test 6 but were dismantled after 14 and 18 days. The results imply that the homogenization of the sealing material has not progressed significantly further despite the 54 extra days of constant 5 MPa water pressure.

The Test 6 conclusions can be summarized as follows:

- The void space sizes between the concrete beams were relatively large and this is suggested to reduce the sealing function.
- Only 1.12 liters (about half the volume of Test 4B and 5) of water was taken up by the system during the drainage and fill-up period. The reason for this is not known. The low water uptake could also have contributed to the poor initial sealing function.
- The density homogenization does not seem to have gone further in Test 6 despite the 54 additional days of 5 MPa water pressure.
- The additional 54 days with 5 MPa water pressure made the bentonite sealing swell into the void spaces between the concrete beams, which reduces the void spaces between the concrete beams.

4.9 Summary and conclusions

4.9.1 General

This section summarizes and discusses the main objectives and conclusions of all tests. Finally the conclusions made for each test are combined and suggestions are made as to how to implement these in a full scale field test.

A summary of all the tests is provided in Table 4-1. The summary contains a brief description of how the drainage and filling period was performed, what pressurization strategy was used and the main pressurization results (e.g. time and pressure at leakage and time when final water pressure is reached). The dry density in the outermost part of the sealing is also presented together with the radial total pressure registered at the time of the final pressure elevation. Additional information from the tests is also given.

Table 4-1. Summary of all the performed tests.

	Drainage and fill-up period length and water uptake	Pressurization strategy	Pressurization results	Dry density in outermost part of sealing and radial swelling pressure	Additional information
Test 1	2 days of drainage and 1 day of fill-up. Low flow rate –0.001 l/min.	Mainly ramps at 100 kPa/h. One period of constant pressure (500 kPa) and occasionally water uptake from burette.	Pressure ramp (100 kPa/h) that reached 2 MPa started on day 22 and completed on day 23.	Dry density was not evaluated. 1,000–1,300 kPa radial total pressure by final ramp start (500 kPa water pressure included).	This was a pilot test to get more acquainted with the equipment. After adjusting some leakage the equipment was working satisfactorily.
Test 2	10 days of drainage and 1 day of fill-up. 0.005 l/min flow rate and 5.75 l water uptake.	Ramps at 100 kPa/h and periods of constant pressure. Final ramp with pauses at every 500 kPa step.	Pressure ramp that reached 2 MPa started on day 36 from 500 kPa. 100 kPa/h with pauses every 500 kPa. Completed day 39.	Dry density was from 1,250–1,350 kg/m^3. About 1,000 kPa radial total pressure by final ramp start (100 kPa water pressure included).	Erosion measured in drainage period; about 1 g/l or less and decreasing. Some backfill bentonite intrusion observed in the filter section.
Test 3	Filter filled directly and drainage through top of filter for 4 days. 0.005 l/min flow rate and 2.74 liters water uptake.	Ramps at 50 kPa/h. Constant pressure of 500 kPa applied for 5 days between 2nd and 3rd ramp.	Pressure ramp that reached 5 MPa started on day 11. 50 kPa/h, completed day 14.	Dry density was from 1,310–1,350 kg/m^3. About 750–950 kPa of radial total pressure by final ramp start (500 kPa water pressure included).	The concrete beams were well fitted to minimize void spaces. Evaluation suggests this improves sealing function.
Test 4A	n/a	Ramp at 500 kPa/h	Leakage after 4 minutes at 30–35 kPa	n/a	No bentonite sealing, only concrete beams cast with cement.
	Drainage and fill-up period length and water uptake	Pressurization strategy	Pressurization results	Dry density in outermost part of sealing and radial swelling pressure	Additional information
Test 4B	Filter filled directly and drainage through top of filter for 20 hours. 0.005 l/min flow rate and 2.29 liters water uptake.	Initially aggressive approach with repeated 100 kPa/h ramps, followed by manual pressure enhancement attempt and finally a 100 kPa/h ramp.	Pressure ramp 7 reached almost 2 MPa after less than 4 days. Finally 4.4 MPa reached on day 14.	Dry density was from 1,250–1,290 kg/m^3. About 1,250–1,400 kPa radial total pressure by final ramp start (500 kPa water pressure included).	Concrete beams cast in cement. Evaluation suggests this improves sealing function.
Test 5	Filter filled directly and drainage through top of filter for 24 hours. 0.005 l/min flow rate and 2.01 liters water uptake.	Pressure enhancement in small steps (50–100 kPa). First ramp start on day 11 (50 kPa/h). Final ramp started day 15 (100 kPa/h).	Sealing leakage already at 500 kPa after 6 days. 5 MPa reached after 18 days.	Dry density was from 1,230–1,330 kg/m^3. About 1,200–1,300 kPa radial total pressure by final ramp start (500 kPa water pressure included).	Large voids between concrete beams (up to 2 mm). Evaluation suggests this reduces sealing function.
Test 6	Filter filled directly and drainage through top of filter for 24 hours. 0.005 l/min flow rate and 1.12 liters water uptake.	Pressure enhancement in small steps (50–100 kPa). First ramp start on day 9 (100 kPa/h up to 1,000 kPa, then 50 kPa/h). Final ramp started day 19 (50 kPa/h).	Sealing leakage at 300 kPa after 3 days. Leakage at 1,850 kPa on day 9. 5 MPa reached on day 22 and held constant for an additional 54 days.	Dry density was from 1,250–1,320 by dismantling. No data form radial total pressure by final ramp start is available.	Large voids between concrete beams (several millimetres). Evaluation suggests this reduces sealing function. Some data lost due to power loss.

4.9.2 Test 1

In the first test the primary goal was to show that all components could be prepared and installed properly in the test equipment and that the basic functions of the design, the test equipment and the data logging system was working satisfactorily. Tap water was used at a flow rate of 0.001 l/min during the fill-up and drainage phase.

The main conclusions were that the components could be installed properly and the test equipment and data logging system worked satisfactorily. The draining function of the design was working well and the components were kept in position and were separated from each other as planned.

4.9.3 Test 2

In Test 2 the flow rate was increased from 0.001 l/min to 0.005 l/min. The test focused on investigating erosion in the draining phase and to make a more extensive density distribution analysis of the bentonite sealing. It was also the first test performed with 1% water salinity.

It was shown in Test 2 that the draining function was working well also at 0.005 l/min and with 1% water salinity. In general, the erosion rate was less than 1 g/l in the drainage outflow, which is considered low. By the time of test dismantling, small amounts of backfill bentonite were found in the filter section. The bentonite intrusion had occurred between the Leca-beams and the windows, probably due to a tiny construction gap. The radial pressure and dry density of the sealing are presented in Table 4-1.

4.9.4 Test 3

In Test 3, a 0.005 l/min flow rate and 1% water salinity was used. The main objective in the test was to reach 5 MPa of water pressure across the seal. At test preparation the concrete beams were carefully fitted to minimize the void spaces between them. The largest voids were measured to about 0.80 mm. The pressure elevation ramping rate was set to 50 kPa/h instead of 100 kPa/h. The filter was filled directly to give the bentonite sealing access to water from start. Also the axial expansion of the bentonite sealing was measured.

Test 3 reached 5 MPa on day 14. The evaluation suggests that the sealing ability was improved by the smaller void spaces between the concrete beams, by giving the sealing component access to water early and by using a reduced pressure elevation ramping rate. The radial pressure and dry density of the sealing are presented in Table 4-1. The dry density in the outermost part of the sealing was similar to Test 2, but the radial total pressures were surprisingly low by the start of the final ramp. The axial expansion in the sealing was about 6–7 mm which corresponds to 12–14%.

4.9.5 Test 4

The main feature of Test 4 was to use concrete beams that were cast in cement to minimize the void space between them as much as possible. This was investigated in two tests; 4A and 4B.

In Test 4A no bentonite sealing component was installed, only the cement cast concrete beams were used. There was water leakage around the cast concrete beams almost instantly at a water pressure of about 30–35 kPa.

Test 4B was fully prepared with all components and performed according to the normal routine but with a slightly more aggressive approach. The filling and drainage period was only 20 hours. An aggressive pressurization strategy was applied with repeated ramping at 100 kPa/h initiated from test start. After only 3 days, a water pressure of 2 MPa was reached, but leakage occurred through the sealing. After this leakage it was hard to recover the water pressure to the same level again but around day 11 the final pressure elevation ramp was initiated. 4.5MP water pressure was reached on day 14 and the sealing seemed to have healed again. The radial pressure and dry density of the sealing were in the same order of magnitude as previous tests and are presented in Table 4-1. It is suggested that molding of the concrete beams improves the sealing ability, mainly based on the results from the early part of the test. The short filling and draining period and the 100 kPa/h hydraulic pressure ramping does not seem to favor the sealing function.

4.9.6 Test 5

The strategy of Test 5 was to a manually apply the hydraulic pressure steps as larger, instantaneous increments. The test also aimed to provide additional information on the influence of large void spaces between the concrete beams (1–2 mm in the largest gaps).

By 500 kPa after 6 days there was leakage through the sealing. When compared to Test 4B, which was reaching 2 MPa after 3 days, suggested that the difference was related to the large voids between the concrete beams in Test 5. Around day 10 there was a leakage in an observation window at 1,500 kPa (no leakage through sealing) and the water pressure was lowered and the window was sealed. When quickly raising the water pressure back to 1,500 kPa, water leakage started through the sealing. It thereby seems important not to increase the water pressure on the sealing too quickly, even if the sealing previously could withstand a high water pressure. The radial pressure and dry density of the sealing were in the same order of magnitude as previous tests and are presented in Table 4-1.

4.9.7 Test 6

Test 6 was performed with a similar manually-applied pressurization method as in Test 5. The void spaces between the concrete beams were somewhat larger larger than Test 5. The test encountered some complications, with a power outage and GDS leakage events, but these are not considered to have affected the results significantly, excepting that all data from the force transducers up to day 21 was lost.

The water pressure was elevated very gradually (50–100 kPa/h) in the beginning but leakage was observed at 300 kPa after less than 3 days of test operation. This is likely because of the large voids between the concrete beams and also a low water uptake in the drainage and fill-up phase. Only 1.12 liters was taken up in this phase and that is about half the volume taken up in Test 4B and 5. On day 22 of testing, the water pressure reached 5 MPa. After this the test was kept running and the pressure held constant at 5 MPa for an additional 54 days before dismantling. At dismantling it was clearly seen that the bentonite had swelled into the voids between the concrete beams. This indicates that open void spaces can be efficiently filled with bentonite in the homogenization process. The available radial pressure and dry density of the sealing are presented in Table 4-1. Despite the bentonite sealing being below 5 MPa of water pressure for an additional 54 days the density homogenization process does not seem to have progressed any further.

4.9.8 Final conclusions and recommendations

The combined main conclusions from the tests are as follows:

- The test components interacted as desired and the different materials were successfully separated from each other. However in some tests the Leca-beams were loosely fitted into the equipment and backfill bentonite managed to intrude into the macadam filter.
- The draining function of the filter worked satisfactorily at both 0.001 and 0.005 l/min.
- The erosion is not considered significant. The amount of eroded material was about 1 g/l or less, which is in the lower region of the erosion prediction model by Sandén and Börgesson (2010).
- The bentonite sealing could successfully withstand 5 MPa of water pressure in all tests were it was tested.
- The size of the void spaces between the concrete beams seems to be of importance for the sealing ability. Casting/grouting of the concrete beams to minimize the void spaces seem to improve the sealing function. The bentonite sealing is however still crucial for the sealing ability.
- Giving the bentonite sealing passive access to water early seems to improve the sealing function significantly.
- In general the 100 kPa/h pressure elevation ramp seems too aggressive. The 50 kPa/h pressure elevation ramp was more successful in raising the pressure without leakage.

- Returning the water pressure to a previously attained higher pressure level must be done carefully to avoid leakage.
- In the tests 5 MPa of water pressure was reached, with radial total pressure ranging from 750–1,400 kPa when the ramp was started (contribution from 500 kPa water pressure included).
- In the tests where 5 MPa of water pressure was reached, the dry densities in the outermost parts of the sealing ranged from 1,250–1,350 kg/m^3 at time of dismantling.
- The water filling of the filter sections should be controlled regarding available volume and the volume of the injected water. In one of the tests (Test 6), the injected water volume was approximately 30% lower than the available volume of the filter and macro voids of the pellet filling, and this seemed to have delayed the bentonite swelling and the following seal.

Based on these conclusions the following suggestions are made for the full scale field test of the tunnel plug;

- The filter draining function should be tested with a water flow rate that represents the expected total flow of a deposition tunnel.
- The erosion during the drainage period should be determined and evaluated to confirm that it is within an acceptable range.
- The size of the void spaces in-between concrete beams and between concrete beams and tunnel wall should be minimized for maximum sealing function. The space between the concrete beams and the tunnel wall should be filled with cement.
- The filter should be filled up with water early to give the bentonite sealing access to water as early as possible.
- The water pressure elevation should be done carefully. If the water pressure needs to be reduced for some reason, the re-pressurization needs to be carefully performed as well.

There was also some data on the radial total pressures and dry densities of the sealing. It is hard to give a direct recommendation for the full scale field test due to the scaling factor. However, a radial total pressure of 750 kPa (including contribution from 500 kPa water pressure) was observed to be lowest in order for the sealing to withstand a ramping of 50 kPa/h that finally reached 5 MPa.

5 Hydro-mechanical modelling of the tunnel plug

5.1 Introduction

This chapter presents the hydro-mechanical modelling work that was performed for the System design of the Dome Plug. This work consists of two-parts:

- Dimensioning calculations of the general plug design. This has mainly consisted of analytical calculations of dimensions for different plug components in different configurations.
- Predictions of the hydro-mechanical processes in the planned field experiment. These predictions were performed stepwise and became increasingly specific during the course of the project.

The components of the plug are illustrated in Figure 5-1. The two main components of the plug construction, apart from the concrete dome, are the i) bentonite seal, which will restrict water flow through the concrete dome and, especially, between the dome and the rock wall; and ii) the permeable filter, which will enable drainage from the tunnel and/or water injection during the hydration of the bentonite seal.

The dimensioning calculations were performed with the aim of limiting the swelling pressure on the concrete dome to 2 MPa. The swelling pressure in the backfill may however reach significantly higher levels (~ 6 MPa). This has initiated the development of a transition zone, a component which due to friction along the tunnel wall can establish a gradient in the axial forces along the tunnel axis.

All bentonite-based components were modeled as if they were made of MX-80 bentonite, simply because the information about other materials was quite limited. More specifically, the material used for the backfill in the dome plug field test (Asha) was regarded as MX-80. Swelling pressures reported by Karnland et al. (2006) indicate however that these two types of bentonite are fairly similar concerning the swelling pressures. A particle density value of 2,780 kg/m^3 was used for MX-80 (Åkesson et al. 2010a) throughout these modeling tasks.

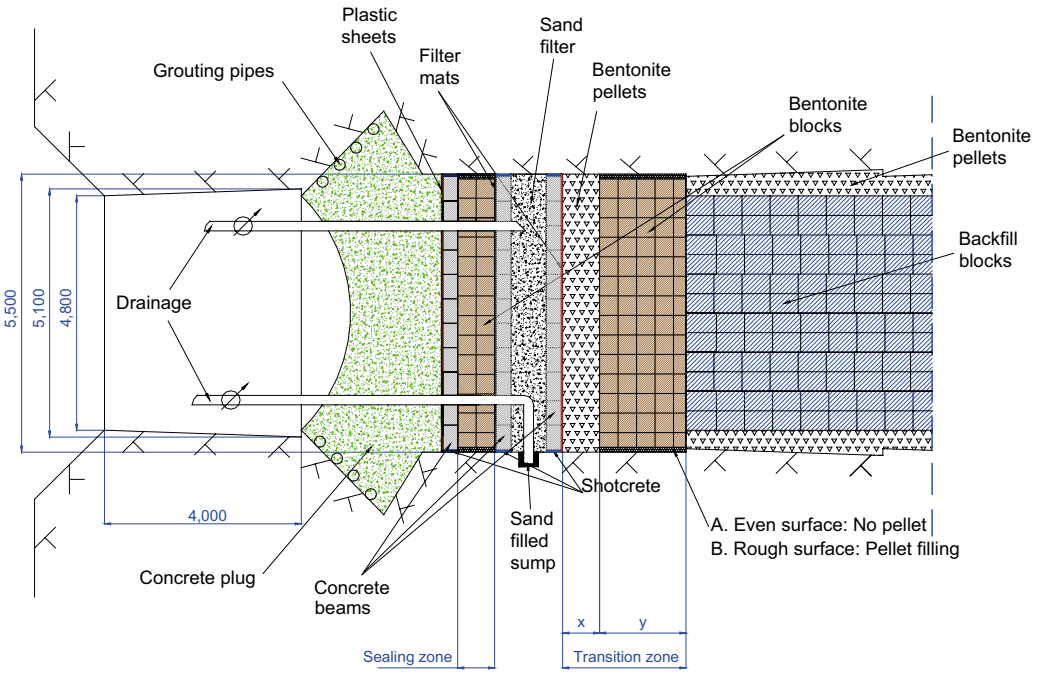

Figure 5-1. *Illustration of main components of plug design.*

The mechanical processes in the plug were generally governed by the main mechanical properties: i.e. swelling pressure relation and friction angle of bentonite for which established data was used. More specific data on the mechanical behaviour, i.e. elastic properties of the filter materials, as well as consolidation/swelling data for MX-80 at relevant densities, were also used.

Apart from the mechanical aspect of the processes, there was also the issue of bentonite hydration and the time-scale for this, and this was largely governed by the hydraulic conductivity data for which established data was used.

The main hydro-mechanical properties on which all calculations are based, are briefly described in Section 5.2 .The modelling work has to some extent been based on results from laboratory test devoted for this project, and these evaluations are presented in Section 5.3. The dimensioning calculations have primarily been performed with an analytical method, developed for this project. This method is presented in Section 5.4, together with results obtained with it. Finally, the numerical modelling is presented in Section 5.5. This work was also two-parted; the first part was related to the plug design and the dimensioning calculations, the second part involved the prediction of the field experiment.

5.2 Hydro-mechanical properties of bentonite

Compacted bentonite exhibits special properties, such as swelling pressure, hydraulic conductivity, shear strength, and water retention properties, which are central for the hydro-mechanical processes in engineered barriers. Compilations of experimental data from tests with MX-80 bentonite have been used for parameterization of functions for some of these functions.

A relation between swelling pressure (p_{swell}) and the void ratio (e) were adopted by Börgesson et al. (1995) on the following form:

$$p_{swell}(e) = p_{swell\,0} \cdot \left(\frac{e}{e_0} \right)^{\frac{1}{\beta}} \tag{5-1}$$

where $p_{swell\,0}$ is the swelling pressure at the reference void ratio e_0 and β is a fitted exponent. In Börgesson et al. (1995), the following parameter setting was adopted for conditions with room temperature, distilled water and void ratios between 0.5 and 1.5: $p_{swell\,0} = 1$ (MPa); $e_0 = 1.1$ (–); $\eta = -0.19$ (–). An alternative relation between p_{swell} and the dry density (ρ_d) was adopted from retention data by Åkesson et al. (2010a) on the form:

$$\log^{10}(p_{swell}) = c_2 \cdot \rho_d^2 + c_1 \cdot \rho_d + c_0 \tag{5-2}$$

with the following coefficients (p_{swell} in kPa): $c_0 = -1.74$; $c_1 = 4.12 \cdot 10^{-3}$; $c_2 = -3.94 \cdot 10^{-7}$. These two functions are illustrated in Figure 5-2. It can be noted that they are quite similar, except for very high dry density for which the TR-95-20 curve exceeds the TR-10-44 curve significantly. The latter relation (TR-10-44) was used exclusively in this work, since this was part of the data qualification for the THM modelling in SR-Site.

A relation between the hydraulic conductivity (K) and the void ratio were adopted by Åkesson et al. (2010a) on the form:

$$K(e) = K_0 \cdot \left(\frac{e}{e_0} \right)^{\eta} \tag{5-3}$$

with the following parameter values: $K_0 = 2.4 \cdot 10^{-13}$ (m/s); $e_0 = 1.0$ (–); $\eta = 5.33$ (–). This relation is illustrated in Figure 5-2 and was used for the numerical models presented in Section 5.5.

The shear strength can be quantified through triaxial compression test during which the sample is driven to failure. The main results from such tests are the mean effective stress (p') and the deviatoric stress (q) at the point of failure. Results from triaxial tests with different densities were presented in Börgesson et al. (1995), and a relation between q and p' were adopted on the following form:

$$q = a \cdot p'^{b} \tag{5-4}$$

with the following parameters: a=2.45 and b=0.77 (if stresses are given in kPa). This relation is illustrated in Figure 5-2 and was used for the numerical models presented in Section 5.5.

The water retention behaviour for free swelling conditions describes the relation between the water content (w) and the relative humidity (RH). This relation is generally path dependent and therefore have different relations been quantified for different initial water contents (see Dueck 2004 and Dueck and Nilsson 2010). All bentonite based components considered in this report have an initial water content of 17%. An empirical set of retention data for such initial water content and for free swelling conditions is shown in Figure 5-2. These measurements were performed at 20°C (Dueck 2004). This data set was used to adopt retention curves for different void ratios, see Section 5.5.5.

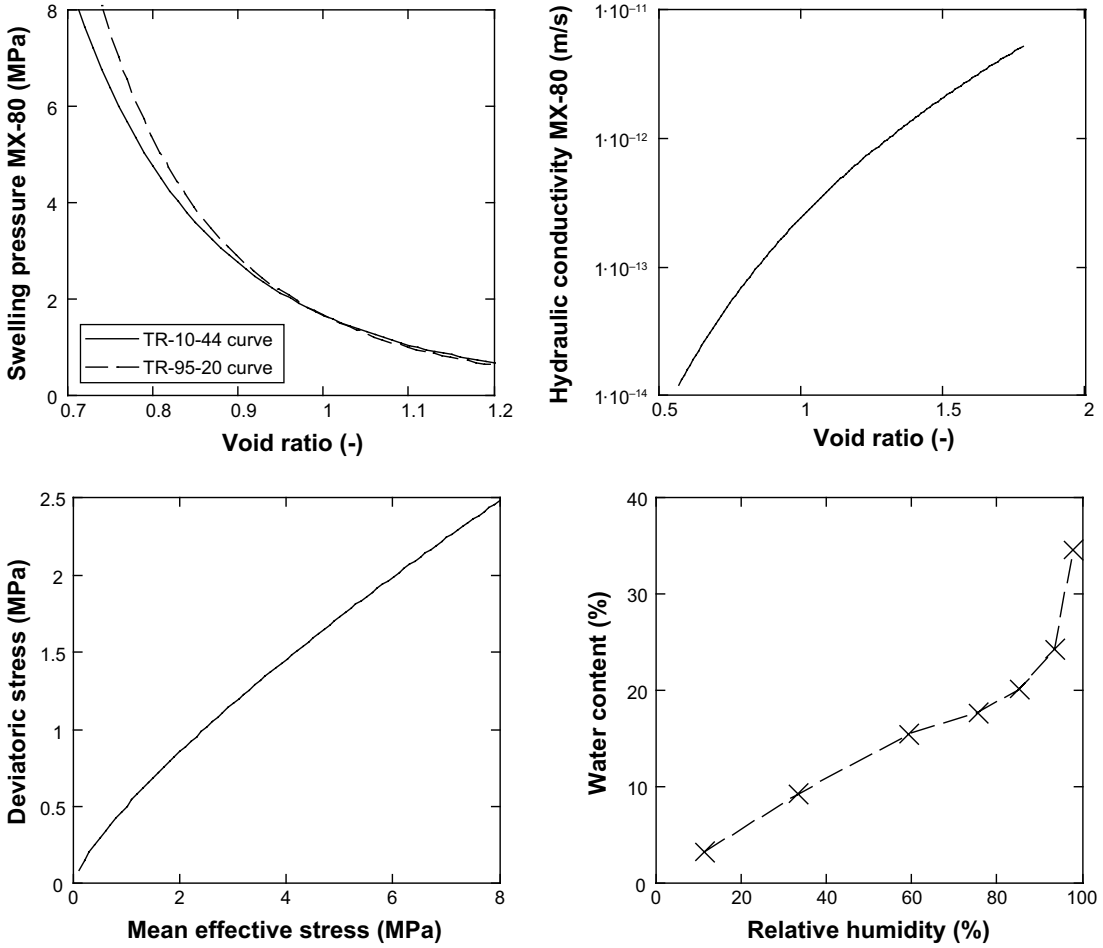

Figure 5-2. *Hydromechanical properties of MX-80 bentonite . Evaluated relations for swelling pressure (upper left), hydraulic conductivity (upper right) and shear strength (lower left). Retention properties for free swelling conditions (lower right).*

5.3 Evaluation of laboratory tests

5.3.1 Introduction

A number of laboratory tests were performed during the initial stage of the project. These tests primarily focused on different filter material and their properties regarding compression and drainage, and for the modelling work the oedometer modulus and Young's modulus were of main interest. Also MX-80 bentonite was analysed in the laboratory tests. For the modelling work, the results from oedometer tests on specimen with a dry density of 1,400 kg/m^3 were of main interest. The evaluations of these test results are presented in the following sections.

5.3.2 CRS tests with filter materials

Four filter materials were analyzed. Three of these were different crushed products with different grain distribution. These products were denoted:

i. Kross 2–4 mm

ii. MakPak 0–5 mm

iii. Harpad 0–4 mm

Data from CRS tests (constant rate of strain) performed on these materials are shown in Figure 5-3.

In addition, tests were performed on Leca block material. Two uniaxial compression tests were first performed, and two CRS test were subsequently preformed. Data from these tests are shown in Figure 5-4.

The adoption of parameter values from evaluations from these tests was not very straightforward and has to some extent evolved during the course of the project.

The oedometer modulus was calculated from the initial (i) and the final (f) load (σ) and density (ρ):

$$M = -\frac{\Delta\sigma}{\varepsilon} = \frac{\sigma_f - \sigma_i}{1 - \frac{\rho_i}{\rho_f}} \tag{5-5}$$

For the crushed products, this modulus was calculated for final densities corresponding to the test condition at a load of 2 MPa (see the red dashed line in Figure 5-3 left), and for the initial density corresponding to unloaded conditions (see lower-end values in Figure 5-3 lower graph). According to this data, the MakPak fraction had the lowest modulus value of approximately 20 MPa, and this value was subsequently used in the analytical calculations presented in Section 5.4 representative for a "loose sand".

In contrast, the crushed products should have higher initial densities if they would have been compacted prior to the compression tests. This has however not been tested, and instead, a default oedometer modulus value of 100 MPa was chosen for a "compacted sand". The initial densities which correspond to this value are shown as the higher-end values in Figure 5-3 (lower graph).

For the field experiment a Young modulus was evaluated from the CRS test of the Kross material (see right graph in Figure 5-3). The strain at 2 MPa was 8.2% which corresponds to an oedometer modulus of 24 MPa. If the Poissons' ratio is assumed to be 0.25 (e.g. Das (1997) gives the interval: 0.15–0.35, for a sand and gravel mixture), then this will correspond to a Young modulus of 20 MPa.

For the Leca blocks an oedometer modulus value was first evaluated directly from uniaxial compression tests (see upper graphs in Figure 5-4). These showed that the strain was approximately 1% at 2 MPa, which would correspond to an oedometer modulus of 200 MPa if the data were obtained in an oedometer. This value was used in the analytical calculations presented in Section 5.4.

CRS tests were subsequently performed with Leca blocks in an oedometer (see lower graph in Figure 5-4). This showed that the strain was approximately 2% at 2 MPa, which corresponds to an oedometer modulus of 100 MPa. If the Poissons' ratio is assumed to be 0.2 (e.g. Möller (1982) recommends this value for concrete), then this will correspond to a Young modulus of 90 MPa. These values were used in the numerical models of the field experiment.

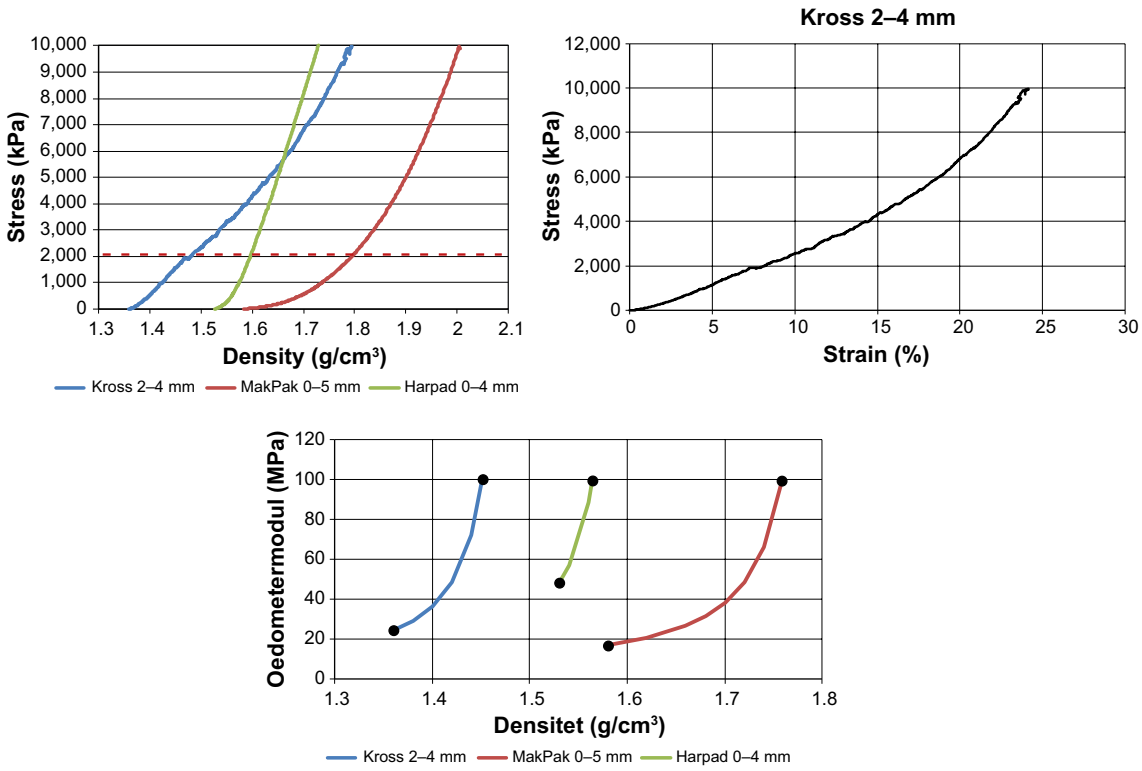

Figure 5-3. *Results from CRS tests with different filter materials. Data presented as axial stress vs. density for all tests (upper left) and axial stress vs. strain for Kross 2-4 material only (upper right). Oedometer modulus as a function of initial stressless density and final measured density at 2,000 kPa (lower graph).*

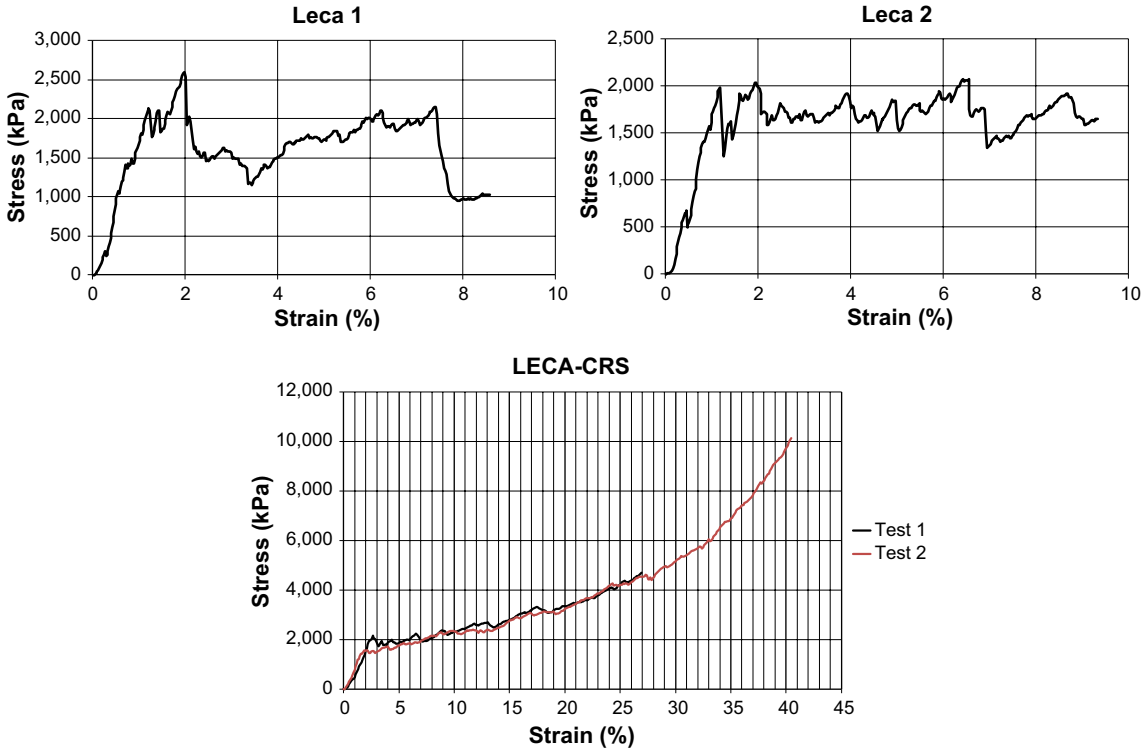

Figure 5-4. *Results from uniaxial compression tests (upper graphs) and CRS tests (lower graph) with Leca blocks.*

5.3.3 Oedometer tests with bentonite

Four oedometer tests were performed on MX-80 bentonite with the intention of obtaining information about the swelling/consolidation behaviour of relevance for the plug design. Four different load steps were applied in two of the tests, and two load steps were applied in the remaining two tests (Table 5-1). The radial stress as well as the void ratio was determined after the initial saturation as well as after each load step.

The results from these tests are compiled in Figure 5-5, and are presented either as stress vs. void ratio (σ-e) relations, or as mean stress vs. deviatoric stress (p-q) relations. These compilations are compared with two swelling pressure relations, Equations (5-1) and (5-2), and one shear strength relation, Equation (5-4), from the literature.

The *σ-e* stress paths, especially regarding the axial stresses, display slightly higher values than the swelling pressure curves. The stress paths with axial stresses also display a significant path-dependence (hysteresis loop), whereas the corresponding paths with radial stresses are quite reversible. The *p-q* stress paths are in most cases below the shear strength relation, although in a few cases they are slightly above.

These test results have been used for evaluation of some of the results from the numerical models (see Section 5.5.6).

Table 5-1. Load steps applied in oedometer tests.

Condition	Axial load (MPa)			
	Test 1	Test 2	Test 3	Test 4
Saturation	2	4	2	4
Load 1	1	2	1	2
Load 2	0.5	1	2	4
Load 3	2	4	–	–
Load 4	4	8	–	–

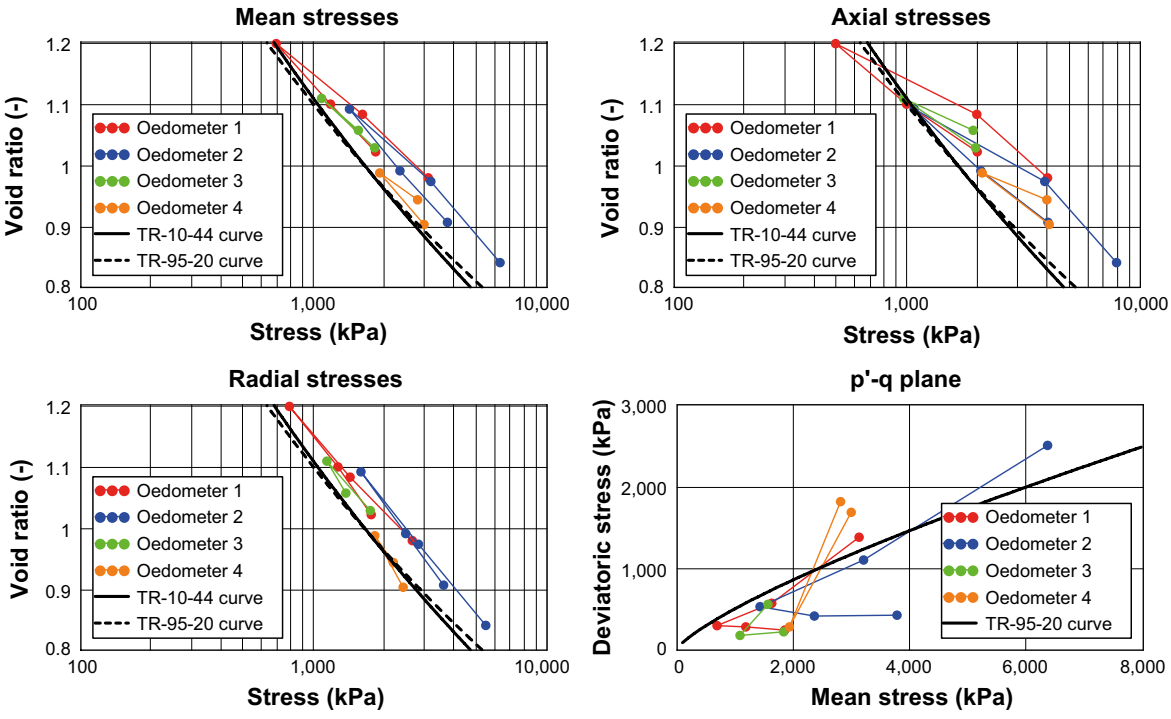

Figure 5-5. *Results from oedometer tests with MX-80.*

5.4 Analytical calculations

5.4.1 Design models

Main assumptions

The first central part of the analytical calculations is based on a specified relationship between the dry density (or void ratio) and the swelling pressure $p_s(\rho_d)$. The swelling pressure is here regarded to be isotropic quantity with the same value in all directions and which doesn't display any hysteresis effects. Two such swelling pressure curves are shown in Figure 5-2, presented by Åkesson et al. (2010a) and Börgesson et al. (1995), respectively.

The second cornerstone of the calculations is the axial force balances in all sections of the tunnel and plug construction in which a gradient of the axial force is balanced by friction along the tunnel wall. The resulting stress distribution implies a density distribution which follows from the swelling pressure curve. And since this density distribution is different from the installed densities of the different components, the displacements of the interfaces between the components can be calculated. All calculations are made for a common friction angle, set to 10° which represents the shear strength of MX-80 at approx. 4 MPa swelling pressure (see Åkesson et al. 2010a).

The main assumptions (isotropic, non-hysteretic swelling pressure and a common friction angle) were made in order to facilitate the analysis presented below with the resources at hand.

Investigated design cases

Three main design alternatives have been investigated: 1) with a seal of bentonite blocks and a transition zone of blocks as well as pellets (Figure 5-6); 2) a seal of bentonite blocks and a transition zone of pellets only (Figure 5-7, left); and 3) a seal of pellets and no transition zone (Figure 5-7, right). Three different filter designs (and stiffness) have been investigated for each one of these alternatives. All cases are summarized together with the lengths of the different components in Table 5-2.

The dimensioning calculation of the first two design alternatives results in the length of the pellets filling of the transition zone, whereas the length of the pellets filling of the seal is calculated in the third alternative. Displacements of different interfaces are also calculated. These calculations are made for the conditions that the pressure on the concrete plug is 2 MPa, and that the swelling pressure of the backfill is 6 MPa. The latter condition corresponds to a dry density of 1,579 kg/m^3, with the used swelling pressure relation. This is slightly higher than the highest installed dry density in the backfill according to SKB (2010) (1,535 kg/m^3). The dry density of the blocks used for the seal and the transition zone is assumed to be 1,400 kg/m^3, whereas the corresponding dry density for pellets in the transition zone is assumed to be 1,000 kg/m^3.

The so-called *inverse calculations* are based on the lengths of the pellets filling found in the dimensioning calculations, and on the modified condition that the swelling pressure of the backfill is 3 MPa (dry density 1,476 kg/m^3). The main result from these calculations is the stress on the concrete plug.

The tunnel as well as the plug is represented as cylinders with a common radius of 2.75 m in the calculations. The possible use of concrete planks in the design is ignored since these planks are assumed to be very stiff and therefore will not contribute to any stress reduction.

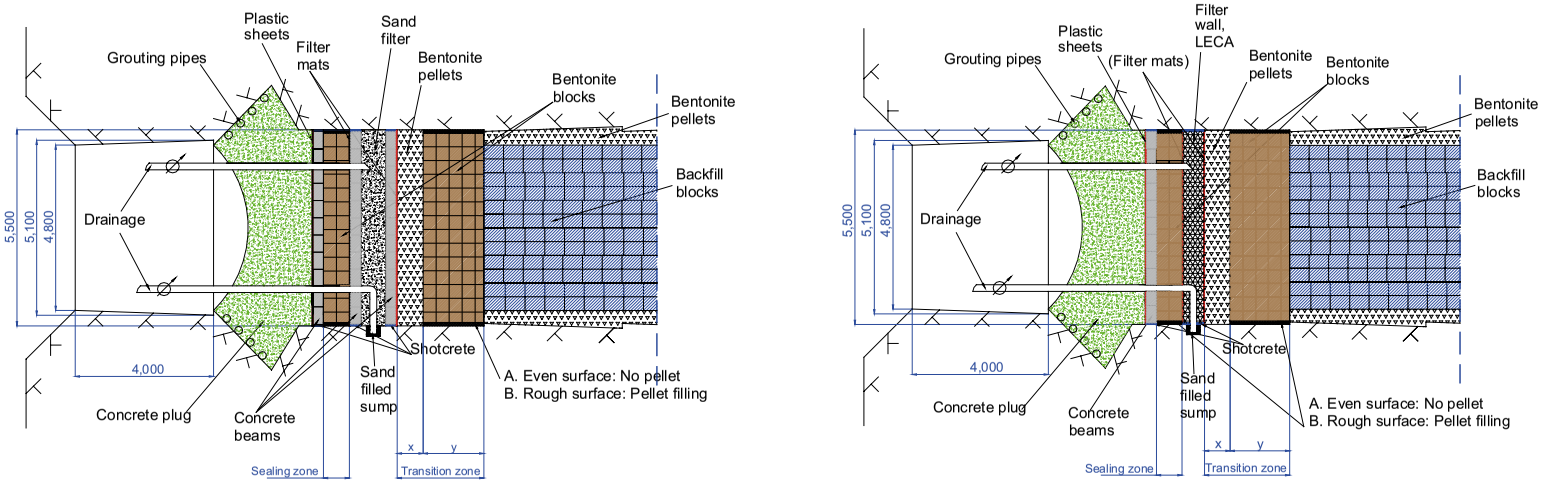

Figure 5-6. *Outline for alternative 1.1 (left) and alternative 1.2 (right).*

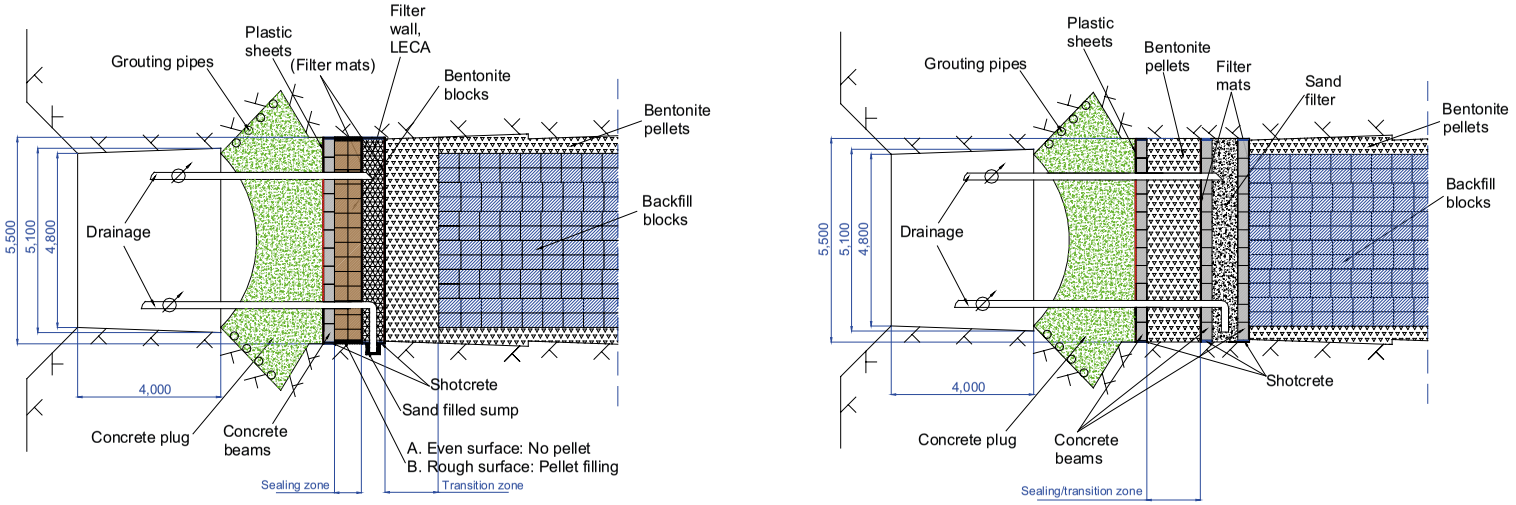

Figure 5-7. *Outline for alternative 2 (left) and alternative 3 (right).*

Table 5-2. Investigated design cases. Calculated lengths marked “Calc”.

Alternative	Seal		Filter			Transition zone	
	Block	Pellet	Sand Loose	Sand comp.	Leca	Pellet	Block
1.1	0.75 m	–	0.75 m	–	–	Calc	1.75 m
1.1	0.75 m	–	–	0.75 m	–	Calc	1.75 m
1.2	0.75 m	–	–	–	0.75 m	Calc	1.75 m
2.1	0.75 m	–	0.75 m	–	–	Calc	–
2.1	0.75 m	–	–	0.75 m	–	Calc	–
2.2	0.75 m	–	–	–	0.75 m	Calc	–
3.1	–	Calc	0.75 m	–	–	–	–
3.1	–	Calc	–	0.75 m	–	–	–
3.2	–	Calc	–	–	0.75 m	–	–

Dimensioning calculations

The friction along the rock wall is assumed to be fully developed which means that a simple relationship can be obtained for the stress distribution:

$$\sigma(z) = \sigma(0) \cdot \exp\left(-\frac{2 \cdot \tan(\phi) \cdot z}{r}\right) \tag{5-6}$$

where σ is the stress (the boundary stress is specified for $z = 0$), r is the tunnel radius and φ is the friction angle. Compressive stresses are defined as a positive quantity. A derivation of this expression was presented by Åkesson et al. (2010b). The different bentonite components in the tunnel/plug design are assumed to equilibrate mechanically in such a way that the final stress distribution in the seal, as well as in the transition zone/backfilling, follows this simple relationship.

The final stress distribution is illustrated in Figure 5-8, together with the initial and final distributions of the dry density. The final density distribution is directly related with the stress distribution through the swelling pressure relation. The integral of the two density profiles are equal.

The first two design alternatives are quite similar, whereas the third alternative is quite different. The procedure for the dimensioning calculations of the first two alternatives is therefore presented together, while the corresponding procedure for the third alternative is presented separately.

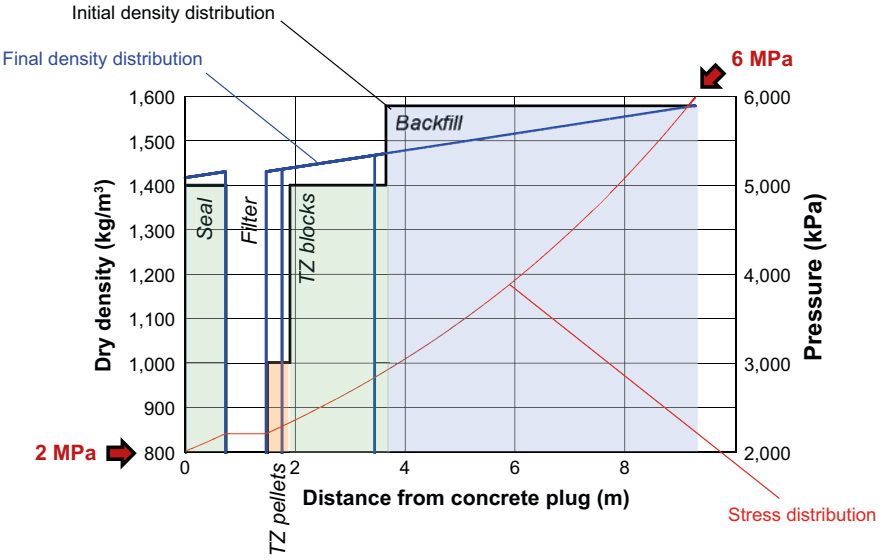

Figure 5-8. *Stress and dry density distributions along the tunnel/plug design.*

Design alternative 1 and 2

The governing lengths for the dimensioning calculations are illustrated in Figure 5-9.

The first step of the dimensioning calculations is to define the final stress distribution in the seal:

$$\sigma_S(z) = 2000\,kPa \cdot \exp\left(\frac{2 \cdot \tan(\phi) \cdot z}{r}\right) \tag{5-7}$$

The dry density distribution is obtained with the inverse function of the swelling pressure relation ($\rho_d(p)$). The displaced length of the seal (L_{SD}) can be sought from this distribution, the initial length (L_S) and the dry density (ρ_S) of the seal:

$$L_S \cdot \rho_s - \int_0^{L_{SD}} \rho_d\left(\sigma_S(z)\right) dz = 0 \tag{5-8}$$

No explicit solution has been found for Equation 5-8, and so a numerical scheme therefore has to be employed. The change in length of the seal (ΔL_S) is given by the initial and the displaced lengths of the seal:

$$\Delta L_S = L_S - L_{SD} \tag{5-9}$$

This change is defined as positive when the length of the seal is decreased.

The stress level at the interface between the filter and the seal (σ_{FS}) is given by the stress distribution and the displaced length of the seal:

$$\sigma_{FS} = \sigma_S\,(L_{SD}) \tag{5-10}$$

This stress is assumed to act throughout the filter. The change in length of the filter (ΔL_F) is given by the stress level as the interface, the initial length (L_F) and the oedometer modulus (M_F) of the filter:

$$\Delta L_F = L_F \frac{\sigma_{FS}}{M_F} \tag{5-11}$$

This change is also defined so that is positive when the length of the filter is decreased. The total change in length of the filter and the seal (ΔL_{FS}) is given as a sum of the changes in length of the seal and filter, respectively:

$$\Delta L_{FS} = \Delta L_S + \Delta L_F \tag{5-12}$$

Coming over to the left hand side of Figure 5-9, a final stress distribution in the backfill and transitions zone is defined:

$$\sigma_B(z) = p_s(\rho_B) \cdot \exp\left(\frac{-2 \cdot \tan(\phi) \cdot z}{r}\right) \tag{5-13}$$

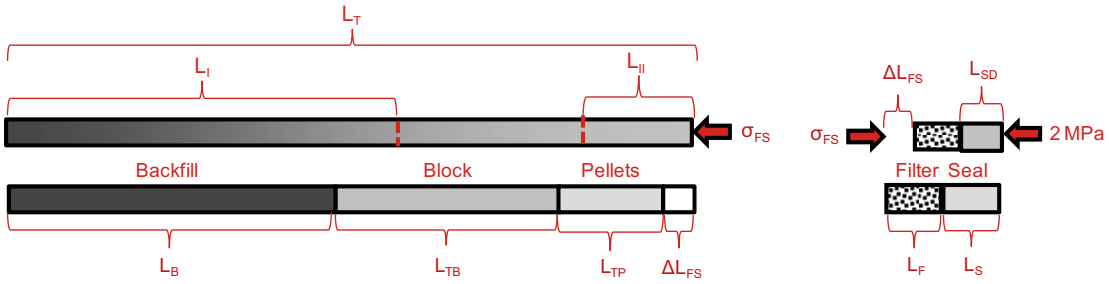

Figure 5-9. *Governing lengths for dimensioning calculations – design alternatives 1 and 2. The lower row shows initial lengths, and the upper row shows final lengths.*

An expression for the total affected length of the backfill and the transition zone (L_T) can be derived by re-arranging this stress distribution. The length is given by the swelling pressure of the "intact" backfill, and thus the dry density of this (ρ_B), and the stress level at the filter (σ_{FS}):

$$L_T = \ln\left[\frac{p_s(\rho_B)}{\sigma_{FS}}\right] \cdot \frac{r}{2 \cdot \tan(\phi)} \tag{5-14}$$

A relation for the initial length of pellets filling in the transition zone can be formulated as:

$$L_{TP} = L_T - L_B - L_{TB} - \Delta L_{FS} \tag{5-15}$$

The initial length of backfill (L_B) constitutes a part of the total affected length. This can be calculated by equating the integral of the density distribution with the sum of products of lengths and densities of the different components (see Figure 5-9):

$$\int_0^{L_T} \rho_d(\sigma_B(z))dz = L_B \cdot \rho_B + L_{TB} \cdot \rho_{TB} + (L_T - L_B - L_{TB} - \Delta L_{FS}) \cdot \rho_{TP} \tag{5-16}$$

This expression can be re-arranged as:

$$L_B = \frac{\int_0^{L_T} \rho_d(\sigma_B(z))dz - L_{TB}(\rho_{TB} - \rho_{TP}) - (L_T - \Delta L_{FS})\rho_{TP}}{\rho_B - \rho_{TP}} \tag{5-17}$$

With this length the initial length of the pellets filling can thus be calculated with Equation (5-15).

The final length of the backfill (L_I) can be sought from the density distribution, the initial length (L_B) and the dry density (ρ_B) of the backfill:

$$L_B \cdot \rho_B - \int_0^{L_I} \rho_d(\sigma_B(z))dz = 0 \tag{5-18}$$

As with Equation (5-8) a numerical scheme has to be employed for this equation. This is also the case for the final length of the pellet filling of the transition zone (L_{II}), which can be sought from the density distribution, the initial length of the pellets filling, and the dry density (ρ_{TP}) of the pellets:

$$(L_T - L_B - L_{TB} - \Delta L_{FS}) \cdot \rho_{TP} - \int_{L_T - L_{II}}^{L_T} \rho_d(\sigma_B(z))dz = 0 \tag{5-19}$$

Design alternative 2 follows basically the same procedure, but with the following simplifications:

- The length of blocks in the transitions zone (L_{TB}) is zero.
- The middle term in the numerator in Equation (5-17) is ignored.
- The final length of the pellets filling L_{II}, and therefore Equation (5-19), is redundant.

Design alternative 3

The governing lengths for the dimensioning calculations are illustrated in Figure 5-10.

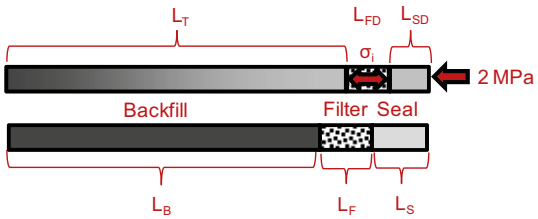

Figure 5-10. *Governing lengths for dimensioning calculations – design alternative 3. The lower row shows initial lengths, and the upper row shows final lengths.*

This procedure begins with the definition of the stress distribution in the backfill, which is identical to Equation (5-13). The total affected length of the backfill is therefore also very similar to Equation (5-14):

$$L_T(\sigma_i) = \ln\left[\frac{p_s(\rho_B)}{\sigma_i}\right] \cdot \frac{r}{2 \cdot \tan(\phi)} \tag{5-20}$$

Still, this length is treated as a function of σ_i, which is the stress acting on and through the filter. This implies that the initial length of the backfill also is a function of σ_i:

$$L_B(\sigma_i) = \frac{\int_0^{L_T(\sigma_i)} \rho_d(\sigma_B(z))\,dz}{\rho_B} \tag{5-21}$$

This is also the case for the final length of the filter:

$$L_{FD}(\sigma_i) = L_F\left(1 - \frac{\sigma_i}{M_F}\right) \tag{5-22}$$

as well as for the final length of the seal:

$$L_{SD}(\sigma_i) = \ln\left[\frac{\sigma_i}{2000}\right] \cdot \frac{r}{2 \cdot \tan(\phi)} \tag{5-23}$$

and the initial length of the seal:

$$L_S(\sigma_i) = \frac{\int_0^{L_{SD}} \rho_d(\sigma_S(z))\,dz}{\rho_S} \tag{5-24}$$

The sum of the initial lengths is equal to the sum of the final lengths:

$$L_B(\sigma_i) + L_F + L_S(\sigma_i) = L_T(\sigma_i) + L_{FD}(\sigma_i) + L_{SD}(\sigma_i) \tag{5-25}$$

The common stress for which different lengths equilibrate can be calculated with this equation. No explicit solution has however been found, and a numerical scheme therefore has to be employed.

With this stress the initial length of the pellets filling can be calculated with Equation (5-24).

Inverse calculations

The dimensioning calculations presented above result in sets of lengths of the different components of the tunnel plug. More specifically, the length of the pellets filling in the transition zone or in the seal is calculated from sets of lengths and properties of the other components, the condition that the pressure on the concrete plug is 2 MPa, and that the "intact" backfill has a swelling pressure of 6 MPa. The aim of the inverse calculations is to quantify the pressure on the concrete plug for the different sets of component lengths and properties, if the swelling pressure of the intact backfill is reduced to 3 MPa.

The general procedure to do this is based on the notion that the system equilibrate so that the stresses are the same on both sides of the filter. Different lengths of the system are therefore formulated as functions of the stress towards the filter. The total length of the system before and after the equilibration should be the same, and this condition is used at to derive an equilibration stress.

The governing lengths for the inverse calculations are illustrated in Figure 5-11.

The total affected length of the backfill and the transition zone is similar to Equations (5-14) and (5-20). In this case, it is formulated as a function of the stress towards the filter:

$$L_T(\sigma_i) = \ln\left[\frac{p_s(\rho_B)}{\sigma_i}\right] \cdot \frac{r}{2 \cdot \tan(\phi)} \tag{5-26}$$

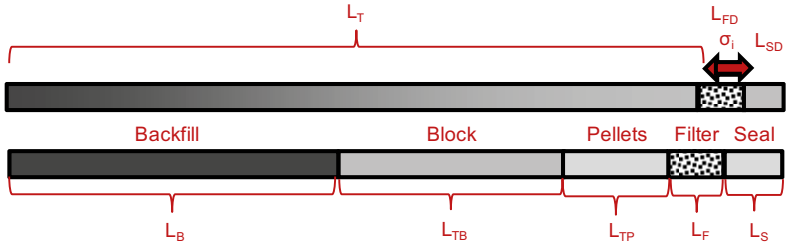

Figure 5-11. *Governing lengths for inverse calculations. The lower row shows initial lengths, and the upper row shows final lengths.*

The initial length of the backfill can also be defined as a function of the stress towards the filter since all the lengths of the transition zone are defined:

$$L_B(\sigma_i) = \frac{\int_0^{L_T} \rho_d(\sigma_B(z))dz - L_{TB}\rho_{TB} - L_{TP}\rho_{TP}}{\rho_B} \tag{5-27}$$

The stress distribution on the backfill side of the filter (σ_B) is the same as in Equation (5-13). The stress distribution in the seal (σ_S) is formulated as:

$$\sigma_S(z,\sigma_i) = \begin{cases} \sigma_i \cdot \exp\left(\frac{2\cdot\tan(\phi)\cdot z}{r}\right) & \text{if} \quad \sigma_i < p_S(\rho_S) \\ \sigma_i \cdot \exp\left(-\frac{2\cdot\tan(\phi)\cdot z}{r}\right) & \text{if} \quad \sigma_i \geq p_S(\rho_S) \end{cases} \tag{5-28}$$

The displaced length of the seal (L_{SD}) can be sought from this distribution, the initial length (L_S) and the dry density (ρ_S) of the seal. In this case, it is formulated as a function of the stress towards the filter:

$$L_S \cdot \rho_s - \int_0^{L_{SD}(\sigma_i)} \rho_d(\sigma_S(z,\sigma_i))dz = 0 \tag{5-29}$$

This is also the case for the final length of the filter:

$$L_{FD}(\sigma_i) = L_F\left(1 - \frac{\sigma_i}{M_F}\right) \tag{5-30}$$

The sum of the initial lengths is equal to the sum of the final lengths:

$$L_B(\sigma_i) + L_{TB} + L_{TP} + L_F + L_F + L_S = L_T(\sigma_i) + L_{FD}(\sigma_i) + L_{SD}(\sigma_i) \tag{5-31}$$

The equilibration stress level (σ_{eq}) can be derived from the equation, at least by numerical means. The sought stress on the plug is finally calculated as $\sigma_S(L_{SD}(\sigma_{eq}),\sigma_{eq})$.

Results

The most relevant results from the analytical calculations are presented in Figure 5-12, Figure 5-13 and Figure 5-14. Each figure shows graphical representations of results from the dimensioning calculations in the upper row, and the inverse calculations in the lower row. The different column represents different filter materials: loose sand (left), compacted sand (middle) and Leca (right). Black lines show initial density distributions; blue lines show final density distributions; and red line show stress distributions. Calculated lengths of pellets filling in transition zone or seal marked in red. Results from design alternative 1, 2 and 3 are shown in Figure 5-12, Figure 5-13 and Figure 5-14, respectively.

A number of key results from the different dimensioning calculations are compiled in Table 5-3:

1. The length of pellets in the transition zone, L_{TP} in Eq. (5-15).
2. The length of pellets in the seal, L_S in Eq. (5-24).
3. The displacement of the interface between the backfill blocks and the transition zone blocks, L_I–L_B in Eq. (5-17) and (5-18).
4. The displacement of the interface between the blocks and the pellets in the transition zone, L_I–L_{II}–L_B–L_{TB} in Eq. (5-14), (5-17) and (5-19) (design alternative 1); the displacement of the interface between the backfill blocks and the pellets in the transition zone, L_I–L_B in Eq. (5-17) and (5-18) (design alternative 2).
5. The displacement of the inner interface of the filter, ΔL_{FS} in Eq. (5-12) (design alternative 1 and 2), or L_I–L_B in Eq. (5-20) and (5-21) (design alternative 3).
6. The displacement of the inner interface of the seal, ΔL_S in Eq.(5-9) (design alternative 1 and 2), or L_S–L_{SD} in Eq. (5-23) and (5-24) (design alternative 3).
7. Minimum backfill dry density for which the method has a solution.
8. Stress on filter, σ_{FS} in Eq. (5-10) (design alternative 1 and 2), or σ_i in Eq. (5-25) (design alternative 3).
9. Total affected length L_T in Eq. (5-14) (design alternative 1 and 2), or σ_i in Eq. (5-20) (design alternative 3).
10. Stress on the plug at a backfill swelling pressure of 3,000 kPa, $\sigma_S(L_{SD}(\sigma_{eq}),\sigma_{eq})$ (see inverse calculations).

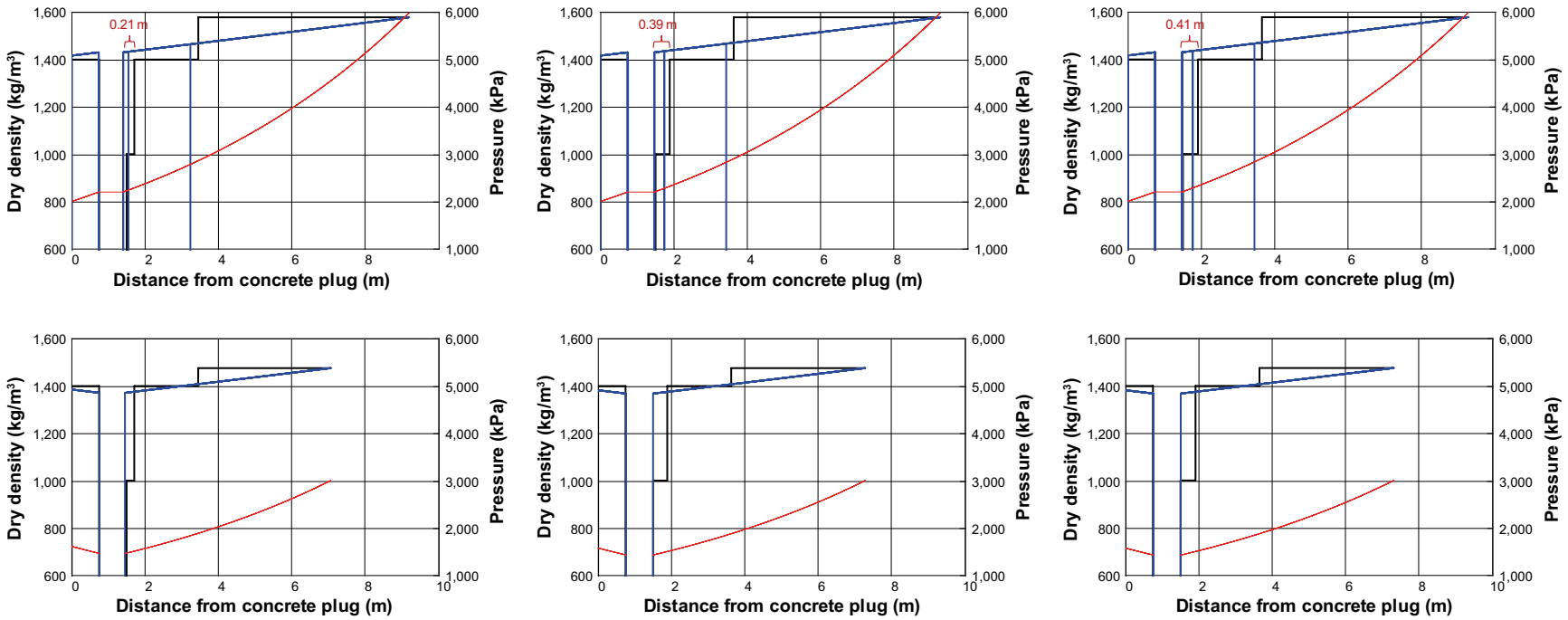

Figure 5-12. *Graphical representation of results from dimensioning calculations (upper row) and inverse calculations (lower row). Design alternative 1 with different filter materials: loose sand (left), compacted sand (middle) and Leca (right). Black lines show initial density distribution; blue lines show final density distribution; and red line show stress distribution. Calculated lengths of pellets filling in transition zone marked in red.*

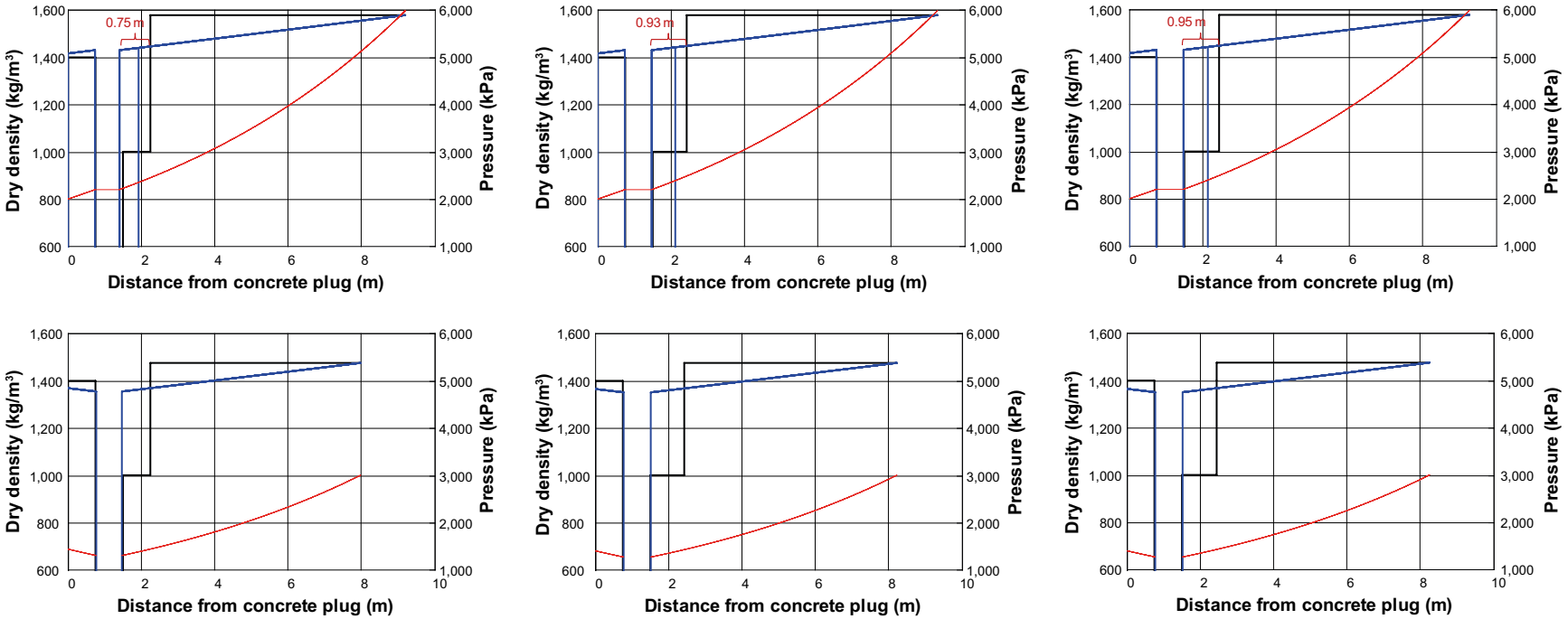

Figure 5-13. *Graphical representation of results from dimensioning calculations (upper row) and inverse calculations (lower row). Design alternative 2 with different filter materials: loose sand (left), compacted sand (middle) and Leca (right). Black lines show initial density distribution; blue lines show final density distribution; and red line show stress distribution. Calculated lengths of pellets filling in transition zone marked in red.*

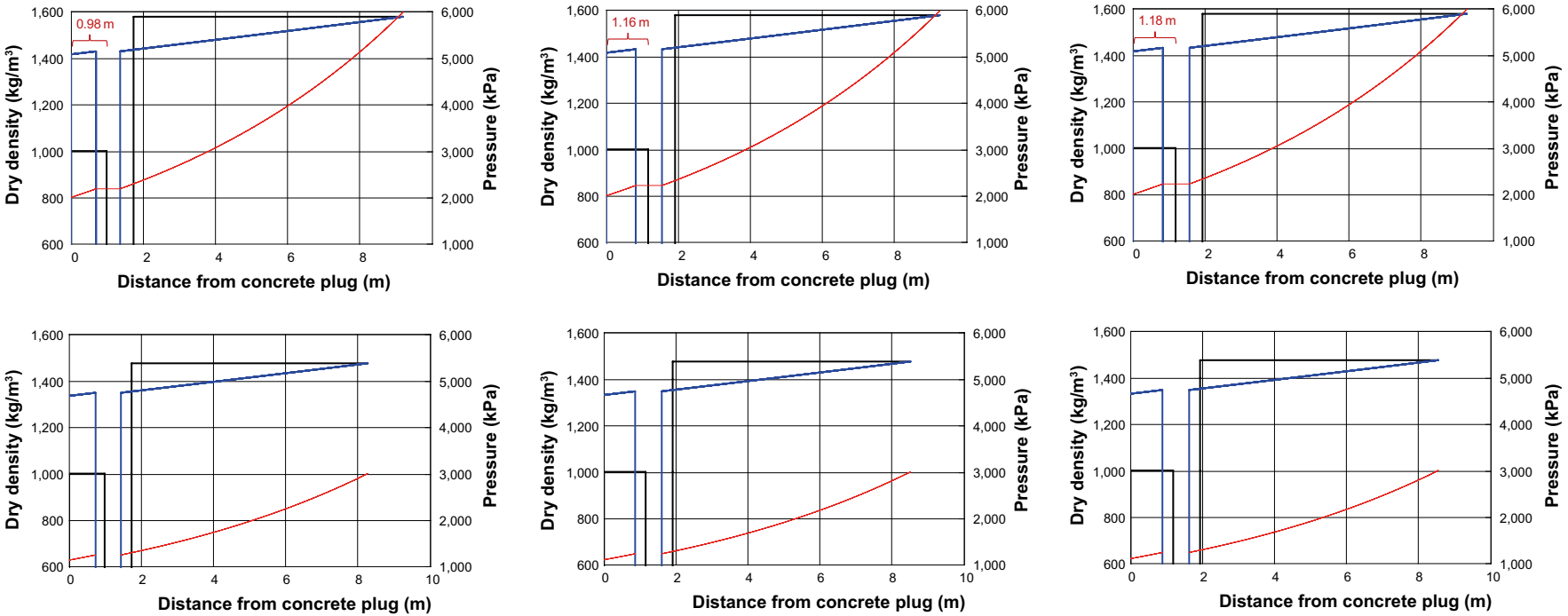

Figure 5-14. *Graphical representation of results from dimensioning calculations (upper row) and inverse calculations (lower row). Design alternative 3 with different filter materials: loose sand (left), compacted sand (middle) and Leca (right). Black lines show initial density distribution; blue lines show final density distribution; and red line show stress distribution. Calculated lengths of pellets filling in seal marked in red*

Table 5-3. Summary of results.

Ro1579; Phi 10; TR-10-44	1.1		1.2	2.1		2.2	3.1		3.2
Seal **Transition zone** **Filter**	**Blocks** **Block/pellet** **Sand loose**	**Blocks** **Block/pellet** **Sand comp.**	**Blocks** **Block/pellet** **Leca**	**Blocks** **Pellets** **Sand loose**	**Blocks** **Pellets** **Sand comp.**	**Blocks** **Pellets** **Leca**	**Pellets** **No** **Sand loose**	**Pellets** **No** **Sand comp.**	**Pellets** **No** **Leca**
Method no:	**1**	**1**	**1**	**2**	**2**	**2**	**3**	**3**	**3**
Modulus filter (MPa):	20	100	200	20	100	200	20	100	200
Length pellet in TZ (m):	0.209	0.389	0.412	0.75	0.93	0.953	–	–	–
Length pellet in seal (m):	–	–	–	–	–	–	0.983	1.161	1.184
Disp. Blocks in TZ (m):	0.217	0.208	0.207	–	–	–	–	–	–
Disp. Pellets in TZ (m):	0.158	0.147	0.145	0.322	0.312	0.31	–	–	–
Disp. Filter (m):	0.095	0.029	0.021	0.095	0.029	0.021	0.374	0.363	0.361
Disp. Seal (m):	0.012	0.012	0.012	0.012	0.012	0.012	0.292	0.346	0.353
Minimum density (kg/m^3):	1,557	1,532	1,529	1,504	1,470	1,464	1,481	1,445	1,437
Stress on filter (kPa):	2,198	2,198	2,198	2,198	2,198	2,198	2,185	2,220	2,225
Total affected length	7.816	7.816	7.816	7.816	7.816	7.816	7.863	7.738	7.722
Stress on plug (kPa) at 3,000 kPa in backfill	1,608	1,573	1,568	1,433	1,398	1,392	1,134	1,104	1,100

5.4.2 Field test dimensioning calculations

Three analytical calculations were performed before the final design of the field test was decided:

- A first dimensioning calculation, which aimed at a final swelling pressure of 2 MPa (effective stress). This resulted in a dry density of the seal blocks, and a block filling area of the backfill blocks.
- A first modified case, with prescribed values of the dry density of the seal blocks and the block filling area of the backfill blocks, in which a width of the pellets-filled slot and a final stress level was calculated.
- A final modified case, with a prescribed value of the width of the pellets-filled slot as well, in which the final stress level was calculated.

All calculations were based on the assumption that all bentonite was completely homogenized and fully water saturated. And by neglecting the wall friction and the internal friction, this would mean that the final density would be the same in the seal and the backfill.

A quite detailed description of the tunnel sections was used, in which the tunnel was simplified as a truncated cone. Tunnel radius was described with the following function:

$$r_T(z) = 2.498 + (z - 14.9)\frac{0.13}{2.15} \qquad (m) \tag{5-32}$$

This was adopted from measurements of the tunnel area at different positions in the tunnel. The tunnel area distribution is shown in (Figure 5-15) together with the main components of the tunnel plug experiment. The volume of a certain section (i.e. between z_1 and z_2), can be calculated as:

$$V_T(z_1, z_2) = \int_{z_1}^{z_2} \pi \cdot r_T(z)^2 \, dz \tag{5-33}$$

All block filling materials (both seal and backfill) were assumed to be associated with a slot volume that was 2% of the block volume. Finally, the dry density of pellets and backfill blocks were assumed to be 900 and 1,750 kg/m^3, respectively, and the block filling area of the seal was assumed to be 16.794 m^2.

The *first dimensioning calculations* were based on the following conditions:

- A final swelling pressure of 2 MPa ~ ρ_d =1,417 kg/m^3.
- The volume of the backfill and the 5 cm pellets filling was regarded to be constant.
- The seal was regarded to swell and to compress the filter.
- According to CRS tests at 2 MPa: the displacement of the seal/filter interface was assumed to be the sum of 8.3% of 0.3 m (macadam) and 2% of 0.3 m (Leca). This meant that the total displacement was 0.03 m.

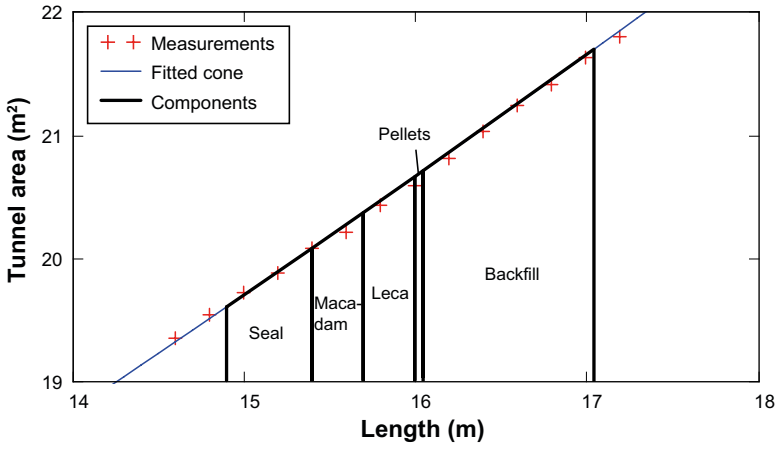

Figure 5-15. *Tunnel area profile.*

The total dry mass of bentonite in the seal should be conserved during homogenisation:

$$V_{SB} \cdot \rho_{SB} + V_{SP} \cdot \rho_P = V_{SF} \cdot \rho_{SF} \quad (5\text{-}34)$$

where V_{SB} is the volume of blocks in the seal (see Figure 5-16); V_{SP} is the volume of pellets in the seal; V_{SF} is the final total (expanded) volume of the seal; ρ_{SB} is the dry density of the seal blocks; ρ_P is the dry density of the pellets filling; and ρ_{SF} is the final homogenized dry density.

The volume of pellets in the seal is obtained by:

$$V_{SP} = V_{SI} - 1.02 \cdot V_{SB} \quad (5\text{-}35)$$

where V_{SI} is the initial total volume of the seal. Note the factor of 1.02, which is due to the 2% addition of slot volume between the blocks.

From these two equations, an expression for the dry density of the seal blocks can be derived:

$$\rho_{SB} = \frac{V_{SF} \cdot \rho_{SF} - (V_{SI} - 1.02 \cdot V_{SB}) \cdot \rho_P}{V_{SB}} \quad (5\text{-}36)$$

With the following values for the different quantities: ρ_P = 900 kg/m^3; ρ_{SF} = 1,417 kg/m^3; V_{SF} = 10.524 m^3; V_{SI} = 9.921 m^3; V_{SB} = 16.794·0.5 = 8.397 m^3, the following value of the dry density of the seal blocks was obtained: ρ_{SB} = 1,631 kg/m^3.

For calculation of the block filling area of the backfill, the total dry mass of bentonite in the backfill, including the pellets filling, should be conserved during homogenisation:

$$V_{BB} \cdot \rho_{BB} + (V_{BP} + V_{PI}) \cdot \rho_P = V_{BF} \cdot \rho_{SF} \quad (5\text{-}37)$$

where V_{BB} is the volume of blocks in the backfill (see Figure 5-16); V_{BP} is the volume of pellets in the backfill; V_{PI} is the volume of pellets filling behind the Leca blocks, V_{BF} is the final total volume of the backfill; ρ_{BB} is the dry density of the backfill blocks; ρ_P is the dry density of the pellets filling; and ρ_{SF} is the final homogenized dry density.

The volume of pellets in the backfill is obtained by:

$$V_{BP} = V_{BF} - V_{PI} - 1.02 \cdot V_{BB} \quad (5\text{-}38)$$

The volume of the blocks in the backfill is given by:

$$V_{BB} = L_{BB} \cdot A_{BB} \quad (5\text{-}39)$$

where L_{BB} is the length of the backfill block filling, and A_{BB} is the block filling area.

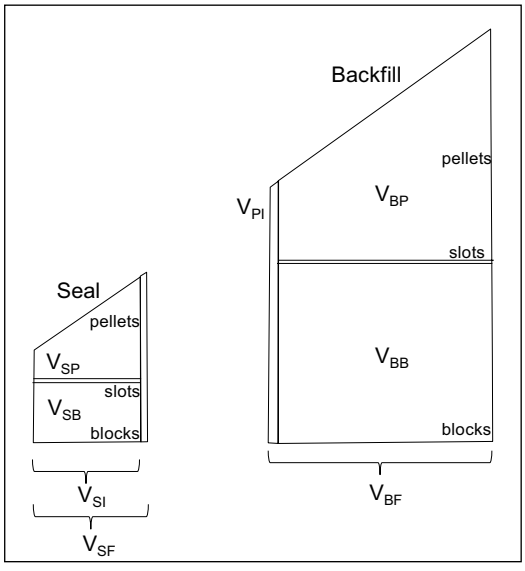

Figure 5-16. *Scheme of different bentonite-filled volumes in tunnel plug experiment.*

From these three equations, an expression for the block filling area of the backfill can be derived:

$$A_{BB} = \frac{V_{BF} \cdot (\rho_{SF} - \rho_P)}{L_{BB} \cdot (\rho_{BB} - 1.02 \cdot \rho_P)} \tag{5-40}$$

With the following values for the different quantities: ρ_P = 900 kg/m^3; ρ_{BB} = 1,750 kg/m^3; ρ_{SF} = 1,417 kg/m^3; V_{BF} = 22.236 m^3; L_{BB} = 1 m, the following value of the block filling area of the backfill was obtained: A_{BB} = 13.817 m^2.

The *first modified case* was considered since it was thought to be beneficial to adhere to the ”standard” block area in backfill (16.452 m^2). The modification was quite simple, since from Eq. (5-40) follows that $A_{BB} \cdot L_{BB}$ is constant if all other variables are constant. This means that L_{BB} can be calculated to: 1 m · 13.817 m^2 / 16.452 m^2 = 0.84 m. From this follows that the width of the pellets-filled slot can be calculated to: 0.05 + 0.16 = 0.21 m.

It was also considered to be beneficial to use quite high dry density in blocks in the seal (1,682 kg/m^3) in combination with the same high block area as in the dimensioning calculation. This would mean that the stress on the plug would exceed 2 MPa. In order to test the consequences a simple analytical tool was developed.

This tool basically considered the installation as two sections with bentonite and one section with the filter (Figure 5-17). Moreover, the changes in length of the seal and the backfill were defined as functions of the pressure at the interfaces ($\Delta z_S(\sigma)$ and $\Delta z_B(\sigma)$).

For the seal, this was based on an expression of the final dry density as a function of the axial position of the interface between the seal and the filter (z_I):

$$\rho_{SF}(z_I) = \frac{V_{SB} \cdot \rho_{SB} + V_{SP} \cdot \rho_P}{V_T(14.9, z_I)} \tag{5-41}$$

This in turn, could together with a swelling pressure curve, be used to formulate an expression of the pressure as a function of z_I.

$$\sigma(z_I) = p_s(\rho_{SF}(z_I)) \tag{5-42}$$

The inverse of this function could, together with the initial position of the interface, be used to formula an expression of the change in length as a function of the pressure:

$$\Delta z_S(\sigma) = z_I(\sigma) - 15.4 \tag{5-43}$$

A similar set of expressions can be formulated for the backfill:

$$\rho_{BF}(z_{II}) = \frac{V_{BB} \cdot \rho_{BB} + (V_{BP} + V_{PI}) \cdot \rho_P}{V_T(z_{II}, 17.05)}$$

$$\sigma(z_{II}) = p_s(\rho_{BF}(z_{II}))$$

$$\Delta z_B(\sigma) = 16 - z_{II}(\sigma) \tag{5-44}$$

In addition, the change in length of the filter was defined as a function of the pressure at the interfaces:

$$\Delta z_F(\sigma) = -\sigma \cdot \left(\frac{L_M}{M_M} + \frac{L_L}{M_L} \right) \tag{5-45}$$

This was based on the oedometer modulus values (M_M and M_L) of the macadam and the Leca, and the initial lengths (L_M and L_L) of these components.

Finally, the sum of these changes in length should be zero:

$$\Delta z_S(\sigma) + \Delta z_F(\sigma) + \Delta z_B(\sigma) = 0 \tag{5-46}$$

and this was used as a condition for seeking the equilibration pressure.

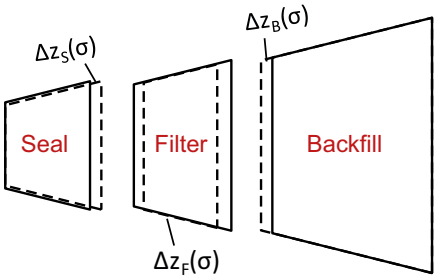

Figure 5-17. *Schematic geometry for homogenization calculation.*

In the first modified case, where the dry density of the seal blocks was 1,682 kg/m^3, the backfill block filling area was 16.452 m^2, and the width of the pellets filled slot was 0.21 m. This resulted in a final stress level of 2.15 MPa, a change in the length of the seal (Δz_S) of 0.041 m, and a corresponding change in the length of the backfill (Δz_B) of –0.008 m.

In the final modified case, the width of the pellets filled slot was changed to 0.15 m, this resulted in a final stress level of 2.48 MPa, a change in the length of the seal of 0.034 m, and a change in length for the backfill of +0.005 m. The equilibration pressure corresponds to a void ratio of 0.92.

5.5 Numerical models

5.5.1 Overview of numerical models

A number of modelling tasks have been pursued during the course of the project, and within each task a number of model cases have been analysed (see Table 5-4). These models were almost exclusively 2D axisymmetric hydro-mechanical models, which were performed with the Code_Bright v3 FEM code. In one case, a plane 1D geometry was used (see below).

The main focus at the start of the project was the *General design models*, which addressed the behaviour of a suggested design of the full-scale tunnel plug, and were thus related to the analytical models in Section 5.4.1. These models included all relevant plug components as well as a significant length of backfilled tunnel. Three cases were analysed.

The next modelling task was the *Field test I models,* which addressed the behaviour of the first version of the planned tunnel plug field test. This consisted of a well-defined cylindrical tunnel section for the plug construction. Two cases were analysed.

The *Field test II models* addressed the behaviour of an updated version of the planned field test. These models were based on the actual section area profile in the TAS01 tunnel, and aimed at investigating the behaviour of different design alternatives, and were thus related to the analytical models in Section 5.4.2. Four cases were analysed. It was found to be very difficult to obtain convergence in these models, and therefore very large elements were employed and only 8 years of result were presented.

Finally, the *Field test predictions*, addressed the behaviour of the final version of the planned field test. These models were based on the actual section area profile, as well as the actual design of the different components; and one of the analytical models in Section 5.4.2 also relates to this design. Three cases were analysed:

- *Base case*. This model was similar to the previous field test models with an idealized hydration through filter and pellets-filled slots.
- *Drained case*. This was identical to the Base case except concerning the hydration, which in this case was limited to the backfill part of the installation. This approach was chosen in order to resemble the initial phase when the filter is drained, but when a substantial inflow is anticipated along the tunnel floor under the backfill blocks.
- *Pressurized case*. The filter in the field tests was planned to be pressurized with several MPa of water, and a protocol for this pressurization scheme has been defined. Some attempts have been made to include this pressurization scheme in the 2D axisymmetric geometry. This has however shown to be even more difficult than the original pressurization with atmospheric water pressure. Instead, a plane 1D geometry was considered in order to enable the inclusion of the planned pressurization scheme.

Table 5-4. Model cases.

Modelling tasks	Name	Description
General design models	PM_NF_32	Base case
	PM_NF_41	Suction control all materials
	PM_NF_43	Suction control all materials + pellets at rock wall in plug
Field test I model	PM_FT_08	Locked boundary at rock wall in plug
	PM_FT_09	Roller boundary at rock wall in plug
Field test II model	PM_TT_34	Seal blocks ρ_d: 1,631 kg/m^3 + 21 cm pellets-filled slot
	PM_TT_35	Seal blocks ρ_d: 1,682 kg/m^3 + 21 cm pellets-filled slot
	PM_TT_36	Seal blocks ρ_d: 1,682 kg/m^3 + 5 cm pellets-filled slot
	PM_TT_37	Seal blocks ρ_d: 1,631 kg/m^3 + 5 cm pellets-filled slot
Field test prediction	PM_TT_101	Base case
	PM_TT_102	Drained case
	PM_FT_1D_4	Pressurized case

Several bentonite components have been represented with different porosity values and different hydro-mechanical parameter values in the different models. The correspondence between dry densities of components (defined in KBS-3, or in the dome plug project), used void ratios and porosities, and the adoption of hydro-mechanical parameters are summarized in Table 5-5. All bentonite components were represented with an initial water content of 17% in the models. This was specified for backfill components in KBS-3, and for the bentonite blocks and the backfill pellets in the dome plug project. The pellets used for the seal in the field test were however, for the sake of simplicity, also modeled with this initial water content, although the actual value was 13%.

Table 5-5. Dry density values of bentonite components; corresponding void ratio and porosity values; and adoption (source or procedure) of hydro-mechanical parameters*.

Modeling task	Backfill blocks	Seal/transition zone blocks	Pellets
GMT	Dry density for backfill blocks in KBS-3: 1,700 kg/m^3 (see Åkesson et al. 2010a). Corresponds to e=0.635 and n=0.388 used in models	Dry density suggested in this project: 1,400 kg/m^3. Corresponds to e=1 and n=0.5 used in models.	Dry density for backfill pellets in KBS-3: 1,000 kg/m^3 (see Åkesson et al. 2010a). Corresponds to e=1.78 and n=0.64 used in models
FTI	HM parameters for MX80 e=0.635 according to Åkesson et al. 2010a.	HM parameters for MX80 adopted for e=1 with procedure presented by Åkesson et al. 2010a.	HM parameters for MX80 e=1.78 according to Åkesson et al. 2010a.
FTII	Dry density for backfill blocks in dome plug field test: 1,750 kg/m^3. With 2% slots this corresponds to e=0.62 and n=0.383, used in models. HM parameters for MX80 adopted for e=0.62 with procedure presented by Åkesson et al. 2010a.	Dry density initially suggested for the seal blocks during the planning of the dome plug field: 1,631 kg/m^3. With 2% slots this corresponds to e=0.74 and 0.425, used in the models. Dry density for seal blocks in dome plug field test: 1,682 kg/m^3. Corresponds to e=0.653 and n=0.395, used in models. HM parameters for MX80 e=0.74 according to Åkesson et al. 2010a.	Dry density for backfill pellets in dome plug field test: 900 kg/m^3. Corresponds to e=2.09 and n=0.676, used in models. HM parameters for MX80 e=1.78 according to et al. Åkesson 2010a.
FTP		Dry density for seal blocks in dome plug field test: 1,682 kg/m^3. With 2% slots this corresponds to e=0.686 and n=0.407, used in models. HM parameters for MX80 adopted for e=0.686 with procedure presented by Åkesson et al. 2010a.	

All used plastic parameter values were adopted in this project, see Section 5.5.5.

5.5.2 Model geometries

An axisymmetric 2D geometry was used to model the *General design models*. The dimensions of the different materials are shown in Figure 5-18. For the tunnel plug these dimensions were suggested within the project, whereas for the backfill the dimensions were adopted from Åkesson et al. (2010b). The used mesh for this geometry is also shown in Figure 5-18. The number of nodes and elements were 2,448 and 2,309, respectively.

An axisymmetric 2D geometry was used to model the *Field Test I models*. The dimensions of the different materials are shown in Figure 5-19. These dimensions were suggested within the project. The used mesh for this geometry is also shown in Figure 5-19. The number of nodes and elements were 704 and 650, respectively.

Two axisymmetric 2D geometries were used to model the *Field Test II models*. The dimensions of the different materials are shown in Figure 5-20 and Figure 5-21. The four main radii values for each geometry were derived from actual areas. The number of nodes and elements were 110 and 90, respectively.

An axisymmetric 2D geometry was used to model the Base case (model PM_TT_101) and the Drained case (model PM_TT_102) in the *Field test predictions*. The dimensions of the different materials are shown in Figure 5-22. The four main radii values were derived from actual areas. The width of the pellets-filled slot between the backfill blocks and the Leca blocks were set to 0.15 m. The used mesh for this geometry is shown in Figure 5-23 . The number of nodes and elements were 289 and 256, respectively.

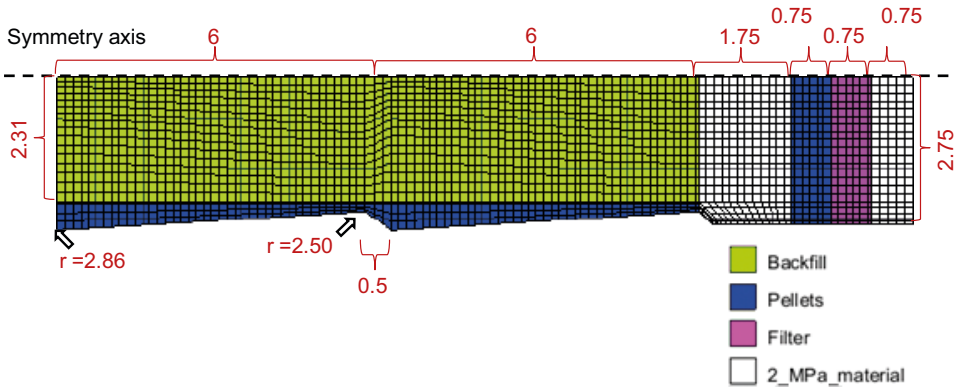

Figure 5-18. *Geometry of General design models.*

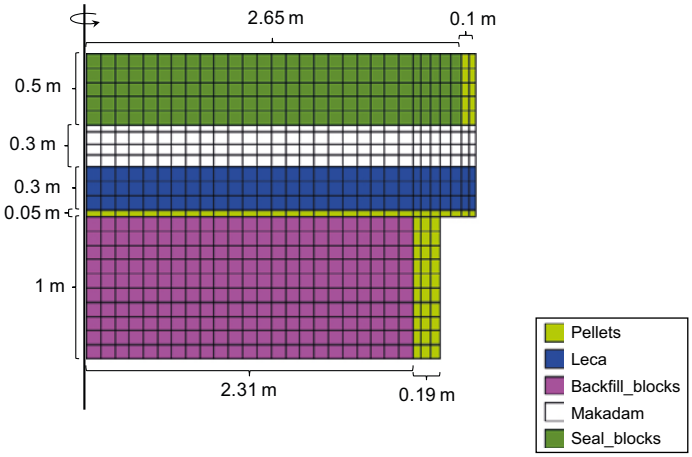

Figure 5-19. *Geometry of Field Test I models.*

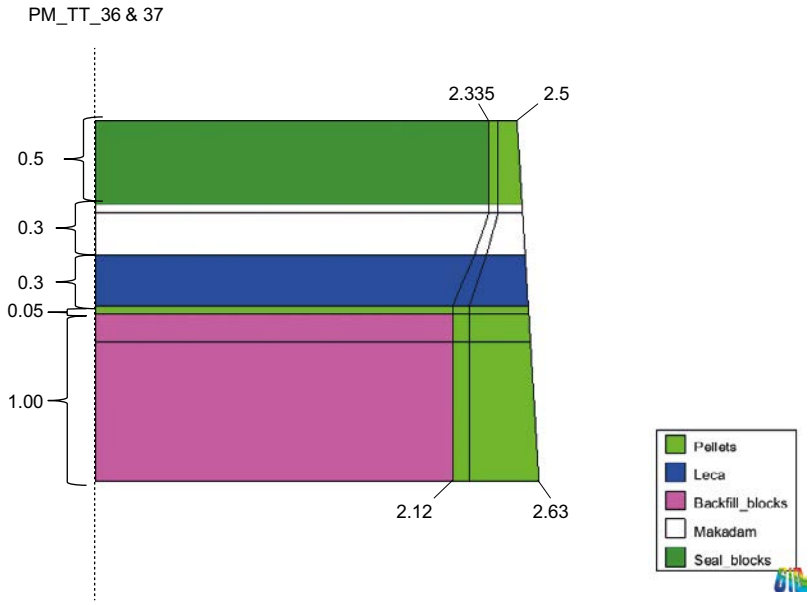

Figure 5-20. *Geometry of Field Test II model with 5 cm pellets-filled slot.*

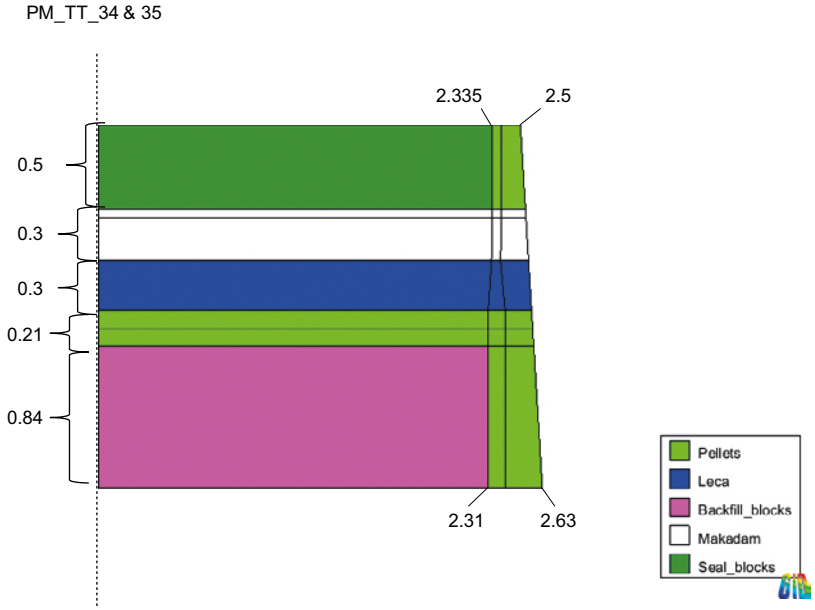

Figure 5-21. *Geometry of Field Test II model with 21 cm pellets-filled slot.*

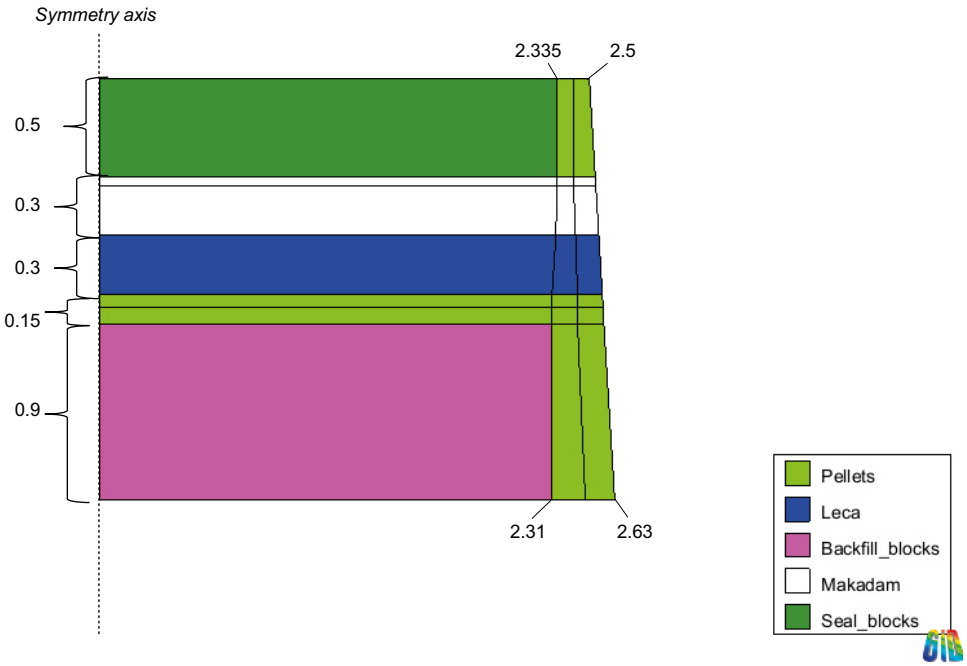

Figure 5-22. *Geometry of Field test predictions – Base case and Drained case.*

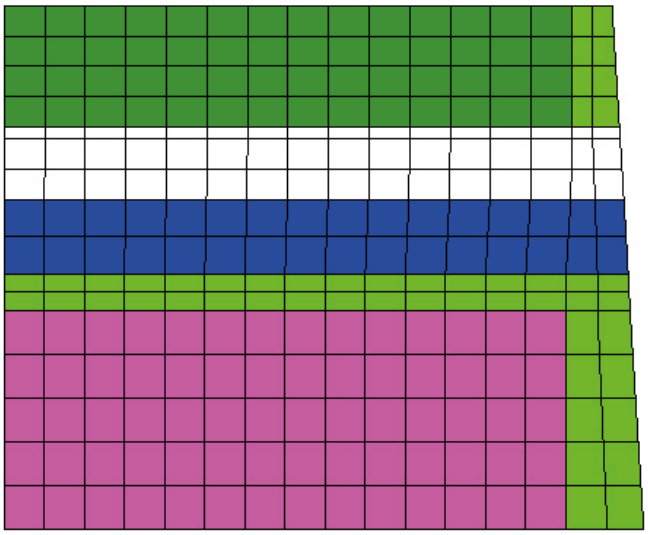

Figure 5-23. *Mesh of Field test predictions – Base case and Drained case.*

A plane 1D geometry was used to model the Pressurized case (model PM_FT_1D_4). The dimensions of the different materials as well as the mesh are shown in Figure 5-24. The number of nodes and elements were 64 and 31, respectively.

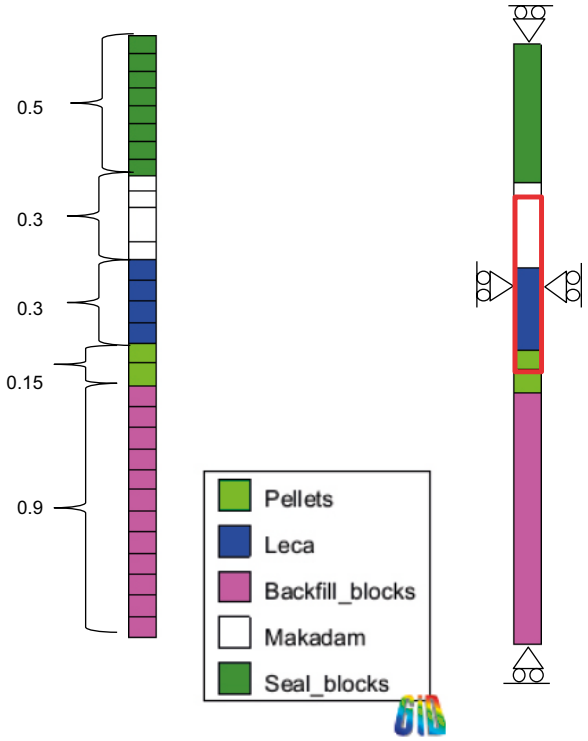

Figure 5-24. *Geometry, mesh and boundary condition of Field test predictions – Pressurized case. Red line denotes the surface boundary.*

5.5.3 Model initial conditions and boundary conditions

All models have had the same initial condition concerning liquid pressure and stresses in all materials. The initial liquid pressure was set to –45.9 MPa, and the total principal stresses were set to –0.11 MPa in all directions. All models were run without gravity, with constant temperature (20°C), and with constant gas pressure (0.1 MPa). The initial stresses thereby corresponded to a net mean stress (p') of 0.01 MPa.

All models were generally supplied with water through the *hydraulic surface boundary* over all filter and pellets fillings, except for the elements adjacent to the bentonite blocks (Figure 5-25, Figure 5-27, Figure 5-28 and Figure 5-29). These surface boundaries were increased from –45.9 to 0.1 MPa during the first 0.01 years. This approach was generalized in the modified cases of the general design models, in which surface boundaries were attached to all materials (see Figure 5-26). Three protocols were used for these boundaries: with a linear increase of liquid pressure during 0.01 years (filter and pellets), 30 years (seal) and 120 years (backfill blocks and transition zone). In the drained case of the field test predictions, the surface boundary only covered the Leca blocks and the pellets around the backfill blocks, and not the macadam and the pellets around the seal blocks as in Figure 5-29. A hydraulic surface boundary was also implemented on the filter and the pellet filling in the plane 1D model (Figure 5-24). The protocol for the liquid pressure at this boundary is shown in Table 5-6.

In all the 2D models, the *mechanical boundaries* towards the concrete dome and the rock wall were fixed, while the roller boundaries were applied to the symmetry axis and the "inner" side of the backfill (Figure 5-25, Figure 5-26, Figure 5-27 left, Figure 5-28 and Figure 5-29). In one case however (Field Test I model case PM_FT_09, see Figure 5-27 right), a roller boundary was applied to the rock wall around the plug construction. The reason for applying a fixed condition at the rock wall is that there were no feasible alternatives. Still, the approach may be relevant to some extent since the axial movements thereby will depend on the shear strengths of the pellets filling. Finally, roller boundaries were applied to all boundaries in the 1D model shown in Figure 5-24.

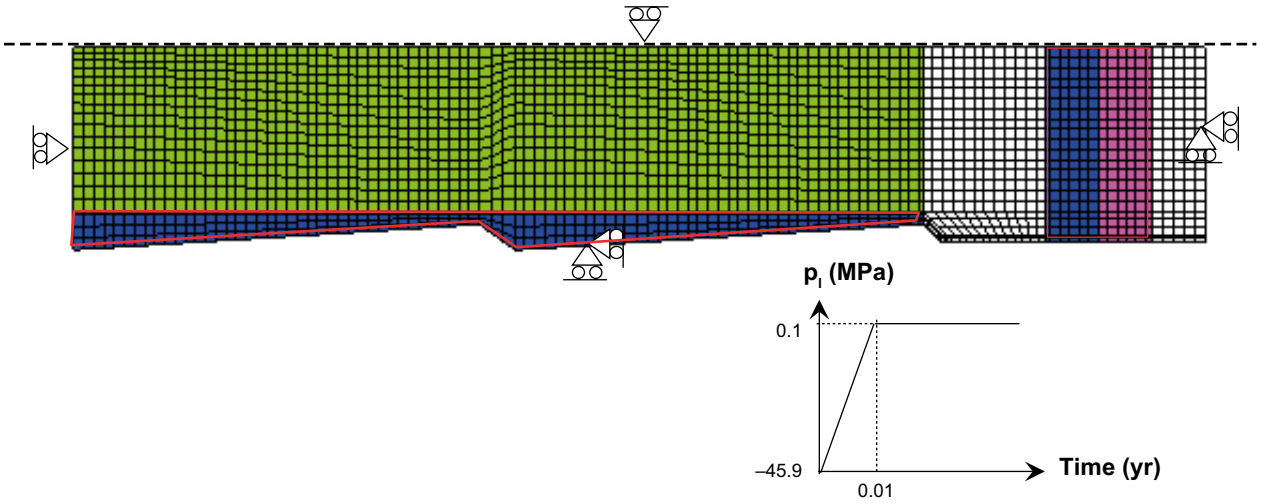

Figure 5-25. Boundary conditions of General design models – Base case. Red lines denote surface boundaries.

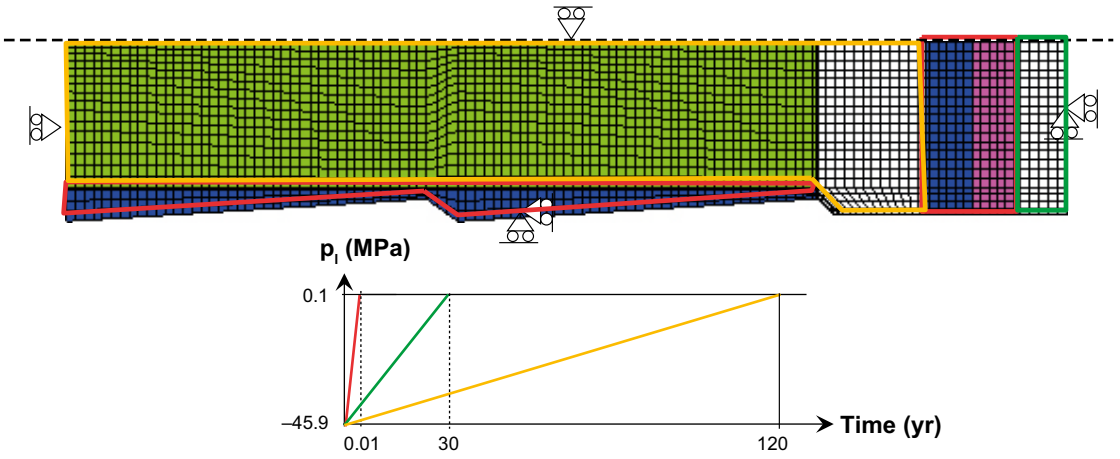

Figure 5-26. Boundary conditions of General design models – modified cases. Red, green and yellow lines denote surface boundaries.

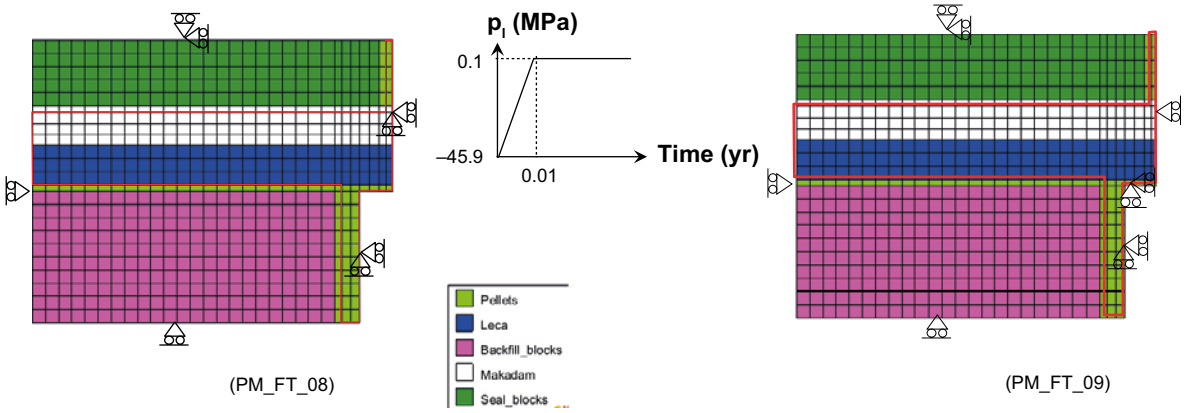

Figure 5-27. Boundary conditions of Field Test I model. Red line denotes the surface boundary.

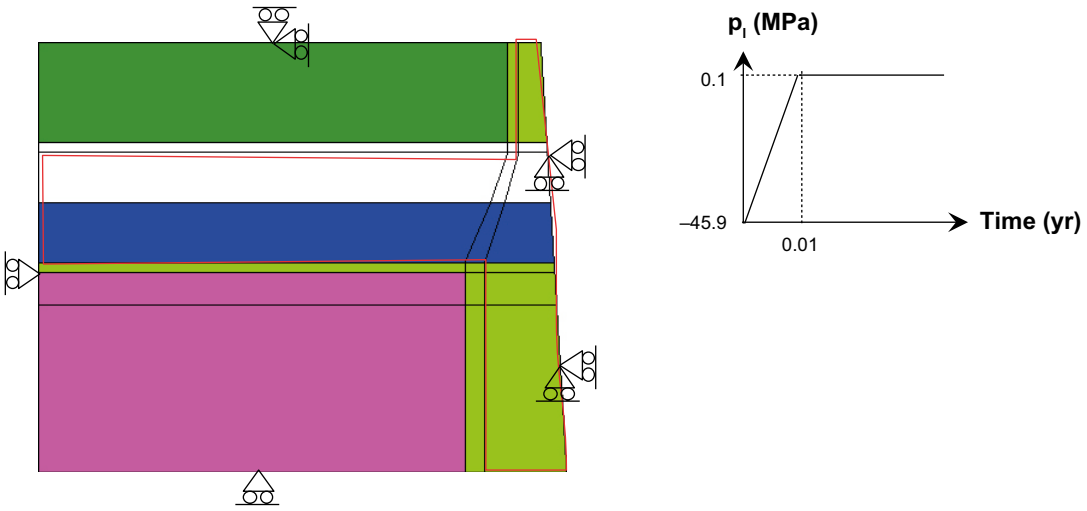

Figure 5-28. Boundary conditions of Field Test II models. Red line denotes the surface boundary.

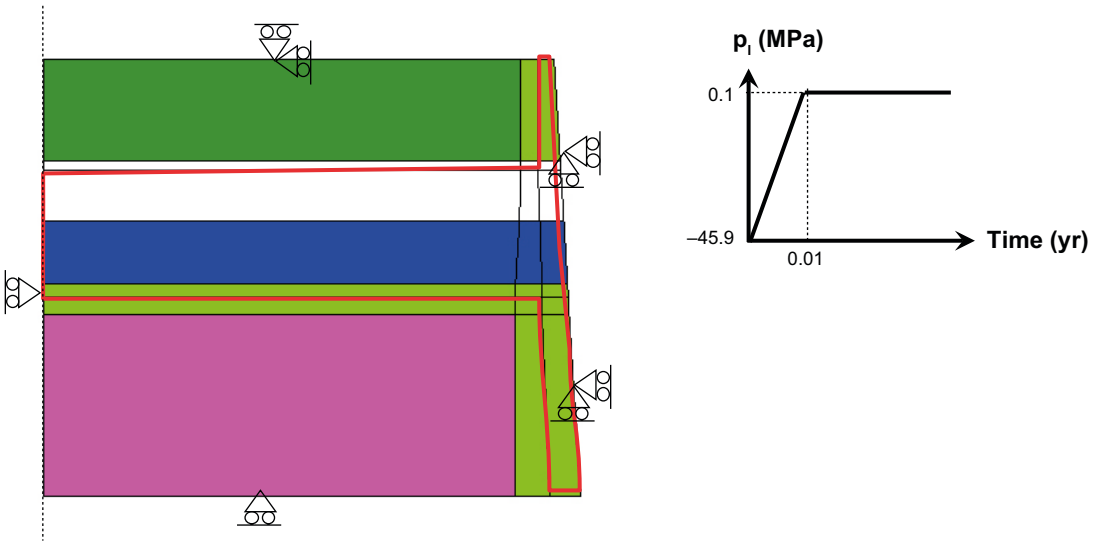

Figure 5-29. Boundary conditions in Field test prediction – Base case. Red line denotes the surface boundary.

Table 5-6. Liquid pressure protocol used in Pressurized case.

Interval	Time period (days)	Liquid pressure (MPa)
1	109–110	–45.9 → 0.1
2	110–119	0.1
3	119–120	0.1 → 5
4	120–150	5
5	150–151	5 → 7
6	151–392	7
7	392–393	7 → 10
8	393–414	10

5.5.4 Material model for bentonite

The hydro-mechanical constitutive laws used are summarized in Table 5-7, which includes Darcy's law, the van Genuchten retention curve, expressions for liquid density and viscosity as well as the mechanical constitutive law.

The elasto-plastic laws used, which are based on the Barcelona Basic Model, are summarized in Table 5-8.

Table 5-7. Summary of used constitutive laws.

Equation	Variable name	Equation	Parameter relationships
Constitutive equations			
Darcy's law	Liquid advective flux	$\mathrm{q}_l = -\frac{\mathrm{k}k_{rl}}{\mu_l}(\nabla p_l - \rho_l \mathrm{g})$	$k = k_0 \frac{n^3}{(1-n)^2}\frac{(1-n_0)^2}{n_0^3}$ $k = k_0 \exp(b(n-n_0))$ $k_{rl} = S_r^3$
Retention curve	Liquid degree of saturation	$S_r(s) = \left(1 + \left(\frac{s}{P_0}\right)^{\frac{1}{1-\lambda}}\right)^{-\lambda}$	
Phase density	Liquid density	$\rho_l(P_l, T) = \rho_{l0} \cdot \exp\left[\beta \cdot \left(P_l - P_{l0}\right) + \alpha \cdot T + \gamma \cdot \varpi_l^h\right]$	
Phase viscosity	Liquid viscosity	$\mu_l = 2 \cdot 10^{-12} \exp\left(\frac{1808.5}{273.15 + T}\right)$	
Mechanical constitutive model	Stress tensor	$d\varepsilon = d\varepsilon^e(d\sigma) + d\varepsilon^p(dp_0^*) + d\varepsilon^h(ds)$	

Table 5-8. Summary of used elasto-plastic laws (based on BBM).

Elastic strain increment:	$d\varepsilon^e = -\frac{1}{3}d\varepsilon_v^e \mathrm{I} + d\mathrm{e}^e$
Elastic volumetric strain increment:	$d\varepsilon_v^e = \frac{dp'}{K},\ K = \max\left\{\frac{(1+e)p'}{\kappa_i(s)}, K_{\min}\right\}$
Suction dependence of κ_i:	$\kappa_i(s) = \kappa_{i0}\left[1 + \alpha_i s\right]$
Elastic deviatoric strain increment:	$de^e = \frac{d\boldsymbol{s}}{2G},\ G = \frac{3(1-2\nu)}{2(1+\nu)}K$
Plastic strain increment:	$d\varepsilon^p = d\Lambda \frac{\partial g}{\partial \sigma}$
Yield surface:	$f = q^2 - M^2(p'+p_s)(p_0-p')$
Plastic potential:	$g = \alpha q^2 - M^2(p'+p_s)(p_0-p')$
Tensile strength:	$p_s(s) = p_{s0} + k \cdot s$
LC-curve:	$p_0(s, p_0^*) = p^c\left(\frac{p_0^*}{p^c}\right)^{\frac{\lambda_0 - \kappa_{i0}}{\lambda(s) - \kappa_{i0}}}$
Suction dependence of λ:	$\lambda(s) = \lambda_0((1-r)\exp(-\beta s) + r)$
Hardening law:	$dp_0^* = \frac{1+e}{\lambda_0 - \kappa_{i0}} p_0^* d\varepsilon_v^p$
Hydraulic strain increment:	$d\varepsilon^h = -\frac{1}{3}d\varepsilon_v^h \mathrm{I}$
Hydraulic volumetric strain increment:	$d\varepsilon_v{}^h = \frac{\kappa_s(p', e)}{(1+e)(s + p_{atm})}ds$
Void ratio and pressure dependence of κ_s:	$\kappa_s(p', e) = \kappa_{s0} f(p', e)$ $f(p', e) = \begin{cases} 1 & \text{if } p' < p_{ref} \\ 10^{-20} & \text{if } p' > p_{swell}(e) \\ 1 - \frac{\ln p' - \ln p_{ref}}{\ln(p_{swell}(e)) - \ln p_{ref}} & \text{otherwise} \end{cases}$ $p_{swell}(e) = 10^{\left[c_0 + c_1\frac{p_s}{1+e} + c_3\left(\frac{p_s}{1+e}\right)^2\right]^{-3}}$

5.5.5 Material parameter values

The numerical models have included different bentonite based materials (backfill blocks, seal and transition zone blocks and pellets) and different filter materials (sand, Leca blocks and macadam), and the specifications and the descriptions of these materials have developed to some extent during the course of the different modelling tasks. The presentation below begins with the bentonite based materials, for which the adoption of hydraulic, elastic and plastic parameters are described separately and ends with filter materials. The parameter values for the bentonite based materials and the filter materials are presented in Table 5-9 and Table 5-10, respectively.

The bentonite blocks that were manufactured for the seal in the field test are made of MX-80 bentonite. The backfill blocks are however made of Asha bentonite. All bentonite in the models are nevertheless regarded as MX-80, simply because the information about Asha is quite limited. Swelling pressures reported by Karnland et al. (2006) indicate however that these two types of bentonite are fairly similar concerning the swelling pressures.

The *hydraulic parameter values for backfill blocks* in the General design models and the Field test I models were the same as for backfill blocks in Åkesson et al. (2010a). The corresponding values in the Field Test II models were the same as for buffer blocks in Åkesson et al. (2010a). Finally, the values for the Field test predictions were adopted for an initial void ratio of 0.62 and a water content of 17%. The retention curve (Figure 5-30) was adopted by using the swelling pressure curve, Equation (5-2), and the model presented by Dueck (2004). The hydraulic conductivity value was derived with the void ratio dependent relation in Equation (5-3).

The *hydraulic parameter values for seal and transition zone blocks* in the General design models and the Field test I models were adopted for an initial void ratio of 1 and a water content 17%. The retention curve was adopted by using retention data for free swelling conditions presented by Dueck (2004), see Figure 5-31. The hydraulic conductivity value was derived with the void ratio dependent relation in Equation (5-3).

The corresponding values in the Field test II models were the same as for a homogenized backfill (e=0.74) in Åkesson et al. (2010a). Finally, the parameter values for the Field test predictions were adopted for an initial void ratio of 0.686 and a water content of 17%. The retention curve (Figure 5-32) was adopted by using swelling pressure curve, see Equation (5-2), and the model presented by Dueck (2004). The hydraulic conductivity value was derived with the void ratio dependent relation in Equation (5-3).

The *hydraulic parameter values for pellets* in all modelling tasks were the same as for pellets in Åkesson et al. (2010a).

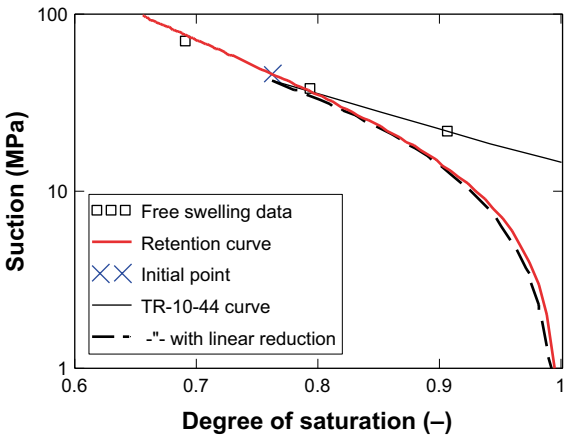

Figure 5-30. *Retention curve for backfill blocks. Void ratio is 0.62 and initial water content is 17%.*

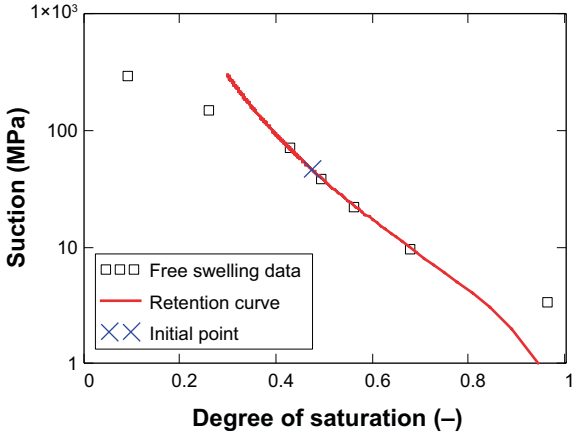

Figure 5-31. *Retention curve for seal/transition zone blocks in General design models and the Field test I models. Void ratio is 1.0 and initial water content is 17%.*

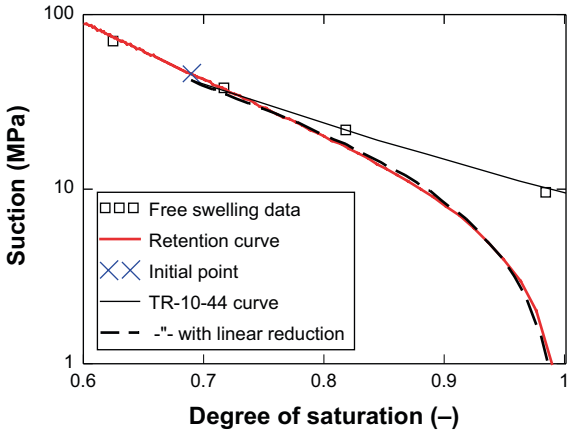

Figure 5-32. *Retention curve for seal blocks in Field test predictions. Void ratio is 0.686 and initial water content is 17%.*

The *elastic mechanical parameters values for all bentonite based materials* were basically the same as for blocks and pellets in Åkesson et al. (2010a). The inbuilt function for the α_{sp} parameter (which governs the pressure dependence of the swelling modulus κ_s) was however changed so that it incorporated the swelling pressure curve used (Equation (5-2)). Moreover, the related p_{ref}-parameter in the swelling modulus was set to lower values than in the original setting by Åkesson et al. (2010a). This was mainly due to that the used swelling pressure curve is lower than the original curve. Finally, the Poisson's ratio for pellets was adjusted to 0.4.

The *plastic mechanical parameter values for all bentonite based materials* were adopted for all the modelling tasks, since these parameter values were based on the used swelling pressure curve. A description of the method for the adoption of these parameters is given by Åkesson et al. (2010a). One major part of this method is the notion of a target void ratio, i.e. the perfectly homogenized void ratio in a specific volume, and in the General design models and the Field Test I models these target void ratios were different for backfill blocks, and seal and transition zone blocks, respectively, whereas in the Field Test II models and the Field test predictions they were same for the different materials. In the former case, the parameter values for the pellets were derived for the target void ratio for the backfill. Finally, the suction dependent LC curve was utilized for the backfill blocks and the seal blocks in the field test predictions, in order to mimic the void ratio dependence of the yield surface (Figure 5-33). A similar approach was recently used by Åkesson et al. (2012).

Table 5-9. Parameter values used for different bentonite based materials in different modelling tasks (GMD: General design model; FTI: Field test I model; FTII: Field test II model; FTP: Field test prediction).

		Backfill blocks				Seal / transition zone blocks				Pellets			
		GDM	FTI	FTII	FTP	GDM	FTI	FTII	FTP	GDM	FTI	FTII	FTP
Initial void ratio	e (–)	0.635	0.635	0.62	0.62	1	1	0.74‡	0.686!	1.78	1.78	2.09	2.09
water content	w (%)	17%	17%	17%	17%	17%	17%	17%	17%	17%	17%	17%	17%
Initial porosity	n (–)	0.388	0.388	0.385	0.383	0.5	0.5	0.425‡	0.407	0.64	0.64	0.676	0.676
Intrinsic	k_0 (m^2)	$2.1\cdot10^{-21}$	$2.1\cdot10^{-21}$	$2.0\cdot10^{-21}$	$1.9\cdot10^{-21}$	$2.4\cdot10^{-20}$	$2.4\cdot10^{-20}$	$4.8\cdot10^{-21}$	$3.2\cdot10^{-21}$	$5.2\cdot10^{-19}$	$5.2\cdot10^{-19}$	$5.2\cdot10^{-19}$	$5.2\cdot10^{-19}$
permeability**)	n_0 (–)	0.388	0.388	0.385	0.383	0.5	0.5	0.425	0.407	0.64	0.64	0.64	0.64
Relative permeability	k_r (–)	S_r^3	S_r^3	S_r^3	S_r^3	S_r^3	S_r^3	S_r^3	S_r^3	S_r^3	S_r^3	S_r^3	S_r^3
Water retention curve	P_0 (MPa)	37.2	37.2	43.5	18.9	2.34	2.34	11.6	10.0	0.162	0.162	0.162	0.162
	λ (–)	0.34	0.34	0.38	0.195	0.20	0.20	0.23	0.185	0.19	0.19	0.19	0.19
Target void ratio		0.83	0.74	0.95	0.92	1	1	0.95	0.92	0.83	0.74†	0.95	0.92
Porous elasticity	κ_{i0} (–)	0.14	0.14	0.14	0.12	0.14	0.14	0.14	0.12	0.15	0.15	0.15	0.15
	α_i	–0.021	–0.021	–0.021	–0.021	–0.021	–0.021	–0.021	–0.021	–0.021	–0.021	–0.021	–0.021
	α_{ils}	0	0	0	0	0	0	0	0	0	0	0	0
	K_{min} (MPa)	20	20	20	20	20	20	20	20	1	1	1	1
Swelling modulus	κ_{s0} (–)	0.3	0.3	0.3	0.3	0.3	0.3	0.3	0.3	0.3	0.3	0.3	0.3
	α_{ss} (–)	0	0	0	0	0	0	0	0	0	0	0	0
	α_{sp}	*)	*)	*)	*)	*)	*)	*)	*)	*)	*)	*)	*)
	p_{ref} (MPa)	1	1	1	0.5	0.5	0.5	0.5	0.5	0.025	0.025	0.025	0.025
Poisson's ratio	v (–)	0.2	0.2	0.2	0.2	0.2	0.2	0.2	0.2	0.4	0.4	0.4	0.4
Plastic stress strain	λ_0 (–)	0.179	0.165	0.198	0.194	0.207	0.207	0.198	0.194	0.254	0.26	0.294	0.29
modulus	r (–)	0	0	0	0.65	0	0	0	0.65	0	0	0	0
	β (MPa^{-1})	0	0	0	0.01	0	0	0	0.01	0	0	0	0
Critical state line parameter	M (–)	0.251	0.238	0.261	0.259	0.278	0.278	0.261	0.259	0.564	0.564	0.705	0.705
Tensile strength	p_{s0} (MPa)	1.8	2.4	1.3	1.4	1.0	1.0	1.3	1.4	0.05	0.05	0.02	0.02
	k (MPa^{-1})	0	0	0	0.035	0	0	0	0.035	0	0	0	0
Non-associativity parameter	α (–)	0.5	0.5	0.5	0.5	0.5	0.5	0.5	0.5	0.5	0.5	0.5	0.5
Pre-consolidation	p_0^* (MPa)	9.84	16	5.55	6.36	4.32	4.32	5.55	6.36	0.242	0.242	0.11	0.11
stress	p_c (MPa)	1	1	1	1	1	1	1	1	1	1	1	1

* inbuilt sp-relation; ** Kozenys law; † Target 0.74 for backfill and 1 for seal; ‡ only e and n changed for cases with e=0.653
! The void ratio was slightly increased in order to take slots between the blocks into account.

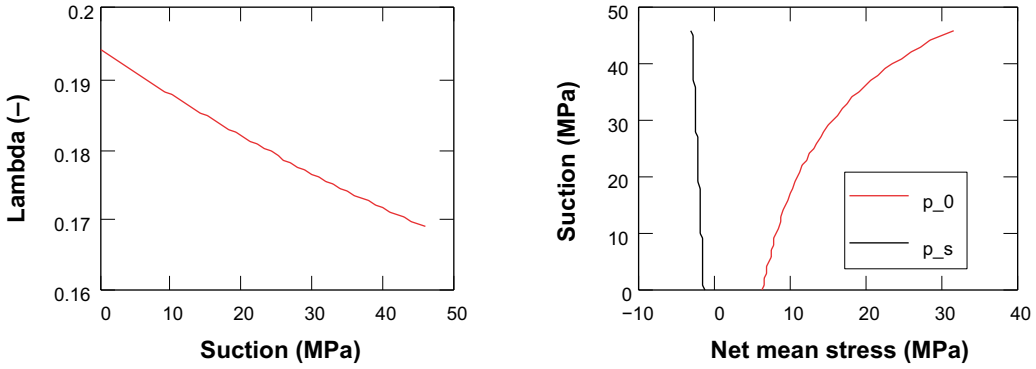

Figure 5-33. *Plastic parameters for blocks in Field test prediction models.*

Lambda is calculated as an average module between two points on the swelling pressure curve, representing the initial void ratio (e_i) and the homogenized target void ratio (e_f)

$$\lambda = -\frac{e_i - e_f}{\ln(p_{swell}(e_i)) - \ln(p_{swell}(e_f))} \tag{5-47}$$

It should be noted that this approach is most relevant for materials that are consolidated, i.e. pellets. For blocks, this approach has been refined so that lambda corresponds to the slope at the target void ratio.

The yield surface is described by the following relation:

$$q^2 = M^2(p' + p_s)(p_0^* - p') \tag{5-48}$$

The tensile strength (p_s) and the critical state parameter (M) are parameters, whereas p_0^* is a hardening variable. The tensile strength (p_s) is regarded to be a void ratio dependent quantity and is derived from the original parameter value adoption by Åkesson et al. 2010. The net mean stress at the critical state point is assumed to be equal to the swelling pressure, ($p' = p_{swell}$). From this it follows that the initial value of p_0^* can be calculated as:

$$p_0^* = p_s + 2 \cdot p_{swell} \tag{5-49}$$

The deviatoric stress q at the critical state point (q_f) is given by Equation (5-4):

$$q_f = a \cdot p_{swell}^b \tag{5-50}$$

The critical state line parameter can thus be calculated as:

$$M = \frac{a \cdot p_{swell}^b}{p_{swell} + p_s} \tag{5-51}$$

Only a few parameters were used for the filter materials (Table 5-10). The *hydraulic parameter values* were the same for all filter materials. The retention curve used was the same as for crushed rock in Åkesson et al. (2010a) (with the modification of a minimum saturation degree of 1%). The intrinsic permeability was set to 10^{-18} m^2. This value should have no effect on the results and was chosen in order to promote numerical convergence. The *elastic parameter values* for the filter sand were the same as for crushed rock in Åkesson et al. (2010a). The corresponding values for Macadam and Leca were derived from laboratory tests, see Section 5.3.2.

Table 5-10. Parameter values used for filter materials.

		Filter sand	Macadam	Leca
Initial porosity	n (–)	0.35	0.35	0.35
Intrinsic permeability	k_0 (m^2)	$1 \cdot 10^{-18}$**)	$1 \cdot 10^{-18}$**)	$1 \cdot 10^{-18}$**)
Relative permeability	k_r (–)	S_r^3	S_r^3	S_r^3
Water retention curve	P_0 (MPa) λ (–)	0.003 0.9*)	0.003 0.9*)	0.003 0.9*)
Young modulus	E (MPa)	60	20	90
Poisson's ratio	v (–)	0.2	0.25	0.2

* mimimum saturation: 0.01
** Lowered to 10^{-50} in Drained case for macadam

5.5.6 Model results

General design models

Results from the Base case model are presented in Figure 5-34 – Figure 5-39.

Final distributions of stresses, void ratio and displacement along the tunnel axis after full saturation has been reached are shown in Figure 5-34. Results from an analytical calculation, performed with the inverse calculation procedure presented in Section 5.4.1, are also shown for comparison. Some differences between these solutions can be noted, e.g. the stress level in the backfill is slightly higher in the numerical model. The main differences between these model approaches are: i) fixed mechanical boundaries along the rock wall; and ii) the irreversible swelling/compression cycles (hysteresis) which imply that consolidated parts yields higher swelling pressure.

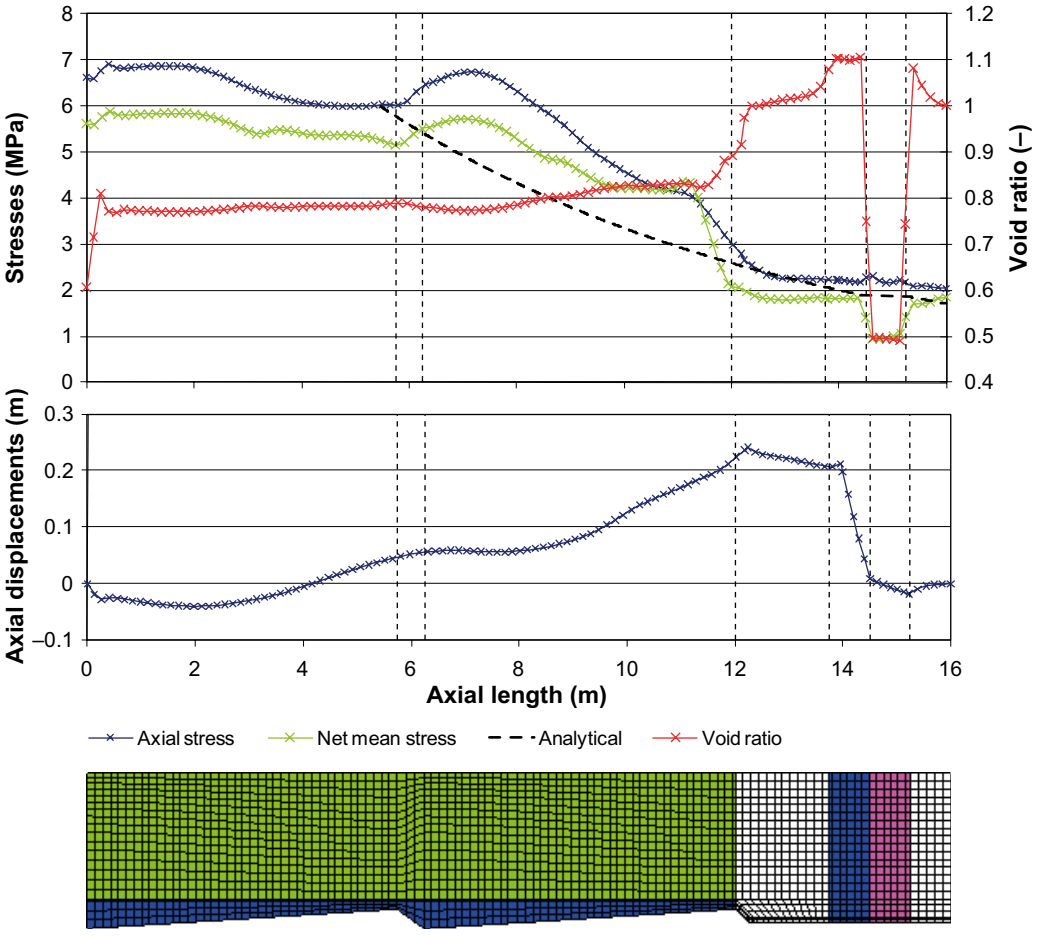

Figure 5-34. Final state border graphs of axial stress and void ratio. Analytical stress distribution added for comparison.

Stress paths in the *e-p'* plane for a selection of nodes along the symmetry axis in the Base Case model are shown in Figure 5-35.The dotted line represents the swelling pressure curve used, see Equation (5-2). Four characteristic path types can be noted:

1. Nodes in pellets increased in mean stress, with almost no swelling, and reached the swelling pressure curve, after which the pellets was compressed beyond the swelling pressure curve. The two slopes reflect that the compression first was elastic and then elasto-plastic.
2. Nodes in the seal and transition zone blocks, close to the pellets filling and filter, increased in mean stress, with some swelling (from 1 to 1.2 in void ratio), and reached the swelling pressure curve, after which the bentonite was compressed beyond the swelling pressure curve.
3. Nodes in the seal and transition zone blocks, at some distance from the pellets filling and filter, increased in mean stress, with only some minor swelling, and reached the swelling pressure curve, after which the bentonite was compressed to some minor extent.
4. Nodes in the backfill blocks, at some distance from the transition zone blocks, increased in mean stress, with some swelling (from 0.635 to 0.8 in void ratio), and reached the swelling pressure curve precisely.

The stress paths for the "expansive" nodes in the seal and transition zone blocks (close to the pellets filling and filter) are further analyzed in Figure 5-36. Stress paths are in this graph shown for the two principal net stresses (axial and radial) versus the void ratio. Experimental stress paths (also principal net stresses) from the oedometer test presented in Section 5.3.3 are shown for comparison. It can be noted that final portions of the stress paths in the model coincide quite well with the experimental paths.

A corresponding comparison for nodes in the pellets filling is shown in Figure 5-37. The experimental stress paths have been reported by Börgesson et al. (1995). Some resemblance can also be noted for these nodes, although the experimental stresses exceeded the modelled stresses to some extent.

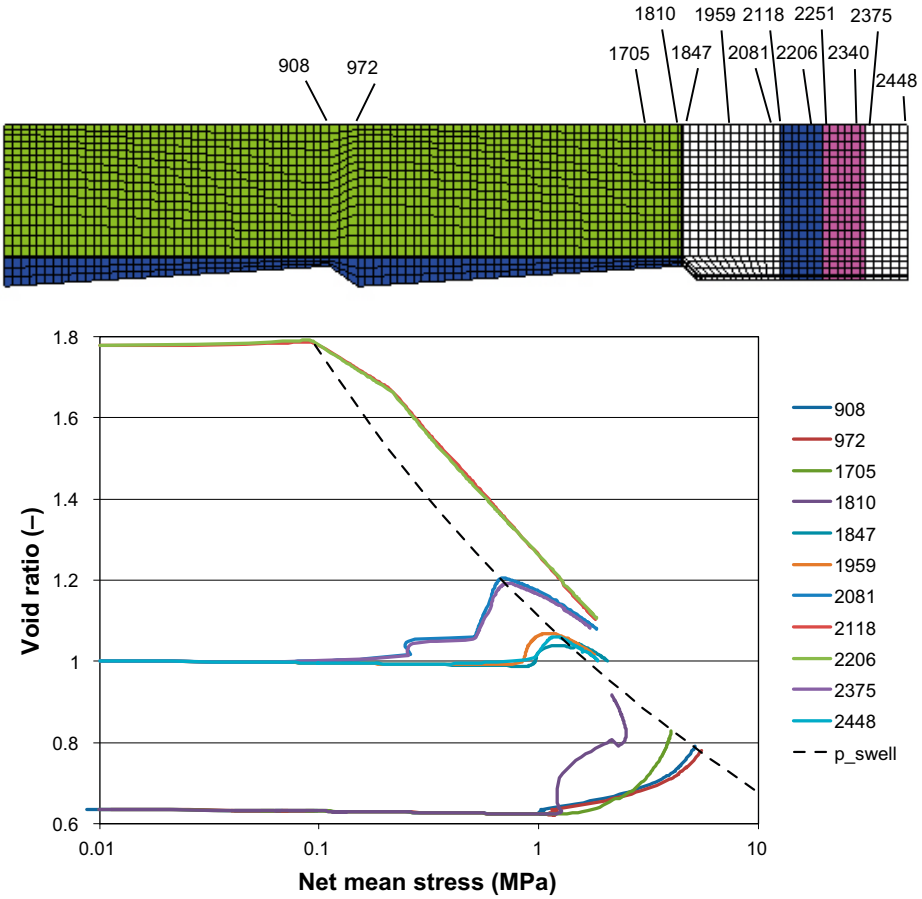

Figure 5-35. *Stress paths in e-p' plane for a selection of nodes.*

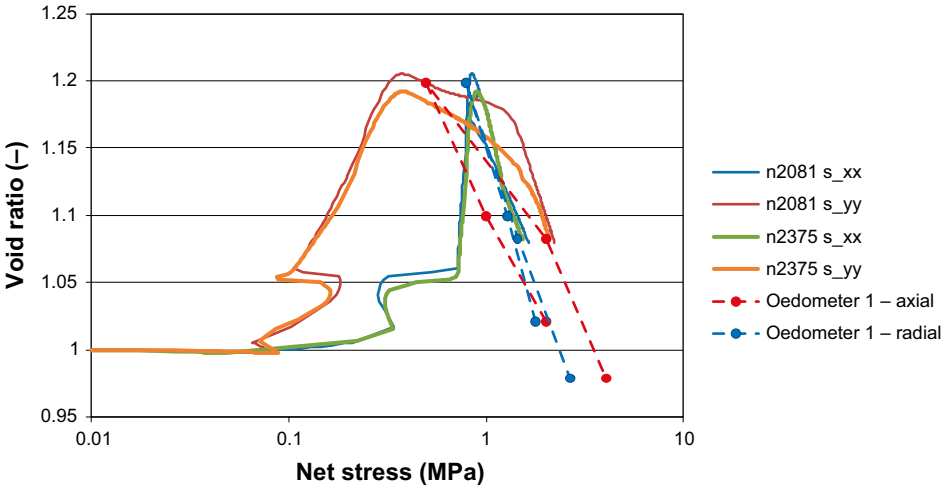

Figure 5-36. *Stress paths in e-σ' plane for two "expansive" nodes in transition zone blocks. Experimental data added for comparison.*

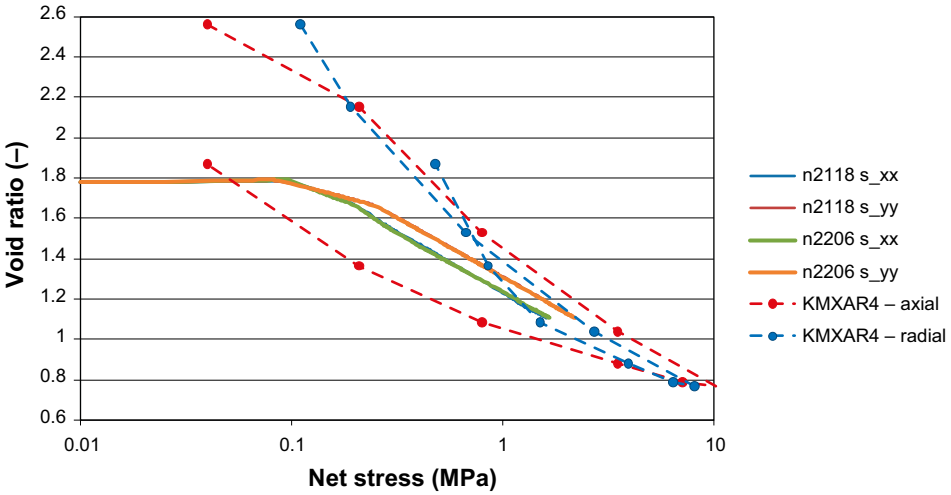

Figure 5-37. *Stress paths in e-σ' plane for two nodes in transition zone pellets. Experimental data added for comparison.*

Radial distributions of axial stresses against the concrete plug are shown in Figure 5-38. It can be noted that the final stresses equilibrate at a level of approximately 2 MPa, as intended. The time to reach this level was quite long (~100 years) and was largely determined by the hydration of the back-fill. One feature of the distributions is the relatively high pressures at the rock wall. This appears to be a consequence of the fixed mechanical boundary at the rock wall which implies that the adjacent bentonite cannot swell to the same extent as in the central part of the seal.

The hydration of the different components is illustrated by the evolution of the saturation degree in "inner" nodes in the backfill, transitions zone and the seal, respectively in Figure 5-39. This picture shows that the time scale to saturate the seal was approximately 30 years, whereas the corresponding time for the transition zone and the backfill was slightly more than 100 years.

The modelled hydration of the seal can be compared with experimental results from a small-scale water uptake test which has been reported by Börgesson (2001), see Figure 5-40. This test had basically the same initial void ratio and the same initial water content as the in the modelled seal. The length of the test was 50 mm, which means that the ratio between the length of seal and the water uptake test was 15. This in turn means that the time-scale for the hydration of the seal should be 225 times longer than for the test, since the ratio of the time-scales should be equal to the square of the length

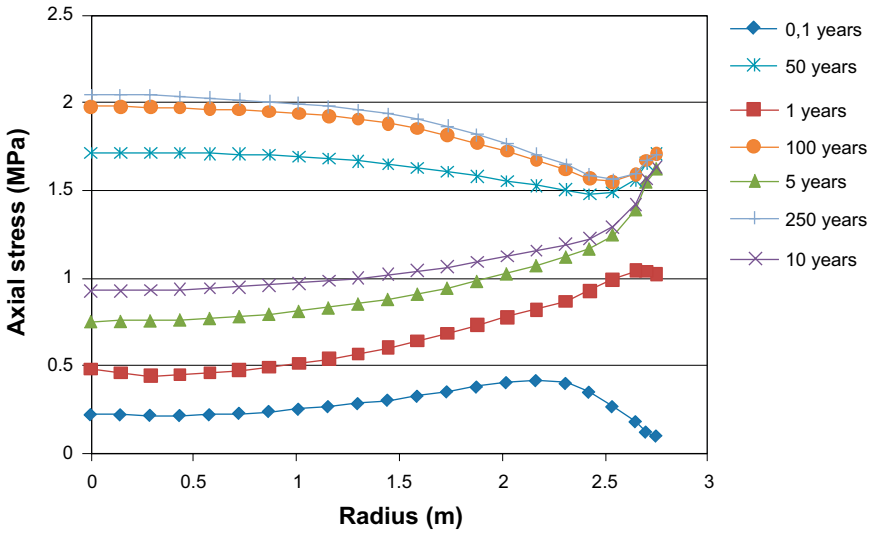

Figure 5-38. *Radial distributions of axial stresses against concrete plug.*

ratio in a diffusion process. The saturation profiles in the lab-test were determined after 1, 2 and 4 weeks, and the corresponding times for the model results in Figure 5-40 is 225 times longer in order to enable a comparison. It can be noted that saturation profiles display some similarities, although the modelled saturation progress is faster than the measured process.

The modified case with suction control in all materials is shown in Figure 5-41, with final distributions of stresses, void ratio and displacement along the tunnel axis after full saturation has been reached. The main differences between these results and the corresponding results from the base case (Figure 5-34) are the relatively high void ratio and low swelling pressure in the backfill in the modified case, and this is probably due to a more extensive homogenization of the backfill. The axial stress distribution in the modified case was also more similar to the analytical solution than the base case was, and this was probably due to the absence (or limitation) of hysteretic effects in this case.

The final state of the plug construction was quite similar in the two models. This is further illustrated Figure 5-42 which shows the evolution of axial displacement and axial stress at five nodes along the tunnel axis. This shows that the evolutions are quite different in the two models although the final states are quite similar.

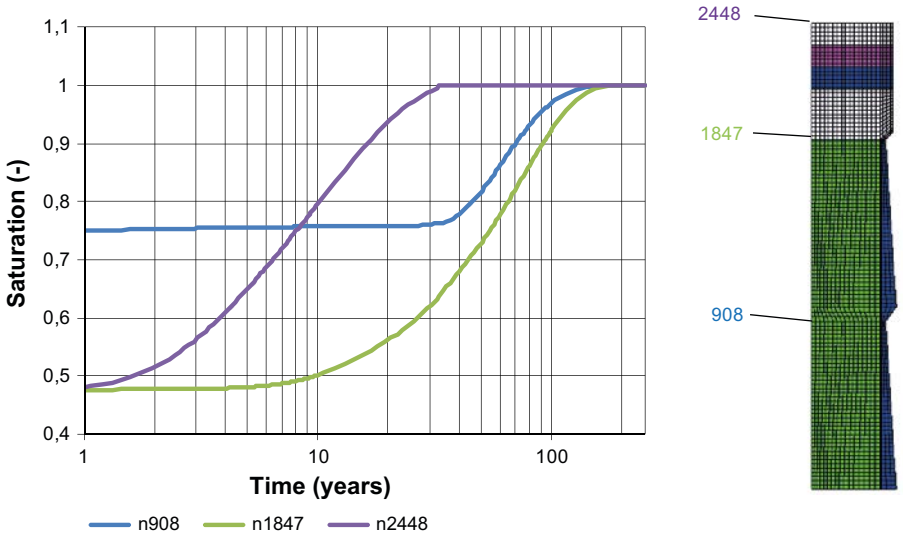

Figure 5-39. *Evolution of saturation in different nodes.*

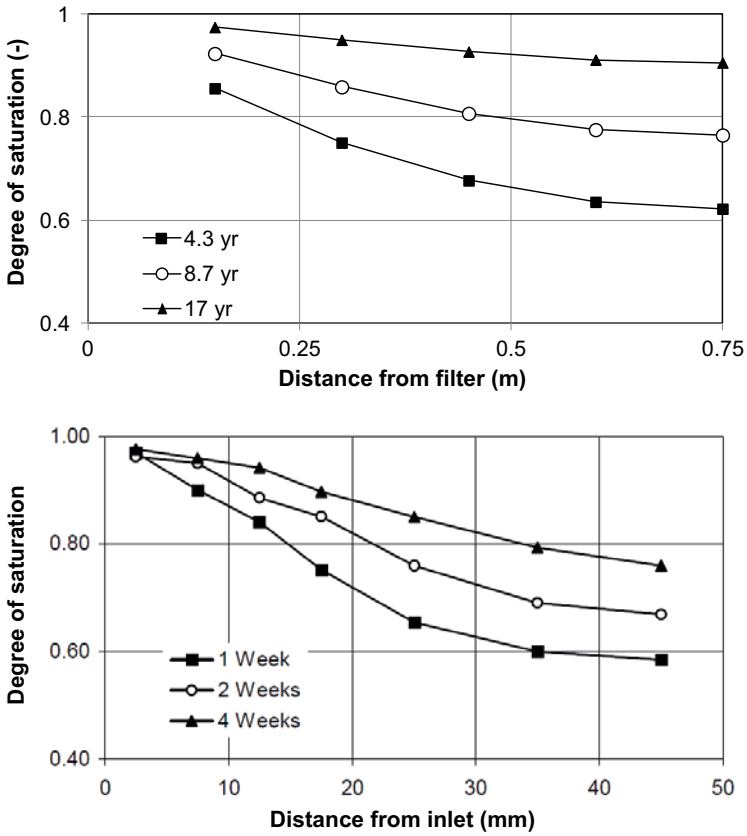

Figure 5-40. *Saturation profiles in seal along symmetry axis for three different points in time (upper). Results from water uptake test with initial target void ratio of 1.0 and initial saturation degree of 50% (lower).*

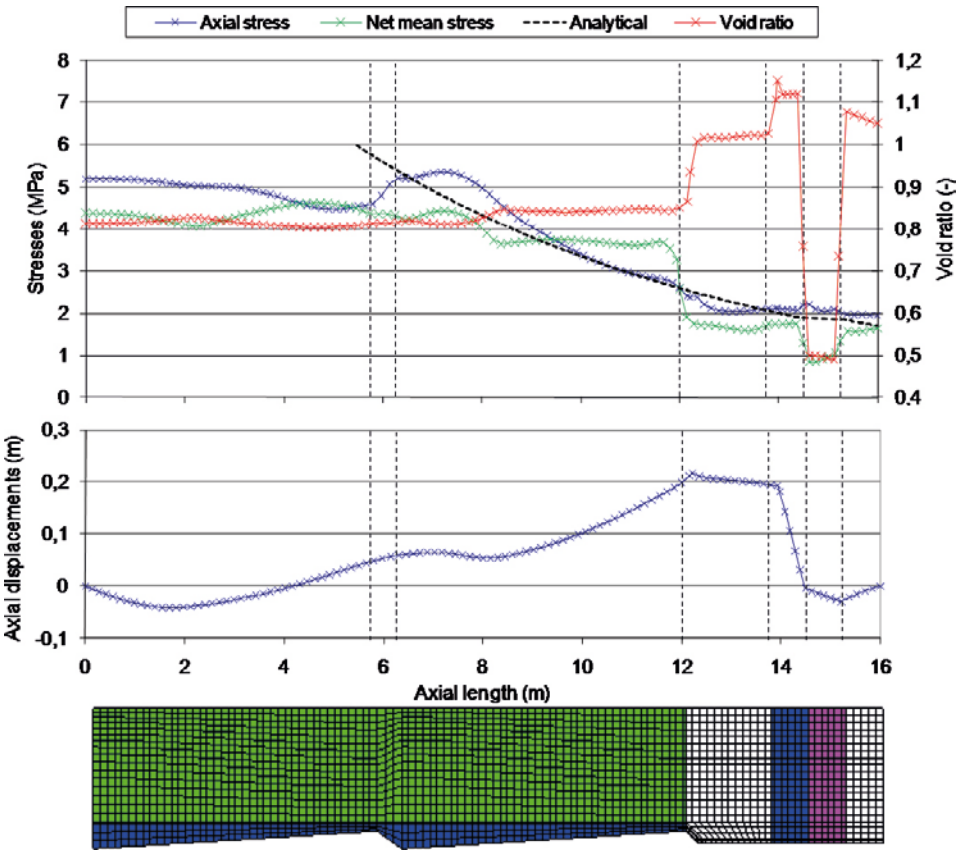

Figure 5-41. *Model PM_NF_41. Final state border graphs of axial stress and void ratio. Analytical stress distribution added for comparison.*

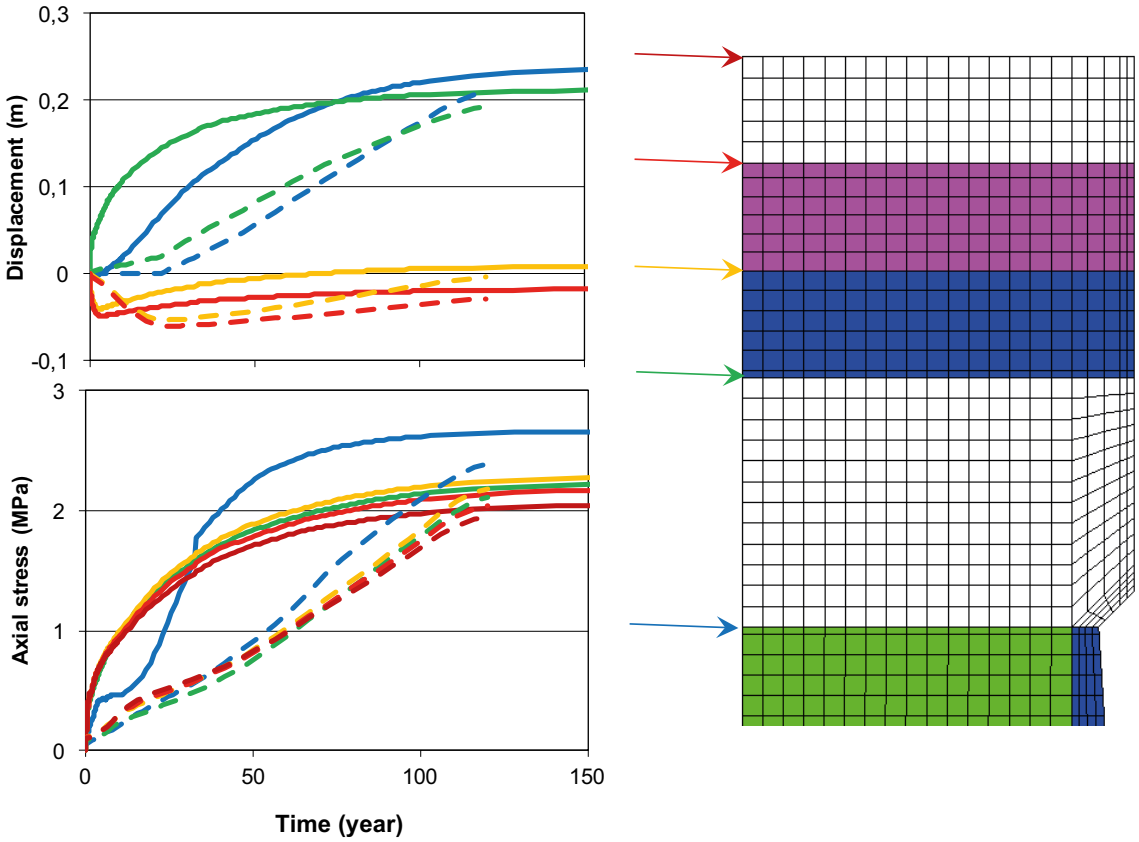

Figure 5-42. *Evolution of axial displacement and axial stress in five nodes along the tunnel axis. Comparison of results from base case (NF_32 – solid lines) and modified case with suction control in all materials (NF_41 – dotted lines).*

The modified case with suction control in all materials, as well as with a *pellets-filled slot in the seal*, is shown in Figure 5-43 with final distributions of stresses, void ratio and displacement along the tunnel axis after full saturation has been reached. The differences between these results and the corresponding results from the modified case without pellets in the seal (Figure 5-41) are small.

Field Test I models

Results from the Base case model are shown in Figure 5-44 to Figure 5-48.

The evolutions of axial displacement in four nodes along the tunnel axis are shown in Figure 5-44. This shows that the analyzed nodes were all displaced outwards, i.e. towards the concrete plug. The largest displacement (75 mm) was found at the interface between the backfill blocks and the pellets filling, whereas the smallest (8 mm) was found at the interface between the seal blocks and the macadam filling.

The evolutions of axial stresses in six nodes are shown in Figure 5-45. This shows the axial stresses followed almost the same trends in the different nodes and all ended up on a level of 3–4 MPa. The stresses were approximately 2 MPa after five years.

Radial distributions of axial stresses against the concrete plug are shown in Figure 5-46. The final stresses equilibrate at a level of approximately 3 MPa in the central part. The time to reach this level was approximately 60 years.

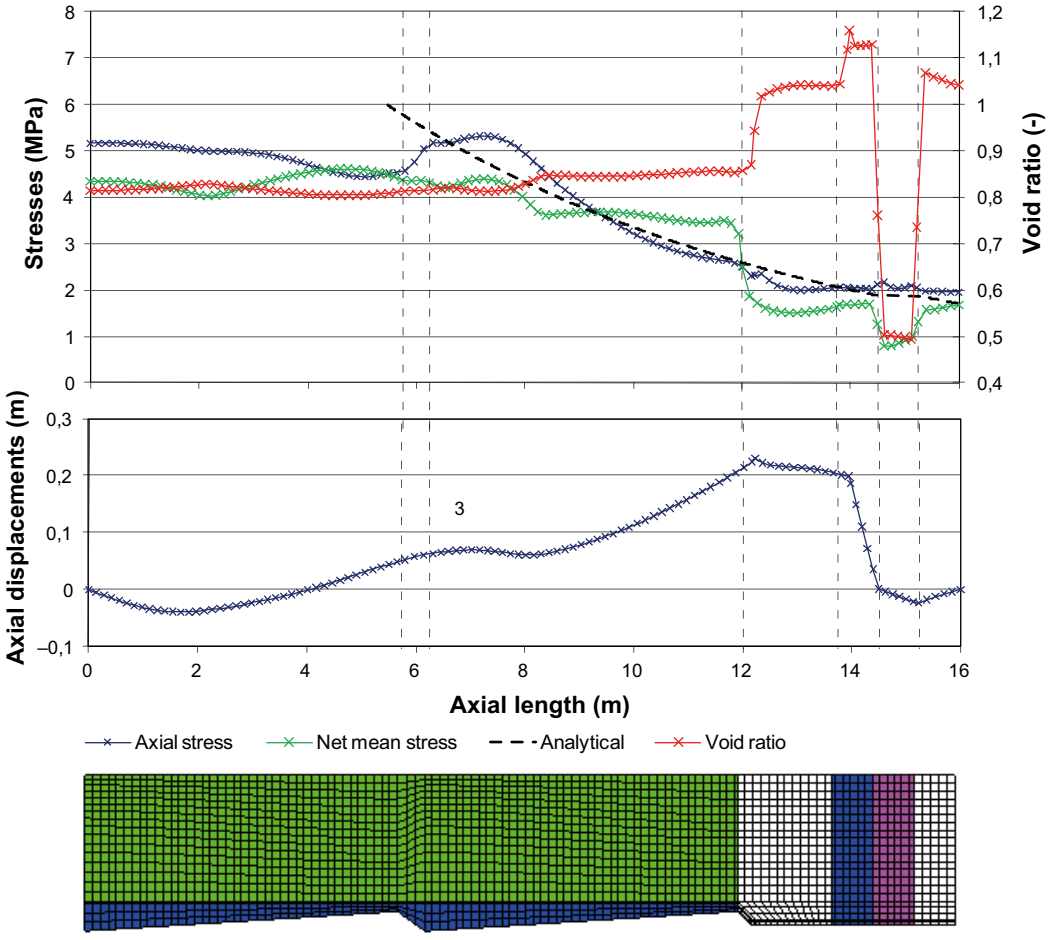

Figure 5-43. *Model PM_NF_43. Final state border graphs of axial stress and void ratio. Analytical stress distribution added for comparison.*

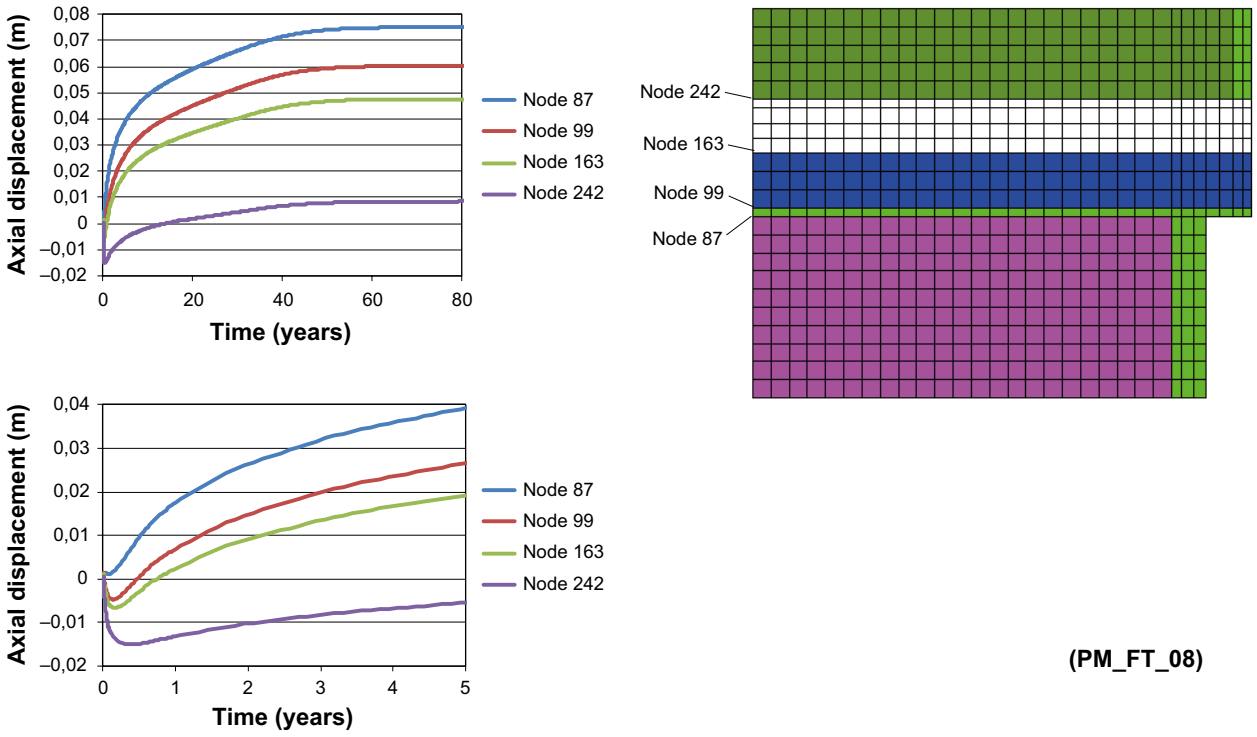

Figure 5-44. *Axial displacements along tunnel axis in field test model.*

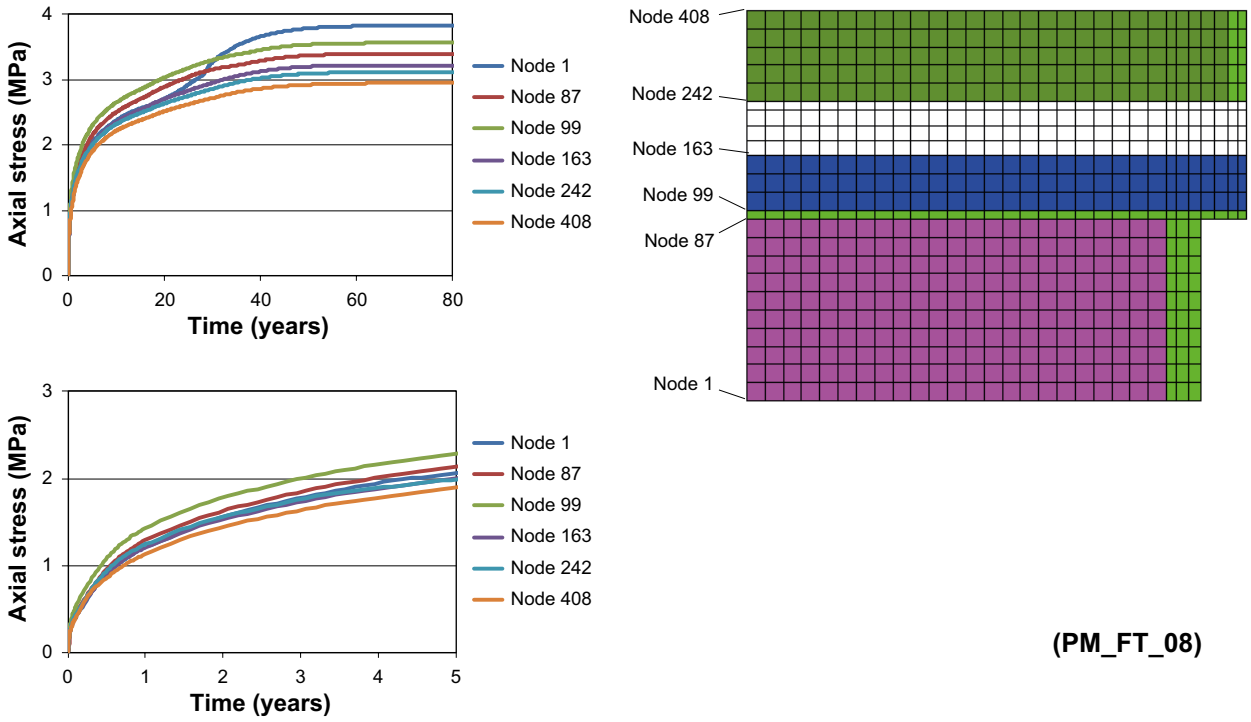

Figure 5-45. *Axial stresses along tunnel axis in field test model.*

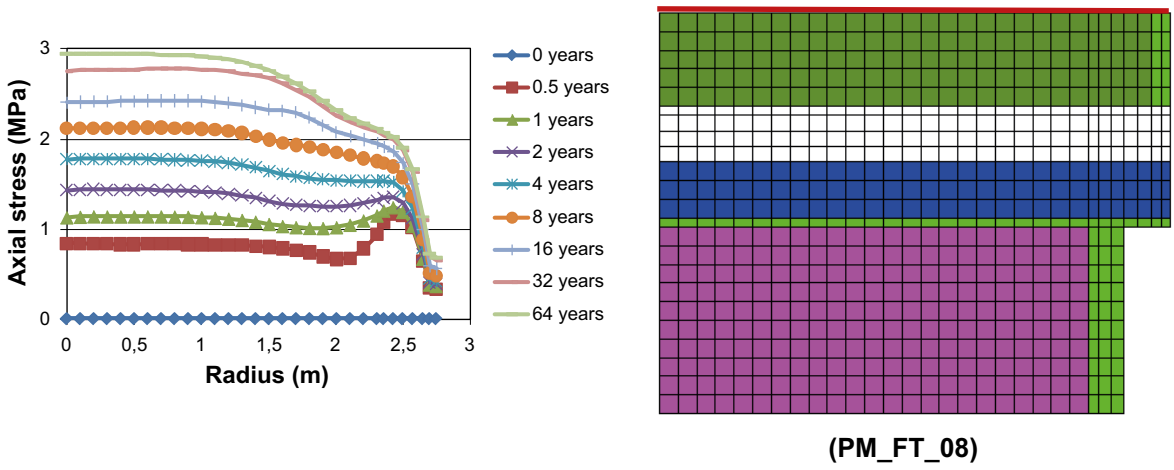

Figure 5-46. *Axial stresses along concrete plug in field test model.*

Radial void ratio distributions in the mid-section of the seal are shown in Figure 5-47. The void ratio in the pellets filling at the rock wall decreased to 1.2. The void ratio in the central part first increased slightly, after which the trend changed so that the final void ratio was slightly lower than the initial value (i.e. 1).

Axial void ratio distributions along the tunnel axis are shown in Figure 5-48. The void ratio in the pellets-filled slot between the backfill blocks and the Leca blocks wall decreased to 1, whereas the void ratio in the inner part of the backfill blocks increased to 0.8.

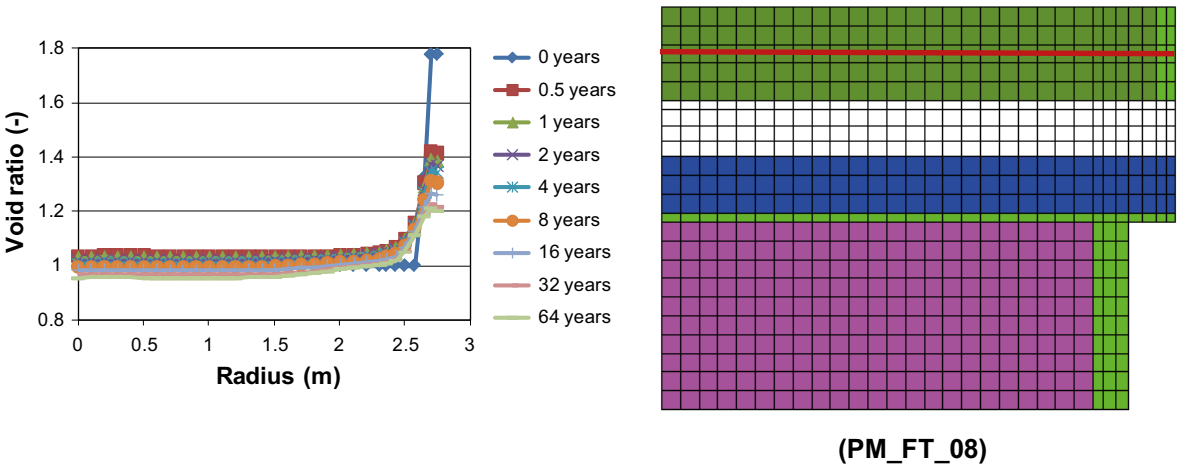

Figure 5-47. *Void ratio distribution along seal in field test model.*

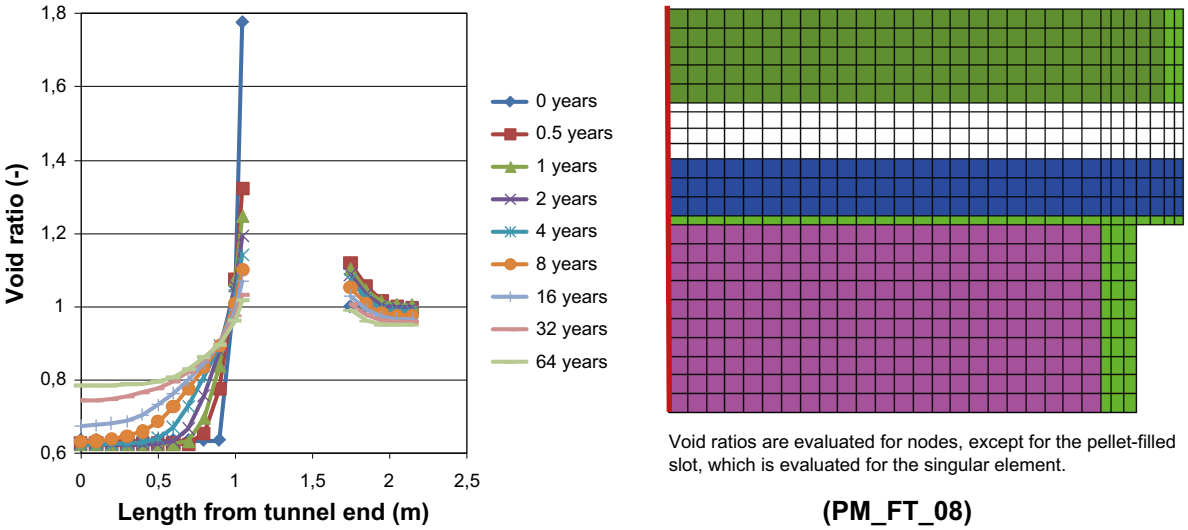

Figure 5-48. *Void ratio distribution along tunnel axis in field test model.*

Field Test II models

The evolutions of axial displacement in three nodes along the tunnel axis during the first 8 years are shown in Figure 5-49 and Figure 5-50. This shows that the analyzed nodes were generally displaced inwards, except for the interface between the backfill blocks and the pellets filling in the two cases with a 21 cm pellets filling, which were displaced outwards. The largest displacements were found for interfaces between the seal blocks and the macadam filling which generally had moved 5 cm after the first two years and had reached 7–8 cm after eight years. The inward displacements are slightly higher in the two cases with the higher dry density of the seal blocks (i.e. models PM_TT_35 and PM_TT_36).

Radial distributions of axial stresses against the concrete plug are shown in Figure 5-51 and Figure 5-52. After two years, the stresses in the central part had increased to 0.6–0.8 MPa, and to 1.2–1.5 MPa in the peripheral parts. The analyzed width of the pellets-filled slot appears to have a larger influence on the stresses after two years, than the influence from the dry density of the seal blocks. After eight years, however, the dry density of the seal blocks appears to have a larger influence.

Stress paths in the e-p' plane for a selection of nodes along the symmetry axis are shown in Figure 5-53 and Figure 5-54. The dotted line represents the used swelling pressure curve. Nodes in pellets increased in mean stress, with almost no swelling, and reached the swelling pressure curve, after which the pellets was compressed beyond the swelling pressure curve. Nodes in the seal and backfill blocks, on the other hand, increased in mean stress and also with some swelling (up to approximately 0.9 in void ratio), and reached the swelling pressure curve.

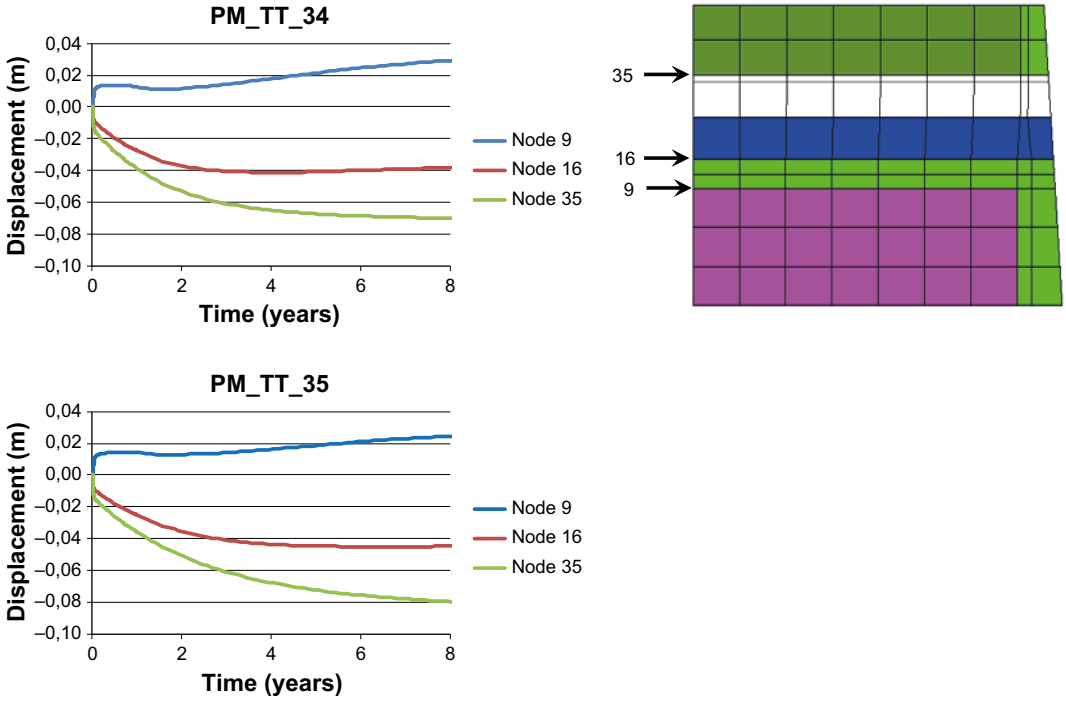

Figure 5-49. *Axial displacement along tunnel axis in models with 21 cm pellets-filled slot.*

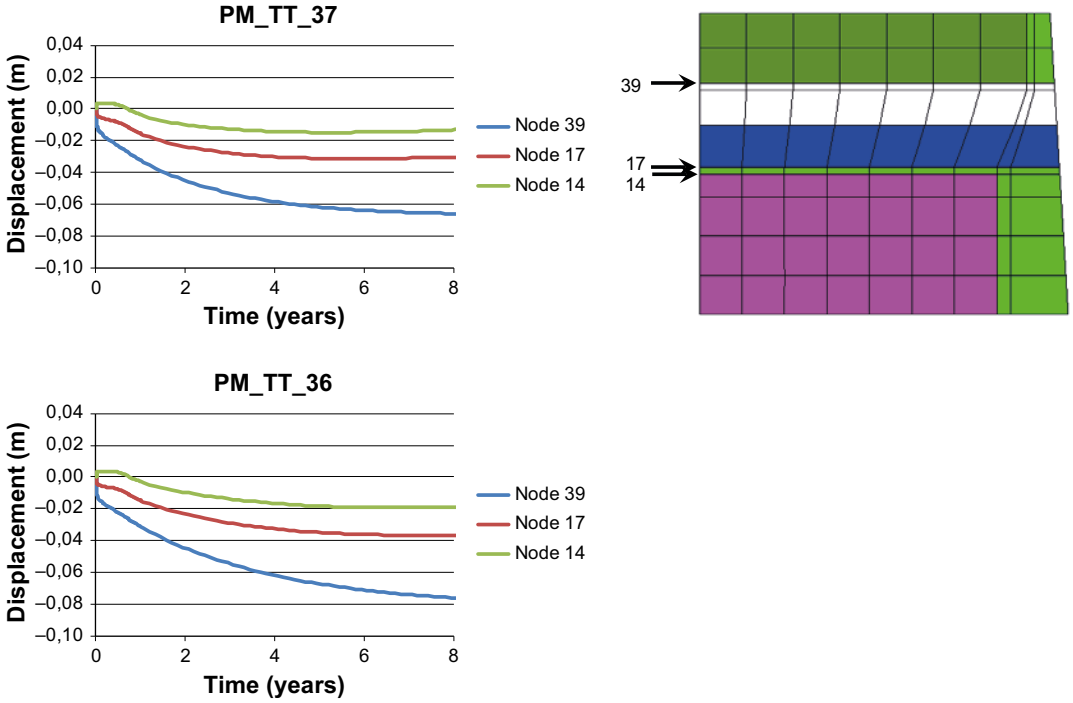

Figure 5-50. *Axial displacement along tunnel axis in models with 5 cm pellets-filled slot.*

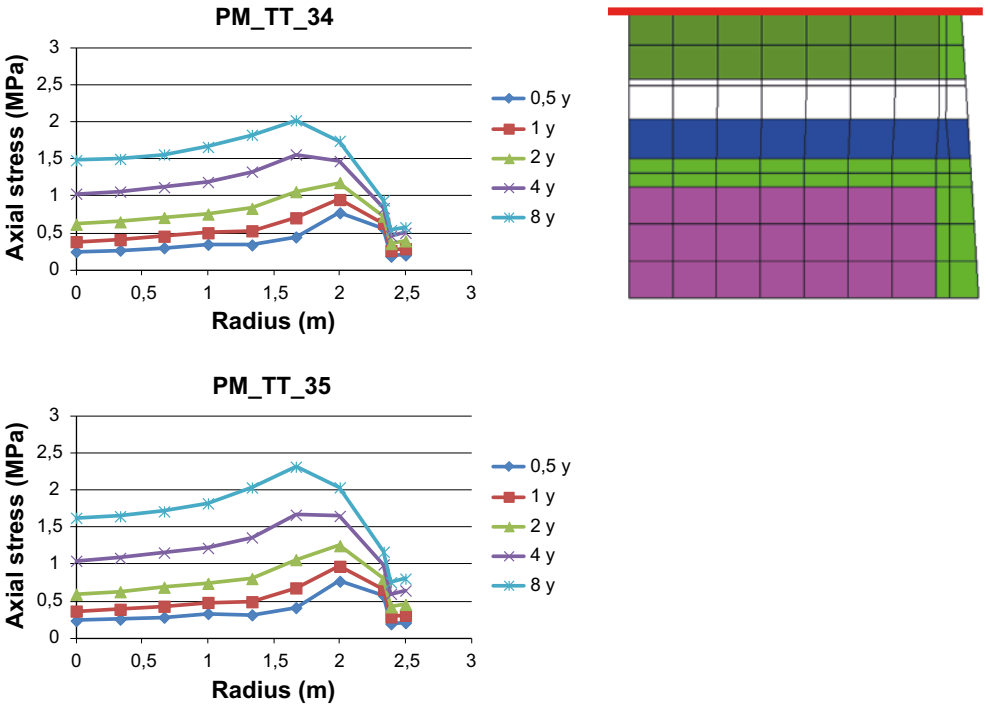

Figure 5-51. *Axial stresses along concrete plug in models with 21 cm pellets-filled slot.*

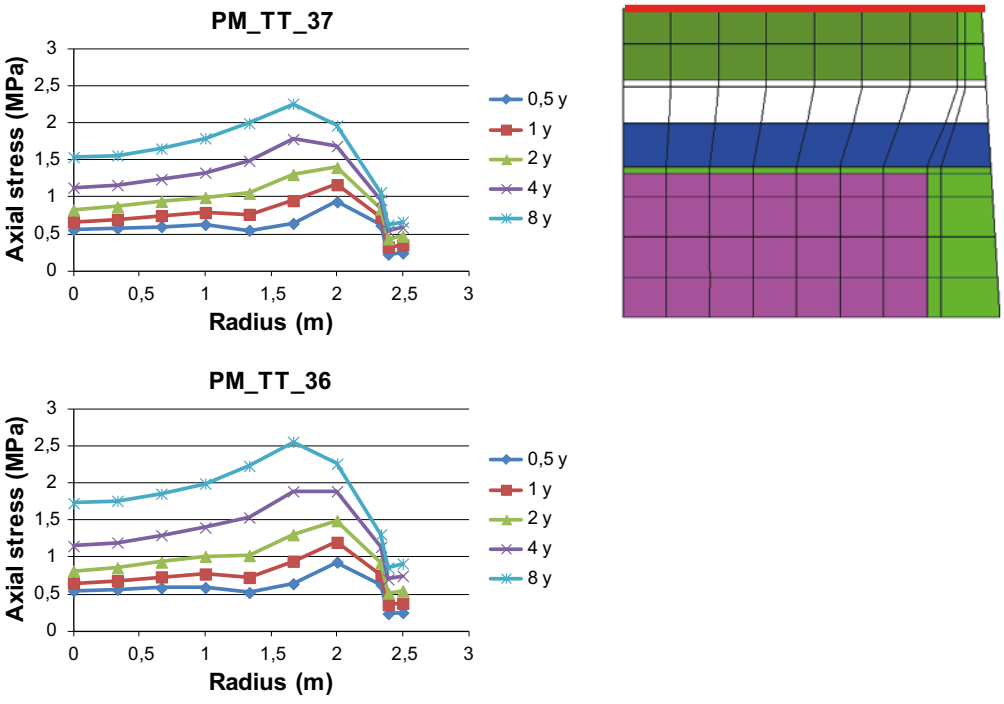

Figure 5-52. *Axial stresses along concrete plug in models with 5 cm pellets-filled slot.*

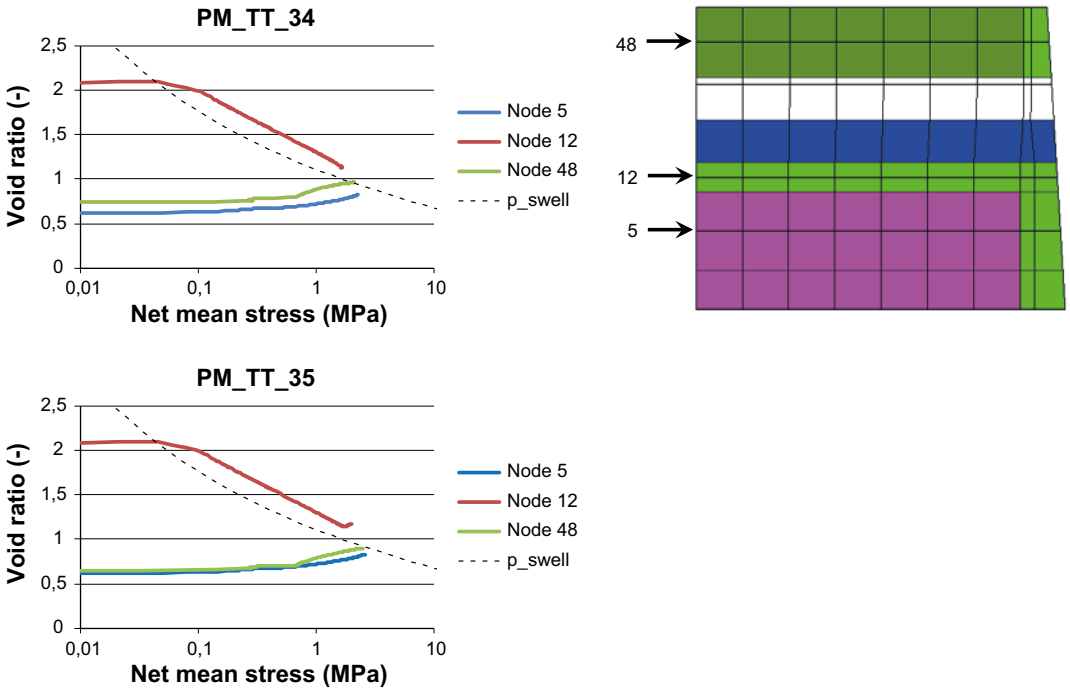

Figure 5-53. *Stress-paths at nodes along tunnel-axis in models with 21 cm pellets-filled slot.*

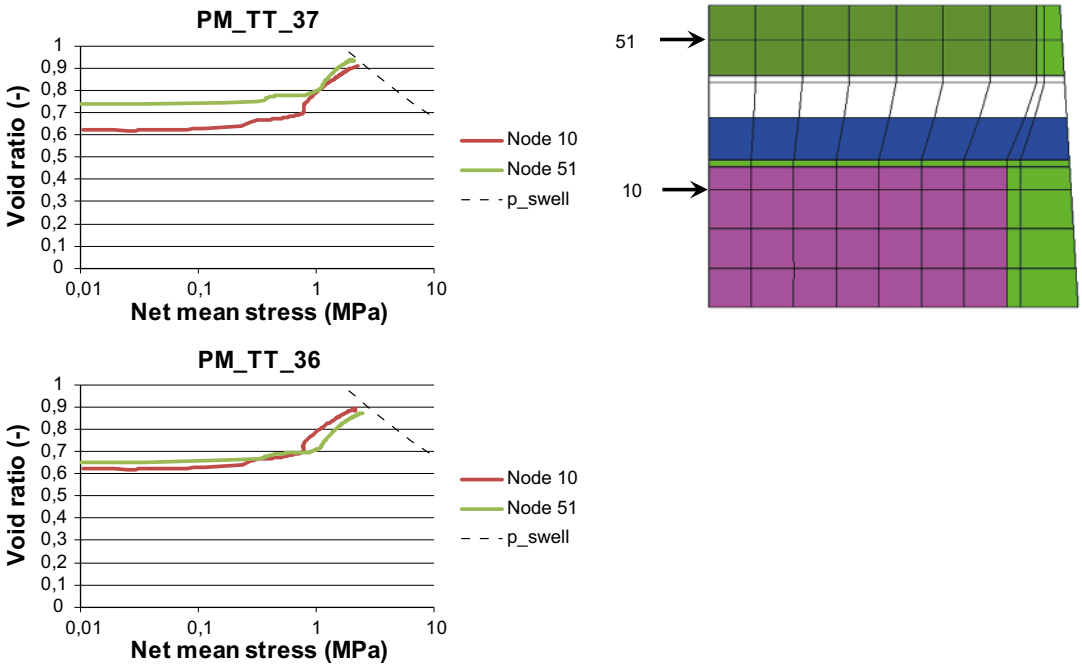

Figure 5-54. *Stress-paths at nodes along tunnel-axis in models with 21 cm pellets-filled slot.*

Field test predictions

Results from the Base case are shown in Figure 5-55 and Figure 5-56. Scan-lines of axial stresses along the interface towards the concrete dome are shown in Figure 5-55, together with history plots of axial stress at six nodes along the tunnel axis, and radial stresses at five nodes along the rock wall outside the bentonite seal. History plots of axial displacements, void ratio and relative humidity for nodes along the tunnel axis are shown in Figure 5-56.

Results from the Drained case are shown in Figure 5-57 with history plots of axial stress along the tunnel axis, radial stresses along the rock wall outside the bentonite seal, and axial displacements along the tunnel axis.

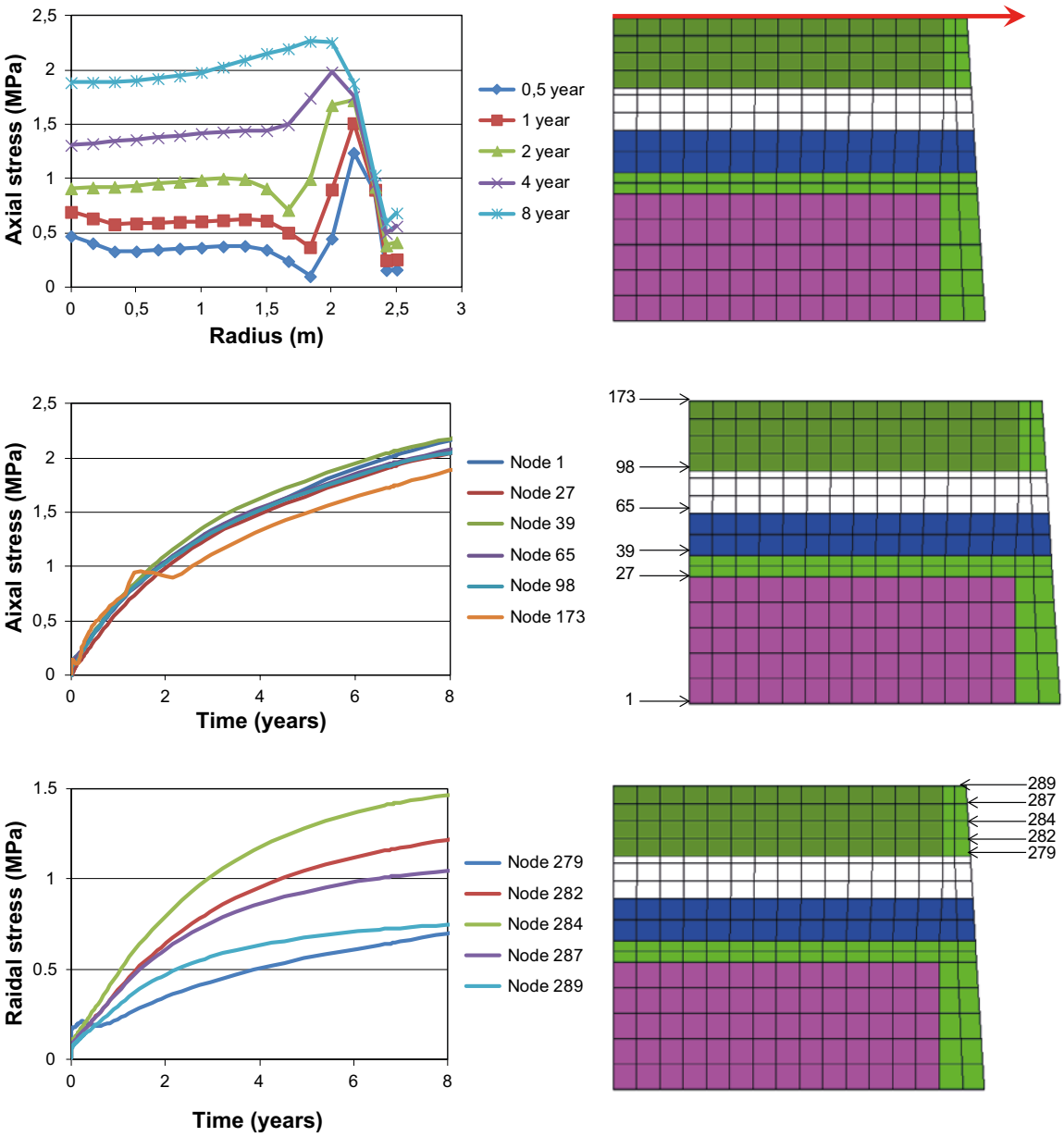

Figure 5-55. *Base case results concerning axial stresses (upper and middle) and radial stresses (lower). The nodal radius in the upper graph is not modified for displacements.*

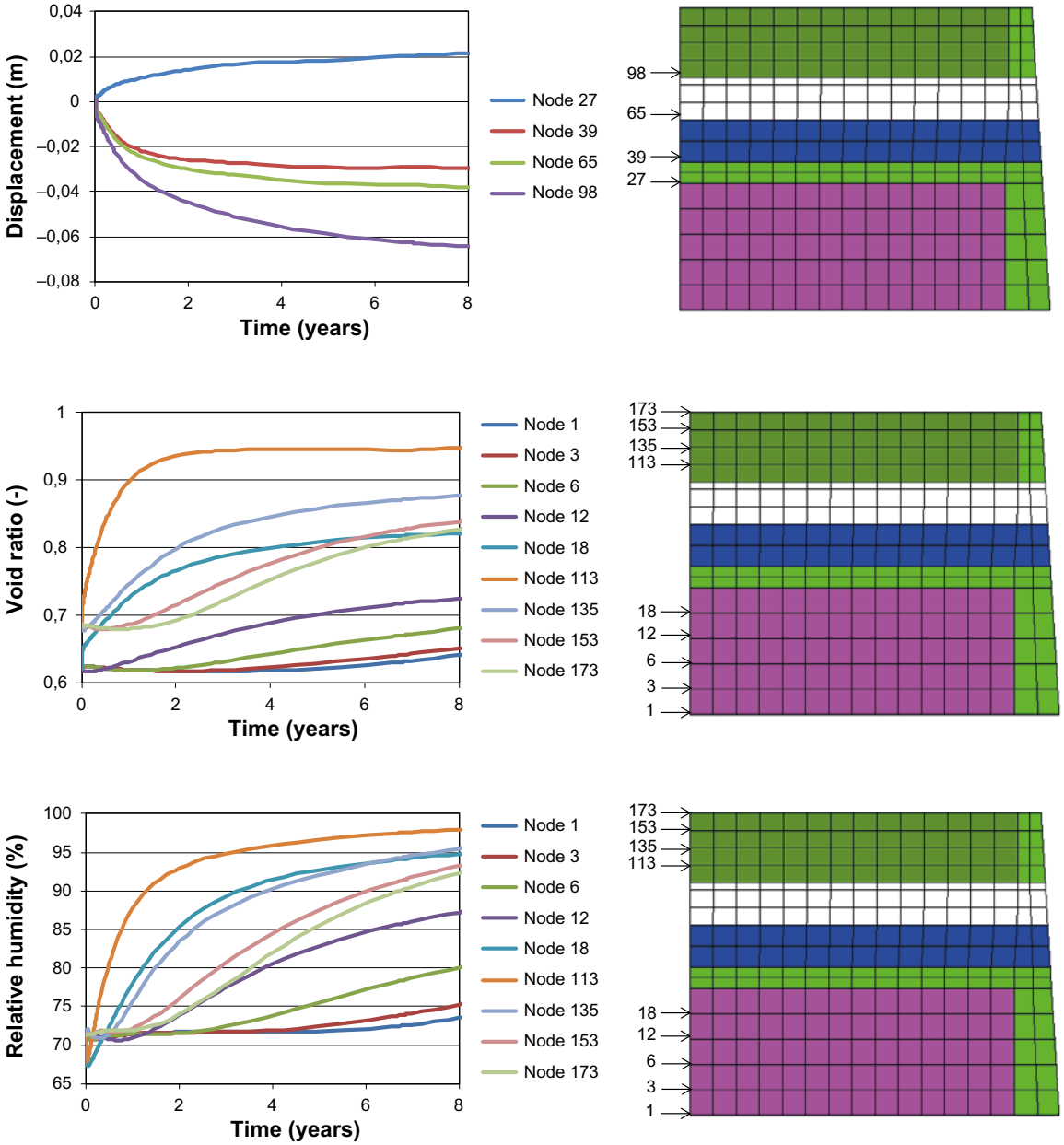

Figure 5-56. *Base case results concerning axial displacement (upper), void ratio (middle) and relative humdity (lower).*

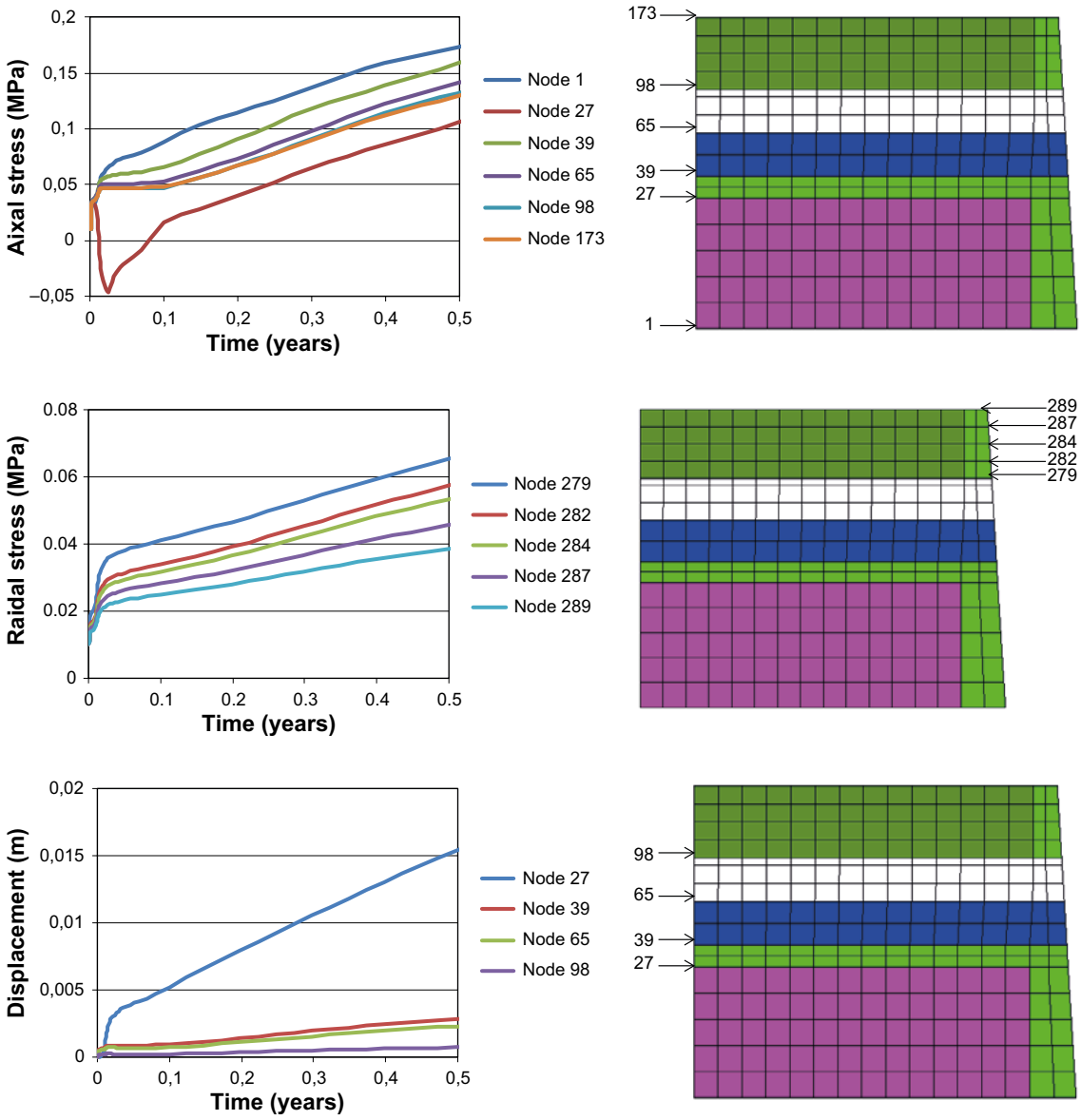

Figure 5-57. *Results from drained case concerning axial stress (upper), radial stress (middle) and axial displacement (lower).*

Results from the Pressurized case are shown in Figure 5-58 with history plots of the axial stress, and axial displacements along the tunnel axis.

All stresses in Figure 5-55, Figure 5-57 and Figure 5-58 are presented as total pressures (positive for compressive stresses) relative an atmospheric pressure of 0.1 MPa.

The current plan is to dismantle the field test after day 415, i.e. after little more than one year. The axial stresses along the tunnel axis are expected to be approximately 0.7 MPa at that time according to the *Base case* model, whereas the radial stresses at the seal towards the rock wall are 0.2–0.5 MPa. The largest displacement along the tunnel axis will occur at the interface between the seal and the filter and will be approximately 4 cm. The inner part of the filter component will be pushed inwards by approximately 2 cm. The extent of hydration will be quite limited at day 415. For example, the relative humidity in the centre of the seal blocks (i.e. 0.25 m from the filter) will only have increased from 71 to 77%. It should be noted however that the evolution will be delayed with the same duration as any drainage period.

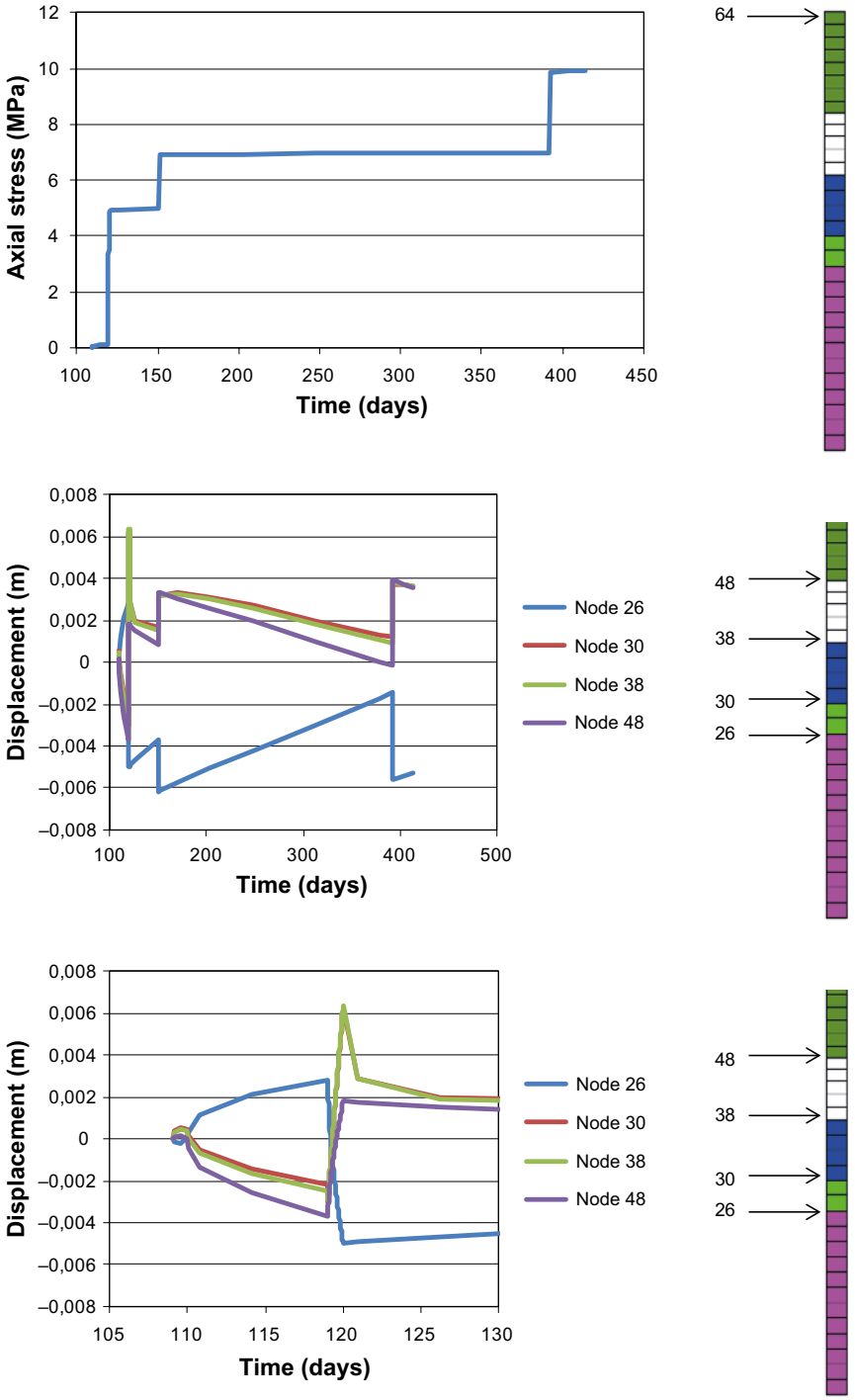

Figure 5-58. *Results from pressurized case concerning axial stress (upper), and axial displacements (middle and lower).*

According to the *Base case* model, there will also be a local increase in axial stress in the peripheral part of the seal with approximately 1.5 MPa at day 415. This is a quite typical behaviour which occurs when bentonite blocks are hydrated from one direction, in this case from the pellets-filled slot towards the rock wall.

The drained period is planned to last for 109 day. The axial stress at the centre of the concrete dome will be 90 kPa at that time according to the *Drained case* model, whereas the radial stress at the seal towards the rock wall will be 30–50 kPa. The displacement of the backfill block interface towards filter will be 1 cm at day 109.

The axial stress in the *Pressurized case* model was almost identical with the applied liquid pressure. This model also indicates that the installed bentonite will be compressed during periods with increasing liquid pressure, so that the displacements of the interfaces towards the filter will be in the order of 5 mm.

The following comments can be made concerning the difference between the results from the three cases:

- The axial stress on the concrete dome will follow the pressurization scheme if this is implemented. The axial stress will follow the Base case results if the filter is water-filled without any significant pressurization. The stress evolution will however be delayed due the drainage period.
- The main displacement is likely to occur at the interface between the seal and the filter, and will probably follow the Base case results. The drainage period will however delay this evolution and the pressurization will probably counteract it to some extent.
- The evolution of RH in the bentonite blocks will probably follow the Base case results. The drainage period will delay this evolution. The pressurization is likely to have a limited impact on these trends however.

Finally, it should be noted that this type of homogenization analysis is associated with uncertainties which limit the predictive capabilities of the models: on one hand there are the sets of data from different measurements and tests, which in general display a significant density dependency; on the other hand there is the adoption of modules and parameter values which are used together with constitutive laws which do not incorporate any density dependency.

Concerning the pressurized case among the field test predictions, it should be noted that the material models applied only have been used for a few pressurized problems in the past. The current pressurized problem may therefore be slightly outside the field of applications for which the material model originally was adopted.

5.6 Concluding remarks

The aims and the designs of the presented models have evolved during the course of the project: from the generic analytical models and the numerical general design models, to increasingly specified numerical field test models.

The analytical models and the general design models were developed with the aim of limiting the final swelling pressure on the concrete plug to 2 MPa, which has been considered to be one of the main design criterions for the plug construction. Since the swelling pressure in the backfill can be considerably higher, this has called for the development of a transition zone, in which a pressure difference between different sections of the plug, can be counter-balanced by the frictional forces against the rock wall.

This aim of the 2 MPa swelling pressure limit has been given less priority during the planning of the field test. One reason for this has been that the time-scale to reach full saturation in a full-scale test is expected to be too long to be studied in a field test. Another reason is that it wasn't possible to manufacture conveniently-sized bentonite blocks with a sufficiently low dry density to keep the system within this limit.

The main results from the different numerical models have been: i) the stress on plug and the stress distribution along the tunnel axis; ii) the displacements of the different components; iii) the extent of homogenization; and iv) the time-scales of hydration.

Some modelling results have been compared with experimental data. One such data set was the different stress paths in the void ratio vs. net stress plane obtained from oedometer tests. The model results showed quite good agreement with the experimental data set, which strengthens confidence in the validity of the mechanical model used. A similar comparison could be made with water saturation profiles from water uptake tests, by choosing model results for relevant time scales. This comparison indicated that the modelled hydration process was slightly faster than the measured hydration.

The work with the numerical models has to a large extent consisted of efforts to reach numerical convergence. In the final models (Field test II models and Field test predictions) the difficulties were quite extensive, which meant that the size of the elements had to be significantly increased, and that results were accepted even if the calculations could not be pursued to full water saturation. Another limitation of the numerical models has been the inability to include contact elements in the model.

During the preparation of this report, however, a new version of the code used (Code_Bright v4.1) has been released, and this facilitates the inclusion of contact elements (in axisymmetric 2D geometries), and also appears to be more numerically stable than the one used in this work. It could therefore be possible to further refine the presented models, if this would be of interest.

6 Conclusions and recommendations

6.1 General

The primary demands on the plug are that the water leakage past the plug is small enough to allow buildup of water pressure inside the plug and to keep erosive water flow from the tunnel at an acceptable level. It is very important that the plug is so tight that the minimum water pressure gradient is moved from the rock/bentonite interface in the tunnel to the plug, since that will give the bentonite time and ability to swell and seal in stagnant water. The plug must also be so tight that the water leakage does not cause unacceptable erosion from the deposition holes until the water pressure in the transport tunnel outside the plug has reached the same level as inside the plug.

In preparation for a plug test at full scale in Äspö HRL, a program for investigating critical parts of a plug and design the plug has been run. The work done for the designing the sealing and draining sections of the plug has included of the following four main subprojects:

- Laboratory testing of the sealing materials, see Chapter 2.
- Laboratory testing of the drainage components, see Chapter 3.
- Scale tests of the sealing and draining function, see Chapter 4.
- Hydro-mechanical modelling of the tunnel plug, see Chapter 5.

The work and the results have been described in the present report. The main results and recommendations are summarised in this Chapter.

6.2 Laboratory testing of the sealing material

The results from the laboratory tests on the sealing material can be summarized as follows:

- **Compaction sealing block**. The tests showed that it was possible to compact blocks with low density and high degree of saturation, although problems could be seen if the water content of the clay was higher than 30%. The desired density of the blocks was increased at a later stage of the project and other tests e.g. the sealing tests showed that blocks with lower water content seemed to swell and seal faster.
- **Strength of the sealing blocks**. The results showed that the strength of the block depends strongly on the water content and on the achieved density of the block. At low water contents (10%), the strength was rather low and the blocks fragile. The low strength was mainly caused by the low density. The tests showed that the highest strength was reached for samples compacted with a water content of 17%. These samples had, however, a dry density higher than desired, which means that the compaction pressure must be adjusted downwards for full scale manufacturing.
- **Compression / expansion properties**. The results from these tests agreed well with what was expected for MX-80 bentonite. The results of these tests were used in Chapter 5 as part of the hydro-mechanical modeling of the plug.
- **Swelling pressure and hydraulic conductivity**. These tests were made in order to investigate if blocks compacted to high degree of initial saturation had the same properties as blocks with low initial degree of saturation. The investigation showed, as expected, that there was no substantial difference, although the hydraulic conductivity values obtained were slightly lower than the reference tests. This difference is attributed to the fact that the blocks compacted to high degree of saturation were more homogenized.
- **Self sealing of fractures**. Three tests were performed in this test series. Two of the tests were performed with bentonite blocks with densities of 1,400 and 1,500 kg/m^3 and with water contents of 35% and 30% respectively i.e. the degree of saturation was very high. The bentonite in these two tests did not manage to seal the artificial fracture (0.01 mm aperture) during the time the tests

were operated. The third test was performed with bentonite blocks with a dry density of 1,500 kg/m^3 and with a much lower water content (13.9%). In this test the behavior was quite different. The bentonite sealed more quickly and a water pressure could be built up on the inflow side of the test assembly (maximum 2 MPa was applied in this test). It is though not clear if the sealing took place in the cylindrical tube containing the blocks or in the artificial slot.

- **Sealing of initial slots**. In these tests, bentonite blocks with different initial densities and water contents were allowed to swell and seal a slot with a gap of either 2 or 4 mm width. The results from the tests showed, as expected that the slot width is of great importance with faster swelling pressure increase with a small gap. Another result was that the initial water content of the bentonite block also influenced the results. The time for swelling, filling up the slot and start of pressure build up was longer for the samples with high initial water contents (and high degree of saturation).

6.3 Laboratory testing of the drainage material

General

This work was done in order to evaluate several different types of draining components that might be used in connection with a concrete tunnel-plug. The draining components will prevent water pressure buildup on the concrete portion of the plug prior to its hardening. The candidate materials tested were three types of geological draining material, two qualities of geotextile and two types of stiff draining materials. An important factor in the evaluation is the expected swelling pressure of about 2 MPa that the components will be exposed to. Compressibility and hydraulic conductivity were tested on all candidates. Modified Proctor compaction tests were also performed on the draining geological materials in order to determine what densities could realistically be expected to be achieved in their as-placed condition. Finally a clogging test was performed on all candidates to investigate if they would maintain their draining ability when exposed to a water flow with high entrained bentonite content. The bentonite slurry concentration was about 10 g/liter MX-80 sodium bentonite.

Geological draining material

Three geological draining materials were tested; a mix of stone dust and macadam with grain sizes < 5 mm, a natural sand/gravel with grain sizes < 4 mm and finally pure macadam with grain sizes 2–4 mm and no fines. Initially a modified Proctor compaction test and a CRS-test were performed on the candidates and then the hydraulic conductivity was measured at three different densities. Macadam 2–4 mm was the candidate with the highest hydraulic conductivity, which was very little affected by an increased dry density. The results from the CRS-tests showed that the other two candidates had a significant reduction in hydraulic conductivity for the densities corresponding to 2 MPa external pressure. In the hydraulic conductivity tests some significant settling was observed in MakPak® < 5 mm and natural sand/gravel < 4 mm. A special test was performed on macadam 2–4 mm but no settling was observed at all. Macadam 2–4 mm was also the absolute superior in the clogging test. Initially the hydraulic conductivity was reduced slightly but over time macadam 2–4 mm seemed to maintain its draining ability.

Geotextile

Two qualities (densities) of the needle felted geotextile were tested; 1,000 g/m^2 and 1,200 g/m^2. Firstly a CRS-test was performed and then the hydraulic conductivity was investigated as a function of stress on the geotextiles. There was no observed difference in compressibility or hydraulic conductivity. The hydraulic conductivity was clearly reduced when the stress on the specimen increased. The clogging test indicated that the geotextile draining ability will be reduced by time and that it should not be used for draining water with eroded bentonite. However it could still function to distribute water if manual wetting of the system is required.

Stiff draining material

The stiff draining material candidates were lightweight concrete and Leca. The Leca specimens had a hydraulic conductivity from $1.17 \cdot 10^{-4}$ to $1.40 \cdot 10^{-4}$ m/s. The lightweight concrete hydraulic conductivity was $1.29 \cdot 10^{-7}$ m/s. The compression strength was highest in the lightweight concrete, about 5.0–5.5 MPa while it was 2–3 MPa for the Leca blocks. In the clogging test the lightweight concrete had an instant pressure buildup and was considered impermeable to the bentonite slurry. The Leca generally showed an initial slight reduction in hydraulic conductivity but was considered to be capable of maintaining its draining ability over a substantial time.

Recommendations

It is strongly suggested to use the macadam 2–4 mm as a geological draining material. This candidate is the clearly superior option in terms of its hydraulic conductivity and also seems to maintain its draining ability when exposed to a water flow with high bentonite content.

The geotextile seem to clog when exposed to a water flow with a content of eroded bentonite and should therefore not be used to drain the system. However it could function as a distributer of water if manual wetting of the system is required.

Leca is the superior stiff draining material in hydraulic conductivity and seem to maintain its draining ability when exposed to a water flow with high bentonite content.

6.4 Scale tests of the sealing and draining function

Several tests of a plug scaled about 1:20 with all components included were performed in the laboratory in order to study the drainage and sealing function of the plug. The combined main conclusions from the tests are as follows:

- The test components interacted as desired and the different materials were successfully separated from each other. However in some tests the Leca-beams were more loosely installed than others and backfill bentonite managed to intrude into the macadam filter, highlighting the importance of construction quality control.
- The draining function of the filter worked satisfactorily at inflow rates of 0.001 l/min and 0.005 l/min.
- The measured amount of eroded material was small, about 1 g/l or less, which is in the lower region of the erosion prediction model by Sandén and Börgesson (2010).
- The bentonite sealing could successfully withstand 5 MPa of water pressure if the hydration and pressurization process was carefully controlled.
- The size of the void spaces between the concrete beams seems to be of importance for the sealing ability. Moulding/grouting of the concrete beams to minimize the void spaces seem to improve the sealing function of the plug.
- Early wetting seemed to improve the sealing function significantly.
- In general the 100 kPa/h pressure elevation ramp seemed too fast. The 50 kPa/h pressure elevation ramp was more successful in raising the pressure without leakage.
- Returning the water pressure to a previously attained high pressure level must be done carefully to avoid leakage.
- The radial total pressure ranged from 750 kPa to 1,400 kPa when the water pressure ramp was started (contribution from a 500 kPa water pressure included) in the tests that resisted 5 MPa water pressure.
- In the tests where 5 MPa of water pressure was reached the dry density in the outermost parts of the sealing was 1.25–1.35 kg/m^3 at dismantling.

Based on these conclusions the following suggestions are made for the full scale field test of the tunnel plug;

- The filter draining function should be tested with a water flow rate that represents the expected total flow of a deposition tunnel.
- The erosion during the drainage period should be measured and evaluated to confirm that it is within an acceptable range.
- The size of the void spaces in-between concrete beams and between concrete beams and tunnel wall should be minimized for maximum sealing function. The space between the concrete beams and the tunnel wall should be filled or groutedcast with cement.
- The filter should be filled up with water early to give the bentonite sealing component access to water as early as possible.
- The pressure elevation should be done carefully. If the water pressure needs to be reduced for some reason, the repressurization needs to be carefully performed as well.

There was also some data on the radial total pressures and dry densities of the sealing. It is hard to give a direct recommendation for the full scale field test due to the scaling factor but a radial total pressure of 750 kPa (including contribution from 500 kPa water pressure) showed to be the lowest swelling pressure that could withstand a ramp of 50 kPa/h that finally reached 5 MPa.

6.5 Hydro-mechanical modelling of the tunnel plug

The modelling work consisted of two major activities:

- Dimensioning calculations of the general plug design. This has mainly consisted of analytical calculations of dimensions for different plug components in different configurations.
- Predictions of the hydro-mechanical processes in the planned field experiment. These predictions were performed stepwise and became increasingly specified during the course of the project.

The aims and the designs of the presented models have evolved during the course of the project: from the generic analytical models and the numerical general design models, to increasingly more specific numerical field test models.

The analytical models and the general design models were developed with an aim to limit the final swelling pressure on the concrete plug to 2 MPa, which has been considered to be one of the main design criterions for the plug construction. Since the swelling pressure in the backfill can be considerably higher, this has called for the development of a transition zone, in which a pressure difference between different sections of the plug, can be counter-balanced by the frictional forces against the rock wall.

This aim of limiting contact pressure to 2 MPa has been given a lower priority during the planning of the field test. One reason for this has been that the time-scale to reach full saturation in a full-scale test is too long to be studied in a field test. Another reason is that it wasn't possible to manufacture conveniently sized bentonite blocks with a sufficiently low dry density.

The main results from the different numerical models have been: i) the stress on plug and the stress distribution along the tunnel axis; ii) the displacements of the different components; iii) the extent of homogenization; and iv) the time-scales of hydration.

Some numerical results have been compared with experimental data:

- One such data set was the different stress paths in the void ratio vs. net stress plane obtained from oedometer tests. The model results showed quite good agreement with the experimental data set, which strengthens confidence in the validity of the mechanical model used.

- A similar comparison was made with water saturation profiles from water uptake tests, by choosing model results for relevant time scales. This comparison indicated that the modelled hydration process was slightly faster than the measured hydration.

The work with the numerical models has to a large extent consisted of efforts to reach numerical convergence. In the final models (Field Test II models and Field Test predictions) the numerical difficulties were quit extensive, indicating that the size of the elements had to be significantly increased. It was therefore necessary to accept as correct the numerical results, for the short-term, even if the calculations could not be pursued to full water saturation. Another limitation of the numerical models has been the inability to include contact elements in the model.

During the preparation of this report, however, a new version of the used code (Code_Bright v4.1) has been released, and this facilitates the inclusion of contact elements (in axisymmetric 2D geometries), and also appears to be more numerically stable than the one used in this work. It could therefore be possible to further refine the presented models as part of ongoing studies in support of full-scale testing.

References

SKB's (Svensk Kärnbränslehantering AB) publications can be found at www.skb.se/publications.

Andersson L, Sandén T, 2012. Optimization of backfill pellets properties. ÅSKAR DP2. Laboratory tests. SKB R-12-18, Svensk Kärnbränslehantering AB.

Börgesson L, 2001. Äspö Hard Rock Laboratory. Compilation of laboratory data for buffer and backfill materials in the Prototype Repository. SKB IPR-01-34, Svensk Kärnbränslehantering AB.

Börgesson L, Johannesson L-E, Sandén T, Hernelind J, 1995. Modelling of the physical behavior of water saturated clay barriers. Laboratory tests, material models and finite element application. SKB TR 95-20, Svensk Kärnbränslehantering AB.

Das B M, 1997. Advanced soil mechanics. 2nd ed. Washington, DC: Taylor & Francis.

Dueck A, 2004. Hydro-mechanical properties of a water unsaturated sodium bentonite: laboratory study and theoretical interpretation. PhD thesis. Lund Institute of Technology, Sweden.

Dueck A, Nilsson U, 2010. Thermo-hydro-mechanical properties of MX-80. Results from advanced laboratory tests. SKB TR-10-55, Svensk Kärnbränslehantering AB.

Fagerström H, 1973. Packningsegenskaper – Förslag till geotekniska laboratorieanvisningar, del 5. In Byggforskningens informationsblad B2:1971. Reviderad utgåva 1973. Stockholm: Statens institut för byggnadsforskning. (In Swedish.)

Karnland O, Olsson S, Nilsson U, 2006. Mineralogy and sealing properties of various bentonites and smectite-rich clay materials. SKB TR-06-30, Svensk Kärnbränslehantering AB.

Möller G (ed), 1980. Betonghandbok. Material. Stockholm: Svensk byggtjänst.

Nyströms Cement, 2011. ALBA Kryprumsgrund (LECA balk). Produktbeskrivning.Available at: http://www.nystromscement.se/uplds/files/alba_kryprumsgrund.pdf [26 October 2011]. (In Swedish.)

Sandén T, Börgesson L, 2010. Early effects of water inflow into a deposition hole. Laboratory test results. SKB R-10-70, Svensk Kärnbränslehantering AB.

Sandén T, Börgesson L, Dueck A, Goudarzi R, Lönnqvist M, 2008. Deep repository – Engineered barrier system. Erosion and sealing processes in tunnel backfill materials investigated in laboratory. SKB R-08-135, Svensk Kärnbränslehantering AB.

Sandén T, Olsson S, Andersson L, Dueck A, Jensen V, Hansen E, Johnsson A, 2014. Investigation of backfill candidate materials. SKB R-13-08, Svensk Kärnbränslehantering AB.

SKB, 2010. Design, production and initial state of the backfill and plug in deposition tunnels. SKB TR-10-16, Svensk Kärnbränslehantering AB.

Svensson D, Dueck A, Nilsson U, Olsson S, Sandén T, Lydmark S, Jägerwall S, Pedersen K, Hansen S, 2011. Alternative buffer material. Status of ongoing laboratory investigation of reference material and test package 1. SKB TR-11-06, Svensk Kärnbränslehantering AB.

Sydsten, 2011. MakPak. Malmö: Sydsten AB. Available at: http://www.sydsten.se/Produkter/Krossprodukter/Stenmj%C3%B6l.aspx [4 October 2011]. (In Swedish.)

Åkesson M, Börgesson L, Kristensson O, 2010a. SR-Site data report. THM modelling of buffer, backfill and other system components. SKB TR-10-44, Svensk Kärnbränslehantering AB.

Åkesson M, Kristensson O, Börgesson L, Dueck A, Hernelind J, 2010b. THM modelling of buffer, backfill and other system components. Critical processes and scenarios. SKB TR-10-11, Svensk Kärnbränslehantering AB.

Åkesson M, Malmberg D, Börgesson L, Hernelind J, Ledesma A, Jacinto A, 2012. Temperature Buffer Test. Final THM modelling. SKB P-12-07, Svensk Kärnbränslehantering AB.

Produktblad Fibertex Geotextil

FIBERTEX NONWOVENS CONSTRUCTION

Product Data Sheet

Fibertex Geotextiles

400.52
Date 02/2015

Fibertex Geotextiles			F-10	F-20	F-22	F-25	F-31	F-32	F-33	F-46	F-55	F-59
Physical Properties												
Weight	EN ISO 9864	g/m²	80	100	120	130	150	175	200	250	315	370
Thickness at 2 kPa	EN ISO 9863-1	mm	0,5	0,5	0,7	0,8	0,8	0,9	1	1,3	1,6	1,6
Mechanical Properties												
Static puncture (CBR-test)	EN ISO 12236	N	800	1100	1500	1600	1800	2000	2500	3400	4000	5100
Tensile strength long. dir.	EN ISO 10319	kN/m	4,6	6,8	8,1	10	12	13	16	20	25	30
Tensile strength trans. dir.	EN ISO 10319	kN/m	4,6	6,6	8,1	10	12	13	16	20	25	30
Elongation at break long. dir.	EN ISO 10319	%	40	35	40	45	38	45	43	50	50	50
Elongation at break trans. dir.	EN ISO 10319	%	50	45	55	55	50	50	50	55	55	55
Dynamic Cone drop	EN ISO 13433	mm	50	35	32	32	26	24	22	17	13	9
Protection efficiency at 300 kPa	EN 13719	%	-	2,6	2,5	2,4	2,3	2,3	2,2	2,2	2,1	2,0
Pyramid puncture resistance	EN 14574	N	-	70	80	110	140	160	200	250	310	400
Hydraulic Properties												
Permeability at 50 mm WH	EN ISO 11058	m/sec	0,1	0,09	0,07	0,07	0,05	0,04	0,03	0,04	0,03	0,02
Permittivity at 50 mm WH	EN ISO 11058	sec^{-1}	2,0	1,8	1,4	1,4	1,0	0,8	0,6	0,1	0,6	0,4
Water flow at 50 mm WH	EN ISO 11058	l/sec/m²	100	90	70	70	50	40	30	40	30	20
Velocity index at 100 mm WH	EN ISO 11058	m/sec	0,16	0,14	0,12	0,12	0,08	0,07	0,06	0,05	0,05	0,03
Water flow at 100 mm WH	EN ISO 11058	l/sec/m²	160	140	120	120	80	70	60	50	50	30
Transmissivity	EN ISO 12958	10^{-6} m²/sec	0,1	0,3	0,3	0,6	0,5	0,8	0,7	1,1	1,5	1,6
Water flow capacity	EN ISO 12958	l/hour/m	0,5	1,0	1,0	2,0	2,0	2,7	2,5	4,0	5,0	6,0
Pore size, $O_{90\%}$	EN ISO 12956	micron	100	100	85	70	75	85	75	70	70	70
Standard Dimensions												
Width		m	4/5	4/5	4/5	4/5	4/5	4/5	4/5	5	5	5
Length		m	100	100	100	100	100	100	100	100	100	100
Roll diameter		cm	25	26	28	30	32	32	34	36	43	45
Roll weight at maximum standard dimension		kg	45	55	65	70	80	95	110	130	165	190

Above technical values are mean values based on measurements in current production and test results from independent test institutes.

Fibertex Geotextiles
Fibertex Geotextiles are used in building and construction works for separation, filtration, drainage, protection, stabilization and reinforcement.
Fibertex Geotextiles are made of virgin polypropylene fibres added HALS UV stabilizer according to EN 12224.
The basic strength of Fibertex Geotextiles is obtained by needle-punching the PP-fibres, which gives strong elastic bonding between the fibres.
Due to the unique production process all Fibertex Geotextiles are added a thermal treatment unless marked with:
M: Needlepunched only

Quality Management
Fibertex production control is certified CE-marking level 2+ for all geotextiles.

CE

1071-CPR-1846

Fibertex Nonwovens A/S is certified according to the international quality management system EN ISO 9001 as well as the environmental management system EN ISO 14001.

Specifications for Tender
The geotextile should be Fibertex type ....or comparable type.
The material should be needlepunched PP with a CBR puncture resistance of ....N, acc. to EN ISO 12236 and a Wide-width tensile elongation of .....% acc. EN ISO 10319.
Water permeability should be .... l/sec/m² acc. to EN ISO 11058 and Pore size $O_{90\%}$ ....micron acc. EN ISO 12956. The geotextile supplier must be certified acc. to ISO 9001 and ISO 14001, and the products must be CE-marked.

Product Data Sheet
Fibertex Geotextiles

Sheet no 400.52
Date 02/2015

Fibertex Geotextiles			F-200M	F-300M	F-400M	F-500M	F-600M	F-650M	F-800M	F-1000M	F-1200M
Physical Properties											
Weight	EN ISO 9864	g/m²	200	300	400	500	600	650	800	1000	1200
Thickness at 2 kPa	EN ISO 9863-1	mm	2	3	3,7	4	4,5	5	6	7	8
Mechanical Properties											
Static puncture (CBR-test)	EN ISO 12236	N	1800	3890	4600	5700	6700	7500	9500	11500	14000
Tensile strength long. dir.	EN ISO 10319	kN/m	12	20	26	32	40	45	50	55	65
Tensile strength trans. dir.	EN ISO 10319	kN/m	12	20	34	40	45	50	65	85	100
Elongation at break long. dir.	EN ISO 10319	%	65	65	70	70	75	75	80	90	85
Elongation at break trans. dir.	EN ISO 10319	%	80	65	70	80	80	90	80	70	65
Dynamic Cone drop	EN ISO 13433	mm	20	16	10	8	5	4	0	0	0
Protection efficiency at 300 kPa	EN 13719	%	2,4	2,3	1,8	1,7	1,6	1,5	1,2	0,8	0,4
Pyramid puncture resistance	EN 14574	N	170	260	400	520	650	700	900	1200	1500
Hydraulic Properties											
Permeability at 50 mm WH	EN ISO 11058	m/sec	0,08	0,05	0,05	0,04	0,03	0,03	0,03	0,02	0,015
Permittivity at 50 mm WH	EN ISO 11058	sec^{-1}	1,7	1	1	0,8	0,6	0,6	0,5	0,4	0,3
Water flow at 50 mm WH	EN ISO 11058	l/sec/m²	80	50	50	45	30	30	25	20	15
Velocity index at 100 mm WH	EN ISO 11058	m/sec	0,13	0,07	0,07	0,06	0,05	0,05	0,04	0,03	0,02
Water flow at 100 mm WH	EN ISO 11058	l/sec/m²	135	70	70	60	50	50	40	35	25
Transmissivity	EN ISO 12958	10^{-4} m²/sec	2,9	4	3	4,3	6	5,7	10	10	12
Water flow capacity	EN ISO 12958	l/hour/m	12	15	12	15	20	20	36	36	43
Pore size, $O_{90\%}$	EN ISO 12956	micron	100	70	80	70	70	70	80	70	60
Standard Dimensions											
Width		m	4/5	4/5	5	5	5,5	5,5	5,5	5,5	5,5
Length		m	100	100	100	100	100	50	50	50	50
Roll diameter		cm	48	60	60	72	73	56	58	69	72
Roll weight at maximum standard dimension		kg	105	155	205	255	335	185	225	280	335

Above technical values are mean values based on measurements in current production and test results from independent test institutes.

Fibertex Paving Fabric			AM-2
Weight	EN ISO 9864	g/m²	150
Thickness at 2 kPa	EN ISO 9863-1	mm	1,2
Static puncture (CBR-test)	EN ISO 12236	N	1500
Tensile strength	EN ISO 10319	kN/m	8
Elongation at break	EN ISO 10319	%	55/55
Dynamic Cone drop	EN ISO 13433	mm	25
Bitumen retention	EN 15381	kg/m^2	1,3
Dimensions	Width	m	3,75/5,0
	Length	m	100
	Roll diameter	cm	35